

**Geophysical monitoring systems to assess
and quantify ground ice evolution
in mountain permafrost**

Dissertation

zur Erlangung des akademischen Grades doctor rerum naturalium
(Dr. rer. nat.)

Vorgelegt dem Rat der Chemisch-Geowissenschaftlichen Fakultät der Friedrich-
Schiller-Universität Jena

von: Dipl.-Geographin Christin Hilbich
geboren am: 20. 02. 1977 in Jena

Gutachter:

1.

2.

3.

Tag der öffentlichen Verteidigung:

Summary

Permafrost (perennially frozen ground) forms a major element of the global cryosphere. Azonal permafrost occurs in the European Alps due to the cold climate at high altitudes. Alpine permafrost is characterised by temperatures only a few degrees below zero and is therefore particularly sensitive to projected climate changes in the 21st century. Current and future warming of the atmosphere will affect periglacial landforms and processes, and potential consequences include hazards due to slope failure and risk to human infrastructure. The ice content of the frozen ground is a key parameter controlling slope stability in periglacial environments. As permafrost is, in contrast to glaciers, basically invisible from the surface, the impacts of global warming are difficult to assess and long time series of mountain permafrost evolution are therefore rare. Traditional observation techniques are mainly based on thermal monitoring in vertical and horizontal dimension, but they provide only weak indications of the ice content.

Addressing the necessity for a method to monitor the long-term mountain permafrost evolution, this thesis contributes to the development of a geophysical monitoring approach that provides information on temporal changes in ground ice content. A geophysical monitoring network comprising permanent geoelectric and refraction seismic profiles at four different landforms in the Swiss Alps was established in the framework of this PhD project.

The objective of this thesis is to investigate the potential of geophysically based techniques for an operational long-term monitoring of mountain permafrost evolution in the context of global warming.

The methodological approach is based on the assumption, that temporal changes in the measured geophysical parameters provide information on changes in the subsurface ice and water content. The so-called time-lapse approach serves to overcome the common problem of the often ambiguous interpretations of absolute resistivity or velocity values of single surveys. Seasonal and long-term changes in the ground ice content were estimated from electrical resistivity tomography (ERT) and refraction seismic tomography (RST) monitoring data sets. The ERT monitoring (ERTM) results were evaluated based on the analysis of apparent resistivities, time series of inverted tomograms, the comparison to temporal variations in subsurface temperatures in nearby boreholes, and the application of appraisal methods. Results from RST monitoring (RSTM) were evaluated based on the reproducibility of travel times and waveforms and the inverted tomograms were compared to ERTM results and borehole temperatures. Finally, ERTM and RSTM data sets are jointly used in the so-called 4-phase model (4PM), that relates the measured geophysical parameters to the respective volumetric fractions of the subsurface material (rock, water, air, ice), to evaluate the potential to quantify temporal changes in volumetric ice, water, and air contents in the subsurface.

The results indicate a huge potential of both monitoring approaches to detect and characterise climate induced ground ice degradation:

The analysis of a comprehensive 7-year *ERTM* data set from a rock slope at Schilthorn (Bernese Alps) revealed a sustained ground ice degradation as a consequence of the heat wave occurring over central Europe in summer 2003. In contrast to borehole temperatures, that returned to the “normal” range already in the following year, *ERTM* data proved a delayed aggradation of ground ice to pre-2003 conditions until 2007 despite favourable temperatures.

A combined analysis of resistivities and borehole temperatures at all test sites showed the strong relation of both parameters and demonstrated the general applicability of the *ERTM* approach to different landforms in mountain permafrost characterised by different surface conditions and ice contents. The obtained resistivity-temperature relations are strongly site-specific and indicate that resistivity values cannot simply be used as a temperature proxy.

Even in the most challenging terrain for the acquisition and processing of *ERTM* data, on coarse blocky landforms with high ice contents, a high potential to resolve temporal changes in ground ice content could be identified. On Murtèl rockglacier (Upper Engadine valley) clear indications for a significant impact of the warm winter 2006/2007 on the permafrost regime were observed by *ERTM* that provide spatially more detailed information than the 1D borehole temperatures. For the Lapires talus slope (Valais), characterised by internal air circulation that contributes to its cooling and thus to permafrost occurrence, it could be shown that *ERTM* bears potential to detect zones of preferential air flow (ventilation funnels), which may contribute to an increased understanding of this microclimatic process.

Limitations of the *ERTM* approach comprise the possible occurrence of inversion artefacts in cases with high ice contents (e.g. massive ice in rockglaciers) and strong resistivity contrasts (e.g. between the unfrozen active layer and ice-rich layers), making a thorough interpretation difficult. Great care has to be taken when absolute resistivity values are to be related to temperature, ice content, or ice origin in rockglaciers. The probability of inversion artefacts can be evaluated by the application of appraisal methods, such as forward/inverse modelling based on synthetic models, the depth of investigation index, or the resolution matrix approach.

To establish a complementary geophysical monitoring method, the applicability of a time-lapse *RSTM* approach was tested for two data sets at Schilthorn and Lapires. The results of this novel approach demonstrate a generally good reproducibility of the waveforms and signal strength for subsequent measurements, and systematic temporal changes in the seismic response from the subsurface. The interpretation of velocity changes from *RST* time-lapse tomograms corresponds to results from *ERTM* and borehole temperatures, but also reveals complementary information that can strongly support the interpretation of *ERTM* data. An important advantage of the *RSTM* approach is, that under certain conditions even an unambiguous identification of ground ice loss is possible. This could be observed at Schilthorn, where a seasonal velocity decrease by more than 3000 m/s clearly proved the initial presence of significant amounts of ground ice in the active layer that disappeared in the following month.

Weaknesses of the *RSTM* approach comprise a limited depth resolution in cases of strong contrasts between active layer and permafrost and for high ice contents, and the much higher efforts of data acquisition and processing compared to *ERTM*.

The application of the *4PM* was extended to time-lapse *RST* and *ERT* data sets. As an extension to previous work, it could be shown that the consideration of temporal changes may provide more realistic estimations than calculating absolute amounts of the constituents of the available pore space. As combined *ERTM* and *RSTM* data sets were acquired for the first time only very recently, further evaluation of the approach will be conducted in future applications.

Zusammenfassung

Permafrost (permanent gefrorenes Material der Lithosphäre) bildet ein wesentliches Element der globalen Kryosphäre. In den Europäischen Alpen finden sich aufgrund des kalten Klimas in großen Höhen azonale Permafrostvorkommen. Dieser Alpine Permafrost weist Temperaturen nur knapp unter 0°C auf und ist damit besonders sensibel für die prognostizierten Klimaänderungen im 21. Jahrhundert. Die gegenwärtige und zukünftige Erwärmung der Atmosphäre wirkt sich auf periglaziale Landformen und Prozesse aus, wobei potenzielle Konsequenzen Naturgefahren aufgrund von Hanginstabilitäten und der Gefährdung von Infrastruktur umfassen. Der Eisgehalt im gefrorenen Untergrund gehört zu den Schlüsselparametern, welche die Stabilität von Hängen in Periglazialgebieten kontrollieren. Da Permafrost im Unterschied zu Gletschern ein unsichtbares Phänomen ist, lassen sich die Auswirkungen der globalen Erwärmung auf die Entwicklung des Gebirgspermafrostes nur schwer erfassen, und lange Zeitreihen der Evolution des Gebirgspermafrostes sind daher rar. Traditionelle Beobachtungsmethoden umfassen die Messung von Oberflächen- und Untergrundtemperaturen, welche aber nur ungenügende Indikatoren für den Eisgehalt darstellen.

Basierend auf dem Bedarf zur langfristigen Beobachtung der Entwicklung des Gebirgspermafrostes trägt die vorliegende Arbeit zur Entwicklung eines Monitoringansatzes bei, der Aussagen über zeitliche Änderungen des Eisgehalts zulässt. Im Rahmen dieser Studie wurde ein geophysikalisches Monitoring-Netzwerk bestehend aus permanenten geoelektrischen und refraktionsseismischen Profilen an vier morphologisch unterschiedlichen Standorten in den Schweizer Alpen aufgebaut.

Das *Ziel dieser Arbeit* war es, das Potenzial geophysikalischer Methoden für ein operationelles Langzeit-Monitoring der Permafrostentwicklung im Hochgebirge im Rahmen der globalen Erwärmung zu untersuchen.

Der *methodische Ansatz* basiert auf der Annahme, dass zeitliche Änderungen in den gemessenen geophysikalischen Parametern Aussagen zu Änderungen im Eis- und Wassergehalt des Untergrundes zulassen. Die Betrachtung der zeitlichen Änderungen (der sogenannte time-lapse Ansatz) dient der Überwindung des generellen Problems der oft uneindeutigen Interpretierbarkeit absoluter Widerstände oder seismischer Geschwindigkeiten einmaliger Messungen. Monitoring-Datensätze der Elektrischen Widerstandstomographie und der refraktionsseismischen Tomographie dienen zur Abschätzung der saisonalen und langfristigen Änderungen des Eisgehaltes. Die Evaluation der Ergebnisse des geoelektrischen Monitorings basierte auf der Analyse von scheinbaren Widerständen, von Zeitreihen invertierter Tomogramme, dem Vergleich mit zeitlichen Änderungen der Untergrundtemperaturen in nahegelegenen Bohrlöchern, sowie der Anwendung von Methoden zur Abschätzung der Genauigkeit der Inversionsergebnisse. Die Ergebnisse des refraktionsseismischen Monitorings wurden anhand der Reproduzierbarkeit der Laufzeiten und Wellenformen und dem Vergleich mit den Ergebnissen des geoelektrischen Monitorings sowie mit Bohrlochtemperaturen beurteilt. Abschließend wurden die geoelektrischen und refraktionsseismischen Monitoring-Datensätze gemeinsam im sogenannten

4-Phasen-Modell (4PM) analysiert, welches die gemessenen geophysikalischen Parameter mit den volumetrischen Anteilen der Materialphasen des Untergrundes (Fels, Wasser, Luft, Eis) in Beziehung setzt, um das Potenzial dieses Modells zur Quantifizierung der zeitlichen Änderungen der volumetrischen Eis-, Wasser- und Luftgehalte im Untergrund zu untersuchen.

Die *Ergebnisse* weisen auf ein enormes Potenzial beider Monitoringansätze zur Erfassung und Charakterisierung klimainduzierter Permafrost- bzw. Bodeneisdegradation hin:

Die Analyse eines umfangreichen *geoelektrischen* Monitoring-Datensatzes vom Nordhang des Schilthorns (Berner Oberland) über 7 Jahre ergab eine nachhaltige Degradation des Bodeneises als Ergebnis der Hitzewelle über Mitteleuropa im Sommer 2003. Im Unterschied zu den Bohrlochtemperaturen, die bereits im darauffolgenden Jahr wieder im „normalen“ Bereich lagen, zeigten die geoelektrischen Monitoringdaten, trotz geeigneter Temperaturverhältnisse, eine Verzögerung der Neubildung des Bodeneises bis ins Jahr 2007.

Durch eine kombinierte Analyse von Widerständen und Bohrlochtemperaturen konnte der starke Zusammenhang zwischen beiden Parametern für alle Standorte nachgewiesen werden. Damit konnte die generelle Anwendbarkeit des geoelektrischen Monitorings für morphologisch unterschiedliche Standorte mit variierenden Oberflächenbeschaffenheiten und Eisgehalten demonstriert werden. Die Beziehung zwischen Widerstand und Temperatur ist dabei stark an den Standort gebunden und impliziert damit, dass gemessene Widerstände nicht notwendigerweise als ein einfacher Proxy für Untergrundtemperaturen zu gebrauchen sind.

Selbst an Standorten mit hohem Eisgehalt und grobblockiger Oberflächenbeschaffenheit, welche die für die Aufnahme und Prozessierung von geoelektrischen Monitoringdaten schwierigsten Bedingungen bieten, konnte ein beachtliches Potenzial bezüglich der Erfassung zeitlicher Änderungen im Eisgehalt identifiziert werden. Auf dem Blockgletscher Murtèl (Oberengadin) wurden mithilfe des Geoelektrikmonitorings deutliche Auswirkungen des warmen Winters 2006/2007 auf das Permafrostregime beobachtet, welche räumlich wesentlich detailliertere Aussagen als die 1D-Bohrlochtemperaturen zuließen. Für die Blockhalde Lapires (Wallis), welche durch interne Luftzirkulation charakterisiert ist, die sich positiv auf das Vorkommen von Permafrost auswirkt, konnte gezeigt werden, dass geoelektrisches Monitoring zur Detektion von Zonen bevorzugter Ventilation und damit zum besseren Verständnis dieses mikroklimatischen Prozesses beitragen kann.

Schwierigkeiten beim geoelektrischen Monitoring bereitet das mögliche Auftreten von Inversionsartefakten in Situationen mit hohem Eisgehalt (z.B. der Eiskern in Blockgletschern) sowie starken Widerstandskontrasten (z.B. zwischen der ungefrorenen Auftauschicht und eisreichen Lagen), welche eine sorgfältige Interpretation erschweren. Große Vorsicht ist daher nötig, wenn absolute Widerstände als Indikator für die Untergrundtemperatur, den Eisgehalt, oder z.B. die Eisgenese in Blockgletschern dienen sollen. Die Wahrscheinlichkeit von Inversionsartefakten kann mithilfe von Methoden zur Abschätzung Qualität der Inversion (sog. appraisal methods) beurteilt werden, wie zum Beispiel der synthetischen Modellierung, des sogenannten Depth-Of-Investigation Indexes, oder dem sogenannten Resolution-Matrix Ansatz.

Um eine komplementäre geophysikalische Monitoringmethode zu etablieren, wurde die Anwendbarkeit eines *refraktionsseismischen* Monitoringansatzes für zwei verschiedene Datensätze untersucht. Die Ergebnisse dieser neuartigen Anwendung demonstrieren eine insgesamt gute Reproduzierbarkeit der Wellenform und Signalstärke für aufeinanderfolgende Messungen sowie systematische zeitliche Änderungen der seismischen Reaktion des Untergrundes. Die Interpretation der seismischen Geschwindigkeitsänderungen in time-lapse Tomogrammen stimmt

mit den Geoelektrikdaten sowie mit den Bohrlochtemperaturen überein, ergibt aber gleichzeitig auch komplementäre Informationen, welche die Interpretation der Geoelektrikdaten wesentlich unterstützen können. Einen wesentlichen Vorteil des refraktionsseismischen Monitorings bietet die Möglichkeit, unter bestimmten Voraussetzungen zweifelsfrei Eisdegradation (oder saisonaler Eisschwund) identifizieren zu können. Am Schilthorn konnte eine saisonale Geschwindigkeitsabnahme von ~ 3000 m/s beobachtet werden, welche sich eindeutig als Eisschwund in der Auftauschicht interpretieren lässt.

Zu den Schwächen des refraktionsseismischen Monitorings gehören eine limitierte Eindringtiefe in Situationen mit starken Geschwindigkeitskontrasten zwischen der Auftauschicht und dem Permafrost, sowie der, im Vergleich zum geoelektrischen Monitoring, wesentlich höhere Aufwand bei der Datenaufnahme und Prozessierung.

In Erweiterung bisheriger Arbeiten wurde das *4PM* auf geoelektrische und seismische *Monitoring*daten angewendet. Es konnte gezeigt werden, dass die Betrachtung zeitlicher Änderungen realistischere Abschätzungen ermöglichen kann als die Berechnung absoluter volumetrischer Gehalte der Materialphasen von Eis, Wasser und Luft im verfügbaren Porenraum des Untergrundes. Eine weiterführende Beurteilung dieses Ansatzes wird in Zukunft im Zuge der Aufnahme weiterer kombinierter geoelektrischer und refraktionsseismischer Monitoringdaten erfolgen.

Table of contents

SUMMARY	I
---------------	---

ZUSAMMENFASSUNG	III
-----------------------	-----

PART I - INTRODUCTION

1 INTRODUCTION	1
1.1 Motivation	1
1.2 Current state of research	1
1.2.1 <i>Sensitivity of Alpine permafrost to climate induced warming</i>	2
1.2.2 <i>Mountain permafrost monitoring</i>	4
1.2.3 <i>Geophysical methods in permafrost research</i>	5
1.2.4 <i>Potential of geophysical methods for the monitoring of permafrost evolution and the quantification of ground ice content</i>	6
1.2.5 <i>Research needs</i>	9
1.3 Objectives	9
1.4 Organisation of the thesis	10
2 GEOPHYSICAL MONITORING RATIONALE	13
2.1 Electrical Resistivity Tomography Monitoring (ERTM) approach	13
2.1.1 <i>Principle of electrical resistivity measurements</i>	13
2.1.2 <i>Sensitivity of the electrical resistivity to temperature and ground ice</i>	14
2.1.3 <i>Electrical resistivity monitoring approach</i>	15
2.1.4 <i>Data acquisition</i>	16
2.1.5 <i>Data processing</i>	17
2.2 Refraction Seismic Tomography Monitoring (RSTM) approach.....	19
2.2.1 <i>Principle of seismic refraction</i>	19
2.2.2 <i>Sensitivity of P-wave velocities to temperature and ground ice</i>	20
2.2.3 <i>Refraction seismic monitoring approach</i>	22
2.2.4 <i>Data acquisition</i>	23
2.2.5 <i>Data processing</i>	24
2.3 Estimation of total fractions of ice, water and air from combined ERT and RST data sets.....	26
3 FIELD SITES	29
3.1 The summit region of Schilthorn (Bernese Alps).....	30
3.2 Murtèl rockglacier (Upper Engadine valley).....	32

3.3	The ventilated Lapires talus slope (Valais).....	33
3.4	The rock plateau at Stockhorn (Valais).....	35

PART II - PUBLICATIONS

4	MONITORING MOUNTAIN PERMAFROST EVOLUTION USING ELECTRICAL RESISTIVITY TOMOGRAPHY: A 7-YEAR STUDY OF SEASONAL, ANNUAL AND LONG-TERM VARIATIONS AT SCHILTHORN, SWISS ALPS	43
5	A GEOELECTRIC MONITORING NETWORK AND RESISTIVITY-TEMPERATURE RELATIONSHIPS OF DIFFERENT MOUNTAIN PERMAFROST SITES IN THE SWISS ALPS.....	59
6	APPLICABILITY OF ELECTRICAL RESISTIVITY TOMOGRAPHY MONITORING TO COARSE BLOCKY AND ICE-RICH PERMAFROST LANDFORMS	69
7	ON THE POTENTIAL OF TIME-LAPSE REFRACTION SEISMIC FOR THE DETECTION OF CHANGES IN GROUND ICE CONTENT.....	99

PART III - SYNTHESIS

8	GENERAL DISCUSSION.....	121
8.1	Reliability of inverted ERT and RST tomograms.....	121
8.2	Reliability of relative resistivity and velocity changes.....	123
8.3	Evaluation of the applicability of ERTM and RSTM within an operational geophysical monitoring network	125
8.3.1	<i>Surface characteristics.....</i>	<i>125</i>
8.3.2	<i>Seasonal differences of data quality and applicability.....</i>	<i>125</i>
8.3.3	<i>Spatial resolution vs. penetration depth.....</i>	<i>126</i>
8.3.4	<i>Temporal resolution</i>	<i>126</i>
8.4	Quantification of ground ice degradation using a combined application of ERTM and RSTM data.....	127
8.4.1	<i>Exemplary data set</i>	<i>128</i>
8.4.2	<i>Deficiencies of the 4-Phase Model (4PM).....</i>	<i>128</i>
8.4.3	<i>Calculation of total ice, water and air contents by the 4PM.....</i>	<i>129</i>
8.4.4	<i>Changes in ice, water and air content determined from a time-lapse application of the 4PM.....</i>	<i>132</i>
8.4.5	<i>Discussion and implications for future applications of the 4PM</i>	<i>134</i>
9	CONCLUSIONS AND OUTLOOK	137
9.1	Main findings of the thesis	137
9.2	Outlook and implications for future research	139

REFERENCES.....	141
APPENDIX.....	151
ACKNOWLEDGEMENTS	163

PART I - INTRODUCTION

Chapter 1

Introduction

Chapter 2

Geophysical Monitoring Rationale

Chapter 3

Field Sites

1 Introduction

1.1 Motivation

Applied geophysics make use of the differences in certain physical properties of different types of rocks or sediments that can be measured from the earth's surface (or from boreholes). Geophysical methods therefore provide the potential to gain information on the subsurface material and structure by non-invasive measurement techniques. Compared to excavations or borehole drillings they are not only much cheaper, but can also cover larger 2D or 3D sections of the subsurface than possible by direct observations. As the subsurface properties basically remain unaffected by the application of geophysical techniques, a huge potential lies in the repetition of measurements for monitoring purposes on several time scales.

Non-destructive and repeatable measurement techniques are especially valuable for application in sensitive environmental systems that are subject to change, such as periglacial environments. Permafrost, defined as material of the lithosphere that remains at or below 0°C for at least two years, is, in contrast to glaciers, a purely thermal phenomenon of the subsurface, which is basically invisible from the surface. Ice - though not part of the definition - may be contained in frozen ground with a range of possible volumetric contents varying from near zero to supersaturated conditions. As distribution and evolution of permafrost is largely governed by climate and its variations, it is particularly sensitive to global warming. This is especially true for Alpine permafrost due to its proximity to melting conditions (Harris et al. 2009).

The investigation of the response of Alpine permafrost to climate change is difficult because of its general inaccessibility and the corresponding lack of long monitoring time series. Traditional observation techniques are basically restricted to temperature measurements in horizontal dimension at the surface (bottom temperatures of the snow (BTS), or ground surface temperatures (GST)), or in vertical dimension in a few boreholes (Haeberli 1973; Vonder Mühll et al. 2007). The application of geophysical techniques to permafrost related problems already started several decades ago (e.g. Timur 1968; Röthlisberger 1972; Barsch 1973; Fisch et al. 1977; King et al. 1988), and is now widely used for the detection, characterisation and mapping of mountain (and polar) permafrost (Kneisel et al. 2008). However, the immense potential of geophysical methods has rarely been exploited yet. The potential of repeated geophysical measurements (geophysical monitoring) for the assessment of mountain permafrost degradation due to global warming will therefore be investigated in this thesis.

1.2 Current state of research

With the latest assessment report of the Intergovernmental Panel on Climate Change (IPCC 2007) a comprehensive compilation of detailed knowledge on current and future warming of the atmosphere is now available. Projected patterns of warming can now be attributed with higher confidence and associated regional-scale features such as changes in precipitation and extreme weather events become less speculative. Warming is expected to be greatest at high

northern latitudes and impact on permafrost is projected in terms of widespread increases in thaw depth over most permafrost regions. Borehole observations in both hemispheres confirm that permafrost temperatures have risen in the last 20-30 years with magnitudes mainly between 0.5-2°C at the depth of the zero annual amplitude (Brown & Romanovsky 2008).

Within the context of climate change the European Alps are affected by greater average warming than commonly projected for Europe as a whole (e.g. Beniston 2006). However, detailed projections concerning the sensitivity of mountain permafrost to climate change do still not exist.

In contrast to polar regions, the distribution of mountain permafrost strongly depends on topographic factors, such as aspect, slope angle and altitude, which in turn influence the net solar radiation, the turbulent heat fluxes and the snow cover distribution (Haeberli 1973; Mitaz et al. 2000; Hoelzle et al. 2001). Strong heterogeneities of these factors in space (topography), or in space and time (snow cover, net radiation) cause complex permafrost distribution patterns, that are complicated by the strong heterogeneity of subsurface material characteristics, such as bedrock, fine and coarse grained debris (Haeberli & Gruber 2008). Within the subsurface material, lateral fluxes of matter and energy caused by circulation of water and air play an important role in steep slopes of mountainous regions. Consequently, alpine permafrost is characterised by highly variable thermal offsets between ground surface and permafrost table. In contrast to mainly flat polar and subpolar lowlands, changes in air temperature cannot simply be related to changes in ground temperature or melting rates in high-alpine terrain (Hoelzle & Gruber 2008; Noetzli 2008; Riseborough et al. 2008). Thus, measuring and modelling of these fluxes and coupling mechanisms for characteristic permafrost substrates still remains a main challenge in alpine permafrost research (Hoelzle et al. 2001; Riseborough et al. 2008).

1.2.1 Sensitivity of Alpine permafrost to climate induced warming

Permafrost temperatures are currently being measured in about 400 boreholes in both hemispheres, with records covering longer periods revealing a general trend of substantial increase in permafrost temperatures during the last decades (Brown & Romanovsky 2008). The magnitude of warming depends on the permafrost temperature, and recent observations from polar permafrost sites show that the rate of warming decreases significantly when permafrost temperatures approach 0°C (Smith et al. 2005; Brown & Romanovsky 2008). According to Smith et al. (2005) and Romanovsky et al. (2008) the apparent stagnation of permafrost temperatures is due to the partial melt of ice within the upper few tens of metres of permafrost, demonstrating that temperature may be a somewhat misleading indicator of permafrost evolution during such transition periods of “internal” melting.

The vast majority of permafrost boreholes is located in polar regions, and similar observational records are only rarely available for the Alpine permafrost. Although a considerable number of permafrost boreholes exist in the European Alps (Vonder Mühll et al. 2007; Harris et al. 2009), the time series are (except for the longest record from Murtèl rockglacier, see Fig. 1.1) still relatively short covering usually about 10 years or less.

Permafrost temperatures in the European Alps are generally only slightly below 0°C. The response time of permafrost to climate induced warming depends on thermal conductivity, ice content, the thickness of the frozen ground and the spatio-temporal distribution of the snow cover (Osterkamp 1983; Smith & Burgess 1998; Luetschg et al. 2008). In general, response

times vary from responses in inter-annual variations of active layer thickness to seasonal events and summer conditions, over decades to centuries for thermal responses below the zero annual amplitude, to centuries or even millennia for basal thawing of permafrost associated with progressive permafrost thinning (Haeberli 1990; Brown & Romanovsky 2008). This indicates that the available time series for the Alps are clearly insufficient for a reliable assessment of trends in the long-term permafrost evolution in response to global warming (Harris et al. 2009).

However, observations from the record breaking summer of 2003 in the Alps demonstrate that extreme atmospheric forcing events may initially be more significant for mountain permafrost evolution than the underlying longer-term climate trends (Brown & Romanovsky 2008; Vonder Mühll et al. 2008). Subsurface temperatures have been significantly affected by the 2003 heat wave and an increased rockfall activity was observed in the Alps, which was attributed to the destabilisation of ice-filled discontinuities (Schiermeier 2003; Gruber et al. 2004a). Also a pronounced acceleration in the creeping velocity of many rockglaciers was observed in recent years and attributed to permafrost warming within the last decade (Roer et al. 2005; Käab et al. 2007; Roer et al. 2008). Delaloye et al. (2008) analysed the creep behaviour of 16 rockglaciers throughout the European Alps during the last 5 to 13 years, and all observed rockglaciers reached an absolute or relative maximal creep rate according to the heat wave in summer 2003.

The last decade was dominated by temperature extremes and climatic anomalies, such that, e.g., of the twelve years between 1995 and 2006 eleven rank among the 12 warmest years in the instrumental record of global surface temperature (IPCC 2007). Apart from the extraordinary hot summer 2003, recent examples for such extreme events in the European Alps are the hot July 2006, the warm autumn/winter 2006/2007 with late snow fall in winter 2006 as well as in 2008 (MeteoSchweiz 2006, 2007). The frequency of extreme weather anomalies has accelerated during the last decades, very likely being intensified in future in terms of increased mean temperature variability, changes in frequency, intensity, and duration of extreme events. Based on the latest IPCC assessment report (IPCC 2007) this includes more hot days, heat waves, heavy precipitation events, and fewer cold days. According to Schär et al. (2004) European summer climate might experience a pronounced increase in year-to-year variability in response to greenhouse-gas forcing making extreme anomalies such as the extraordinary hot summer 2003 more likely to occur. These short-term weather anomalies (in particular extreme summer air temperatures) will mainly affect the depth of the active layer, whereas the long-term evolution of mean air temperatures are reflected by the permafrost temperature below the zero annual amplitude (Harris et al. 2009). Observation of the *response of permafrost to such extreme atmospheric forcing* will thus be a key challenge to understand and predict its future evolution in the context of global warming.

In mountain permafrost environments subsurface warming can have a severe impact on the *stability* of rock walls or debris slopes (Noetzli et al. 2003; Gruber et al. 2004; Haeberli et al. 2004; Fischer et al. 2006; Gruber & Haeberli 2007; Huggel et al. 2008). Temperatures slightly below 0°C were identified to cause minimal stability conditions of ice-filled rock joints (Davies et al. 2001; Günzel 2008). Knowledge of the amount of ice contained in rock walls or debris slopes is therefore crucial for a physically based assessment of the hazard potential due to degrading permafrost (Haeberli et al. 2001; Harris et al. 2001a; Maurer et al. 2003; Gruber et al. 2004; Gude & Barsch 2005; Fischer et al. 2006). Moreover, the ice content is an important parameter for modelling the future evolution of the ground thermal regime in permafrost ar-

eas (Salzmann et al. 2007a; Noetzli 2008). However, due to the remote location of permafrost areas and the corresponding logistical and financial difficulties in obtaining spatially differentiated data sets, *knowledge about the ice content in permafrost areas is still scarce*.

1.2.2 Mountain permafrost monitoring

Since permafrost is primarily a thermally defined phenomenon, commonly applied observation techniques are based on thermal aspects of permafrost evolution. In existing European (PACE21: Permafrost and Climate in the 21st Century, Harris et al. 2003) and Swiss (PERMOS: Permafrost Monitoring in Switzerland, Vonder Muhll et al. 2008) permafrost monitoring networks, subsurface temperature data are being obtained through a network of shallow and deep (down to 100 m) boreholes. The PERMOS programme started in 1999 and currently involves 15 permafrost borehole temperature monitoring sites (**Fig. 3.1**), with the longest time-series at Murtel rockglacier recording since 1987. Further elements of the monitoring programme comprise the measurement of ground surface temperatures (GST), snow cover thickness as well as periodically aerial photograph analyses at selected sites (Vonder Muhll et al. 2007).

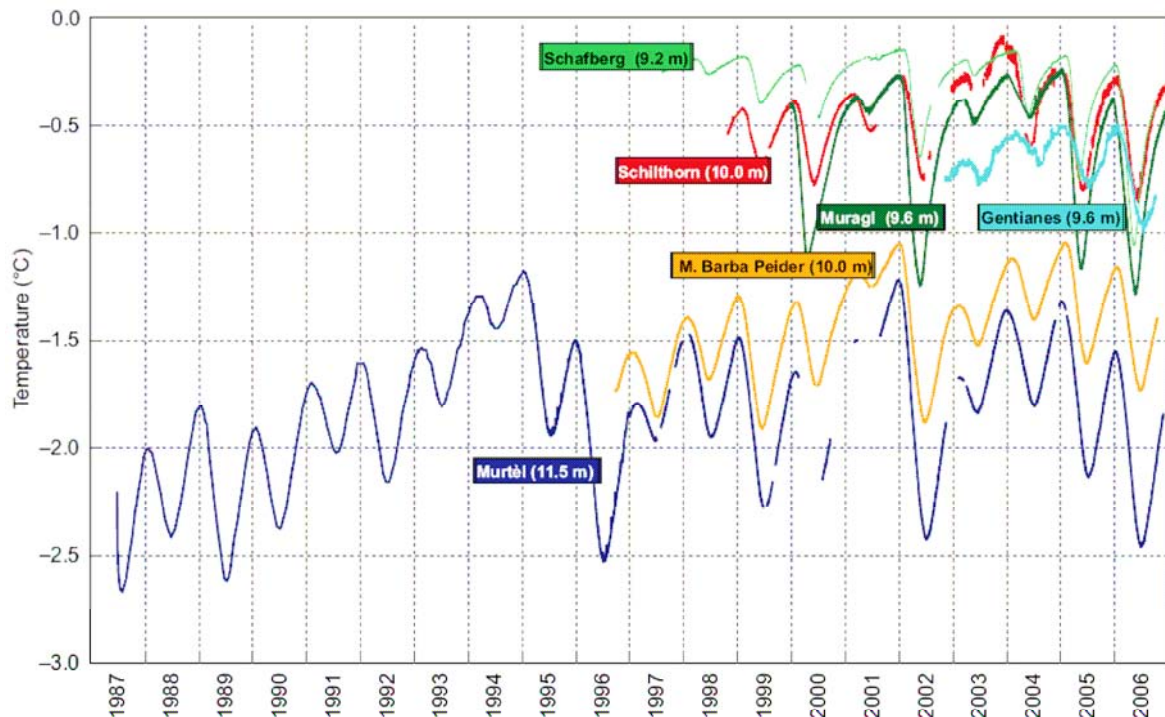


Fig. 1.1: Comparison of temperature records for selected PERMOS boreholes in roughly 10 m depth until 2006 (PERMOS 2009). Location of the borehole sites is indicated in Fig. 3.1.

However, long-term degradation processes in terms of thawing phenomena cannot necessarily be identified by thermal permafrost monitoring alone, since ice content is not only dependent on temperature evolution but also on the availability of unfrozen water during the freezing period, and, as stated above, an apparent stagnation of temperatures close to the melting point may mask the general trend of permafrost evolution. Moreover, considering slope stability and permafrost modelling (e.g. Noetzli et al. 2008; Riseborough et al. 2008), not only temperature changes but also the ice content of the subsurface plays an important role (Gruber & Haeblerli 2007; Harris et al. 2009). The sensitivity of mountain permafrost to climate change is therefore

strongly dependent on the amount of ice present in the considered permafrost occurrences (Smith & Burgess 1998; Harris et al. 2001b; Luetschg & Haeberli 2005; Haeberli et al. 2006; Noetzli 2008), indicating that ice content should be addressed in operational monitoring programmes.

1.2.3 Geophysical methods in permafrost research

Geophysical methods have long been recognised to provide detailed information of the frozen subsurface. The long tradition of the application of geophysical methods in permafrost areas originates from engineering related problems in arctic environments. A comprehensive review on geophysics in the study of permafrost is given by Scott et al. (1990). Detailed studies of the applicability of many different geophysical methods to specific scientific and engineering aspects in polar permafrost are provided by e.g. Ingeman-Nielsen et al. (2005), or Yoshikawa et al. (2006).

Similar to the polar regions, first geophysical measurements under much more challenging conditions in high alpine terrain go back to the 1970s (Barsch 1973; Fisch et al. 1977; Haeberli 1978), but the first systematic studies on the applicability of different methods to different permafrost related questions and landforms are much younger. The strong heterogeneity of alpine terrain and permafrost distribution and characteristics requires a separate evaluation taking into account the peculiarities of high mountains, such as applicability in rough or steep terrain, or resolution of small-scale heterogeneities. A comprehensive evaluation of different geophysical methods (including first applications of tomographic methods) for the detection, mapping and characterisation of mountain permafrost is given by Hauck (2001), Hauck & Vonder Mühll (2003), and a recently compiled reference guide for the application of geophysical methods in periglacial environments edited by Hauck & Kneisel (2008). They demonstrate that, during the last decade, traditional survey methods, such as vertical electrical soundings or refraction seismic surveys based on one or two shot points, have been replaced by much more sophisticated 2D and 3D surveys and tomographic inversion schemes (e.g. Lanz et al. 1998; Loke 2003; Sandmeier 2008). The progress in computational technology is accompanied by a substantially increased resolution potential and decreased processing time.

An evaluation of the applicability of electrical resistivity tomography (ERT), refraction seismic tomography (RST) and ground penetrating radar (GPR) for the use on rockglaciers is provided by Maurer & Hauck (2007). Kneisel (2004, 2006) investigated the applicability of ERT to different morphologies (rockglaciers, glacier forefields, solifluction lobes, ice-cored moraines, scree slopes, etc.). The use of seismic refraction was demonstrated by Musil et al. (2002) and Hausmann et al. (2007) for the characterisation of the interior of rockglaciers, and by Ikeda & Matsuoka (2002) and Ikeda (2006) for the differentiation between active and inactive rockglaciers. Internal boundaries in rockglaciers could be delineated with ground penetrating radar by Lehmann & Green (2000), Berthling et al. (2003) and Maurer & Hauck (2007). Electromagnetic induction methods can be used for deep sounding of the permafrost base (Hauck et al. 2001; Bucki et al. 2004). These are only a few examples of numerous applications of geophysical methods to mountain permafrost.

Due to the complexity of the subsurface and the different capabilities in discriminating between certain materials a combination of complementary geophysical methods is often favoured to avoid ambiguities in the interpretation of the results (Vonder Mühll et al. 2002; Kneisel & Hauck 2003; Ikeda 2006; Otto & Sass 2006; Maurer & Hauck 2007). Even so, a

priori geological information is generally required to calibrate the results and substantially increase the reliability of geophysical interpretations (Ingeman-Nielsen et al. 2005). Among the various possible combinations, refraction seismics and ERT is probably the most promising for mountain permafrost studies (Hauck & Vonder Mühll 2003; Kneisel et al. 2008). The *resistivity contrast* between ice and unfrozen water is very large but can be small between ice, air and certain rock types, as all three behave as electrical insulators. Conversely, *seismic P-wave velocities* exhibit a large contrast between very slow velocities in air and high velocities in ice, allowing a reliable discrimination of ice and air in the pore space of the subsurface material by the combined application of both methods. Other combinations, including ERT, electromagnetic induction methods, GPR, and refraction seismics have been applied as well (Hauck et al. 2003; Bucki et al. 2004; Hauck et al. 2004; Ingeman-Nielsen et al. 2005; Yoshikawa et al. 2006; Maurer & Hauck 2007).

Among the multiple methods that have been evaluated for their use in permafrost related research increased potential has been attributed to ERT, GPR and seismic refraction. Basic results from the comparison of the applicability of these three methods are briefly summarised in Tab. 1.1. The assessment of the use of other geophysical methods by different authors (such as electromagnetic techniques (EM), nuclear magnetic resonance (NMR), induced polarisation (IP), gravimetry etc.) yielded less uniform results what may partly be due to the specific demands of their application. Some of these methods suffered from low near-surface resolution (e.g. EM), or their less “universal” nature, e.g. the limitation of NMR studies to sites without any infrastructure causing electromagnetic noise.

1.2.4 Potential of geophysical methods for the monitoring of permafrost evolution and the quantification of ground ice content

Current challenges are associated with geophysical monitoring approaches to assess short- and long-term changes in the subsurface material composition as a complementary, cost-effective and 2D alternative to 1D borehole temperature monitoring. In principle, a variety of geophysical methods can be used to monitor changes by repeated measurements using the same survey geometry (Harris et al. 2009). Due to its high sensitivity to the unfrozen water content, ERT is probably the first choice for a permafrost monitoring with respect to ice content (Fortier et al. 1994). In recent years ERT monitoring (ERTM) techniques have become more and more popular in applied geophysics and are used in seasonal hydrological applications (e.g. Aaltonen 2001; Aaltonen & Olofsson 2002; French et al. 2002; Daily et al. 2004) and tracer and contaminant studies (e.g. Kemna et al. 2002; Slater et al. 2002; Singha & Gorelick 2006), but these systems are not applicable for high-mountain and remote permafrost areas. A first ERTM approach for frozen ground has been introduced by Hauck (2002). Data acquisition started in 1999 and has been continued until present allowing a comprehensive evaluation of the performance of ERTM for mountain permafrost studies. This is the topic of *publication #1* (chapter 4).

Based on this pilot study on ERTM in mountain permafrost, similar measurement strategies were started for frozen rock walls (Krautblatter & Hauck 2007) and glacier forefields (Kneisel 2006). However, with regard to measurement effort (man-power, measurement time, accessibility of the field sites), regular data acquisition with high temporal resolution over long periods remains difficult. In contrast to surface related processes in permafrost terrain (e.g. frost wedging, frost heave, solifluction (Matsuoka & Humlum 2003)), *no continuously logging geophysical monitoring approach exists to date*. Motivated by the successful results of the ERTM pilot study

(*publication #1*, chapter 4), a first fully automatic ERTM system is now being developed (in cooperation with GEOLOG, Augsburg) within the recently started research programme SPCC (Sensitivity of mountain permafrost to climate change, 2008-2011, funded by the German Research Foundation). A 14-days test period on Schilthorn provided promising results (unpublished data), and regular data acquisition with the newly developed automatic ERTM (A-ERTM) system on Schilthorn will start in spring 2009.

The above mentioned studies usually address only structural or qualitative characteristics of the frozen ground (e.g. the depth to the permafrost table) without determining its quantitative composition. For a reliable assessment of the sensitivity of mountain permafrost to climate change, the *material properties* (in particular the ice content) of the subsurface must be determined. In partly or permanently frozen ground subsurface material may consist of four different phases: two solid phases (rock/soil matrix and ice), liquid (unfrozen pore water), and gaseous (air-filled pore space and cavities). Except for laboratory analyses of field probes obtained in boreholes (e.g. Arenson et al. 2002; Arenson et al. 2003), the composition of the subsurface material cannot be determined by direct observations.

Moreover, the destructive nature of excavations or the drilling of boreholes makes repeated observations of the ground composition in terms of a monitoring impossible. *Geophysical techniques allow for a monitoring on any time scale*, however, their indirect nature requires a relation between the measured variable (e.g. electrical resistivity, seismic velocity) and the respective parts of the material composition (rock, water, air, ice).

Although geophysical methods have been widely used in permafrost research, very few studies have attempted to establish quantitative or semi-quantitative relationships between measured physical properties and permafrost parameters such as temperature or ice and unfrozen water content. Fortier et al. (1994) correlated measured electrical resistivities with ice and unfrozen water contents (calibrated by the calorimetric method) to predict changes in unfrozen water and ice contents of the frozen ground from resistivity logging. Quantitative combinations of electric and seismic data sets were introduced by Daniels et al. (1976), who used resistivity data for calculating the increase in seismic P-wave velocity due to the frozen layer. Hauck & Wagner (2003) applied fuzzy logic to combine resistivity and seismic velocity data sets for identifying regions with ground ice occurrences. Based on gravimetrically derived densities Hausmann et al. (2007) calculated the relative ice content using a three-phase model (rock, ice and air) for the ice-rich permafrost within a rockglacier. A relation of measured electrical resistivity, seismic P-wave velocity and the 4 phases present in permafrost material was introduced by Hauck et al. (2008). This so-called 4-phase model (4PM) is based on two well-known geophysical mixing rules for electrical resistivity (Archie 1942) and seismic P-wave velocity (Timur 1968) and can be used to approximate the respective volumetric fractions of each phase (e.g. the ice content).

Tab. 1.1: Compilation of potentials and limitations of the application of ERT, RST and GPR to permafrost related problems (compiled from Hauck 2001; Ingeman-Nielsen et al. 2005; Yoshikawa et al. 2006; Maurer & Hauck 2007; Kneisel et al. 2008)

ERT	
General remarks	ERT has been proven to be a powerful tool for a wide variety of landforms and purposes in all of the above mentioned evaluation studies. The method is applicable under various surface conditions, provided that there is sufficient electrical contact between electrodes and the ground. It has the broadest potential from all applied methods.
Potential	<ul style="list-style-type: none"> • detection and mapping of horizontal extent of discontinuous permafrost and the depth of the active layer • indication and delineation of massive ground ice • discrimination of massive ice and overburden permafrost • estimation of ice and unfrozen water content • monitoring the temporal evolution of permafrost and visualising transient processes
Limitations	<ul style="list-style-type: none"> • limited vertical resolution • the depth to bedrock is often not sufficiently well clarified • differentiation between ice, air and specific rock types can sometimes be difficult • as galvanic contact between electrodes and ground is required, the method is only applicable on snow-free surfaces • the often high contact resistances only allow the injection of weak electrical currents into the ground, causing low signal-to-noise ratios for some electrode arrays (e.g. Dipole-Dipole) • good electrical contact between the electrodes and the ground is essential
RST	
General remarks	RST was found to be equally well suited for most of the targets mentioned for ERT, but as the difference between the signals of frozen and unfrozen ground is smaller the interpretation of the results is more difficult. Also the efforts in data acquisition and processing are higher than for ERT.
Potential	<ul style="list-style-type: none"> • contribution to the differentiation of air, ice and rock for complementary use with ERT • determination of the lateral distribution of frozen ground and active layer thickness • detection of interfaces between loose and more compacted material, e.g. the base of active layer, regions of degraded permafrost, or the top of bedrock • if bedrock topography is the target of interest seismic data are essential • higher resolution of structural characteristics than ERT
Limitations	<ul style="list-style-type: none"> • high efforts for data acquisition and processing • Sensitivity of P-wave velocities to temperature changes in partly frozen material is lower than that of resistivities (due to the fact that seismic waves travel along the frozen part of the material as opposed to resistivity that depends on the unfrozen water)
GPR	
General remarks	GPR is a fast survey method that does not need direct contact to the ground, what makes it very popular for the use in permafrost terrain
Potential	<ul style="list-style-type: none"> • discrimination of massive ice and overburden permafrost • determination of the lateral extent of permafrost as well as the depth to the permafrost table • allows the determination of shear horizons within rockglaciers
Limitations	<ul style="list-style-type: none"> • limited penetration depth (particularly in fine-grained (clay) or wet material) • limited resolution of the boundary between massive ice and frozen host material or bedrock • not useful when many chaotic reflectors are present in the subsurface (certain rockglaciers)

1.2.5 Research needs

Summarising the previous sections, the most important research questions concerning the assessment of the sensitivity of mountain permafrost to climate change can be formulated as follows:

- A more sophisticated permafrost modelling requires field measurements of *processes within the main types of ground material such as bedrock, fine-grained debris and coarse, ice-rich debris* (Harris et al. 2009). This should include the consideration of the influence of the snow cover, the role of ice within fine and coarse debris and in bedrock, and the mass and heat transfer by percolating water.
- An increased need for detailed information on the *varying response of heterogeneous landforms in mountain permafrost* was identified, especially, as both the distribution and the amount of ground ice can be highly variable (Harris et al. 2001b; Luetschg & Haeberli 2005; Haeberli et al. 2006).
- To estimate the stability of slopes and rock walls the development of *suitable approaches for a determination of the subsurface material composition* (in particular the ice and unfrozen water content) is essential. The amount of ice present within the subsurface is also a critical input parameter for permafrost modelling approaches (Noetzli 2008; Riseborough et al. 2008).

This emphasises the need for innovative methodological approaches:

- For the assessment of climate induced permafrost degradation *suitable monitoring approaches for the observation of changes in the subsurface composition (ice and unfrozen water contents) are required*, which account for the strong spatial heterogeneity of mountain permafrost (Gruber & Haeberli 2007; Harris et al. 2009).
- To address the problem of the often remote study sites and the need for regular and temporally high-resolution data sets, *a fully operational automatic ERT monitoring system is required*.
- To reduce the ambiguities inherently involved in geophysical methods, a further need is the *development of a complementary geophysical monitoring approach* (e.g. seismics), which is not available to date.

1.3 Objectives

The above mentioned research needs concerning the observation of permafrost evolution and its sensitivity to climate change emphasise the necessity for a geophysically based method to monitor and quantify the composition of the subsurface material in high alpine permafrost terrain, and in particular the ice content evolution in both spatial and temporal dimension.

The central objective of this thesis is to analyse the potential of geophysical monitoring techniques for the assessment and quantification of seasonal and long-term changes in the ground ice content of mountain permafrost.

The main focus is hereby on:

- a *generalised evaluation of the ERT monitoring approach* (introduced by Hauck 2002 for one specific permafrost site in the Swiss Alps) for its applicability to different time scales and to different landforms (with variable surface and subsurface conditions),
- the *analysis of the potential of a complementary monitoring approach* using time-lapse refraction

- seismic measurements,
- the *quantification of relative changes in the subsurface composition due to seasonal dynamics or climatic anomalies* (to prove the applicability for the assessment of long-term changes due to global warming),
 - the *estimation of changes in the volumetric ice and water content* within the pore space of the subsurface material.

1.4 Organisation of the thesis

This thesis consists of three main parts:

Part I: Following this introduction and overview on the current state of research, the geophysical monitoring approaches for both applied methods (ERT and RST) are described in chapter 2. In addition, the approach to quantify (changes in) the volumetric ice and water content based on geophysical data sets is presented. Chapter 3 provides an overview on the characteristics of the different landforms at the study sites.

Part II: The main scientific work of this thesis is presented in four chapters dealing with the major objectives defined above. In chapter 4 (consisting of a paper published in *Journal of Geophysical Research*, Hilbich et al. 2008b) the general applicability of ERT monitoring of permafrost degradation on different time scales has been proven for the Schilthorn site. Chapter 5 (consisting of a paper published at the *9th International Conference on Permafrost*, Hilbich et al. 2008a) deals with the extension of the approach to an ERTM network at four different landforms and evaluates first measurement results based on reference borehole temperature data. A special focus is laid on the assessment of the reliability and applicability of the ERTM approach to particularly challenging coarse blocky and ice-rich permafrost sites in chapter 6 (consisting of a paper published in *Permafrost and Periglacial Processes*, Hilbich et al. in press). The potential of a complementary time-lapse refraction seismic monitoring approach is evaluated and compared with the ERTM approach in chapter 7 on the basis of repeated measurements at two different permafrost sites. This chapter will be shortly submitted to *The Cryosphere*.

Part III: A discussion of the results of this thesis is provided in chapter 8, including a comprehensive outlook on the combined application of ERTM and RSTM for the quantification of climate induced ground ice degradation. Finally, a summary gives an overview on the main findings of this thesis and an outlook on future research needs.

2 Geophysical monitoring rationale

This chapter gives an overview of the geophysical background of the methods used in this study, their sensitivity to permafrost related physical properties (i.e. temperature and ice content), and the monitoring approach and strategy. The last section introduces an approach for a quantification of ground ice contents based on ERT and RST data and the implications for the application to monitoring data sets.

2.1 Electrical Resistivity Tomography Monitoring (ERTM) approach

2.1.1 Principle of electrical resistivity measurements

The overall purpose of resistivity measurements is to determine the subsurface resistivity distribution that can be related to distinct material properties. By injecting a direct current via two electrodes into the ground the resulting potential difference can be measured between two other electrodes fixed at the ground surface. As different subsurface materials cause variations in resistance to current flow, distinctive variations in the measured potential difference provide information on the subsurface structure and materials.

The resistance to current flow is a consequence of the material dependent specific electrical resistivity ρ_s shown in Fig. 2.1. Using Ohm's law the so-called apparent resistivity ρ_a can be calculated from the current I and voltage difference values ΔV :

$$\rho_a = K \frac{\Delta V}{I} \quad (1)$$

where K is a geometric factor relating the applied current and the measured potential difference to the geometric array of the four electrodes (Burger et al. 2006). Varying the geometry (i.e. lateral position and spacing) of these four electrodes used for a resistivity measurement (the so-called quadrupoles) changes the size and position of the subsurface section over which the bulk electrical resistivity is determined, which allows for a differentiation of lateral and vertical variations in the resistivity distribution of the ground. Penetration depth is thereby controlled by electrode spacing. Modern multi-electrode resistivity systems can automatically measure various quadrupole combinations along a profile line.

The apparent resistivity ρ_a (Equation 1), equals the specific (that is the “true”) resistivity ρ_s of the subsurface only for homogeneous conditions, which is rarely the case. For heterogeneous ground conditions the specific resistivity distribution is derived from the measured apparent resistivity values using inversion methods implemented in commercially available software programmes (see section 2.1.5).

Depending on the array geometry applied in a resistivity survey 1D, 2D and 3D resistivity images of the subsurface can be obtained, the spatial resolution is thereby a function of the

number and spacing of electrodes as well as the applied quadrupole geometry. The most common quadrupole configurations are the Wenner, Schlumberger (or a combination of both), and the Dipole-Dipole configurations (Burger et al. 2006).

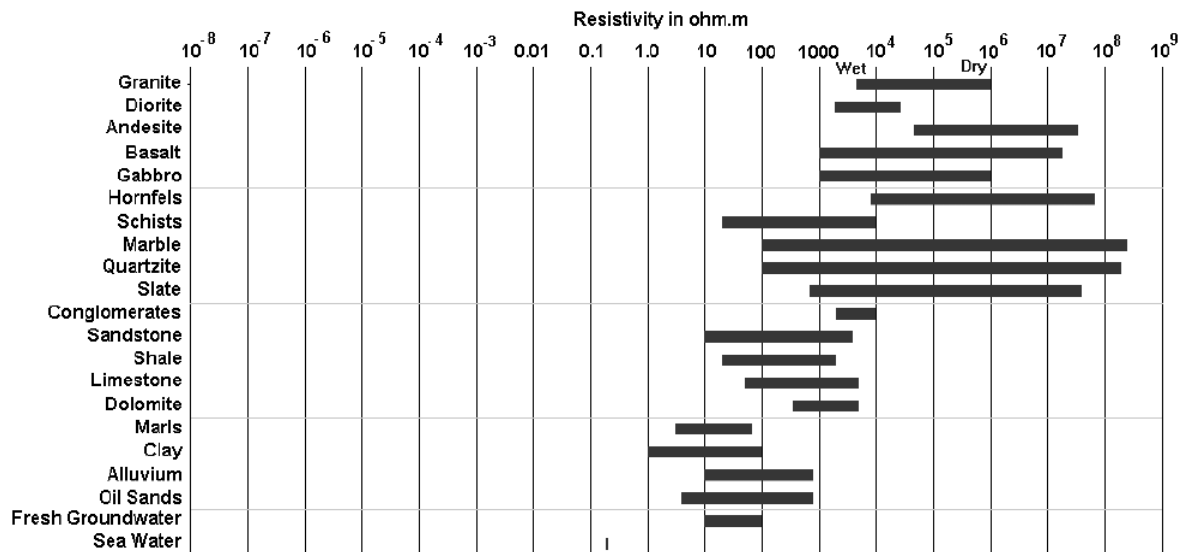


Fig. 2.1: Specific electrical resistivity of different materials (modified after Loke 2003).

Most minerals in sediments and rocks have very high specific resistivities of $>10^9 \Omega\text{m}$ (Schön 2004). However, in general, the conduction in subsurface material is electrolytic and takes place through the presence of conductive fluids. The material dependent specific resistivities of rocks and sediments (Fig. 2.1) are therefore largely controlled by the electrolytic conduction of water that is distributed across grain boundaries or contained in pores, fractures and faults (Schön 2004). The electrical resistivity of a substrate or rock is inversely proportional to porosity and degree of saturation (Fortier et al. 1994), which can be described by an empirical relationship called Archie's second law relating the effective resistivity ρ of a medium (consisting of a rock or soil matrix and pore water) to the resistivity of the pore water ρ_w , the porosity Φ and the saturation S_w :

$$\rho = \rho_w \Phi^{-m} S_w^{-n} \quad (2)$$

where the cementation factor m (according to Rubin & Hubbard 2005 between 1.3-2.0 for unconsolidated sand to consolidated sandstone) and the saturation exponent n (according to Schön 2004 considered to equal 2 for most rocks) are empirically determined parameters (Archie 1942). Due to the *large and overlapping ranges of resistivity values* (mainly due to the water content) only a rough discrimination between saturated and unsaturated unconsolidated sediments and rocks is possible without additional information. In general, the resistivity of a specific substrate depends on porosity, water saturation, pore water salinity, structure of pore volume, and temperature.

2.1.2 Sensitivity of the electrical resistivity to temperature and ground ice

The sensitivity of electrical resistivity to temperature is closely related to the unfrozen water content (Olhoeft 1978), and arises from different effects, above and below the freezing point. At positive temperatures the resistivity of the pore water increases with decreasing tempera-

ture as a consequence of increasing viscosity of the pore water, which, in turn, decreases the mobility of the ions in the water. This can be quantitatively described as a linear function of the resistivity ρ_0 measured at a reference temperature T_0 and the temperature coefficient of resistivity α , which has a value of about 0.025 K^{-1} for most electrolytes (Keller & Frischknecht 1966):

$$\rho = \frac{\rho_0}{1 + \alpha(T - T_0)} \quad (3)$$

Below the freezing point resistivities increase exponentially due to successive freezing of the pore water with decreasing temperatures. The subzero relationship between resistivity and temperature can be expressed through:

$$\rho = \rho_0 e^{-b(T)} \quad (4)$$

where ρ_0 and b (in K^{-1}) are constants (McGinnis et al. 1973). The factor b controls the rate of increase and can be determined from Equation (4) if resistivity data for different subzero temperatures are available. This exponential relation of resistivity and temperature (Equation 4) demonstrates that *resistivity values of frozen ground can range through a few orders of magnitude* between 1-5 $\text{k}\Omega\text{m}$ to several hundred $\text{k}\Omega\text{m}$ or even a few $\text{M}\Omega\text{m}$ (e.g. Hoekstra & McNeill 1973). The large differences in resistivity values for frozen and unfrozen materials are due to the nature of the pore water, that is electrically conductive above the freezing point and becomes an insulator with the transformation to ice below the freezing point.

Relating the temperature dependence to time, the resistivity increase during freezing depends mainly on the porosity and the degree of water or ice saturation, respectively (Kneisel et al. 2008). During freezing a relative increase in ionic load causes a depression of the freezing point of the remaining pore water. Thus, the unfrozen pore water content can be comparatively high enabling a significant electrolytic conduction *even at temperatures well below 0°C* (Scott et al. 1990).

2.1.3 Electrical resistivity monitoring approach

As shown above, electrical resistivity measurements yield information on the physical properties of the ground, that are mainly controlled by the strong dependence of resistivity on temperature, and thus by the ice and unfrozen water content. Assuming that general conditions (such as lithology, stratigraphy, state of weathering, pore space) remain constant over an observation period of several years to decades, repeated electrical resistivity measurements yield information on variations in the subsurface ice and water content with changing temperature and time (Delaney et al. 1988; Fortier et al. 1994).

The monitoring strategy is based on the semi-automatic monitoring set-up tested by Hauck (2002) during a one-year pilot study at Schilthorn (see chapter 3 for site description). This set-up guarantees constant measurement conditions in terms of electrode position and spacing and allows measurements throughout the year, even when the profiles are covered with several meters of snow. More details and an illustration of the principle of the fixed electrode array at Schilthorn can be found in *publication #1* in chapter 4. The same approach was applied to other sites with varying numbers of electrodes and spacing adapted to the respective requirements and objectives (see chapter 3).

To evaluate the applicability of the monitoring approach to the detection of long-term (e.g. decadal) changes in ground ice content, an analysis of different time scales, ranging from short-term (daily) and seasonal to inter-annual (*publication #1*, chapter 4), as well as a comparison of temporal resistivity with borehole temperature changes at different landforms was conducted (*publication #2*, chapter 5). In addition, the reliability of the resistivity inversion in the context of the monitoring data, especially concerning anticipated permafrost degradation signals, is analysed in *publication #3* (chapter 6).

2.1.4 Data acquisition

The principle of data acquisition is equal for all four test sites (fixed electrode array, measurements by plugging a resistivity meter to the switch box that connects the cables from all electrodes). However, surface conditions are different for the different permafrost sites and the depth range of interest as well as the size of the landform requires variations in the length of the respective profile lines. Similarly, the spatial resolution is a function of the minimum electrode spacing. For logistical reasons the number of electrodes of a profile was restricted to a maximum of 48 (to enable automatic measurements with the multi-electrode system *Syscal Junior* from IRIS Instruments). The electrode array installed at each test site constitutes therefore a compromise between desired investigation depth and spatial resolution. The respective set-ups are summarised in **Tab. 3.1**.

As good electric contact between electrode and ground surface is essential to enable current flow between different electrodes, a particular challenge in conducting electrical resistivity measurements in high alpine terrain is the coupling of the electrodes (steel stakes) to the ground. The contact resistance of an electrode is a function of the common surface between electrode and ground (LaBrecque et al. 2004), thus it becomes obvious that steel stakes fixed between large blocks of rockglaciers or other coarse blocky landforms provide only punctual contact and contact resistances are generally high. Considerable efforts were therefore undertaken to fix the electrodes as deep and as firm as possible in blocky ground. By this, contact resistances could be reduced to a maximum of about 500 Ω , which is according to IEEE (1983) regarded to allow sufficient current flow. In critical cases significant improvement was achieved by parallel coupling of two electrodes (partly screwed into the blocks). However, particularly on coarse blocky landforms electrode contact varies considerably between summer and winter and between dry and moist surface conditions, by this influencing the success of a survey. As there is no possibility to improve the coupling when the electrodes are covered by snow, many measurements conducted in wintertime did not provide sufficient electrode contact, restricting the ERTM results of the Murtèl and Stockhorn sites (see chapter 3) to the summer season. Another factor influencing ground contact of the electrodes is the movement of blocks in case of creeping permafrost (e.g. rockglaciers), where the coupling may decrease (but also increase) with time and should be checked occasionally.

According to Kneisel et al. (2008) in periglacial environments the choice of the appropriate electrode configuration depends on the difficult surface conditions. Maximum current injected into the ground is often quite low, making geometrical factors of distinct electrode configurations a critical factor in the decision for the best configuration. Wenner or Wenner-Schlumberger configurations are therefore much more popular than e.g. the Dipole-Dipole configuration, even though the latter may provide superior lateral resolution. The Wenner-Schlumberger array provides a better depth resolution than the Wenner array, but it requires a larger number of measurements, e.g. 529 instead of 360 for 48 electrodes. As many measure-

ments had to be made *manually* by connecting four pin plugs to the switch box for all quadrupoles of a certain configuration (see Fig. 3, chapter 4) in the beginning of the study, for practical reasons the Wenner array was chosen for the ERT monitoring study. Measurement time for a Wenner measurement (manual) was still about three hours for 48 electrodes.

The development of an *adaptor* connecting the electrode array to a multi-electrode resistivity system, effectively reduced the measurement effort and allows now the measurement of multiple configurations.

As the monitoring approach is *not fully automated yet*, for logistical reasons measurements could only be carried out at irregular time instances. Weather and snow conditions (e.g. danger of avalanches) often prohibited access to the study sites, further limiting the total number of measurements per site. A particular focus was on the summer season at all test sites, especially on August and September, that is at the time of maximum active layer depth. Measurements at these dates will be continued for long-term comparison of inter-annual differences.

2.1.5 Data processing

Geophysical inversion

A common characteristic of applied geophysics is the indirect measurement of interior properties of the earth from the surface. Linking the measured data by a mathematical relationship with the specific properties of the earth, that is the model, represents the *inverse problem* in geophysics. The term inverse problem is used in contrast to the *forward problem*, which represents the prediction of the model response (synthetic data) on the basis of a given subsurface model and a set of specific model parameters. The solution of the forward problem is unique. The inverse theory deals with the reverse problem, which is substantially harder to solve: starting with the measured data the goal is to determine the corresponding model m that is related to the data d by a function g (Menke 1984):

$$\mathbf{d} = \mathbf{g}(\mathbf{m}) \tag{5}$$

Accordingly, to calculate a resistivity image from ERT data it is necessary to carry out an inversion that produces a model with the specific resistivity distribution on a 2D model grid from the observed apparent resistivities (calculated from the measured voltages, Equation 1). In all practical ERT applications the inverse problem is ill-posed and non-unique to solve, requiring the inversion to be solved iteratively by minimising the misfit between the data and the model response (optimisation-based technique) (Stummer et al. 2004).

The inversion algorithm starts with the determination of a starting model, usually a homogeneous half-space with the resistivity set to the average of the apparent resistivities. By forward modelling corresponding apparent resistivities are calculated, which are then compared to the observed data. If the convergence criterion (defined in an objective function, e.g. the difference between data and model) is met, the initial model is considered to adequately represent the true resistivity distribution. If the convergence criterion is not met, a search algorithm is applied that tries to reduce the difference between the predicted and observed apparent resistivity values by adjusting the resistivity of the model blocks in the estimated resistivity model. From the new model the apparent resistivities are calculated and compared again to the observed data, and the procedure is repeated until the inversion has converged, e.g. the misfit between data and model is less than a predefined value (Daily et al. 2004b).

However, the solution of an inverse problem is only a first step towards answering the questions concerning a resistivity image (Routh & Miller 2006). Due to the fact, that a continuous function of model parameters is estimated from a discrete data set, the solution of the inverse problem depends on the regularisation and the model parameterisation used in the inversion. Also the data are always contaminated with measurement errors providing an additional source of discrepancy. An important step after the inversion is therefore the quantification of the error between the estimated and the true model. The determination of the uncertainty in the estimated model is called *appraisal problem* (Scales & Snieder 2000). The whole cycle of the forward problem, the inverse (or estimation) problem, and the appraisal problem is illustrated in Fig. 2.2. Although image appraisal is essential to get an impression which features in the inverted image are influenced by artefacts due to the inversion and which regions are constrained by the data, it is not included in operational inversion routines, but has to be conducted separately. The application of appraisal techniques is the focus of *publication #3* and will be further discussed in chapter 6.

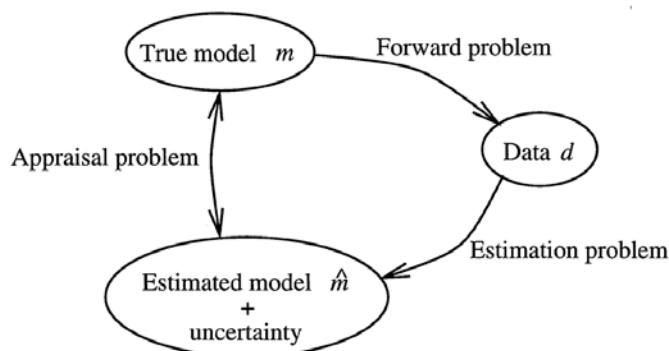


Fig. 2.2: Illustration of the relation between forward, inverse (or estimation), and appraisal problem (Scales & Snieder 2000).

ERT inversion with RES2DINV

The processing of the electrical resistivity data sets was carried out with the software programme RES2DINV (ver. 3.56), which performs a smoothness constrained inversion using finite difference forward modelling and Gauss-Newton inversion techniques (Loke & Barker 1995; Loke & Barker 1996). The robust (L_1 -norm) inversion scheme was used for all data sets, as it is best suited to reproduce sharp boundaries (e.g. the interface between active layer and permafrost table, or the shape of ice lenses) (Loke et al. 2003). For the robust inversion scheme the measure of the misfit between observed data and inverted model is given by the absolute data misfit value in percent.

Within the context of *ERT monitoring*, a special inversion technique is applied to analyse the change in model resistivities of subsequent measurements. Recalling that each inversion attempts to minimise the difference between the observed and calculated apparent resistivity values for an individual data set, the degree of adaptation and thus the uncertainties involved in model estimation may be different for independent data sets. Consequently, there is no guarantee that calculated resistivity differences from independently inverted data sets of subsequent measurements are only due to actual temporal changes in the subsurface resistivity (Loke 1999). A specific *time-lapse inversion* technique based on cross-model constraints is therefore applied that uses the model obtained from the inversion of an initial data set as a refer-

ence model to constrain the inversion of the later time-lapse data sets (Loke 1999). The absolute changes in the model resistivity values are minimised by using a robust smoothness constraint. As a result, the percentage change in the model resistivity obtained from the inversion of a later time data set compared with the reference model from the inversion of the first data set is determined. Moreover, by using Archie's law (Equation 2) and assuming initially saturated conditions RES2DINV provides the possibility to relate the temporal resistivity change to the percentage desaturation of the subsurface material. This allows a rough approximation of the amount of freezing or thawing that has occurred between two measurement dates and will be considered in *publication #1* in chapter 4.

2.2 Refraction Seismic Tomography Monitoring (RSTM) approach

2.2.1 Principle of seismic refraction

Seismic refraction makes use of the first arrivals from compressional waves (P-waves), generated by a seismic source (e.g. a sledge hammer or explosives), at the receivers (geophones) providing information on the propagation velocity within the subsurface. As the propagation velocity of P-waves (v_p) is different for a variety of subsurface materials (Fig. 2.3), the time it takes a wave to travel between source and receivers (travel time) can be used to extract information on the subsurface material and the depth of distinct interfaces (e.g. between unconsolidated sediments and bedrock, or between the unfrozen active layer and the permafrost table) acting as refractors. A necessary condition of the refraction seismic method is an increase of seismic velocities with depth, because seismic wave energy would otherwise be refracted away from the surface and could not be detected at the receivers. In case of decreasing velocities with depth in parts of the subsurface the recorded first arrivals only partly reflect the subsurface structure and low velocity layers (remaining mostly unnoticed) distort the results.

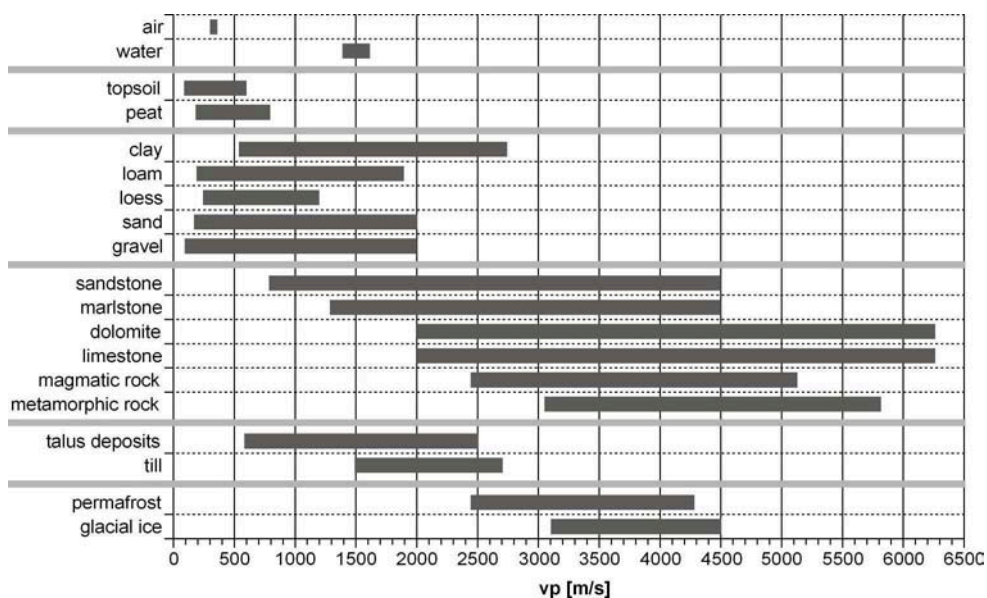


Fig. 2.3: Seismic P-wave velocities (v_p) of different subsurface materials compiled after Fertig 1997, Hecht 2000 and other authors (Schrott & Hoffmann 2008).

The fundamentals of the refraction seismic technique will not be repeated here in detail (for a comprehensive introduction see e.g. Burger et al. (2006)). In the following, the sensitivity of the method to permafrost related problems will be highlighted, and the refraction seismic monitoring approach (including data acquisition and processing) will be explained.

2.2.2 Sensitivity of P-wave velocities to temperature and ground ice

From Fig. 2.3 it is seen that the compressional velocity for ice (including ground ice and glacial ice) can range from 2500 to 4500 m/s. Similar to the large ranges of compressional velocities for different rock types (due to different states of weathering or fracturing) this range reflects a) different amounts of air or rock inclusions in the ice matrix of glaciers, and b) different amounts of ice contained in the pores of a rock or soil matrix under permafrost conditions.

Röthlisberger (1972) gives a value of about $v_p = 3500$ m/s for pure ice. The often lower velocities of ice are attributed to air contained in the sample (Timur 1968), whereas higher values indicate that also rock particles with higher seismic velocities are enclosed in the ice matrix (Röthlisberger 1972). This is because seismic velocity of a mixture depends on the seismic velocity of its constituents. The oldest and most popular expression that relates seismic velocity v to the porosity Φ (and the interstitial water) of a medium is Wyllie's equation (1956):

$$\frac{1}{v} = \frac{1-\Phi}{v_r} + \frac{\Phi}{v_w}, \quad (6)$$

where v_r is the P-wave velocity of the solid rock, and v_w that of the interstitial pore water.

Timur (1968) extended this two-phase time-average equation to a three-phase time-average equation to account for an *ice-liquid-rock matrix* under permafrost conditions:

$$\frac{1}{v} = \frac{(1-f_i)\Phi}{v_w} + \frac{f_i\Phi}{v_i} + \frac{1-\Phi}{v_r}, \quad (7)$$

with f_i being the fraction of the pore space filled with ice, and v_i the seismic velocity of the ice. Equation 7 demonstrates that the presence of ice in the pore spaces of sediments can cause large increases in seismic velocity compared to the velocity when the interstitial water is unfrozen (Timur 1968). Since ice is much stiffer than water, the wave speed is a strongly increasing function of the ice-to-water ratio. However, rock is much stiffer than either ice or water, therefore the wave speed is also a decreasing function of the porosity Φ (Zimmerman & King 1986). Under field conditions in mountain permafrost, not only liquid and ice but also air is contained in the pore spaces, which can similarly be included in the time-average equation (shown in section 2.3). The relation of compressional velocities for two- and three-phase media (calculated based on Equations 6 and 7) to porosity is illustrated in Fig. 2.4.

Analysing the relation of compressional velocity and the gaseous (air), liquid (water), and two solid (rock/soil, ice) components of the subsurface as a function of temperature reveals that the bulk velocity of a medium generally *increases with freezing* (see Fig. 2.5). The shape of the velocity-temperature-curve is a function of lithology, pore structure, and the nature of the interstitial fluids leading to a sharp increase of v_p in water-saturated rocks with decreasing temperature, whereas it is nearly independent of temperature in dry rocks (Timur 1968). In contrast to the characteristics of consolidated rocks investigated by Timur (1968), the velocity difference between frozen and unfrozen conditions is *more pronounced for unconsolidated coarse-grained sediments* (as a function of the water-filled porosity) (cf. Fig. 2.5; Scott et al. 1990).

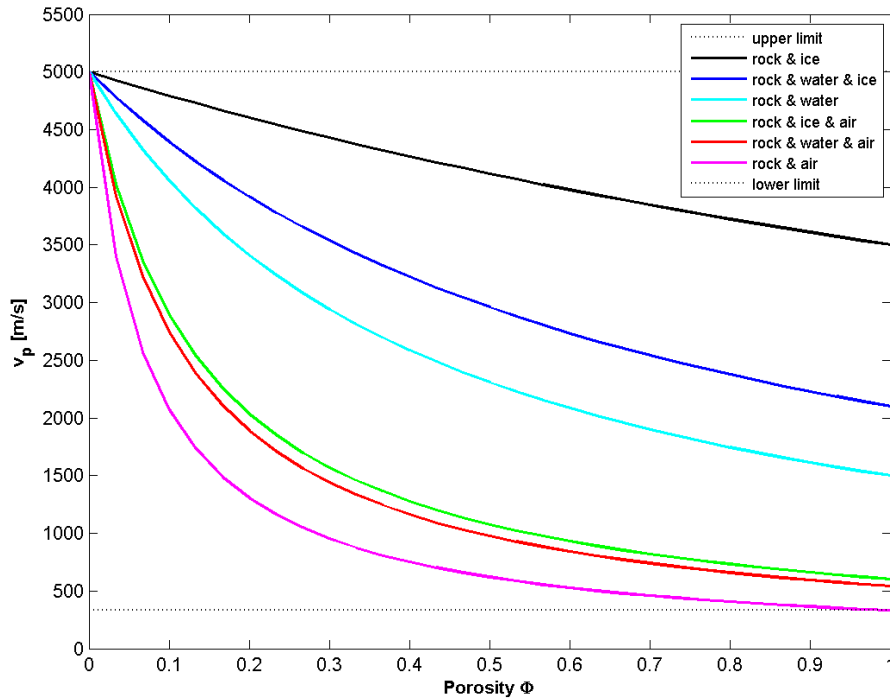


Fig. 2.4: Illustration of the relations of two- and three-phase media to porosity (calculated after Wyllie et al. (1956) and Timur (1968)). The curves for three-phase media were calculated for equal fractions of water, ice and air, respectively. The compressional velocity was set to 5000 m/s for rock, 3500 m/s for ice, 1500 m/s for water, and 330 m/s for air. The incorporation of the gaseous phase in the Timur equation will be introduced in section 2.3.

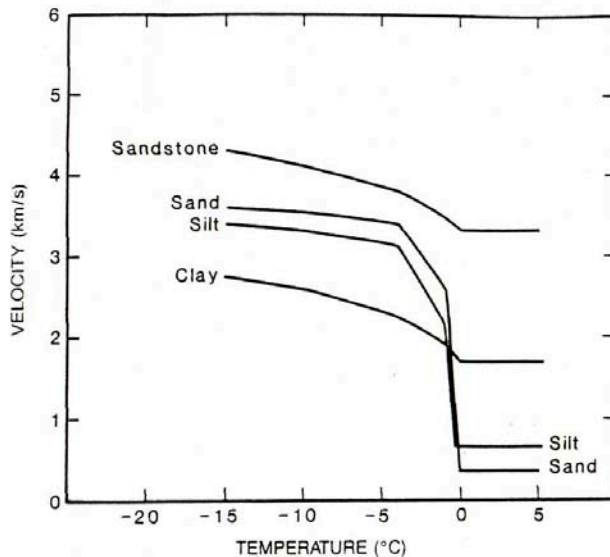


Fig. 2.5: P-wave velocity of different subsurface materials as a function of temperature (Scott et al. 1990).

An important characteristic of frozen ground is, that in the typical temperature range of several degrees below the freezing point it still contains considerable amounts of unfrozen water in the pores (Pandit & King 1979; Sondergeld & Rai 2007), which is due to the increased ion concentration in the remaining liquid water lowering the freezing temperature. In his experiments with consolidated sandstones Timur (1968) found that during freezing the system consists of an ice-liquid-rock matrix, which transforms to a solid-solid system (ice-rock matrix) at

temperatures of ca. $-21\text{ }^{\circ}\text{C}$, where all water was frozen and the P-wave velocity remained constant (at its maximum) during further cooling. Similarly, Pandit & King (1979) found free water in the pore space of sedimentary rocks even at -15°C .

It can be concluded that the analysis of compressional wave velocities in permafrost is theoretically *capable of identifying subsurface changes due to freezing or thawing* processes (depending on the spatio-temporal resolution of a survey). However, as the seismic refraction technique is based on increasing velocities with depth the method is generally not applicable to analyse the lower boundary of permafrost or taliks (Röthlisberger 1972).

2.2.3 Refraction seismic monitoring approach

Time-lapse seismic monitoring is an important research topic in exploration geophysics (Vesnaver et al. 2003; King 2005), but the detection of changes in reservoir velocity and compaction (due to oil production) is preferably done using reflection seismics due to their high resolution potential. Seismic reflections from the upper 5-15 m of the earth are usually overwhelmed by contaminating effects from different coincident-arriving waves and more affected by scattering effects in highly heterogeneous material with shallow low velocity layers (typical for mountain permafrost sites). Therefore, reflection data rarely provide information on the very shallow parts of an unconsolidated sedimentary section (Lanz et al. 1998). According to Lanz et al. (1998) and Musil et al. (2002) *refraction seismic tomography* is more appropriate for exploring the upper 50 m of the subsurface.

A first approach in reservoir monitoring using time-lapse refraction seismics for the estimation of reservoir velocity changes was introduced only recently by Landrø et al. (2004). It is based on the fact, that a velocity change in a reservoir (due to oil production) by only 1% will change the critical angle of refraction and thus the critical offset for refracted waves, i.e. their first appearance at the surface. For oil reservoirs located at depths of $> 1000\text{ m}$ this change in critical offset amounts to several tens of meters, showing the huge potential of this method (Landrø et al. 2004). For shallow targets the corresponding difference in critical offsets would be reduced to a few centimetres to decimetres, making this approach inappropriate for the monitoring of mountain permafrost evolution. Concerning shallow applications, *no time-lapse refraction seismic approach is known to date*, neither for permafrost, nor for other fields of interest.

As shown above, the refraction seismic technique is generally capable of discriminating unfrozen and frozen sediments or massive ice, and is thus a standard method for determining active layer thickness (e.g. Kneisel et al. 2008). However, the ranges of P-wave velocities for ice and bedrock (both frozen and unfrozen) are very similar (Fig. 2.3), making a differentiation of stratigraphic details in bedrock and/or below the permafrost table often difficult. Conversely, P-wave velocities *differ significantly for ice and water* (Fig. 2.3), enabling the detection of changes in the ice and water content within the pores and fractures of the subsurface material by repeated measurements, provided that general conditions (lithology, stratigraphy, state of weathering, pore space) remain unchanged over the observation period. Despite the limitations concerning qualitative stratigraphic interpretation, even comparatively small temporal changes in P-wave velocities may indicate zones with significant ground ice content changes due to seasonal variations or long-term climate change. Repeated seismic measurements are therefore supposed to provide the *potential of an independent monitoring method* (complementary to ERT) to determine relative ice (and water) content changes of the subsurface.

To reliably detect such changes via refraction seismic monitoring necessary conditions include a constant source-receiver-geometry between subsequent measurements and an amount of P-wave velocity change that is well above the noise level.

The *development and validation of an appropriate RST monitoring approach* involves an evaluation of a hierarchy of methods:

- (a) The comparison of time-lapse seismograms and analysis of reproducibility of the seismic signal,
- (b) The analysis of time-lapse travel time curves with respect to resolving possible shifts in travel times and changes in P-wave velocities
- (c) The comparison of inverted tomograms including the quantification of spatio-temporal velocity changes (time-lapse tomography).

A first application and an evaluation of this time-lapse refraction seismic approach will be conducted at different permafrost sites, and its potential and limitations for application in high mountain permafrost environments will be analysed in chapter 7.

2.2.4 Data acquisition

As geophones and corresponding cables are much more costly than the corresponding electrodes/cables of the ERTM set-up, the arrays could not be installed permanently. Moreover, in contrast to electric methods, the signal generation is much more laborious and cannot be automated. The field work effort for seismic monitoring (including lay-out of the survey line and data acquisition) is therefore much higher than for ERTM. Horizontal resolution is comparable to the respective ERT profiles.

To enable comparability to the ERTM results the acquisition of the refraction seismic profiles was always conducted in the immediate vicinity of the respective ERT profiles at all sites, i.e. geophones were placed close to the corresponding electrodes. In all cases where large blocks were available the geophones were fixed via screws to the blocks, assuring an optimal coupling to the ground (Fig. 2.6). As the screws were permanently fixed they also guaranteed identical geophone positions during subsequent measurements. In cases of fine-grained unconsolidated surface material the geophones were fixed to the ground via spikes and positions were marked to enable relocation for later measurements.



Fig. 2.6: Example of a geophone mounted on a fixed screw to a large block.

For RST the density of sources should ideally be comparable to that of the receivers (Maurer & Hauck 2007), shot points were therefore placed at the midpoint between each pair of geophones.

A common characteristic of mountain permafrost sites is their usually remote location in rough and/or steep terrain. Many geophysical surveys are therefore restricted to the use of light weight equipment and simple efforts in signal generation. This is especially true for monitoring approaches that depend on repeated measurements. A particular aim of this study was therefore to analyse the potential of the RSTM approach based on a simple set-up. Although the quality of a survey may significantly be improved by high resolution data sets (large number of geophones, small spacing, powerful seismic sources (explosives or shot guns)), data acquisition was restricted to a maximum of 24 geophones and a sledge hammer (3-5 kg) hitting a steel plate (or fixed blocks) as seismic source. Signal stacking of minimum 10-15 stacks was necessary to achieve an adequate signal-to-noise ratio. Depending on the overall length of the profiles up to 40 stacks were carried out for the far shots.

As access to the ground surface is needed, measurements are basically restricted to the summer season when the snow cover is absent, which would be a serious limitation for an operational seismic monitoring approach. However, with some additional effort the snow cover may be removed manually along the seismic line to enable a measurement under early summer conditions when the active layer is still widely frozen.



Fig. 2.7: A seismic survey conducted after the removal of the snow cover in early summer (Schilthorn, July 2007).

2.2.5 Data processing

Data processing (first arrival picking, travel time analysis, tomographic inversion) was done using the software REFLEXW (Sandmeier 2008). As for the inversion of electrical resistivities (section 2.1.5), the reconstruction of the velocity pattern of the subsurface (model) is based on the automatic adaptation of synthetic travel times, calculated by forward modelling, to observed travel times (data). The tomographic inversion in REFLEXW uses a so-called SIRT (Simultaneous Iterative Reconstruction Technique) algorithm that is based on iterative adaptation (Sandmeier 2008). A starting model has to be defined that consists ideally of a gradient model with increasing velocities with depth reflecting the gross structure of the study area. Lanz et al. (1998) suggest better to overestimate than to underestimate the initial velocity gra-

dient to ensure sufficient ray coverage. Starting from this initial model synthetic travel times are calculated by forward modelling, which are then compared to the observed data. Based on the travel time residuals (synthetic – observed travel times) the initial model is adapted and synthetic traveltimes are again calculated for the new model. This iterative process stops as soon as distinct stopping criteria are fulfilled, e.g. if the relative change between subsequent iterations is smaller than a predefined value, or a maximum number of iterations is reached. In contrast to the inversion of ERT data, in RST inversion the ray paths depend heavily on the initial velocity model, such that convergence of the tomographic inversions usually requires a larger number of iterations (10-15) (Lanz et al. 1998). For the time-lapse data sets the same settings were used for all inversions.

Topography of the surface relief was incorporated into the travel time analysis by redefining the geometry of the shots and receivers based on topographic xz-values, and into the tomographic inversion by setting the velocities of cells above the irregular surface to that of air and fixing them during the inversions (Sandmeier 2008).

The reliability of the final inversion model can be judged qualitatively on the basis of the ray distributions obtained by so-called ray tracing, which is the determination of the ray paths with the shortest travel times between all source-receiver offsets (Sandmeier 2008). Ray density and the number of crossing rays in one grid cell generally decrease with depth, but depending on the heterogeneity of the subsurface the ray coverage may be highly variable in the final model, with regions not being sampled by rays indicating low confidence in the velocity estimates (Lanz et al. 1998). Velocities determined near the base of the lowermost ray paths likely represent average values for the deep regions traversed (Musil et al. 2002).

Quantitative measures to evaluate the reliability of the final tomograms are provided by REFLEXW by the *total absolute time difference* and the *total time difference* between the observed and calculated travel times. The total absolute time difference defines the sum of the absolute time differences independent from the sign (positive or negative difference) and gives an estimate on the overall adaptation of the tomogram. Conversely, the total time difference takes into account the sign of the differences and gives an estimate whether the mean model leads to too small or too large traveltimes, i.e. an interface is too shallow or too deep (Sandmeier 2008).

To summarise the preceding sections, for permafrost research using geoelectric and refraction seismic methods it can be concluded that:

- *At a given temperature* the electric resistivity and P-wave velocity of a frozen subsurface layer are a function of the material, its porosity and the respective fractions of ice, water and air in the pore space, and may thus be highly variable for different sites and temperatures.
- At a given site the *change in resistivity and velocity of a frozen subsurface layer with temperature* is only a function of the phase change between water and ice in the pore space. It must be taken into account that in mountain permafrost environments water may flow into or out of the system, which may complicate the interpretation of changes of both parameters.

Another effect that may be regarded is the hysteresis in both parameters upon temperature cycling, causing different resistivity and velocity values for the same temperature depending on the direction of temperature change (Timur 1968; Sondergeld & Rai 2007). However, this effect is observed in high resolution laboratory studies and is assumed to be negligible for field applications dealing with higher noise levels.

2.3 Estimation of total fractions of ice, water and air from combined ERT and RST data sets

To be able to use the geophysical monitoring data from different test sites to quantify a) total fractions of ice (or water), or b) the volumetric loss of ice within a certain time span due to atmospheric warming, a relation between the measured geophysical parameters (electrical resistivity, seismic velocity) and the respective fractions of the subsurface material (rock, water, air, ice) is required. Accordingly, for each model block of the 2D ERT and RST tomograms the total volume is considered as the sum of the volumetric fractions f of the four components for rock r , water w , ice i , and air a . For each model block the equation:

$$f_w + f_r + f_i + f_a = 1 \quad \text{with} \quad 0 \leq f_w, f_r, f_i, f_a \leq 1 \quad (8)$$

must be fulfilled.

The equation by (Archie 1942) (Equation 2) relates the electrical resistivity to the porosity of the rock and the resistivity of the pore water. Similarly, the equation by Wyllie et al. (1956) (Equation 6) relates seismic P-wave velocities to the porosity and the interstitial water. The extension of the latter by a third medium (ice) by Timur (1968) (Equation 7) provides a more differentiated relation. As emphasised by Timur (1968), also a fourth medium (air) should be taken into account for the estimation of seismic velocities under field conditions. As a first step, the equation can be further extended to (after Hauck et al. 2008):

$$\frac{1}{v} = \frac{f_w}{v_w} + \frac{f_r}{v_r} + \frac{f_i}{v_i} + \frac{f_a}{v_a} \quad (9)$$

This extension of Timur's equation states that the reciprocal of the P-wave velocity ($1/v$) of a mixture, the so-called slowness, is equal to the sum of the slownesses of the respective components (water, rock, ice, air), each weighted by its volumetric fraction f (Hauck et al. 2008).

As the pore water has a superior influence on the bulk resistivity of a medium (compared to the resistivity of the minerals of the rock matrix (except for clays)), Archie's law (Equation 2) only considers the resistivity of the pore water. The volumetric fraction of air is a function of porosity Φ and water saturation S_w . Archie's Law does not consider the presence of ice. However, similar to air, ice is an electrical insulator, thus, from a physical point of view, it makes no difference whether the pore space *not* saturated with water is filled with air and/or ice. Using Equation 8 the volumetric fractions of the porosity and the saturation in Equation 2 can be expressed as follows:

$$S_w = \frac{f_w}{\Phi} = \frac{f_w}{1 - f_r} \quad (10)$$

Equations (2), (8) and (9) form a set of equations that relates the four unknown volumetric fractions of water, rock, ice, and air to the material constants $\rho_w, v_w, v_r, v_i, v_a$ and the (material dependent) free constants in Archie's Law m and n . Hauck et al. (2008) combined Equations (2), (8), (9), and (10), solved for the ice content f_i and revealed:

$$f_i = \frac{v_i v_a}{v_a - v_i} \left[\frac{1}{v} - \frac{f_r}{v_r} - \frac{1 - f_r}{v_a} + \left(\frac{a \rho_w (1 - f_r)^n}{\rho (1 - f_r)^m} \right)^{1/n} \left(\frac{1}{v_a} - \frac{1}{v_w} \right) \right] \quad (11)$$

Similarly, equations for the air content f_a and the water content f_w were derived:

$$f_a = \frac{v_i v_a}{v_i - v_a} \left[\frac{1}{v} - \frac{f_r}{v_r} + \frac{1}{v_i} (f_r - 1) - \left(\frac{a \rho_w (1 - f_r)^n}{\rho (1 - f_r)^m} \right)^{1/n} \left(\frac{1}{v_w} - \frac{1}{v_i} \right) \right] \quad (12)$$

$$f_w = \left(\frac{a \rho_w (1 - f_r)^n}{\rho (1 - f_r)^m} \right)^{1/n} . \quad (13)$$

These equations (11-13) constitute the so-called four-phase model (4PM) introduced by Hauck et al. (2008). As four unknown variables are contained in only three governing equations, there is no unique solution to the system of equations. As a first approximation, one variable (e.g. the porosity) may be estimated and prescribed. Furthermore, the material constants ρ_w , v_w , v_r , v_p and v_a as well as the cementation and saturation exponents m and n are prescribed according to common values described in literature (Schön 2004; Rubin & Hubbard 2005). ρ_w , v_w , v_p and v_a may be considered equal for most permafrost conditions, conversely, v_r has to be adjusted depending on the prevailing type of bedrock (see Fig. 2.3). The resistivity of water discharging from springs related to the permafrost occurrence may be measured in the field and used as indication for ρ_w .

As a result, from coincident tomographic ERT and RST data sets the 4PM calculates volumetric fractions of three of the four unknowns, that is ice, air and water, if the fourth unknown, the rock content $f_r (= 1 - \Phi)$, is prescribed.

However, the calculated fractions of ice, water, and air are a function of the prescribed porosity model and consequently only a rough approximation of the true subsurface conditions. A more realistic approach is therefore to calculate the respective fractions of ice, water and air relative to the pore volume (Hauck et al. 2008). This approach also offers the possibility to *use the 4PM in a time-lapse context* for subsequent ERT and RST data sets and to estimate the *temporal change in the volumetric contents of ice, water and air* relative to a given porosity (that is assumed to remain constant over time). In chapter 8, a comprehensive outlook will be given on the extension of the 4PM approach introduced by Hauck et al. (2008) to a time-lapse 4PM approach by an exemplary data set to evaluate the performance for monitoring purposes. The potential of this time-lapse approach concerning the reliability of the estimation of changes rather than absolute values will be discussed.

3 Field sites

All field sites chosen for the establishment of the geophysical monitoring network are part of the Swiss PERMOS network (Vonder Mühll et al. 2007; Vonder Mühll et al. 2008) and are located in different climatic regions of the Swiss Alps. They have been chosen among the other PERMOS sites (see Fig. 3.1) due to the availability of deep borehole information (≥ 20 m), and as representatives for typical permafrost occurrences including a rockglacier, a talus slope, a bedrock plateau, and a rock slope covered by debris.

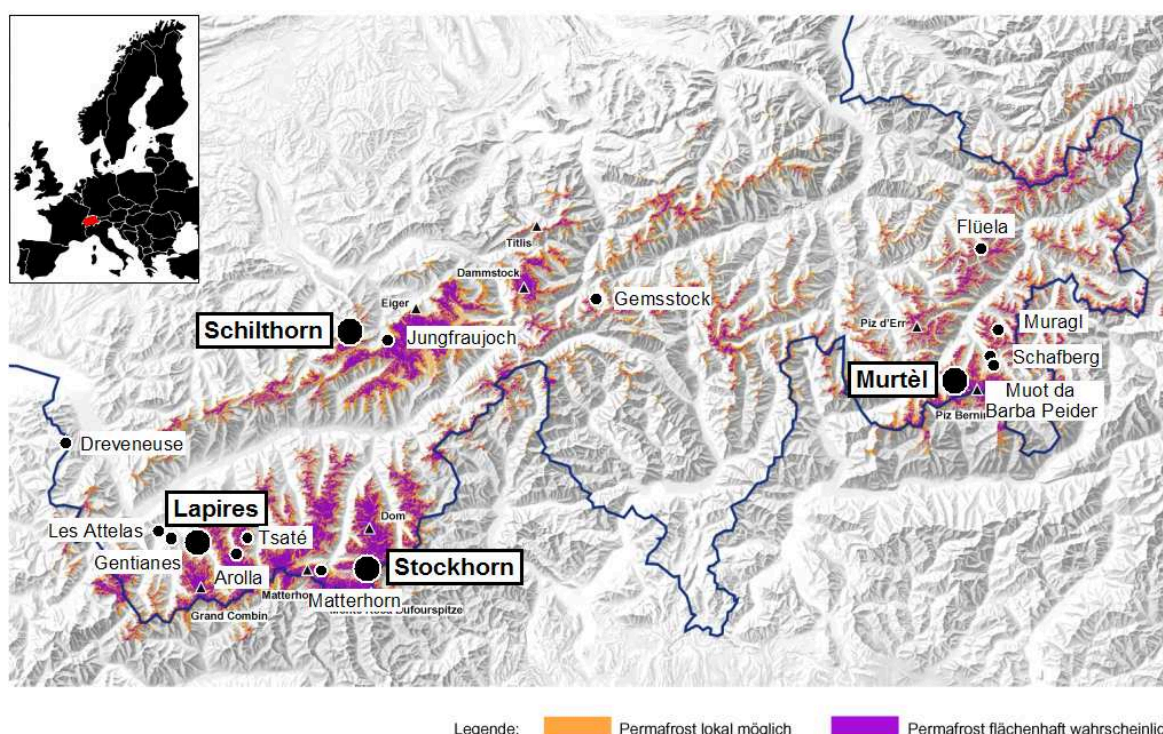


Fig. 3.1: Map of the modelled potential permafrost distribution in Switzerland (violet: permafrost likely, orange: permafrost possible, map: ©BAFU 2006) with all PERMOS borehole sites indicated by black dots (the four test sites used in this study are highlighted).

The selected test sites comprise morphologically different landforms with different contents of ground ice to analyse ...

- ... site-specific differences in the response of permafrost dynamics to atmospheric forcing,
- ... the applicability of geophysical monitoring to various geomorphological landforms and surface conditions,
- ... the effect of ice content for permafrost sensitivity to climate change.

To extend the time series into the past and to cross-check the geophysical monitoring data with independent data, sites have been chosen where detailed data on permafrost characteris-

tics and dynamics from previous or currently ongoing studies exist and previous geophysical data are available for the analysis of long-term (i.e. decadal) changes in ground ice content evolution. Previous ERT measurements that are coincident with the newly installed monitoring profiles exist for Schilthorn, Murtèl, and Lapires (see Tab. 3.1). Long-term monitoring over several decades is intended at all four test sites within the framework of the PERMOS network. The sites are described in the following sections, main characteristics are summarised in Tab. 3.1 at the end of this chapter.

3.1 The summit region of Schilthorn (Bernese Alps)

The Schilthorn massif with the summit at 2970 m altitude is located close to Mürren in the Bernese Alps, Switzerland, at the transition between the Prealps in the north and the principal chain of the Bernese Alps in the southeast (Fig. 3.1). The Schilthorn massif consists of metamorphic sedimentary rocks dominated by deeply weathered dark limestone schists with a fine-grained debris cover (up to several meters thick) around the summit area (Imhof et al. 2000; Vonder Mühl et al. 2007).

During the construction of the Schilthorn summit station between 1965 and 1967 permafrost was found in terms of up to ~ 0.5 m thick ice lenses in the heavily jointed bedrock (Imhof et al. 2000). Within the framework of the European PACE project (Harris et al. 2003) between 1998 and 2000 three boreholes were drilled into the north facing slope approximately 60 m below the ridge to monitor thermal permafrost evolution. In addition, meteorological data (Vonder Mühl et al. 2007) and spatially distributed ground surface temperature data (Noetzli et al. 2008) are collected throughout the year.

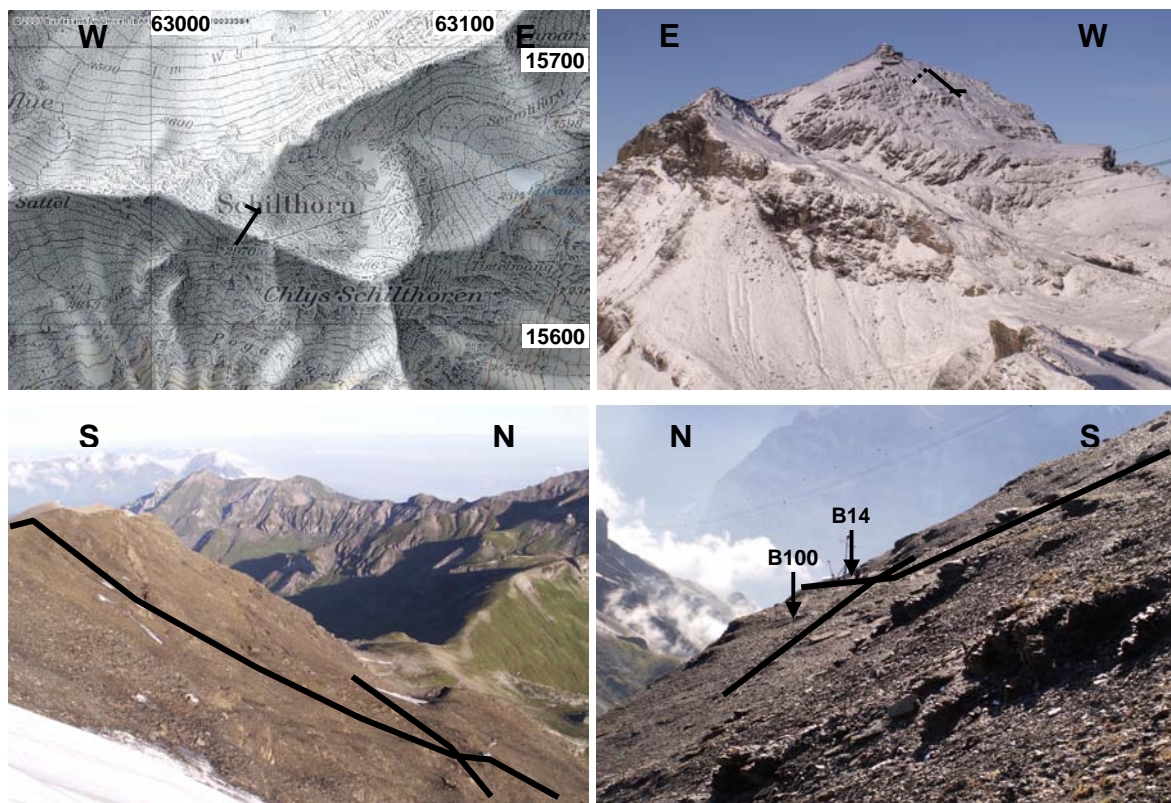


Fig. 3.2: Map (PK25, ©Swisstopo 2007) and photos of the Schilthorn summit region (northern slope) with the position of both ERTM profiles (vertical and horizontal) highlighted by black lines. Note, that the part of the vertical profile located on the southern slope is not visible here.

Permafrost conditions at Schilthorn are rather warm, and according to the mostly dry cuttings obtained by drilling, where no particular ice lenses were hit, ice content seems to be very low (Imhof et al. 2000, pers. communication D. Vonder Mühl). The average maximum active layer thickness is relatively high and amounts to about 5 m (see *publication #1*, chapter 4). The temperatures from two boreholes recorded between 1999 and 2008 are plotted for the uppermost 10 m in Fig. 3.3.

Previous geophysical measurements (RST, ERT) have been conducted along several profiles by Hauck (2001). The first ERT monitoring system in alpine terrain was installed at Schilthorn in summer 1999 (see Fig. 3.2). 12 measurements with a monthly resolution were conducted for a one-year period between September 1999 and September 2000 (Hauck 2002). Between 2002 and 2004 another 81 data sets were recorded within three diploma theses (Schudel 2003; Völksch 2004; Scherler 2006). Since summer 2005 further data sets are being acquired within the PhD project presented in this thesis. The comprehensive analysis of this unique data set and the implications for the applicability of ERT monitoring on different time scales are presented and discussed for the period between 1999 and 2006 in *publication #1* (chapter 4).

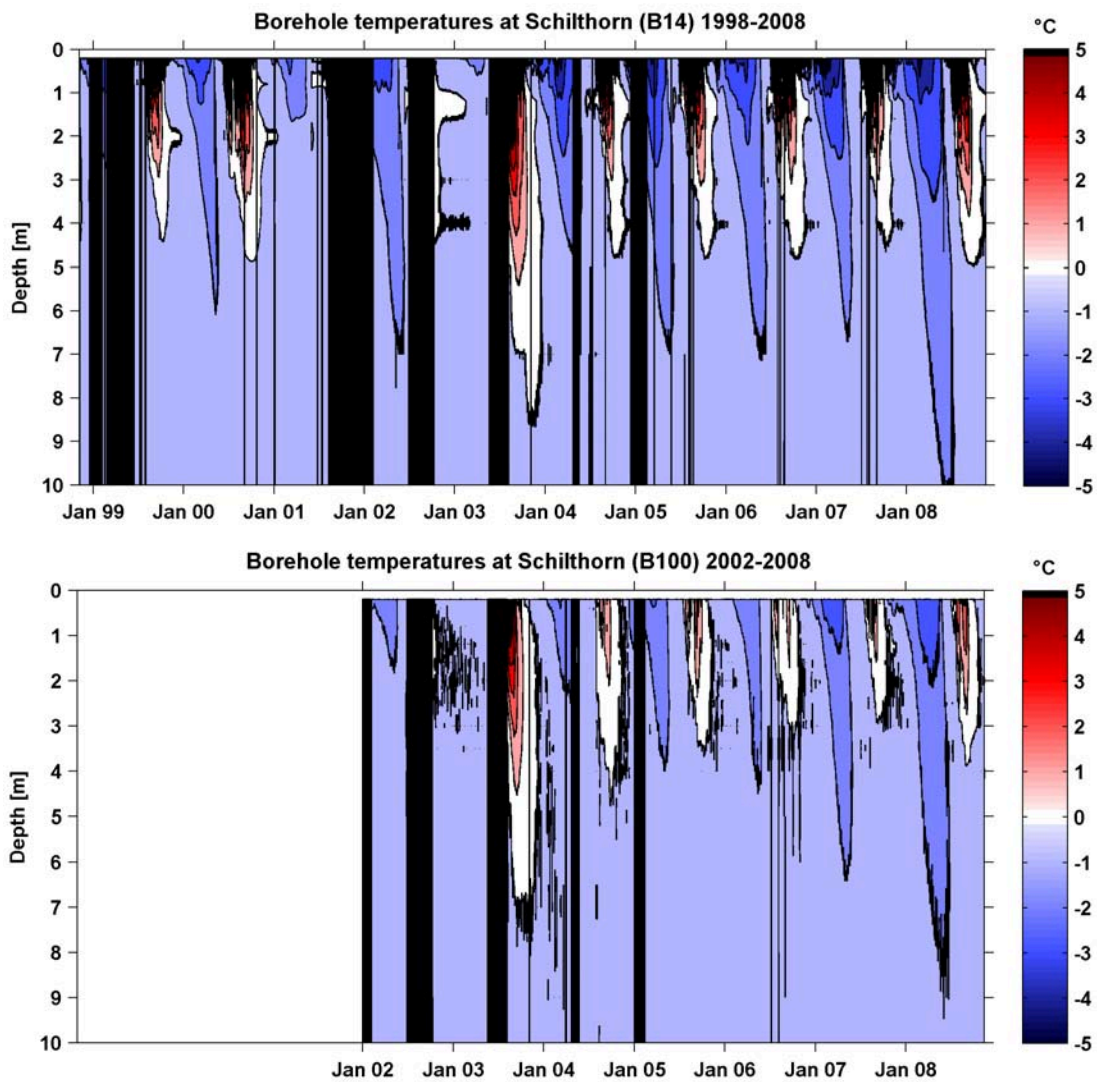


Fig. 3.3: Borehole temperatures at Schilthorn from the 14 m borehole (B14, upper panel) and the 100 m vertical borehole (B100, lower panel) shown as time-depth plot for the uppermost 10 m, respectively. Black vertical bars denote missing data. Data were provided by PERMOS (responsible: J. Noetzli, University of Zurich).

In addition to this relatively small ERTM profile (58 m length), a second ERTM profile of 184 m length was installed in orthogonal direction across the Schilthorn crest in summer 2006 (see Fig. 3.2) to obtain a cross section of the entire Schilthorn crest. Data acquisition was partly done within another diploma project (Krauer 2008) and is contemporaneously managed for both ERTM profiles since summer 2007. First results of the time-lapse ERT data from this vertical profile were analysed in combination with ground temperature measurements and numerical modelling to investigate the 3D thermal regime below the crest (see Noetzli et al. (2008) in Appendix B).

Refraction seismic tomography measurements have been conducted on both ERTM profiles, and RSTM started in August 2006 for the horizontal profile. Two RSTM data sets from summer 2008 are presented and analysed in chapter 7.

3.2 Murtèl rockglacier (Upper Engadine valley)

Murtèl rockglacier is an active rockglacier of about 400 m length and has developed within a small cirque at the foot of a NW exposed talus slope near Piz Corvatsch on the northern slope of the Upper Engadine valley (see Fig. 3.1). Lithology is dominated by granodiorite and schist (Vonder Mühl et al. 2007). A striking feature of this rockglacier is its pronounced ogive-like surface relief with elevation differences between the furrows and ridges of up to 8 m and diameters of the boulders of up to several meters. The rockglacier is supersaturated with ice providing up to 90% ice content (Arenson & Springman 2005). Creep rates are comparatively slow with average surface velocities between 5 and 15 cm/a (Kääb et al. 1998).

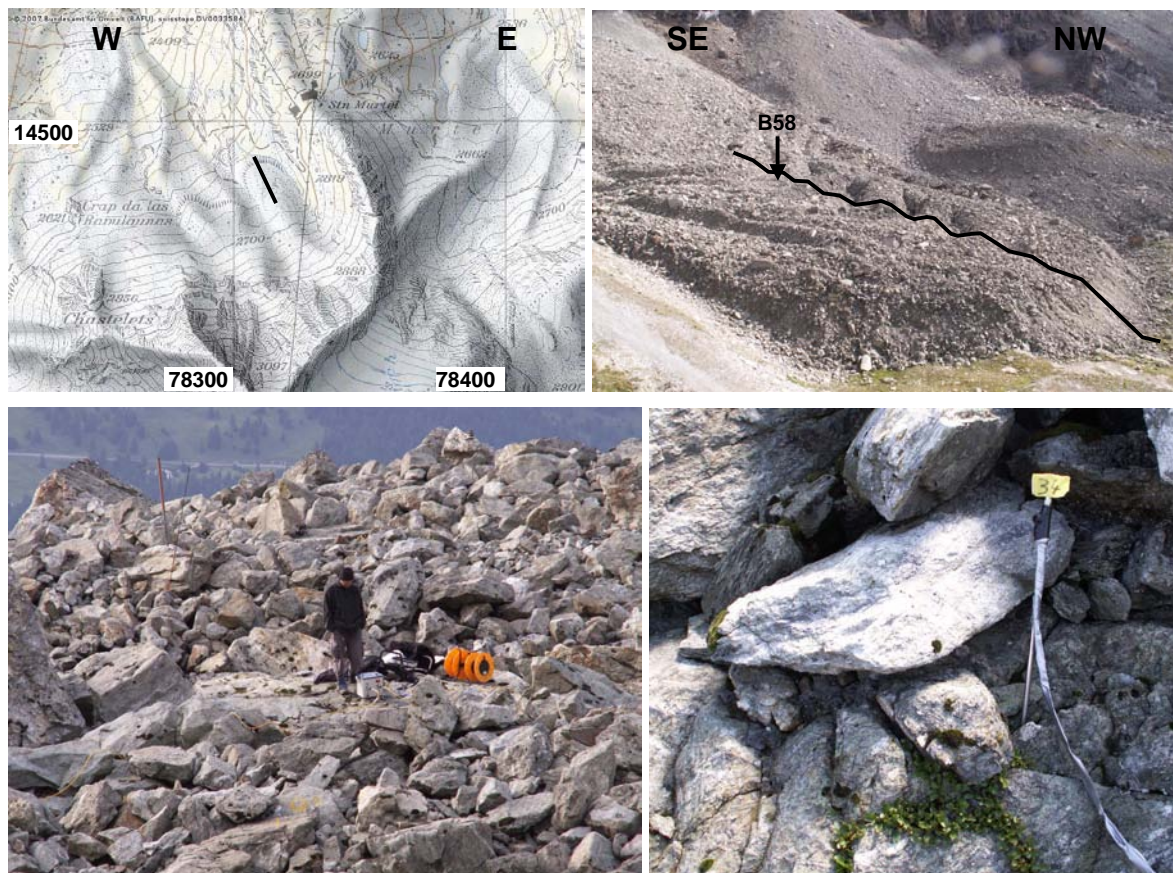


Fig. 3.4: Map (PK25, ©Swisstopo 2007) and photos of the Murtèl rockglacier with the position of the ERTM profile highlighted by a black line.

Murtèl rockglacier is one of the most intensely investigated rockglaciers worldwide (first investigations go back to the early 1970s (e.g. Barsch 1973; Haeberli 1973). Borehole temperatures are recorded since 1987 (Haeberli et al. 1998; Hoelzle et al. 2002; Vonder Mühll et al. 2007) and provide the longest temperature record in Alpine permafrost (see Fig. 3.5). The stratigraphy revealed by borehole drilling and basic results from geophysical data from Murtèl rockglacier are described in detail in *publication #3* (chapter 6), together with data from previous geophysical surveys and photogrammetry.

Across the lower part and the tongue of the rockglacier a longitudinal ERTM profile was installed in August 2005. The position of this profile (highlighted in Fig. 3.4) was chosen to cover previous ERT and RST profiles conducted in 1998 and 2004, respectively (Maurer & Hauck 2007). In addition, a cross profile was measured in August 2006 that intersects the longitudinal profile approximately in the middle (not shown).

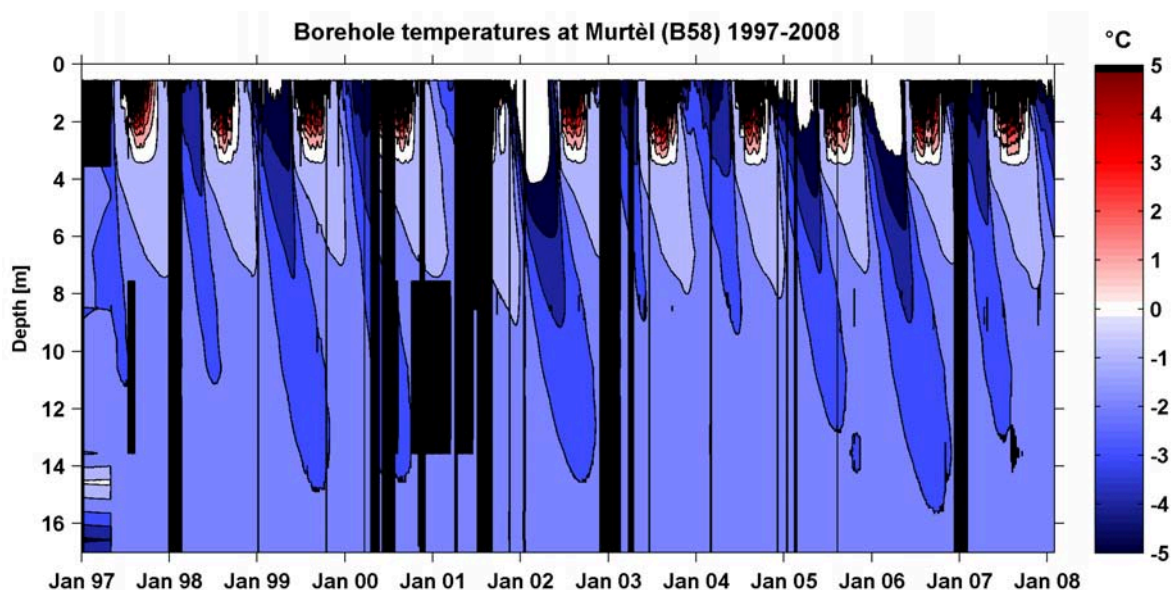


Fig. 3.5: Borehole temperatures at Murtèl rockglacier from the 58 m borehole (B58, only 32 m are equipped with thermistors) shown as time-depth plot for the uppermost 17 m. Black vertical bars denote missing data. Data were provided by PERMOS (responsible: J. Noetzli, University of Zurich).

3.3 The ventilated Lapires talus slope (Valais)

The Lapires site is a vast concave talus slope located near Nendaz at the foot of the Pointe des Lapires summit in the Valais. It is oriented in NE direction and extends over more than 500 m width between 2350 and 2700 m altitude. Lithology consists of metamorphic clasts (mainly gneiss) (Vonder Mühll et al. 2007). The surface was formed by multiple processes, such as avalanches, rockfall, debris flows, solifluction, etc. (Delaloye et al. 2001). Excavations for the installation of two cable car pylons in summer 1998 exposed sediments more or less saturated with ice (Lambiel 1999; Delaloye et al. 2001). The investigations carried out between 1998 and 2006 to map the permafrost distribution and to understand its controlling factors are summarised in *publication #3* in chapter 6.

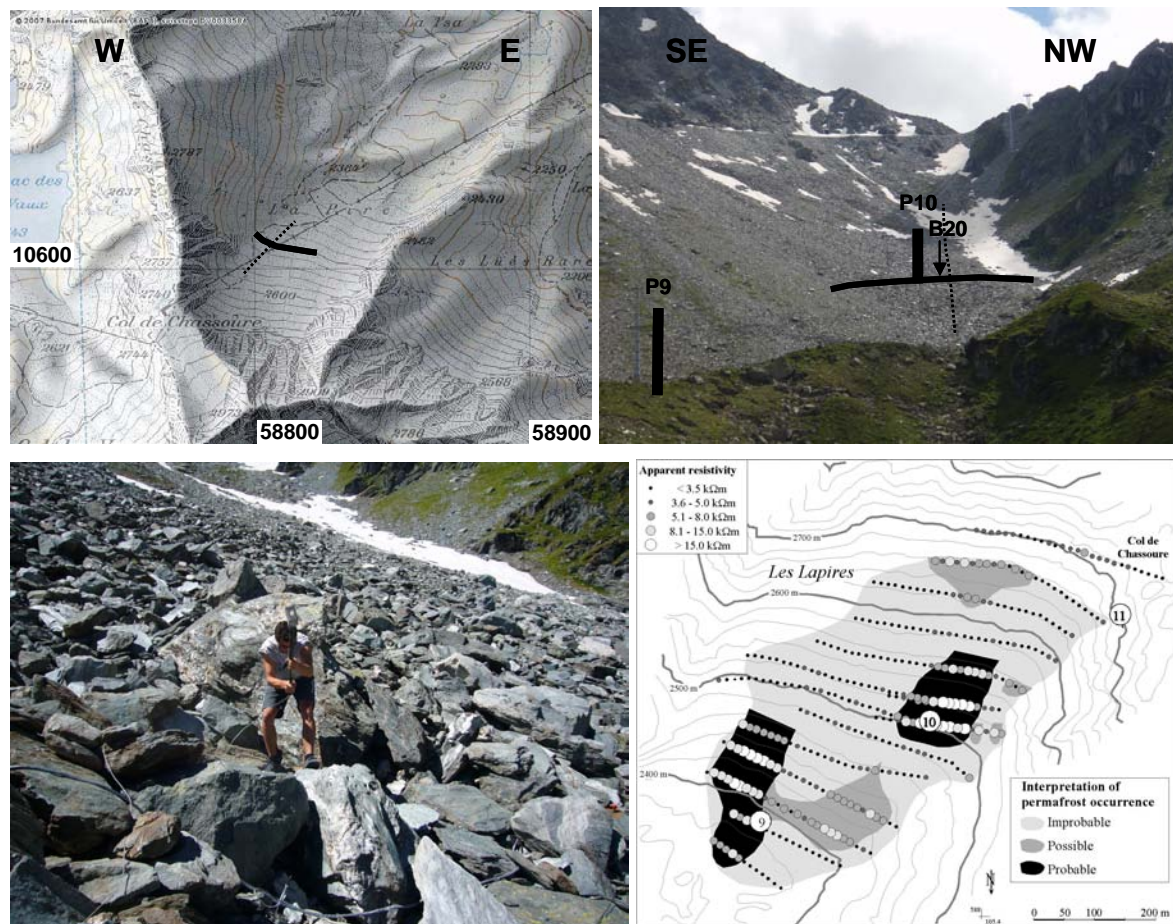


Fig. 3.6: Map (PK25, ©Swisstopo 2007) and photos of the Lapires talus slope with the position of both ERTM profiles (vertical (dashed) and horizontal) highlighted by black lines. The map in the lower right panel shows the permafrost distribution derived from BTS and resistivity measurements by Delaloye (2004).

A borehole (B20) was drilled in 1999 near the pylon P10 (see Fig. 3.6 for position) and subsurface temperatures are recorded within the pylon (since 1998) and in the borehole (since 1999). Temperature evolution since 1998 is illustrated in Fig. 3.7, the thermal regime can be described as temperate (warm) permafrost. According to Delaloye & Lambiel (2005) the existence of permafrost at this site is (at least partly) due to an internal air circulation that contributes to the cooling of the talus slope.

In August 2006 a permanent ERTM profile was installed in horizontal direction traversing the pylon P10 and the borehole (see Fig. 3.6). The profile is in alignment with a previous ERT survey from 1999 (Delaloye et al. 2001). The installation of a second ERTM profile in vertical direction was finished in summer 2008 (in cooperation with D. Abbet and R. Delaloye, University of Fribourg) and further ERT measurements were conducted along additional profiles (pers. communication D. Abbet and R. Delaloye, University of Fribourg) providing a comprehensive data set on the resistivity distribution within the talus slope. RST measurements were conducted along both ERTM profiles in summers 2007 and 2008. Two RSTM data sets from summer 2008 are presented and analysed in chapter 7.

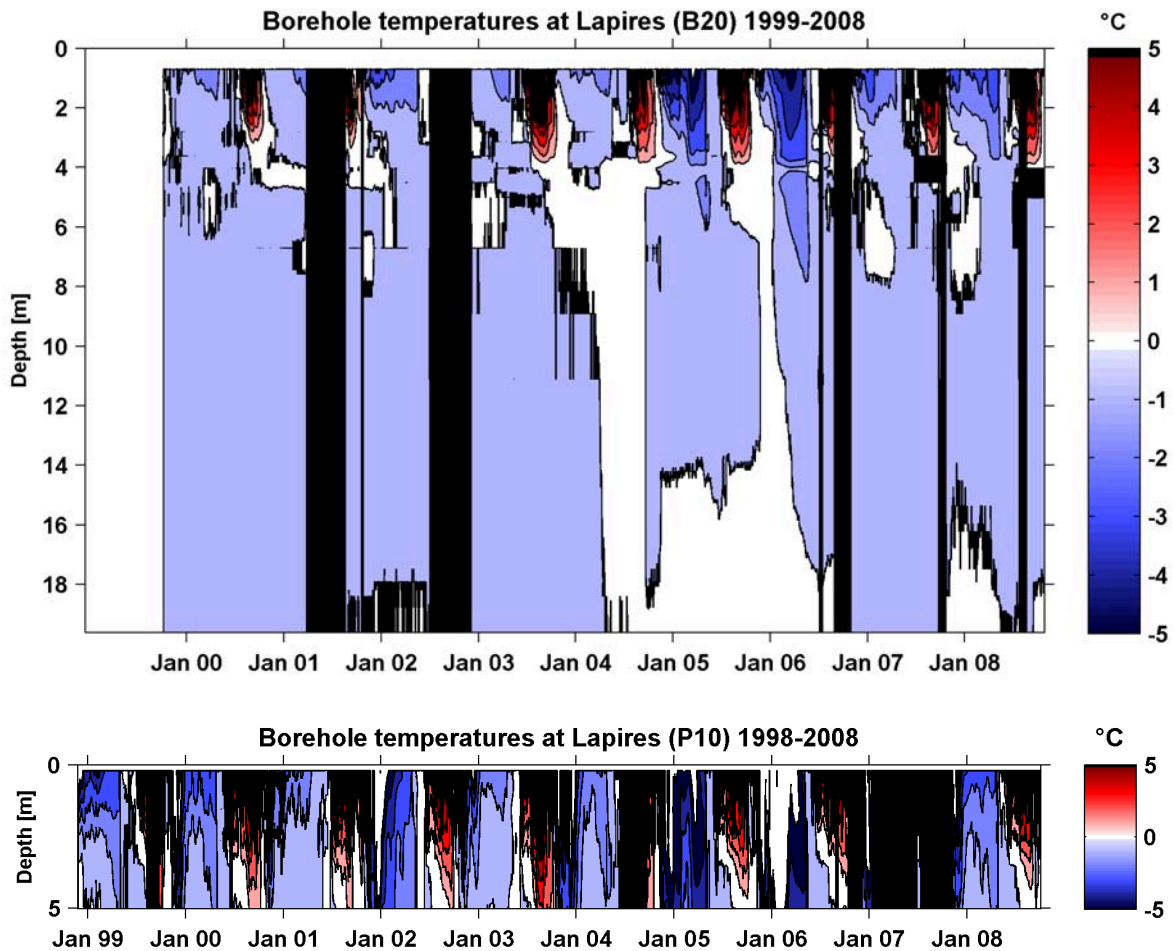


Fig. 3.7: Borehole temperatures at Lapires from the 20 m borehole (B20, upper panel) and the 5 m thermistor chain at the pylon P10 (lower panel) shown as time-depth plot for the uppermost 19.6 m and 5 m, respectively. Black vertical bars denote missing data. Data were provided by PERMOS (responsible: R. Delaloye, University of Fribourg; C. Lambiel, University of Lausanne).

3.4 The rock plateau at Stockhorn (Valais)

The Stockhorn plateau is located on a EW oriented mountain crest between the Gornergrat and the Stockhorn summit, near Zermatt (Valais), and is with 3410 m altitude the highest test site of this study. The small rock plateau extending over ca. 50-100 m width and several hundred meters length separates the steep and glacier-covered northern rock face from the non-glaciated and gently inclined south face (Fig. 3.8). The lithology consists of Albit-Muskowit schists and the surface is characterised by patterned ground that has developed in a thin debris cover. Significant amounts of ground ice could be observed in large ice-filled cracks during construction works of a new ski lift in summer 2007 (see Fig. 3.9). In summer 2000 two boreholes have been drilled on the plateau as part of the PACE project (Harris et al. 2003) that are affected by the strong 3D topography effects of this site (Gruber et al. 2004b): although they are only 30 m apart, the 100 m deep borehole close to the north face exhibits significant colder temperatures than the 17 m deep borehole located close to the southern edge of the plateau (see Fig. 3.10).

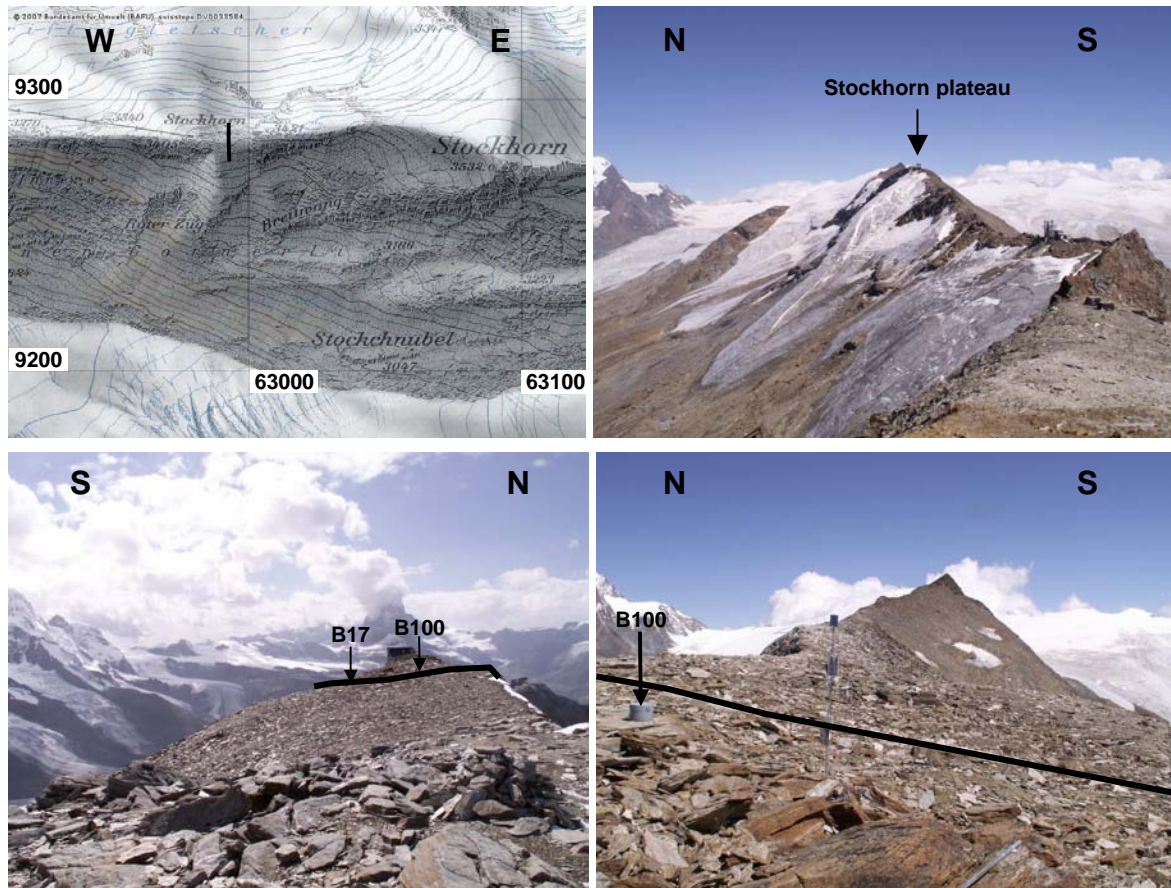


Fig. 3.8: Map (PK25, ©Swisstopo 2007) and photos of the Stockhorn plateau with the position of the ERTM profile highlighted by a black line. Note, that the parts of the profile located on the northern and southern slopes are not visible here.



Fig. 3.9: Ice-filled crack observed close to the monitoring profile at the Stockhorn plateau (Photo: M. Baum 2007).

First ERT surveys were conducted across the plateau by Hauck (2001). The ERTM profile was installed in summer 2005 from the northern edge of the plateau in NS direction 96 m to the south. In summer 2007 the profile was extended by about 12 m into the north face to increase the overall investigation depth of the ERTM profile and to improve the resolution of 3D topography effects in the resistivity distribution. The position of the ERTM profile is indicated in Fig. 3.8 (note, that the photos basically show the 50 m wide plateau and the parts of

the profile extending over the northern and southern slopes are not visible). Selected ERT tomograms from the Stockhorn plateau are presented together with resistivity-temperature relations in *publication #2* in chapter 5.

First RST surveys started in summer 2006, and during an extensive monitoring study in August and September 2007 a high-resolution data set of coinciding ERTM and RSTM measurements was acquired in the framework of two diploma theses (Baum 2008; Klein 2008) in order to analyse the resolution potential of both methods.

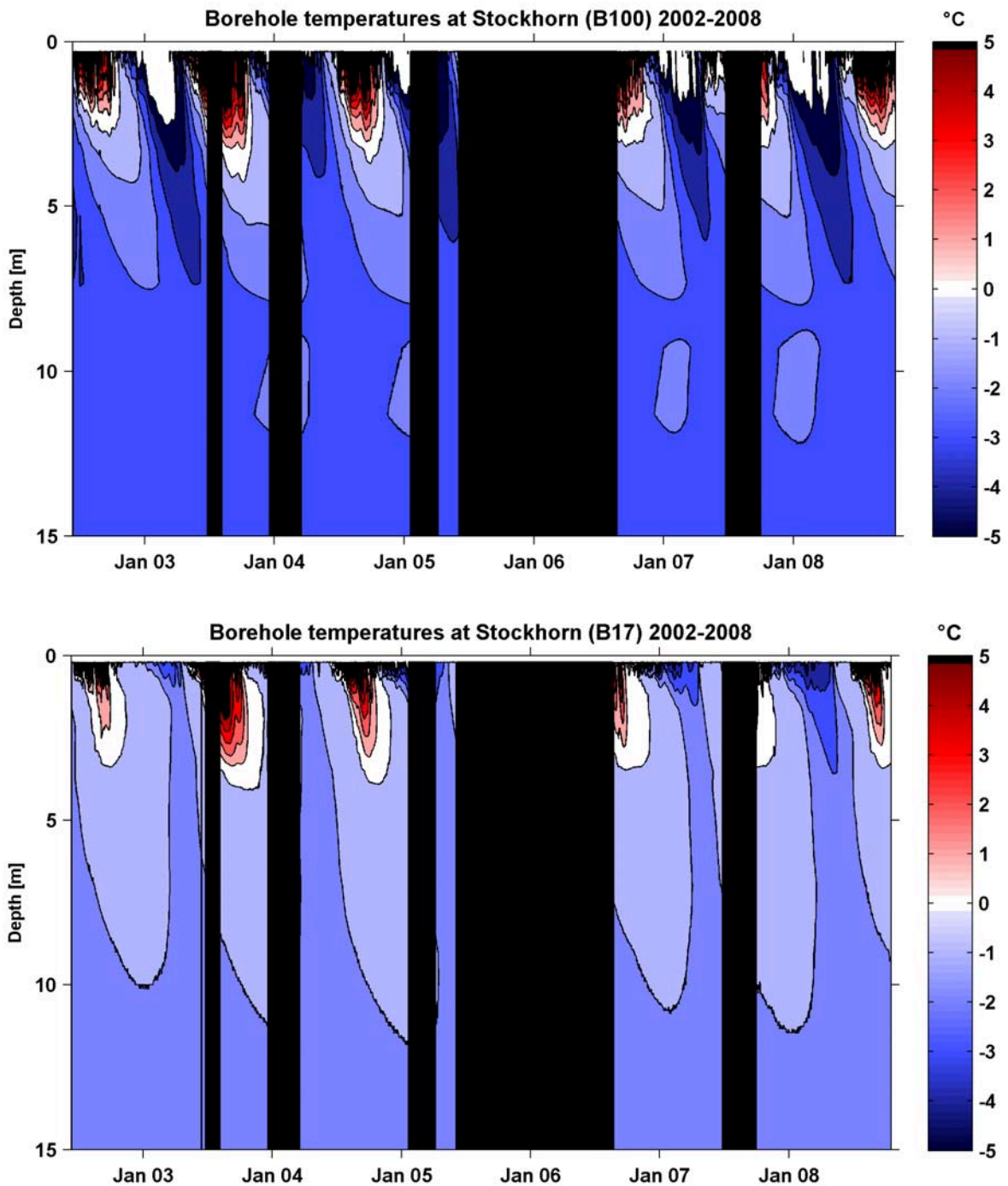


Fig. 3.10: Borehole temperatures at Stockhorn from the 100 m borehole (B100, upper panel) and the 17 m borehole (B17, lower panel) shown as time-depth plot for the uppermost 15 m, respectively. Black vertical bars denote missing data. Data were provided by PERMOS (responsible: M. Hoelzle, University of Fribourg).

Tab. 3.1: Summary of main characteristics of the test sites in this thesis (based on Vonder Mühl et al. 2007).

	Schilthorn	Stockhorn	Lapires	Murtèl
site description	north facing slope beneath summit	rock plateau on a crest	ventilated talus slope	coarse blocky rockglacier
lithology	Limestone schists bedrock covered with several meters debris	Albit-Muskowit schists bedrock covered with 0-1 m debris	Gneiss	Granodiorite, Schist
altitude	2910 m	3410 m	2500 m	2670 m
slope angle/aspect	30° NNE	8° S	25° NE	10° NNW
MAAT	-4.3°C	-5.5°C	0.5°C	-3°C
precipitation	2700 mm	1500 mm	1200-1500 mm	2000 mm
boreholes (drill date)	13.7 m (1998) 100 m (2000) 92 m oblique (2000)	17 m (2000) 98.3 m (2000)	19.6 m (1998)	58 m (1987) 21 m (2000) 62 m (2000)
other measurements	air temperature relative humidity net radiation snow depth wind speed/direction BTS/GST	air temperature relative humidity net radiation snow depth wind speed/direction BTS/GST	air temperature shortwave radiation reflected shortwave radiation BTS/GST	air temperature surface temperature relative humidity net radiation snow depth wind speed/direction BTS/GST
comments	temperate (warm) permafrost	-	temperate (warm) permafrost, internal air circulation	-
ERTM				
location	cross profile in N-slope	N-S-profile across plateau	cross profile	longitudinal profile
# of electrodes	30	55	43	48
spacing	2 m	2 m	4 m	5 m
profile length	58 m	94 m	168 m	235 m
investigation depth	10 m	15 m	25 m	40 m
ERTM since (# of measurements)	8/1999 (130)	8/2005 (26)	8/2006 (19)	8/2005 (16)
previous measurements at same location	8/1998 (Hauck 2001)	8/1998 (Hauck 2001)	8/1999 (Delaloye 2004)	7/1998 (Hauck 2001)
RSTM				
# of geophones	24	24	24	24
spacing	2 m	2/4 m	8 m	10 m
profile length	46 m	46/92 m	184 m	230 m
RSTM since (# of measurements)	8/2006 (5)	8/2006 (14)	6/2007 (3)	7/2007 (1)
previous measurements at same location	-	-	-	Maurer & Hauck (2007)

PART II – PUBLICATIONS

Chapter 4

Monitoring mountain permafrost evolution using electrical resistivity tomography: A 7-year study of seasonal, annual, and long-term variations at Schilthorn, Swiss Alps. *Journal of Geophysical Research (in press)*

Chapter 5

A geoelectric monitoring network and resistivity-temperature relationships of different mountain permafrost sites in the Swiss Alps. *Proceedings of the 9th International Conference on Permafrost, Fairbanks, Alaska (2008)*

Chapter 6

Applicability of ERT monitoring to coarse blocky and ice-rich permafrost landforms. *Permafrost and Periglacial Processes (2008)*

Chapter 7

unpublished: On the potential of time-lapse refraction seismic for the detection of changes in ground ice content. *To be submitted to The Cryosphere*

4 Monitoring mountain permafrost evolution using electrical resistivity tomography: A 7-year study of seasonal, annual and long-term variations at Schilthorn, Swiss Alps

Citation

Hilbich, C., Hauck, C., Hoelzle, M., Scherler, M., Schudel, L., Völksch, I., Vonder Mühl, D. & Mäusbacher, R. 2008. Monitoring mountain permafrost evolution using electrical resistivity tomography: A 7-year study of seasonal, annual, and long-term variations at Schilthorn, Swiss Alps. *Journal of Geophysical Research* **113**: F01S90.

This paper presents a comprehensive and unique data set from geoelectric monitoring at a mountain permafrost site for 7 years¹. The data set is systematically evaluated regarding the reliability of observed changes on different time scales, and the resistivity changes are interpreted in terms of their significance for permafrost evolution. A special focus is laid on the response to the heat wave during summer 2003.

Main findings

- ▷ The subzero temperature dependence of electrical resistivity is directly associated with the content of ground ice and unfrozen water.
- ▷ Analysis of apparent resistivities revealed a good overall data quality and a resolution potential for temporal changes on the order of a few days.
- ▷ Analysis of time-lapse inversion models revealed resistivity changes consistent with subsurface temperature changes, but also changes not conforming to long-term temperature evolution, especially in relation to the hot summer of 2003. The former changes are attributed primarily to seasonal variations in the permafrost regime, whereas the latter are believed to indicate increases in the content of unfrozen water due to substantial ground ice degradation as a consequence of the 2003 heat wave. In contrast to subsurface temperatures, resistivity changes indicate a sustained degradation for several years, which is therefore more severe than that determined by thermal monitoring.
- ▷ The discrepancy between temperature and resistivity evolution is interpreted to be caused by a limited availability of unfrozen water (prohibiting refreezing to the previous amount of

¹ In Appendix A the time series was extended for the full observation period (until 2008) for selected figures.

ice in the following winter) or by changes in materials characteristics, e.g. pore volume change by subsidence.

- ▷ The identification of sustained ground ice degradation shows the potential of a combined thermal and geoelectric monitoring approach compared to thermal monitoring only. The study therefore not only confirms the general applicability of ERTM to the assessment of long-term ground ice degradation but also shows additional benefits arising from ERTM.

Monitoring mountain permafrost evolution using electrical resistivity tomography: A 7-year study of seasonal, annual, and long-term variations at Schilthorn, Swiss Alps

C. Hilbich,¹ C. Hauck,² M. Hoelzle,³ M. Scherler,³ L. Schudel,³ I. Völksch,^{3,4}
D. Vonder Mühl,⁵ and R. Mäusbacher¹

Received 22 March 2007; revised 20 July 2007; accepted 27 September 2007; published 26 January 2008.

[1] A combined geophysical and thermal monitoring approach for improved observation of mountain permafrost degradation is presented. Time-lapse inversion of repeated electrical resistivity tomography (ERT) measurements allows both active layer dynamics and interannual permafrost conditions to be delineated. Analysis of a comprehensive ERT monitoring data set from a 7-year study at Schilthorn, Swiss Alps, confirmed the applicability of ERT monitoring to observations of freezing and thawing processes on short-term, seasonal, and long-term scales. Long-term resistivity changes were evaluated on the basis of seasonal resistivity variations showing an annual cycle with high resistivities in frozen and low resistivities in unfrozen state. One important result is the detection of a sustained impact of the extraordinarily hot European summer of 2003 on the permafrost regime, which is more severe than previously assumed from borehole temperatures. Combined analyses of ERT monitoring and borehole temperature data revealed substantial ground ice degradation as a consequence of the 2003 summer, which did not recover in the following years despite suitable subsurface temperature conditions. Resistivity changes that are nonconforming to long-term temperature evolution are attributed to the limited availability of liquid water and/or changes in material characteristics (e.g., pore volume changes as a result of subsidence).

Citation: Hilbich, C., C. Hauck, M. Hoelzle, M. Scherler, L. Schudel, I. Völksch, D. Vonder Mühl, and R. Mäusbacher (2008), Monitoring mountain permafrost evolution using electrical resistivity tomography: A 7-year study of seasonal, annual, and long-term variations at Schilthorn, Swiss Alps, *J. Geophys. Res.*, 113, F01S90, doi:10.1029/2007JF000799.

1. Introduction

[2] Climate-induced warming of the near-surface atmospheric layer and a corresponding rise of ground temperatures will lead to substantial changes in the water and energy balance of regions underlain by permafrost. The increased frequency of extreme weather periods, such as the hot summer of 2003 in the European Alps [Schär *et al.*, 2004; Intergovernmental Panel on Climate Change (IPCC), 2007] and associated slope instabilities [Harris *et al.*, 2001a; Gruber *et al.*, 2004a], makes monitoring of mountain permafrost evolution (with a high resolution in space and time) more and more important.

[3] Since permafrost is a phenomenon primarily defined thermally, common observation techniques are based on thermal aspects of permafrost evolution. As in existing European (Permafrost and Climate in the 21st Century, PACE21 [Harris *et al.*, 2001b, 2003]) and Swiss (PERMOS [Vonder Mühl *et al.*, 2004]) permafrost monitoring networks, subsurface temperature data can be obtained from a network of shallow and deep (down to 100 m) boreholes. If the geotechnical impact (slope instability) as well as modeling of permafrost distribution and evolution are to be taken into account, not only temperature changes but also ground ice content play an important role in permafrost observation [Harris *et al.*, 2001a, 2001b]. Potential slope instability strongly depends on subsurface material characteristics, such as porosity, crack size and orientation, hydraulic properties, and the fractions of pore space filled with air, ice, and unfrozen water [Arenson *et al.*, 2002, 2003]. Consequently, the sensitivity to climate change of mountain permafrost is influenced greatly by the amount of ice present within different permafrost occurrences [Harris *et al.*, 2001a; Luetsch and Haeblerli, 2005; Haeblerli *et al.*, 2006]. However, except for laboratory analyses of field samples obtained in boreholes [e.g., Arenson *et al.*, 2003;

¹Geographical Institute, Friedrich Schiller University of Jena, Jena, Germany.

²Institute for Meteorology and Climate Research, Forschungszentrum Karlsruhe, University of Karlsruhe, Karlsruhe, Germany.

³Geographical Institute, University of Zurich, Zurich, Switzerland.

⁴Now at Swiss Federal Institute for Forest, Snow and Landscape Research, Birmensdorf, Switzerland.

⁵SystemsX, ETH Zurich, Zurich, Switzerland.

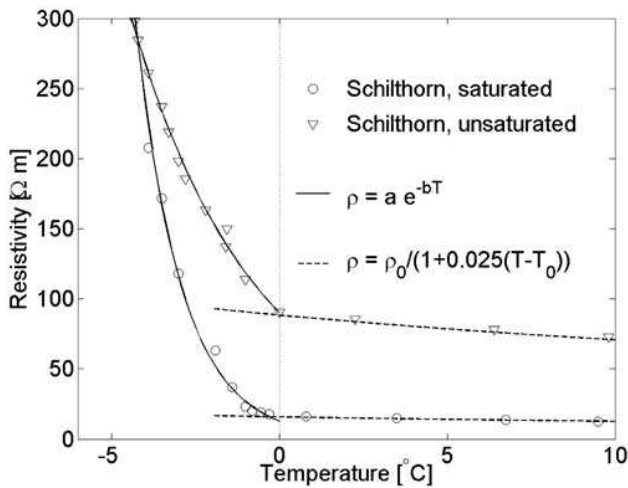


Figure 1. Temperature dependence of electrical resistivity in a sample from Schilthorn, Swiss Alps, for different water contents. The solid line describes the exponential relation between resistivity, ρ , and temperature, T , for temperatures below the freezing point (a and b are constants), while the dashed line describes the relation for unfrozen conditions (modified after Hauck *et al.* [2005]) (Copyright John Wiley & Sons Limited. Reproduced with permission).

Arenson and Springman, 2005], the composition of subsurface material can be inferred only from indirect geophysical investigations [Musil *et al.*, 2002; Maurer and Hauck, 2007]. Hence Haeberli *et al.* [2006] emphasize the strong need for detailed subsurface information at mountain permafrost sites, especially as the distribution and amount of ground ice can be highly variable.

[4] To predict successfully the evolution of ground temperatures in a changing climate and, at the same time, analyze its potential impact, surface and subsurface monitoring techniques must be extended from temperature monitoring at point locations (boreholes) to three-dimensional geophysical monitoring of freezing and thawing processes. Surface-based geophysical methods constitute a cost-effective and noninvasive alternative in determining three-dimensional fields of subsurface properties, such as ice content, porosity, unfrozen water content, and type of lithospheric material (for a review, see Scott *et al.* [1990], Hauck and Vonder Mühll [2003a], and Maurer and Hauck [2007]). Because of the indirect nature of geophysical measurements, subsurface structures and processes remain unchanged, which makes geophysical methods suitable for monitoring purposes [Suzuki and Higashi, 2001; French *et al.*, 2002; Hauck, 2002]. In principle, a variety of geophysical methods can be used to monitor changes by repeated measurements with the same sensor positions and survey geometry. Electrical resistivity tomography (ERT) provides a remarkable potential, as measured electrical resistivity is a temperature-dependent signal [e.g., Telford *et al.*, 1990]. This temperature dependence is most pronounced for temperatures below the freezing point, indicating the close relation between the fraction of pore space filled with unfrozen water and electric conduction (Figure 1) (discussed in detail by Hauck [2001]). During freezing, measured electrical resistivity will rise exponentially as

unfrozen water content within a substrate decreases. Thus the electrical resistivity is sensitive to phase changes between water and ice (which are also influenced by other effects, such as impurities) and therefore is directly associated with the ice content of the subsurface material.

[5] Its high sensitivity to unfrozen water content makes ERT possibly the first choice in permafrost monitoring with respect to ice content. ERT monitoring techniques have become more and more popular in seasonal hydrological applications [Aaltonen and Olofsson, 2002; French *et al.*, 2002; Daily *et al.*, 2004] and tracer and contaminant studies [e.g., Kemna *et al.*, 2002; Slater *et al.*, 2002; Singha and Gorelick, 2006a]. However, in contrast to surface-related processes in permafrost terrain (e.g., frost wedging, frost heave, solifluction [Matsuoka and Humlum, 2003]), no continuously logging geophysical monitoring approach exists to date.

[6] In the summer of 1999, a semiautomatic ERT monitoring system was installed at Schilthorn (Bernese Alps, Switzerland, cf. Figure 2) [Hauck, 2002]. On the basis of a 1-year data set, the author showed that this semiautomatic ERT monitoring approach was able to detect and visualize subsurface freezing and thawing processes on a seasonal basis, i.e., the onset of freezing in autumn, propagation of the freezing front during winter, and thawing of the active layer in summer. However, because of the limited data and the short measurement period, it could not be evaluated, whether the method can also be applied to processes both on very short (days) and longer timescales (interannual variations). Reliable application of ERT monitoring in analyzing long-term (decadal) changes in ice content evolution would allow spatially variable permafrost degradation to be assessed in connection with climate change. This paper presents results of a permafrost monitoring pilot study so far covering 7 years by analyzing the potential of ERT permafrost monitoring on these different timescales.

2. Electrical Resistivity Tomography (ERT)

[7] Direct current resistivity techniques are employed to measure electrical resistance in the subsurface by passing a current between two electrodes and measuring the potential difference between two other electrodes coupled to the ground. Multiplying an appropriate geometric factor, which is a function of the distance between the four electrodes, yields the so-called apparent resistivity, ρ_a , which equals the specific resistivity, ρ_s , solely for homogeneous ground conditions. When a multielectrode array is used for acquiring a set of four-electrode measurements (quadrupoles) with different center points and spacings, a two-dimensional distribution of measured apparent resistivities is obtained (cf. Figure 3). Iterative tomographic inversion of apparent resistivity data finally yields a two-dimensional model of specific resistivities, which represents the true resistivity distribution of the subsurface section [Daily *et al.*, 2004; Loke and Barker, 1995].

[8] Under the assumption that general conditions (lithology, pore space, electrode coupling, etc.) remain constant over several years of observation, measured changes in resistivity basically can be attributed to changes in the unfrozen water content. In the absence of changes in water contents as a result of rain or snowmelt, these resistivity

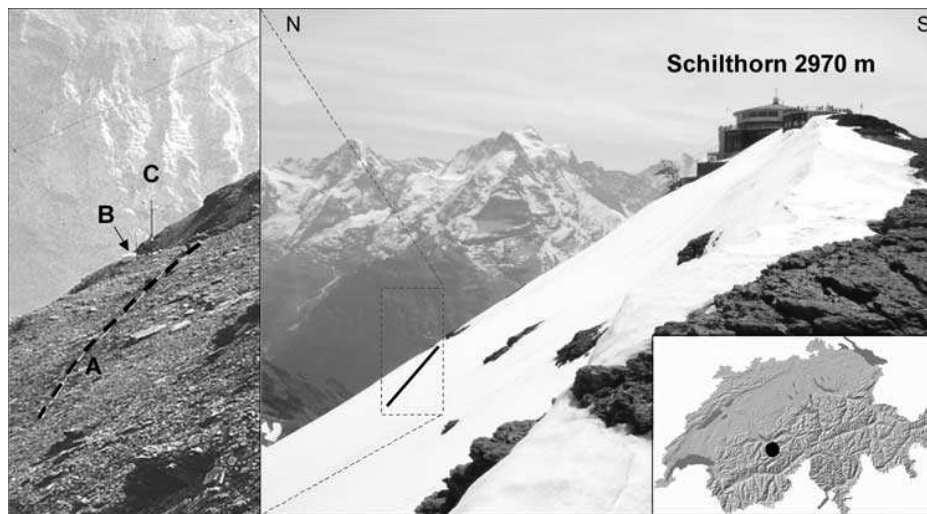


Figure 2. Photo of the field site with locations of the resistivity profile (site A) parallel to the north facing slope, the boreholes (site B), and the meteo station (site C). The location of Schilthorn in the Swiss Alps is indicated in the inset at bottom right.

changes can be related to freezing or thawing processes and subsurface temperature changes, respectively [Hauck, 2002]. In the rather dry high mountain regions of the European Alps, where most precipitation occurs as snow, temporal changes in unfrozen water content due to rain or snowmelt usually can be distinguished from freezing and thawing processes because of their seasonal character, with a peak in late spring and early summer and a rather fast draining of liquid water due to the absence of water keeping

layers in the shallow subsurface [Hauck, 2002]. For most of the year, a resistivity increase can be associated with freezing, and a decrease, with thawing processes. Nevertheless, data interpretation remains difficult, since an increase in resistivity may be due to changes in the contents of ice (freezing) or air (melting followed by draining of unfrozen water). In general, local resistivity data can differ from resistivities resulting from inversion of ERT data collected at the field site because (1) reconstructed tomo-

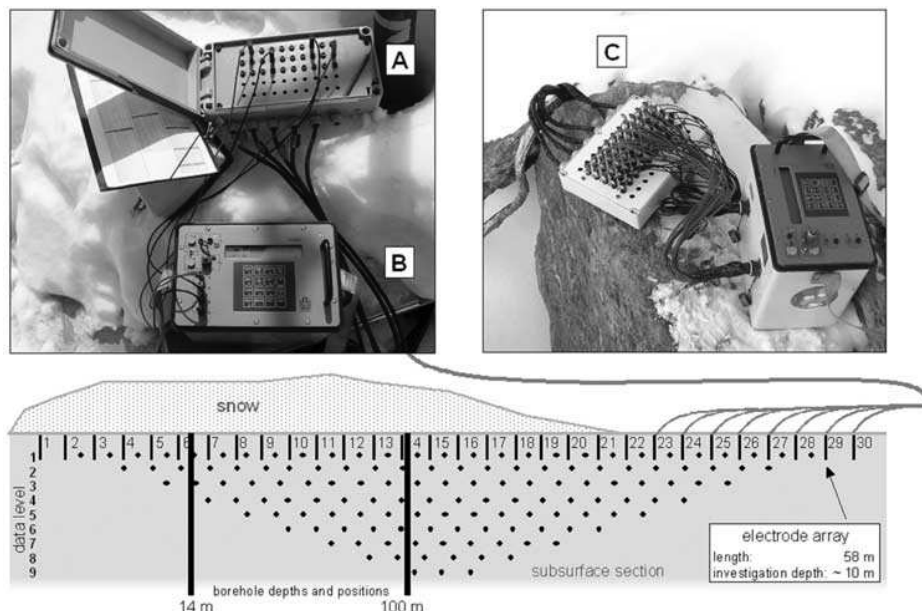


Figure 3. Working principle of the ERT monitoring system operating at Schilthorn: Electrodes are buried in the ground (1 m deep) and are connected to a manual switchbox (marked A) by buried cables. ERT measurement can be performed by connecting any resistivity meter (marked B) to the switchbox with four pin plugs and switching the pin plugs for the quadrupoles of a specific configuration. Optionally, a matching adaptor (marked C) for a defined multielectrode resistivity meter can be used for automatic measurement of the entire configuration.

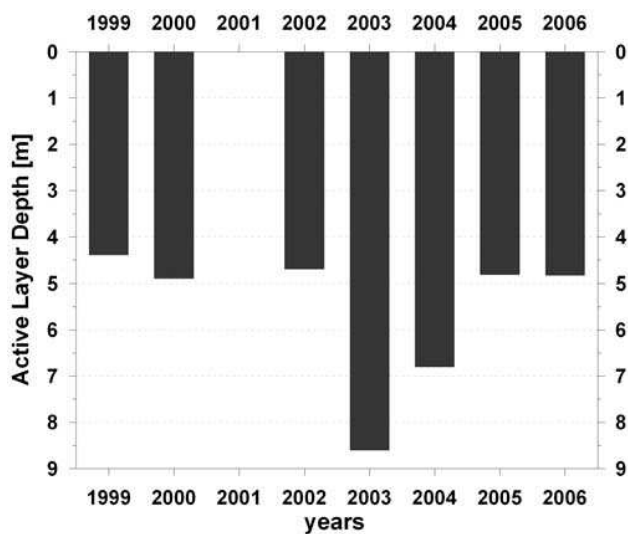


Figure 4. Maximum thickness of the active layer at Schilthorn for the period of 1999–2006 (no data for 2001).

grams are subject to inversion artifacts (e.g., due to extreme gradients between resistive anomalies underlain by conductive anomalies, and vice versa), (2) sensitivity diminishes with the distance from the source electrodes and depends on local and time-dependent resistivity distribution, and (3) inverse models are over parameterized, thus requiring the imposition of smoothing constraints (regularization) to facilitate convergence of the inverse solution [e.g., *Hauck et al.*, 2003; *Hauck and Vonder Mühll*, 2003b; *Singha and Gorelick*, 2006a, 2006b]. In this context, *Day-Lewis et al.* [2005] state that geotomography tends to overpredict the extent, and underpredict the magnitude, of geophysical targets. Further difficulties arise from measurement errors or data gaps in time series, e.g., sporadic failures of electrode coupling, as well as spatial variations in resistivity due to ion content or temperature fluctuations (cf. Figure 1).

[9] Appropriate time sequences can be used to perform so-called time-lapse inversions where the resistivity model obtained from inverting the initial data set is used to constrain inversion of later measurements. By this, percentage change in subsurface resistivity as a function of time is calculated [*Loke*, 1999]. Results of ERT monitoring can be directly linked to changes in frozen and unfrozen water content of the subsurface and therefore to permafrost evolution, thus providing a method complementary to temperature measurements.

3. Field Site

[10] The Schilthorn massif with the summit at 2970 m a.s.l. is located in the Bernese Alps, Switzerland, at the transition between the Prealps in the north and the principal chain of the Bernese Alps in the southeast (Figure 2). The lithology of Schilthorn is dominated by micaceous shales [*Imhof et al.*, 2000], which are deeply weathered on the surface, thus covering the bedrock with a layer of fine-grained debris including sandy and silty material (up to several meters thick) around the whole summit area. Almost no vegetation has developed around Schilthorn summit.

[11] Following some first indications of permafrost (ice lenses) during construction of the Schilthorn summit station between 1965 and 1967 [*Imhof et al.*, 2000], the site was chosen for long-term permafrost observation within the framework of the European PACE project [*Harris et al.*, 2003]. In 1998 and 2000 three boreholes (14 m vertical, 100 m vertical and 100 m inclined) were drilled into the north facing slope approximately 60 m below the ridge to monitor permafrost temperatures at various depths [*Vonder Mühll et al.*, 2004] (see Figure 2). In addition, meteorological data (air temperature, relative humidity, net radiation, snow depth, wind speed/direction) are recorded at the borehole location. Spatially distributed data are collected from measurements of the bottom temperature of snow in winter and ground surface temperatures throughout the year.

[12] According to borehole data, permafrost thickness is at least 100 m, but comparatively warm at temperatures close to 0°C [*Vonder Mühll et al.*, 2000; *Harris et al.*, 2003]. Comparatively thick active layer depths of about 5 m recorded since 1999 also reflect temperate permafrost conditions (cf. Figure 4). The Schilthorn, which is part of the Swiss permafrost monitoring network (Permafrost Monitoring in Switzerland (PERMOS)), can thus be characterized as a site with a substantial/thick occurrence of permafrost, but because of the proximity to critical temperatures near the freezing point, with a pronounced susceptibility to degradation. Also, alpine topography, with its three-dimensional geometry, controls the subsurface thermal field by aspect- and altitude-related climate variables on the surface. This leads to complex three-dimensional patterns of temperature distribution and heat flow within mountain tops, such as Schilthorn. Isotherms are steeply inclined and there are strong lateral heat flows resulting in a heat flux oriented more horizontally through the mountain top than vertically [*Noetzli et al.*, 2007].

[13] Since the impact of global warming in high alpine environments is believed to be most pronounced in permafrost close to melting conditions [*Harris et al.*, 2001a], the Schilthorn is an excellent site for long-term observations of ground ice evolution.

4. ERT Data Acquisition and Data Processing

[14] A permanent semiautomatic ERT monitoring system was installed in the immediate vicinity of the boreholes in 1999 to determine changes in electrical resistivity associated with changes in permafrost evolution [*Hauck*, 2002] (cf. Figure 2). The ERT monitoring system consists of a fixed array of 30 electrodes with a spacing of 2 m, which are connected by buried cables to a manual switchbox where the resistivity meter can be connected for the various quadrupole measurements in a tomographic survey (Figure 3). This permanent setup allows access throughout the year, even in winter, when the electrode array is covered with snow. Using the same Wenner electrode configuration as by *Hauck* [2002], measurements resulting in 135 single data points at nine data levels with a depth of investigation of approximately 10 m (cf. Figure 3) were recorded for each time instance. The electrode array is located on a small terrace roughly 60 m below the crest parallel to the north facing slope, and therefore is not influenced by topography.

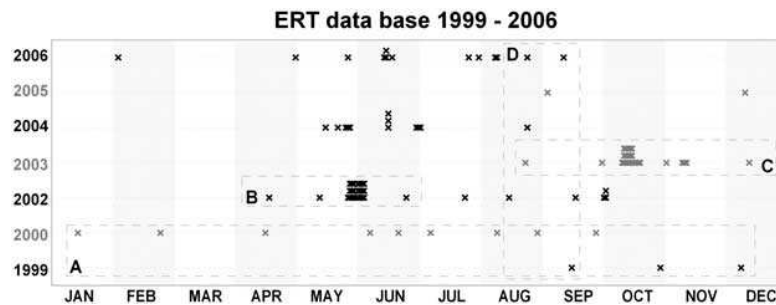


Figure 5. Illustration of the available data set of 110 individual measurements between 1999 and 2006. Two or three vertical dots indicate several measurements a day. Dashed lines delineate data sets chosen for analyzing short-term (marked B and C), seasonal (marked A), and long-term (marked D) variations of electrical resistivity.

[15] Since installation of the ERT monitoring system in September 1999 a data set of 110 individual tomographic measurements was acquired, providing a comprehensive database for analyzing effects of short-term (days to weeks), seasonal (months) and long-term (several years up to decades) variations in electrical resistivity and their implications for ground ice monitoring (Figure 5).

[16] The significance of measured resistivity changes concerning their association with freezing or thawing processes in the subsurface (as opposed to measurement noise or other spurious influences) can be assessed by analyzing the apparent resistivity data on different timescales. In a first step, measured apparent resistivities were averaged for each depth level (as indicated in Figure 3), providing nine horizontal mean values for each measurement date. By this spatial averaging spurious noise and geologic background variations along the profile can be smoothed out (highly erroneous values were removed initially) and the mean change between subsequent measurements can be assessed. Consistent freeze or thaw signals will produce clear trends of resistivity levels increasing or decreasing with time independent of spatial heterogeneities and with a characteristic time lag toward increasing depths. On the other hand, disturbances due to bad electrode-ground coupling or localized water accumulations would result in irregularly high or low values, indicating nonsystematic changes.

[17] After assessing the reliability of the apparent resistivity data sets obtained, the robust inversion scheme [Claerbout and Muir, 1973] of the RES2DINV software [Loke and Barker, 1995] was used to produce 2D specific resistivity tomograms of the subsurface. Compared to the analysis of apparent resistivities referred to above, ERT inversion tomograms often provide less precise indications of temporal changes, because regularization constraints within the inversion scheme may lead to a blurred spatial representation of the changes in resistivity observed. The robust constraint (as opposed to the more smoothing least squares constraint) was chosen to minimize this effect and model more accurately the resistivity changes observed.

[18] To minimize artifacts produced by numerical inaccuracies of individual inversions, the time-lapse inversion method was applied which jointly inverts time sequence data sets on the basis of a common reference model [Loke, 1999]. Time-lapse inversions produce 2-D tomograms illustrating the percentage change in resistivity between two

subsequent data sets. Moreover, a relation between the bulk electrical resistivity of a mixture, pore water resistivity, its porosity and saturation, the so-called Archie's law [Archie, 1942], allows the temporal resistivity change to be attributed to the percentage desaturation of the subsurface material, thus giving a first approximation of the amount of freezing or thawing between two measurement dates.

[19] A potential source of uncertainty lies in choosing an appropriate convergence criterion for the iterative inversion process. Inversions of the data sets typically converge after 3–5 iterations, indicated by a change in RMS error between consecutive iterations of less than 5%. However, sometimes the choice between two iterations as the “final” result is difficult to make. Even though, under Schilthorn conditions, this error source usually accounts for less than 1%, resistivity changes of less than 5% should not be overinterpreted [Hauck and Vonder Mühll, 2003b].

5. Results

5.1. Analysis of Borehole Temperatures

[20] Borehole temperatures are recorded in three boreholes 14 and 100 m deep, respectively. Figure 6 shows the borehole temperatures observed for the two vertical boreholes located within the ERT profile (for positions, see Figure 3). Although the distance between the boreholes is only 15 m, the temperature records differ remarkably in terms of amplitude within the upper few meters. However, observations and model studies can explain this feature as being due to higher moisture contents in the shallow subsurface near the 100 m borehole because of preferential water flow paths from the upper slope, whereas the 14 m borehole is located on a small plateau. As latent heat transfer during phase changes between frozen and unfrozen water as well as evaporation attenuate overall temperature changes due to atmospheric forcing, the higher water content leads to attenuated temperature amplitudes in the 100 m borehole compared to the 14 m borehole. The differences in the amounts of water in the active layer are also reflected in different zero curtain lengths for the two borehole sites. Despite these spatial inhomogeneities, seasonal temperature changes are consistent and reflect the delayed response of subsurface temperatures to atmospheric forcing as a function of depth. Although there are a few data gaps masking the complete temperature pattern, the extra-

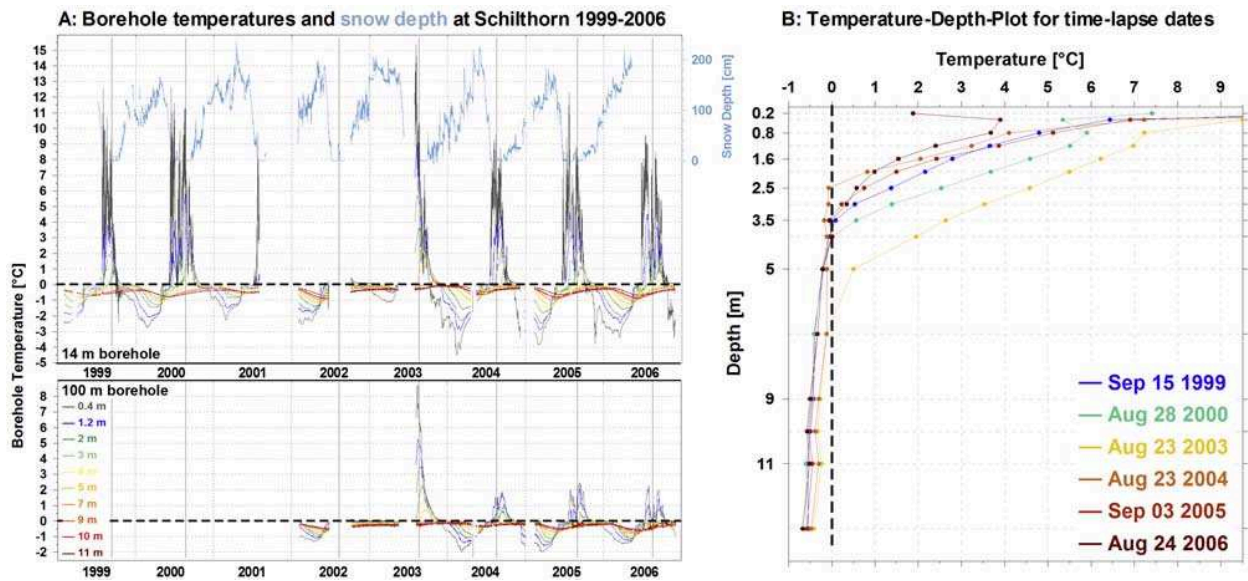


Figure 6. Borehole temperatures in 1999–2006. (a) Borehole temperatures plotted for both (top) the 14 m and (bottom) the 100 m boreholes for all thermistors covering the investigation depth of the ERT profile. The top blue graph marks snow depths. The gray vertical lines indicate measurement dates used for time-lapse inversion (see Figure 10). (b) Temperature-depth plots for the respective time-lapse measurement dates. For clarity, temperatures above 9.5°C are not shown.

ordinary role of the summer of 2003 is clearly visible in the data. This will be considered in detail in the context of ERT measurements outlined in section 6.

5.2. Analysis of Apparent Resistivity Values

[21] Apparent resistivity data of all surveys were analyzed for four different timescales (daily, monthly, seasonal and annual, Figure 7). Figure 7a illustrates an example of mean

resistivity change for each data level during nine days in October 2003 with up to three measurements a day. Daily fluctuations are small (a pronounced daily cycle is not expected to be present in October). However, a slight but distinct increase in resistivity is observed for all data levels. These data are highly reproducible in terms of a monotonous increase with time and yielding a total difference of approximately 50 Ωm in nine days, which is 5% of the

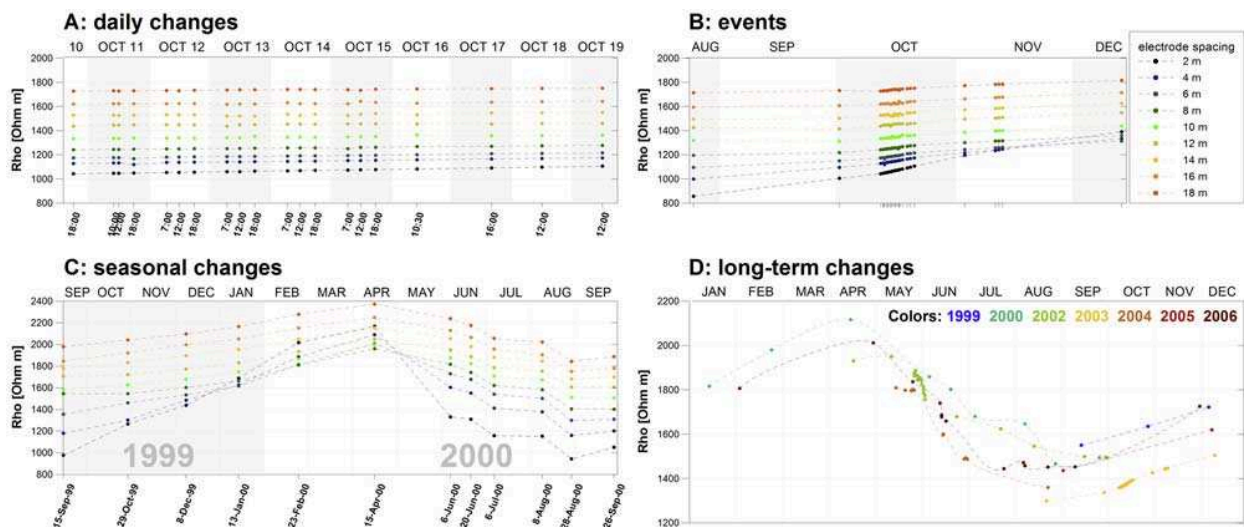


Figure 7. Illustration of apparent resistivity data for various timescales indicated in Figure 5. Timescales are (a) daily scale from 10–19 October 2003, (b) event scale (freezing period from October to December 2003), and (c) seasonal scale (quasi-monthly changes from September 1999 to September 2000). Figures 7a–7c show mean values per data level (cf. Figure 3). Colors mark different data levels, with upper levels coinciding with narrow electrode spacing shown in black and blue and lower levels shown in red. Also shown is (d) the bulk apparent resistivity (one mean value for the full profile) displayed as an annual cycle for the whole period of observation. Colors mark different years.

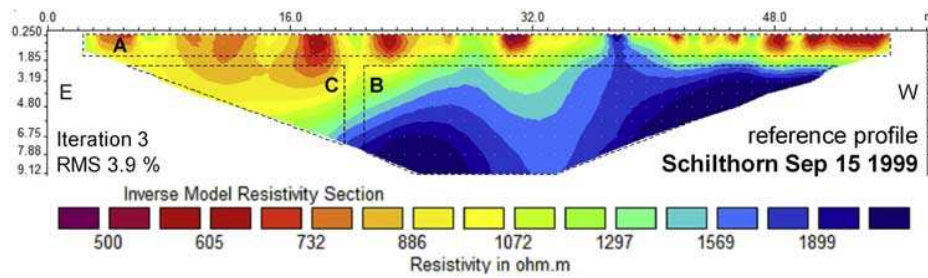


Figure 8. ERT inversion model results for the reference profile of 15 September 1999.

absolute resistivity values observed, thus proving the significance of small-scale resistivity changes recorded within a few days.

[22] With respect to the associated seasonal context, namely freezing of the active layer in early winter, rising values in Figure 7a document the onset of the freezing process, which intensifies in November and December, as illustrated in Figure 7b. On this monthly scale, a delayed response of deeper layers to temperature forcing on the surface is visible. The advancing freezing front is reflected in an accelerated increase in near-surface resistivities compared to deeper parts of the profile, which is in good agreement with borehole temperatures (see section 5.3).

[23] On a seasonal scale, the advancing freezing front in late winter (increasing resistivity) as well as the active layer melting in summer (decreasing resistivity) can be observed by quasi-monthly measurements between September 1999 and September 2000 (Figure 7c, discussed in more detail by Hauck [2002]). This seasonal scale also illustrates a changing variability of measured resistivities with depth over the year, variability being twice as high in late summer as in late winter because of low resistivities within the active layer. Seasonal changes over a whole year (see Figures 7c and 7d) are characterized by minimal resistivities in the active layer in late summer, followed by a distinct increase beginning in late autumn and peaking in spring, and decreasing resistiv-

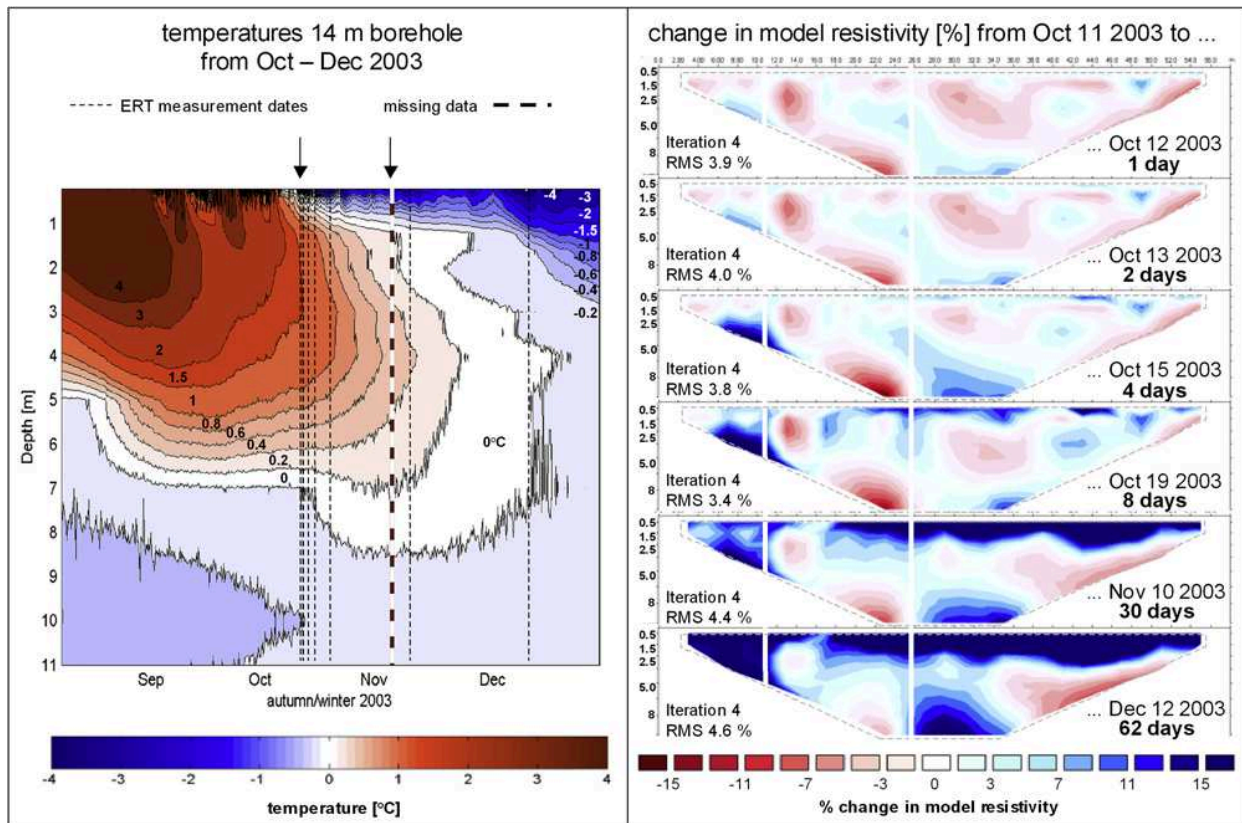


Figure 9. (left) Borehole temperatures and (right) percentage change of specific resistivity between October and December 2003. Borehole temperatures are plotted for the 14 m borehole as isotherms for equal temperatures for the investigation depth of the ERT profile. Note that contour line spacing is decreased at around 0° for clarity. Dashed vertical lines indicate the dates of measurements used for time-lapse inversion. Borehole locations within the ERT profile are marked by white vertical lines.

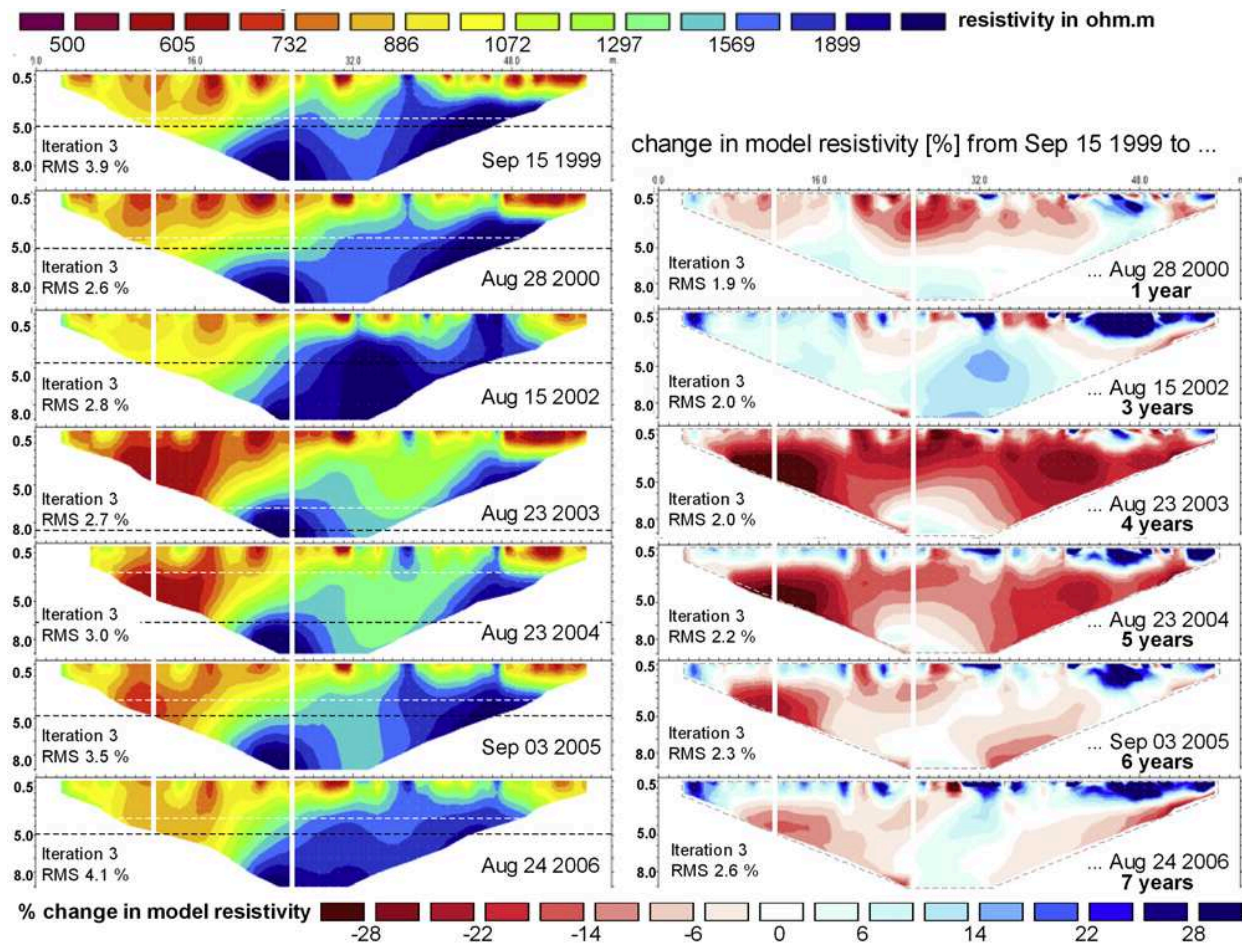


Figure 10. Tomograms of (left) the respective midsummer dates for 1999–2006 and (right) percentage change in specific resistivity within years (1999–2006). Positions of the boreholes (14 m left, 100 m right) within the ERT profile are marked by white vertical lines. Depths of active layers are marked both for the measurement date (white dashed line) and for the maximum thickness of the active layer (black dashed line).

ities as a consequence of snowmelt and the active layer thawing in summer. This pattern proceeds with some delay at greater depths.

[24] Finally, displaying each data set with only one mean resistivity value for the full profile on an annual scale, allows a long-term comparison of all measurements to be made (Figure 7d). Although the lack of data for 2001 and the absence of data for the winter months of nearly all years observed offers but incomplete insights into long-term trends of resistivity change, pronounced differences between bulk resistivities in the respective years can be seen. Especially the exceptionally warm summer of 2003 (yellow) in Central Europe, with mean summer (June, July, August) temperatures exceeding the 1961–1990 mean by $\sim 3^{\circ}\text{C}$, and the 1864–2000 mean by 5.1°C [Schär *et al.*, 2004], is reflected in the lowest values recorded since 1999.

[25] Even though simple averaging of apparent resistivities helps to evaluate data quality and illustrate the significance of the data set for permafrost monitoring purposes, data inversion is necessary for reliable and spatially differentiated assessment of freezing and thawing processes. This will be addressed in the next section.

5.3. Analysis of Time-Lapse Inversion Models

[26] Data inversion of selected reference profiles was carried out as a prerequisite for time-lapse inversions. Figure 8 shows the inverted reference profile of September 1999 to illustrate subsurface resistivity distribution. The profile can be separated into a heterogeneous surface zone (zone A), a resistive zone in the western part (zone B), and a less resistive zone in the eastern part at greater depth (zone C). According to Hauck [2001], who conducted additional geophysical surveys to characterize the field site, the more highly resistive region corresponds to firm bedrock, while the region with lower resistivities is associated with more strongly weathered material.

[27] On the basis of another reference profile of 11 October 2003, Figure 9 shows the tomograms of a time series of six subsequent surveys extending into the freezing period between October and December 2003. On the first two days, resistivity changes by less than $\pm 5\%$, which is close to the measurement uncertainty as characterized, e.g., by the root-mean-square error of inversion, which varies between

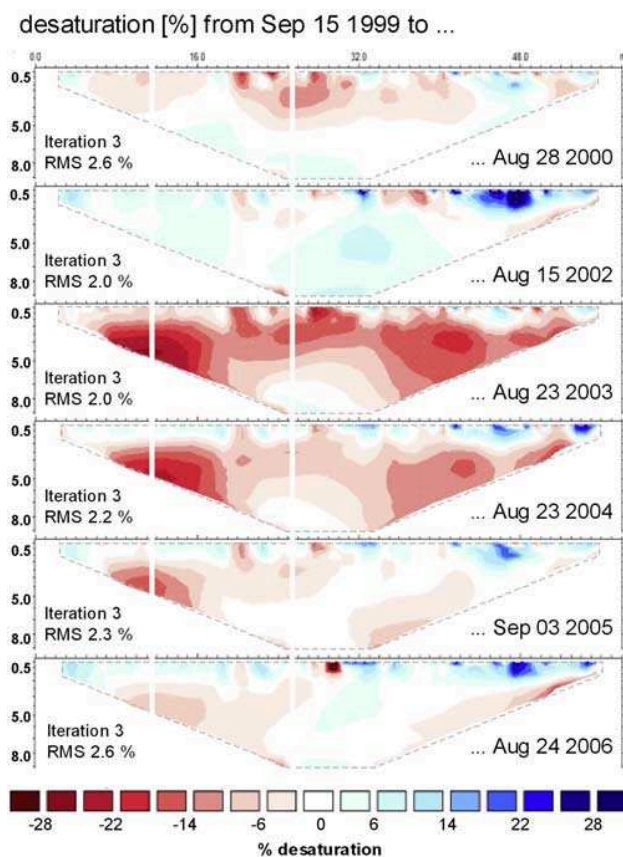


Figure 11. Percentage change in saturation for several years (1999–2006) on the basis of the reference model in September 1999.

3% and 5%. Nevertheless, the anomaly structures displayed seem to be consistent in reproducibility over several days.

[28] On the fourth day, a distinct blue colored region representing a resistivity increase of 15 to 40% (based on the reference profile) begins to develop on the surface and increases in thickness with time. This resistivity increase reflects the advance of the freezing front from the surface, starting in late autumn and approaching deeper parts of the profile in the winter. Comparison with the temperature measurements in Figure 9 shows surprisingly good agreement in time and depth. According to the borehole data, the ground surface in the eastern part of the profile (14 m borehole) was already frozen at the beginning of the time sequence while the central part (100 m borehole) still exhibited positive temperatures. Similarly, the time-lapse tomograms show only little change in the already frozen eastern surface region compared to the distinct resistivity increase in the central and western surface regions of the profile.

[29] Unlike short-term variations over several weeks, which are limited to shallow depths, long-term variations of specific resistivities over several years are more pronounced in the deeper parts of the profile. Figure 10 shows results of time-lapse inversion for measurements at comparable dates in midsummer (mid-August to mid-September) over a period of 7 years, based on the reference profile of 15 September 1999 (Figure 8). No ERT data are available for

2001. Annual changes in resistivity can be compared only if there are comparable data sets; that is, the measurement dates must be representative of the period of observation to preclude seasonal variations in the signals compared. The data set available offers but a limited choice for covering the whole period of observation, as the measurement dates of the data set stem from several independent case studies performed over the years and were not obtained on a regular basis. Nevertheless, except for 2001, special attention has been devoted to regular measurements in midsummer, i.e., the period from mid-August to mid-September, to permit a long-term study of permafrost evolution to be conducted. Figure 7d indicates this midsummer period to be characterized by the lowest bulk resistivity of the profile of the year, thus providing an appropriate time for interannual comparison.

[30] Apart from minor anomalies near the surface, the greatest variations occur at depths of 3 m and more (Figure 10). Superficial anomalies should not be taken into account in analyzing long-term variations of specific resistivity as they are associated with differences in moisture content under varying atmospheric conditions at the times of measurement. Clear indications of resistivity changes, both positive or negative, are visible below this surface layer, indicating a response independent of prevailing weather conditions at the time of measurement. The striking features in Figure 10 are the distinct increase in resistivity of up to 15% in the summer of 2002 and the extreme decrease in resistivity of 15% to 35% in the summer of 2003. Borehole data (Figures 4 and 6) show the depth of the active layer to have doubled in 2003 compared to 2002 which is reflected in the large changes in resistivity in those years, and which is clearly associated with the extraordinary cold year of 2002 and the extraordinary hot summer of 2003 in the European Alps [MeteoSchweiz, 2002, 2003; Schär et al., 2004].

[31] In 2005 and 2006, the depths of the active layer in the borehole logs were restored to pre-2003 conditions (~5 m). At the respective measurement dates (some 4–6 weeks before the time of maximum thaw depth), thaw depth was consistently around 4.5–5 m in 1999, 2000, 2005, and 2006 (no data for 2002), as is indicated by the dashed lines in Figure 10 (left). However, time-lapse tomograms after 4, 5, and 6 years suggest that the pronounced drop in resistivity in 2003 was not fully offset in 2004 or 2005 even though subsurface temperatures in the winter periods were lower than in the years before 2003 (Figure 6). This apparent permafrost degradation will be discussed further in section 6.

[32] Another approach to estimating the extent of ice melt or ice formation is by calculating the percentage desaturation for the time-lapse profiles. A well-known geophysical relation called Archie's law, which relates the resistivity of a porous medium to its saturation [Archie, 1942], can be used to convert resistivity change into percentage desaturation. A mean value of 2.0 for the so-called saturation exponent in Archie's law [see, e.g., Hauck, 2002] was chosen, but in general the sensitivity of calculated saturation to a range of plausible values for the saturation exponent is low in this case (only around 1 to 3%). The calculated percentage desaturation for the time-lapse profiles in Figure 10 is shown in Figure 11. In general, the resultant desaturation is low ($\pm 5\%$) for the years before 2003 and after 2004 for most parts of the profile. Maximum desaturation values (summer of 2003) are around -20 to -30% (relative to the

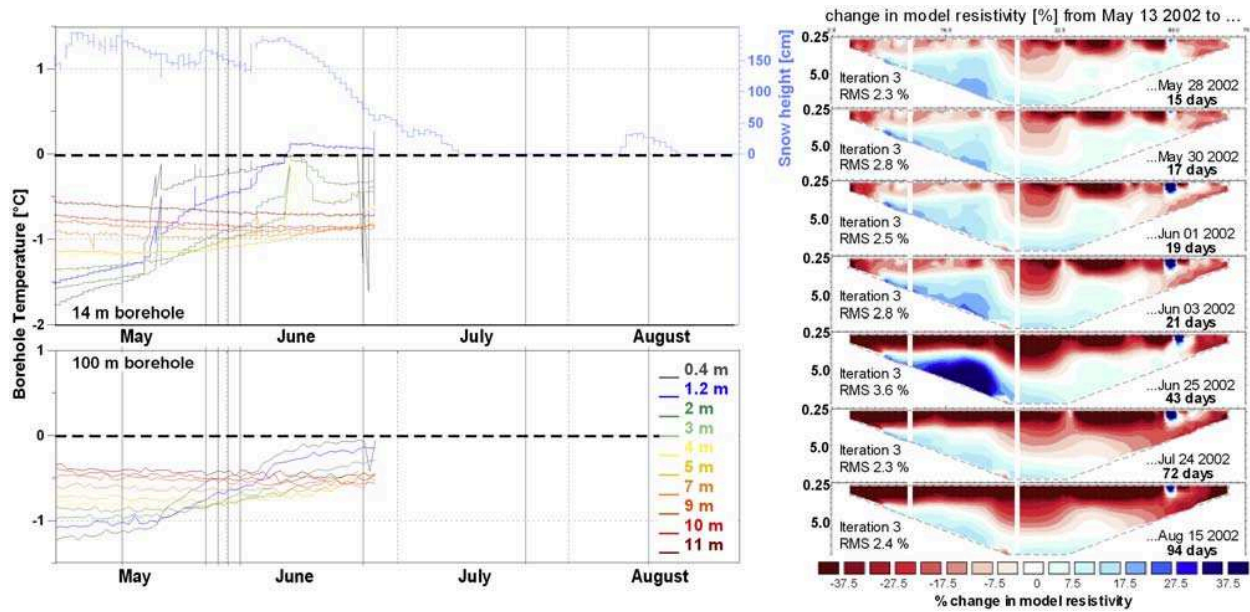


Figure 12. (left) Borehole temperature and snow depth data and (right) percentage change in specific resistivity between May and August 2002). Borehole temperatures are plotted for both (top left) the 14 m and (bottom left) the 100 m boreholes for all thermistors covering the investigation depth of the ERT profile (no borehole data for July and August). The gray vertical lines indicate measurement dates used for time-lapse inversion. Borehole locations (14 m left, 100 m right) within the ERT profile are marked by white vertical lines.

summer of 1999), corresponding to up to 15% loss of ice content for a hypothetical case of 50% porosity and saturated initial conditions (which is only an upper bound for the field site at Schilthorn, where saturation is much less than 100%) [Hauck, 2002]. Improved approximation of the pore space and initial saturation of the subsurface section would allow relative changes in ice and unfrozen water contents to be computed from repeated ERT measurements.

6. Discussion

[33] Results of the 7-year time series shown above clearly indicate the applicability of ERT monitoring in investigating permafrost evolution on different timescales, i.e., short-term, seasonal, and interannual changes. Over the short term, characteristic changes in resistivity can be attributed either to the freezing period in late autumn and early winter or to subsurface thawing processes in late spring and summer. For the former case, Figure 9 clearly indicates that resistivity increases in depth sections where the temperature reaches zero degrees and less, but does so with a typical time lag as a function of depth. Changes in resistivity due to freezing range from 30% to more than 75%.

[34] The reverse can be observed during and after snowmelt in late spring and summer. Melting of the active layer can be recognized in both borehole temperatures and resistivity decrease. However, unlike in the freezing case, changes in resistivity cannot be explained entirely by phase changes from ice to water. Meltwater from the snow cover infiltrates into the upper parts of the profile, causing both a drop in resistivity due to the growing content of unfrozen water (independent of subsurface melting) and a rise in temperature near the flow paths. This can be observed for

periods when the snow cover is still relatively thick (>1 m, cf. Figure 12), thus preventing radiation control of the ground surface temperature. During this period, active layer temperatures increase (but are still below zero), and specific resistivities decrease on the order of 5 to 20% (Figure 12). After accelerated melting of the remaining, very wet, snow cover, and with subsurface temperatures rising above zero degrees, resistivity decreases by 45 to 65% relative to the initial frozen conditions (see Figure 12).

[35] In addition to the vertical infiltration of meltwater, horizontal advection may play a significant role in Alpine terrain. The study site clearly is affected by the down slope movement of (melt) water from the beginning of snowmelt until the last snow patch disappeared in the upper part of the slope. Consequently, vertical and horizontal water infiltration processes need to be taken into account in interpreting changes in resistivity associated with ground ice melting.

[36] While seasonal timescales provide information about the “natural” range of bulk resistivity changes due to freezing and thawing cycles of the active layer, monitoring interannual differences allows the long-term evolution of the permafrost regime to be estimated. While the changes in resistivity between the summer of 1999 to 2000 and 1999 to 2002 seem to reflect the interannual variability of permafrost dynamics due to atmospheric forcing, the hot summer of 2003 obviously had a sustainable effect on the local permafrost regime for more than 1 year. The depth of the active layer increased from approximately 4–5 m (1999–2002) to almost 9 m in 2003, as is evident from borehole information (Figure 4), but also clearly visible in the ERT tomograms. While the temperature regime seems to have recovered in 2005 from the 2003 heat anomaly, the corresponding resistivity values have not. Although resis-

tivities measured in this profile section increased again in 2005, they did not exceed 1700 Ωm in those parts where resistivity had reached 2500 Ωm in the years before 2003 (see Figure 10). This difference is small compared to seasonal variations, but large in an interannual context. As inversion RMS errors are much lower than this observed discrepancy, the decrease of resistivity can be considered significant as a consequence of the heat wave in 2003. Subzero temperatures were nearly identical before 2003 and after 2004 and cannot explain the differences in resistivity (cf. Figure 6b). Hence a substantial loss of ground ice is assumed to be due to the summer 2003 anomaly, which obviously did not, or not entirely, recover in the following years.

[37] The temperature regime did not prevent ice formation, as subzero temperatures (in winter) were even lower after 2003 than before (see Figure 6a). The post-2003 resistivity decrease therefore must be associated with a limited availability of unfrozen water or with a reduced pore volume (due to subsidence processes) as a consequence of ice melt. The former assumption is relatively unlikely because meltwater from adjacent snow patches is delivered almost throughout the whole summer (but no moisture data exist up to now). In contrast to the initial assumption of a very low ice content [Imhof *et al.*, 2000; Vonder Mühll *et al.*, 2000; Harris *et al.*, 2003], the latter possibility could indicate previous supersaturation, at least in parts of the subsurface section, that did not (yet?) recover. However, further study is necessary to prove this hypothesis.

[38] In view of further atmospheric warming and the projected higher frequency of summer heat waves such as in 2003 [Schär *et al.*, 2004; IPCC, 2007], the degradation of ground ice observed must be evaluated with respect to possible thresholds (e.g., extent of ice melt, regeneration time) to the reversibility of permafrost degradation under current and future climate conditions (regeneration of ground ice). The results of this study indicate that extreme weather events can disturb the permafrost system (not necessarily the temperature regime, but the ice content) for years. The time series presented is still too short for reliable predictions to be made, but is indicative of pronounced sensitivity of the Schilthorn permafrost site to atmospheric forcing. Questions arise as to the extent in which the permafrost regime can buffer atmospheric heat transfer, and about the critical threshold (e.g., frequency of disturbances) of long-term degradation. The “warm” subsurface conditions with low ice content of areas with temperate permafrost, such as Schilthorn, are especially sensitive to degradation. Moreover, because of the extreme topography, degradation will produce three-dimensional effects [Gruber *et al.*, 2004b].

7. Conclusions and Outlook

[39] A combined geoelectric and thermal monitoring approach using electrical resistivity tomography (ERT) and borehole temperature data for long-term observation of permafrost evolution is presented. The approach was validated at the Schilthorn, Swiss Alps, mountain permafrost field site, characterized by thick permafrost occurrence, but, because of the proximity to critical temperatures near the freezing point, with a pronounced susceptibility to ground ice degradation. Key results of a 7-year time series

including more than 110 ERT tomograms along a 60 m long (corresponding to 10 m depth of investigation) survey line are as follows.

[40] 1. The subzero temperature dependence of electrical resistivity is directly associated with the content of ground ice and unfrozen water, which is the target value to be assessed.

[41] 2. Analysis of apparent resistivities serves to evaluate data quality and scale-dependent characteristics in resistivity change patterns, illustrating the significance of the data set for permafrost monitoring.

[42] 3. Analysis of time-lapse inversion models with respect to subsurface temperature reveals important insights both into changes in resistivity consistent with temperature (directly associated with phase changes from water to ice and vice versa) and these not conforming to long-term temperature evolution. The former changes are attributed primarily to short-term phenomena, i.e., seasonal variations in the permafrost regime, whereas the latter changes are believed to indicate increases in the content of unfrozen water due to substantial ground ice degradation (exceeding the interannual variability) as a consequence of the extraordinary hot summer of 2003 which was not offset within 1 year. This degradation is more severe than is determined by subsurface temperatures. The discrepancy observed between temperature and resistivity evolution is mainly controlled by the availability of liquid water or by changes in materials characteristics (e.g., pore volume change by subsidence).

[43] 4. Uncertainties arise from the lack of moisture data, as moisture variations can mask the temperature dependence of resistivity data.

[44] 5. Long-term changes in resistivity are evaluated on the basis of seasonal variations in resistivity, providing the “natural” range of values observed.

[45] 6. Calculating changes in saturation in a first approximation helps to determine relative changes in ice and water contents. However, initial saturation and the pore volume of subsurface material are critical factors to determine.

[46] 7. Indications of substantial degradation of ground ice in general, and melting of supersaturated areas in particular, show the potential of a combined thermal and ERT monitoring approach compared to thermal monitoring only.

[47] Concerning the remarkable increase in the depth of the active layer at Schilthorn from, typically, approximately 5 m to 9 m in the summer of 2003, long-term permafrost changes at this particular site are difficult to assess because of the insufficient depth (about 10 m) of the monitoring profile. However, ERT monitoring profiles are currently investigated to depths of approximately 30 m at several sites in the Swiss Alps within the GO4ICE (Geophysical observation and four-phase modeling of the ice content evolution) project as part of the Permafrost Monitoring Switzerland (PERMOS) network. The data set shown for the Schilthorn monitoring site demonstrates the general applicability of long-term permafrost monitoring by ERT systems to assess relative changes in ice content with time.

[48] Automation of ERT data acquisition is in progress to guarantee better temporal resolution of measurements and therefore easier comparison of ERT data sets from different years. Besides continuing ERT monitoring, future work will focus on the additional acquisition of repeated refraction seismic data. A combination of electric and elastic mixing rules based on resistivity and seismic velocity data sets

seems a promising approach for an absolute quantification of ice and water contents in the pore space.

[49] **Acknowledgments.** The authors would like to thank Schilthornbahn AG for logistical, and the PERMOS network (financed by BAFU, Switzerland) for financial support.

References

- Aaltonen, J., and B. Olofsson (2002), Direct current (DC) resistivity measurements in long-term groundwater monitoring programmes, *Environ. Geol.*, *41*(6), 662–671, doi:10.1007/s00254-001-0447-1.
- Archie, G. E. (1942), The electrical resistivity log as an aid in determining some reservoir characteristics, *Trans. Am. Inst. Min. Metall. Pet. Eng.*, *146*, 54–62.
- Arenson, L. U., and S. M. Springman (2005), Triaxial constant stress and constant strain rate tests on ice-rich permafrost samples, *Can. Geotech. J.*, *42*(2), 412–430.
- Arenson, L., M. Hoelzle, and S. Springman (2002), Borehole deformation measurements and internal structure of some rock glaciers in Switzerland, *Permafrost Periglacial Processes*, *13*, 117–135, doi:10.1002/ppp.414.
- Arenson, L. U., N. Almasi, and S. M. Springman (2003), Shearing response of ice-rich rock glacier material, in *Proceedings of the International Conference on Permafrost*, 8th, edited by M. Phillips, pp. 39–44, A. A. Balkema, Brookfield, Vt.
- Claerbout, J. F., and F. Muir (1973), Robust modeling with erratic data, *Geophysics*, *38*(5), 826–844.
- Daily, W., A. Ramirez, A. Binley, and D. LaBrecque (2004), Electrical resistance tomography, *Leading Edge*, *23*(5), 438–442, doi:10.1190/1.1792225.
- Day-Lewis, F., K. Singha, and A. Binley (2005), Applying petrophysical models to radar travel time and electrical resistivity tomograms: Resolution-dependent limitations, *J. Geophys. Res.*, *110*, B08206, doi:10.1029/2004JB003569.
- French, H. K., C. Hardbattle, A. Binley, P. Winship, and L. Jakobsen (2002), Monitoring snowmelt induced unsaturated flow and transport using electrical resistivity tomography, *J. Hydrol.*, *267*, 273–284, doi:10.1016/S0022-1694(02)00156-7.
- Gruber, S., M. Hoelzle, and W. Haeblerli (2004a), Permafrost thaw and destabilization of Alpine rock walls in the hot summer of 2003, *Geophys. Res. Lett.*, *31*, L13504, doi:10.1029/2004GL020051.
- Gruber, S., L. King, T. Kohl, T. Herz, W. Haeblerli, and M. Hoelzle (2004b), Interpretation of geothermal profiles perturbed by topography: The Alpine permafrost boreholes at Stockhorn Plateau, Switzerland, *Permafrost Periglacial Processes*, *15*, 349–357, doi:10.1002/ppp.503.
- Haeblerli, W., et al. (2006), Permafrost creep and rock glacier dynamics, *Permafrost Periglacial Processes*, *17*, 189–214, doi:10.1002/ppp.561.
- Harris, C., M. C. R. Davies, and B. Etzelmüller (2001a), The assessment of potential geotechnical hazards associated with mountain permafrost in a warming global climate, *Permafrost Periglacial Processes*, *12*, 145–156, doi:10.1002/ppp.376.
- Harris, C., W. Haeblerli, D. Vonder Mühll, and L. King (2001b), Permafrost monitoring in the high mountains of Europe: The PACE Project in its global context, *Permafrost Periglacial Processes*, *12*, 3–11, doi:10.1002/ppp.377.
- Harris, C., D. Vonder Mühll, K. Isaksen, W. Haeblerli, J. L. Sollid, L. King, P. Holmlund, F. Dramis, M. Guglielmin, and D. Palacios (2003), Warming permafrost in European mountains, *Global Planet. Change*, *39*, 215–225, doi:10.1016/j.gloplacha.2003.04.001.
- Hauck, C. (2001), Geophysical methods for detecting permafrost in high mountains, Ph.D. thesis, 204 pp., Mitt. der Versuchsanst. fuer Wasserbau, Hydrol. und Glaziol. der Eidg. Tech. Hochsch., Zurich, Switzerland.
- Hauck, C. (2002), Frozen ground monitoring using DC resistivity tomography, *Geophys. Res. Lett.*, *29*(21), 2016, doi:10.1029/2002GL014995.
- Hauck, C., and D. Vonder Mühll (2003a), Evaluation of geophysical techniques for application in mountain permafrost studies, *Z. Geomorphol.*, *132*, suppl., 159–188.
- Hauck, C., and D. Vonder Mühll (2003b), Inversion and interpretation of two-dimensional geoelectrical measurements for detecting permafrost in mountainous regions, *Permafrost Periglacial Processes*, *14*, 305–318, doi:10.1002/ppp.462.
- Hauck, C., D. Vonder Mühll, and H. Maurer (2003), Using DC resistivity tomography to detect and characterize mountain permafrost, *Geophys. Prospect.*, *51*, 273–284, doi:10.1046/j.1365-2478.2003.00375.x.
- Hauck, C., D. Vonder Mühll and M. Hoelzle (2005), Permafrost monitoring in high mountain areas using a coupled geophysical and meteorological approach, in *Climate and Hydrology of Mountain Areas*, edited by C. De Jong et al., pp. 59–71, John Wiley, Hoboken, N. J.
- Imhof, M., G. Pierrehumbert, W. Haeblerli, and H. Kienholz (2000), Permafrost investigation in the Schilthorn massif, Bernese Alps, Switzerland, *Permafrost Periglacial Processes*, *11*, 189–206, doi:10.1002/1099-1530(200007/09)11:3<189::AID-PPP348>3.0.CO;2-N.
- Intergovernmental Panel on Climate Change (IPCC) (2007), Summary for policymakers, in *Climate Change 2007: The Physical Science Basis: Contribution of Working Group I to the Fourth Assessment Report of the Intergovernmental Panel on Climate Change*, edited by S. Solomon et al., pp. 1–18, Cambridge Univ. Press, New York.
- Kemma, A., J. Vanderborght, B. Kulesa, and H. Vereecken (2002), Imaging and characterisation of subsurface solute transport using electrical resistivity tomography (ERT) and equivalent transport models, *J. Hydrol.*, *267*, 125–146, doi:10.1016/S0022-1694(02)00145-2.
- Loke, M. H. (1999), Time-lapse resistivity imaging inversion, paper presented at 5th Meeting of the Environmental and Engineering Society European Section, Budapest.
- Loke, M. H., and R. D. Barker (1995), Least-squares deconvolution of apparent resistivity, *Geophysics*, *60*(6), 1682–1690, doi:10.1190/1.1443900.
- Luetschg, M., and W. Haeblerli (2005), Permafrost evolution in the Swiss Alps in a changing climate and the role of the snow cover, *Norw. J. Geogr.*, *59*, 78–83, doi:10.1080/00291950510020583.
- Matsuoka, N., and O. Humlum (2003), Monitoring periglacial processes: New methodology and technology, *Permafrost Periglacial Processes*, *14*, 299–303, doi:10.1002/ppp.461.
- Maurer, H., and C. Hauck (2007), Geophysical imaging of alpine rock glaciers, *J. Glaciol.*, *53*(180), 110–120.
- MeteoSchweiz (2002), Witterungsbericht Jahr 2002, MeteoSchweiz, Zurich, Switzerland.
- MeteoSchweiz (2003), Witterungsbericht Jahr 2003, MeteoSchweiz, Zurich, Switzerland.
- Musil, M., H. Maurer, A. G. Green, H. Horstmeyer, F. O. Nitsche, D. Vonder Mühll, and S. Springman (2002), Shallow seismic surveying of an Alpine rock glacier, *Geophysics*, *67*(6), 1701–1710, doi:10.1190/1.1527071.
- Noetzi, J., S. Gruber, T. Kohl, N. Salzmann, and W. Haeblerli (2007), Three-dimensional distribution and evolution of permafrost temperatures in idealized high-mountain topography, *J. Geophys. Res.*, *112*, F02S13, doi:10.1029/2006JF000545.
- Schär, C., P. L. Vidale, D. Lüthi, C. Frei, C. Häberli, M. A. Liniger, and C. Appenzeller (2004), The role of increasing temperature variability in European summer heatwaves, *Nature*, *427*, 332–336, doi:10.1038/nature02300.
- Scott, W. J., P. V. Sellmann, and J. A. Hunter (1990), Geophysics in the study of permafrost, in *Geotechnical and Environmental Geophysics*, edited by S. Ward, pp. 355–384, Soc. of Explor. Geophys., Tulsa, Okla.
- Singha, K., and S. Gorelick (2006a), Hydrogeophysical tracking of three-dimensional tracer migration: The concept and application of apparent petrophysical relations, *Water Resour. Res.*, *42*, W06422, doi:10.1029/2005WR004568.
- Singha, K., and S. Gorelick (2006b), Effects of spatially variable resolution on field-scale estimates of tracer concentration from electrical inversions using Archie's law, *Geophysics*, *71*(3), 83–91, doi:10.1190/1.2194900.
- Slater, L., A. Binley, R. Versteeg, G. Cassiani, R. Birken, and S. Sandberg (2002), A 3D ERT study of solute transport in a large experimental tank, *J. Appl. Geophys.*, *49*, 211–229, doi:10.1016/S0926-9851(02)00124-6.
- Suzuki, K., and S. Higashi (2001), Groundwater flow after heavy rain in landslide-slope area from 2-D inversion of resistivity monitoring data, *Geophysics*, *66*(3), 733–743, doi:10.1190/1.1444963.
- Telford, W. M., L. P. Geldart, and R. E. Sheriff (1990), *Applied Geophysics*, 2nd ed., 790 pp., Cambridge Univ. Press, Cambridge, U. K.
- Vonder Mühll, D., C. Hauck, and F. Lehmann (2000), Verification of geophysical models in Alpine permafrost using borehole information, *Ann. Glaciol.*, *31*, 300–306.
- Vonder Mühll, D., J. Noetzi, I. Roer, K. Makowski, and R. Delaloye (Eds.) (2004), Permafrost in Switzerland 2002/2003 and 2003/2004, *Glaciol. Rep. Permafrost 4/5*, Cryos. Comm. of the Swiss Acad. of Sci., Zurich, Switzerland.
- C. Hauck, Institute for Meteorology and Climate Research, Forschungszentrum Karlsruhe, University of Karlsruhe, Postfach 3640, Karlsruhe D-76021, Germany.
- C. Hilbich and R. Mäusbacher, Geographical Institute, Friedrich Schiller University of Jena, Löbdergraben 32, Jena D-07743, Germany. (c7hich@uni-jena.de)
- M. Hoelzle, M. Scherler, and L. Schudel, Geographical Institute, University of Zurich, Winterthurerstrasse 190, Zurich CH-8057, Switzerland.
- I. Völkisch, Swiss Federal Institute for Forest, Snow and Landscape Research, Zürcherstrasse 111, Birmensdorf CH-8903, Switzerland.
- D. Vonder Mühll, SystemsX, ETH Zurich, Rämistrasse 101, Zurich CH-8092, Switzerland.

5 A geoelectric monitoring network and resistivity-temperature relationships of different mountain permafrost sites in the Swiss Alps

Citation

Hilbich, C., Hauck, C., Delaloye, R. & Hoelzle, M. 2008. A geoelectric monitoring network and resistivity-temperature relationships of different mountain permafrost sites in the Swiss Alps. *Proceedings of the 9th International Conference on Permafrost*, Fairbanks, Alaska **1**: 699-704.

This paper presents the geoelectric monitoring network established at four permafrost sites in the Swiss Alps. ERT results from summer are compared qualitatively to measurements during winter to show the different characteristics of seasonal variations at the respective landforms. In addition, the complete ERTM data sets of all landforms are analysed in terms of resistivity-temperature relations in vertical profiles at borehole positions.

Main findings

- ▷ At all monitoring sites a clear relation between resistivity and subsurface temperature is evident, showing the potential of ERTM for the assessment of climate related ground ice degradation.
- ▷ Total resistivity ranges and the amplitudes of temporal changes differ markedly for the observed landforms due to site-specific differences in material properties, seasonal dynamics, temperature ranges and the hierarchy of dominating factors.
- ▷ The striking and sustained impact of the hot summer 2003 on the permafrost regime at Schilthorn could vividly be demonstrated by analysing deviations from the temperature-resistivity curve. These deviations from the main branch of the temperature-resistivity curve persisted until 2007 after a slow recovery in the years following the heat wave.
- ▷ Small seasonal changes are recorded at rockglacier Murtèl due to its thermal inertia, whereas high seasonal dynamics are observed at the other sites as a consequence of internal ventilation (Lapires talus slope), high unfrozen water and low ice contents (Schilthorn) and 3D topography effects (Stockhorn).

A geoelectric monitoring network and resistivity-temperature relationships of different mountain permafrost sites in the Swiss Alps

Christin Hilbich

Department of Geography, University of Jena, Germany

Christian Hauck

Institute for Meteorology and Climate Research, University of Karlsruhe/Forschungszentrum Karlsruhe, Germany

Reynald Delaloye

Geosciences Department, Geography Unit, University of Fribourg, Switzerland

Martin Hoelzle

Glaciology, Geomorphodynamics and Geochronology, University of Zurich, Switzerland

Abstract

An Electrical Resistivity Tomography (ERT) monitoring network has been installed in different permafrost landforms in the Swiss Alps. Repeated ERT measurements yield information on changes occurring in the physical properties of the ground with changing temperature and time. Because the sensitivity of electrical resistivity to temperature is mainly due to the amount of unfrozen water in the pore space of the subsurface material, temporal resistivity changes can be related to freezing and thawing processes. The combined analysis of borehole temperature and ERT monitoring data is used to determine temporal changes of ice and unfrozen water. Key results from this approach include (a) the determination of site-specific total resistivity ranges (as a function of ice content) and amplitudes of seasonal resistivity changes, (b) the demonstration of 3D-topography effects on resistivity distribution in ridge situations, and (c) the identification of depth dependent resistivity-temperature relationships as a function of depth related unfrozen water contents.

Keywords: Electrical Resistivity Tomography; Monitoring; Mountain Permafrost; PERMOS; Temperature

Introduction

Within the context of climate change the European Alps are affected by greater average warming than commonly projected for Europe as a whole (Beniston et al. 1997). The consequences of global warming for permafrost have been investigated and observed in polar regions for many years (e.g. Osterkamp et al. 1983, Nelson et al. 2001, Frauenfeld et al. 2004, IPCC 2007). In contrast to mainly flat polar lowlands, mountain permafrost is strongly influenced by topographic factors (aspect, slope angle, altitude), affecting net solar radiation and snow cover distribution (Hoelzle et al. 2001). Spatial and temporal heterogeneities of these factors cause complex permafrost distribution patterns that are complicated by heterogeneous subsurface material compositions (bedrock, fine and coarse grained debris). Consequently, also the ice content differs markedly between different permafrost landforms.

In addition to temperature, ice content is one of the most critical parameters for the evaluation of the impact of global warming on rockwall stability. Direct observations of ice content are scarce and difficult to obtain. Indirect information from Electrical Resistivity Tomography (ERT) has great potential for detecting the presence of ice, because the specific resistivities of frozen and unfrozen material are markedly different. With repeated ERT measurements under constant general conditions, temporal changes of resistivities are assessed and can be related to freezing and thawing processes (Hauck 2002, Hilbich et al. 2008). However, reliable and quantitative conclusions

concerning climate related changes in ice content can only be drawn when resistivity changes related to external water input (e.g., from precipitation, snowmelt or lateral water flow) can be excluded (or distinguished from ice melt).

The newly installed ERT monitoring network within the Swiss permafrost monitoring network PERMOS (Fig. 1) provides a unique data set that facilitates study of the relations between measured resistivities and borehole temperatures in different permafrost landforms. Sites in the network include the *Schilthorn* (Bernese Alps) permafrost site, which has the longest (> 8 years) record of ERT measurements (Hilbich et al. 2008). In this paper we analyze the potential of coupled ERT and temperature monitoring to improve resistivity-based estimates of total amounts and temporal changes of ice content in permafrost regions.

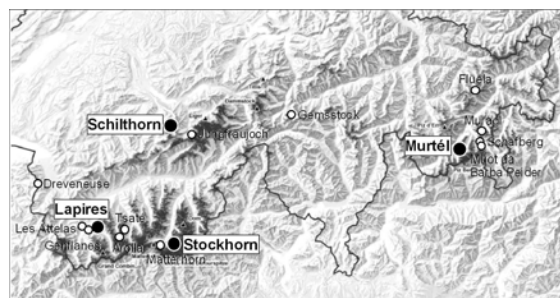


Figure 1: The PERMOS network in the Swiss Alps with borehole temperature monitoring sites (white dots) and combined borehole and ERT monitoring sites (black dots) (map: BAFU 2007).

Theory and Methods

Borehole temperatures

In existing European and Swiss permafrost monitoring networks (PACE21, PERMOS (Harris 2001, Vonder Mühl et al. 2004)), subsurface temperature data are obtained in a network of shallow and deep (down to 100 m) boreholes. The PERMOS programme started in 1999 and involves 16 permafrost borehole monitoring sites with the longest time-series at rockglacier *Murtèl* (Upper Engadine), recording since 1987. However, long-term climate-related degradation processes in terms of thawing phenomena cannot necessarily be identified by thermal permafrost monitoring alone, as the ice content depends on temperature evolution and also on the availability of unfrozen water during the freezing period (Hilbich et al. 2008).

Electrical Resistivity Tomography (ERT)

The electrical resistance of the ground can be determined by passing a current between two electrodes and measuring the resulting potential difference between two other electrodes coupled to the ground. Repeating this procedure along an electrode array for a number of different 4-electrode combinations (quadrupoles) with different center points and spacing reveals a two-dimensional distribution of electrical resistances within a subsurface section. By multiplying a geometric factor representing the distance between the four electrodes the apparent resistivity ρ_a is obtained for each data point of a certain multi-electrode configuration. Using the software package RES2DINV (Loke & Barker 1995), a 2D model of specific resistivities ρ_s , i.e., the true resistivity distribution of the subsurface section, can be calculated from ρ_a by an iterative tomographic inversion process. All ERT data presented in this contribution were measured with the WENNER configuration, and the robust inversion scheme (Clairbout & Muir 1973) of the software RES2DINV was applied.

ERT monitoring

Within the ERT monitoring network a fixed electrode array was installed at four characteristic permafrost sites in the Swiss Alps. All electrodes of one array are permanently connected via cables to a contact box, which serves as an adaptor to a resistivity meter and can be accessed throughout the year (described in detail in Hilbich et al. 2008). Measurements can be carried out by only one person, even in winter, when the electrode array is covered with snow. ERT monitoring started in 1999 at the *Schilthorn* site, in 2005 at the *Murtèl* and *Stockhorn* sites, and in 2006 at the *Lapires* site (see section Field sites) and comprises roughly 10 measurements per site to date, except for *Schilthorn* with more than 100 measurements.

Dependence of resistivity on temperature

According to an empirical relationship called Archie's Law the resistivity of a medium (consisting of a rock or soil matrix and pore water) can be related to the resistivity

of the water, the porosity and the fraction of the pore space occupied by liquid water (Telford et al. 1990).

The sensitivity of electrical resistivity to temperature arises from different effects, above and below the freezing point. At positive temperatures the resistivity of the pore water increases with decreasing temperature as a consequence of increasing viscosity of the pore water, which, in turn, decreases the mobility of the ions in the water. This can be quantitatively described as a linear function of the resistivity ρ_0 measured at a reference temperature T_0 and the temperature coefficient of resistivity α , which has a value of about 0.025 K^{-1} for most electrolytes (Telford et al. 1990):

$$\rho = \frac{\rho_0}{1 + \alpha(T - T_0)}. \quad (1)$$

Below the freezing point resistivities increase exponentially due to successive freezing of the pore water with decreasing temperatures. The subzero relationship between resistivity and temperature is given by:

$$\rho = \rho_0 e^{-b(T)}, \quad (2)$$

where ρ_0 and b (in K^{-1}) are constants (e.g. Hauck 2002). The factor b controls the rate of decrease and can be determined from Equation (2) if resistivity data for different subzero temperatures are available.

Repeated ERT measurements therefore yield information on the changes occurring in the physical properties of the ground with changing temperature and time (Fortier et al. 1994). Plotting ground temperatures from boreholes (interpolated to the depths of the model blocks of the tomograms) against ρ_s extracted from ERT data at borehole positions (marked in Figures 4 - 6) then allows comparison of the relation between T and ρ_s for different sites.

Field sites

ERT monitoring sites have been chosen to represent different permafrost landforms, different climatic regions in the Swiss Alps and with respect to the availability of deep boreholes (> 20 m). The landforms include the north facing rock slope of *Schilthorn* (Bernese Alps), the rock plateau *Stockhorn* (Valais), the talus slope *Lapires* (Valais) and the active rockglacier *Murtèl* (Upper Engadine) (Fig. 1). All ERT profiles were placed close to at least one borehole to enable a calibration of the indirect geophysical measurements with direct observations of the subsurface material composition as made during drilling, and subsurface temperature records of the boreholes. A detailed description of the test sites is given in Table 1.

Results and Discussion

8-year ERT monitoring Schilthorn

The ERT monitoring at *Schilthorn* started in September 1999 and comprises more than 100 datasets, making it the longest ERT monitoring record in mountain permafrost

research. A comprehensive analysis of this time series is given in Hilbich et al. (2008). Figure 2 shows the inter-annual changes between measurements in late summer for each year except 2001.

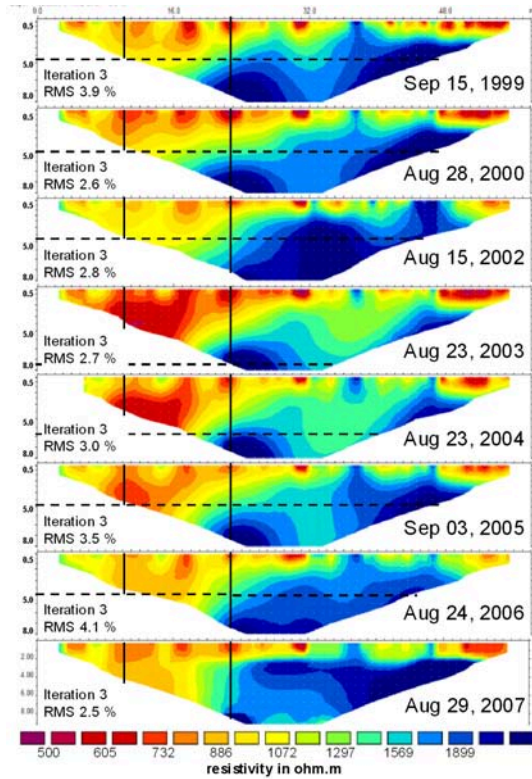


Figure 2: ERT monitoring results of Schilthorn: inter-annual comparison of late summer resistivity distribution (modified after Hilbich et al. 2008).

One of the most prominent features of the dataset is the effect of the extraordinarily hot summer of 2003 on mountain permafrost in the European Alps. According to the borehole temperatures the summer of 2003 caused an immense deepening of the active layer to almost twice the depth of the years before (horizontal dashed lines in Fig.

2). But, in contrast to the subsurface temperatures, which returned rapidly to almost “normal” conditions in 2004, measured resistivities took about 4 years to recover to pre-2003 conditions. As stated before, temporal resistivity changes are assumed to be caused by freezing and thawing processes that are themselves controlled by temperature. The close relation between temperature and resistivity is evident from Figure 3, where borehole temperatures and specific resistivities at the borehole position are shown for the upper four meters and for a one year period (September 1999 to 2000).

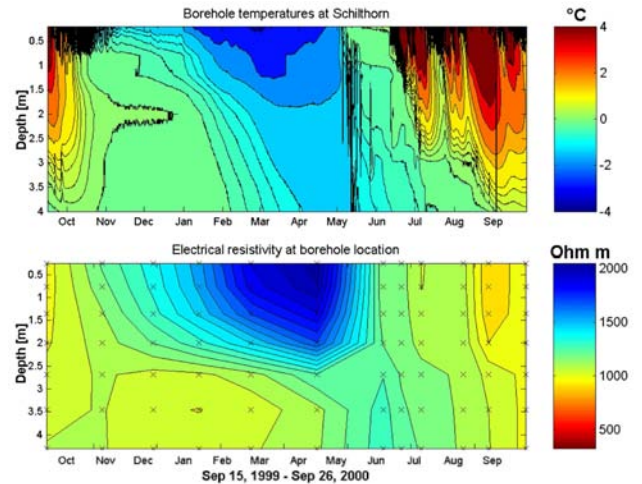


Figure 3: Comparison of temperatures (top) and interpolated resistivities at borehole location (bottom) for September 1999 - September 2000 at Schilthorn. Resistivity data points used for interpolation are shown as black crosses.

ERT monitoring at different landforms

First results from ERT monitoring in different permafrost landforms reveal pronounced differences in total resistivity values and the amplitude of seasonal resistivity dynamics. The first is due mainly to site-specific material characteristics (lithology, pore volume, fractions of pores filled with air, ice and unfrozen water, etc.), but the latter can have different causes. Besides local climatic

Table 1: Characterization of the ERT monitoring sites and the available boreholes within the PERMOS network

	Schilthorn	Stockhorn	Lapires	Murtèl
Site description	north facing slope beneath summit, bedrock covered with 0 to several meters debris	rock plateau on a crest, bedrock covered with 0-1 m debris	talus slope with internal ventilation	blocky rockglacier
Lithology	Limestone schists	Albit-Muskowit schists	Gneiss	Granodiorit, Schists
Altitude (a.s.l.)	2910 m	3410 m	2500 m	2670 m
Slope, aspect	30° NNE	8° S	25° NE	10° NNW
Location	Cross profile in N-slope	N-S-profile across plateau	Cross profile	Longitudinal profile
Boreholes	14 m (since 1998) and 100 m vertical, 100 m oblique (since 2000)	17 m, 100 m (since 2000)	20 m (since 1998)	20 m, 60 m, 60 m (since 1987/2000)
ERT Monitoring since	8/1999	8/2005	8/2006	8/2005
Profile length, investigation depth	58 m 10 m	94 m 15 m	168 m 25 m	235 m 40 m

effects controlled by altitude, aspect, snow regime, etc., such morphological characteristics as differences in substrate, active layer thickness, thermal conduction in the active layer, etc. play an important role for the amount to which seasonally variable atmospheric forcing is transferred into the ground. This becomes evident not only from the site-specific subsurface temperature regime but also from the resistivity changes throughout a year. Figures 4, 5, and 6 show tomograms with typical summer (top) and winter (bottom) resistivity distributions for the bedrock (*Stockhorn*), rockglacier (*Murtèl*) and talus slope (*Lapires*) sites. From the qualitative comparison the most important site-specific characteristics are discussed qualitatively in the following paragraphs:

Stockhorn

The *Stockhorn* profile is located on a plateau between the steep ($> 80^\circ$) northern rock face, and the steeply inclined southern slope. Permafrost distribution is therefore assumed to be affected by 3D topography effects as described by Gruber et al. (2004) and Noetzli et al. (2008). Three-dimensional effects become evident in the ERT monitoring data by pronounced active layer freezing (increasing resistivities during winter) in the northern part, while similar characteristics are missing in the southern part. This corresponds well with observations of the snow cover, which is usually thicker and persists longer in the northern part. In general, the site is exposed to pronounced resistivity changes in the whole subsurface section (to about 20 m depth), which is attributed to 3D topographic effects of the ridge, influencing radiation and turbulent heat transfer to the ground.

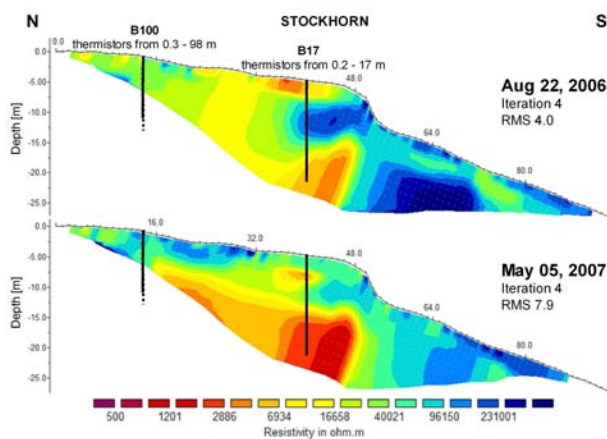


Figure 4: ERT tomogram for typical summer (top) and winter (bottom) conditions at rock plateau *Stockhorn*.

Murtèl

Rockglacier *Murtèl* is generally characterized by extremely high resistivities (300 k Ω m to > 2 M Ω m) in the interior part caused by the large volume of massive ice. The air in the blocky top layer effectively isolates the ice core from summer heating. Consequently, seasonal resistivity changes are only observed in the active layer (ca. 3 – 3.5 m) and the tongue. Although changes in the inverted resistivities of the ice core can be quite high (not

resolved by the color scale) no systematic seasonal change or trend can be observed from the monitoring data so far. Due to a limited sensitivity of the inversion model to high resistive zones at greater depth, spatial or temporal variations of such high resistivities on the order of M Ω m should not be over-interpreted (Marescot et al. 2003). An exception concerns the slightly less resistive vertical zone below the depression at 100-105 m horizontal distance, which is observed in all ERT data (see upper panel in Fig. 5). In summer this resistivity contrast is usually more pronounced than in winter. Due to the uncertainties mentioned above this zone with decreased (but still very high) resistivities is difficult to interpret, but may be an indication of a slightly higher amount of unfrozen water (under subzero temperature conditions), possibly indicating water flow or a zone of higher debris content.

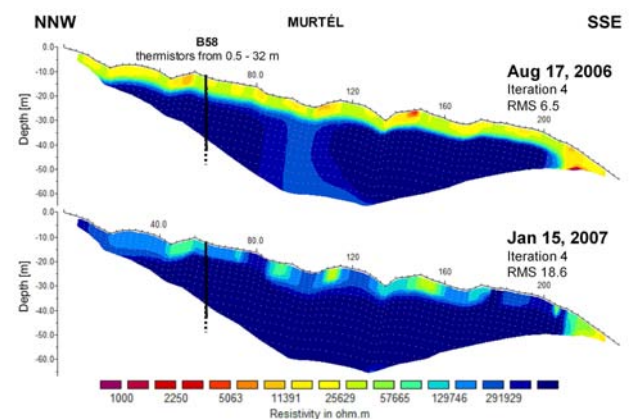


Figure 5: ERT tomogram for typical summer (top) and winter (bottom) conditions at rockglacier *Murtèl*.

Lapires

The *Lapires* site can be characterized as a talus slope thermally influenced by internal ventilation with a special pattern of permafrost and ground ice occurrence partially reflecting of this internal air circulation (reported in detail by Delaloye & Lambiel 2005). The highly resistive feature in the central part of the tomogram indicates the zone where ground ice is likely to be present. In general, such high resistivities (here > 40 k Ω m) can be caused by high amounts of ice or air within the pore space of the blocky talus slope (Hauck & Kneisel 2008). ERT monitoring results reveal substantial seasonal changes in resistivities within this zone, possibly indicating a change in material properties over the course of the year. In combination with direct observations during drilling of the borehole and subsurface temperature records, decreasing resistivities at the bottom of this feature during winter and increasing resistivities in summer appear to be related to the air circulation. This may indicate ice formation in summer and thawing processes in winter, but the process remains difficult to understand physically. However, the resistive anomaly can also be influenced by the presence of a cable car pylon in the middle of the profile, represented by very low resistivities in the upper few meters. This low resistive anomaly may cause a low confidence of the resistivity measurement and the inversion process beneath. Further

tests are necessary to judge the significance of resistivity changes as indication for changes in material properties.

Active layer freezing during winter (up to 4 m) is however clearly evidenced at this site.

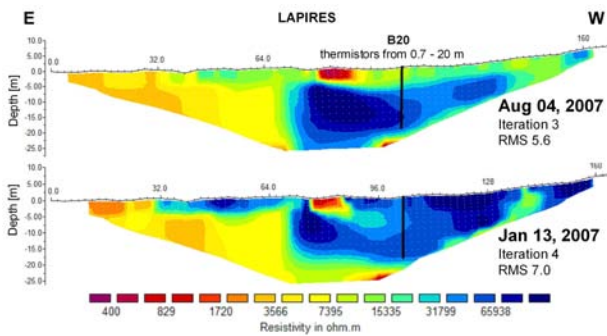


Figure 6: ERT tomogram for typical summer (top) and winter (bottom) conditions at talus slope *Lapires*.

Resistivity-temperature relationships

Resistivity-temperature (ρ - T) relationships are plotted for all four test sites in Figures 7 and 8. Figure 7 shows the results for *Schilthorn* (active layer from 0 – 4.3 m depth), where the largest data set is available. For temperatures above the freezing point results agree well with theory (Equation (1)) with slightly but continuously increasing resistivities with decreasing temperature.

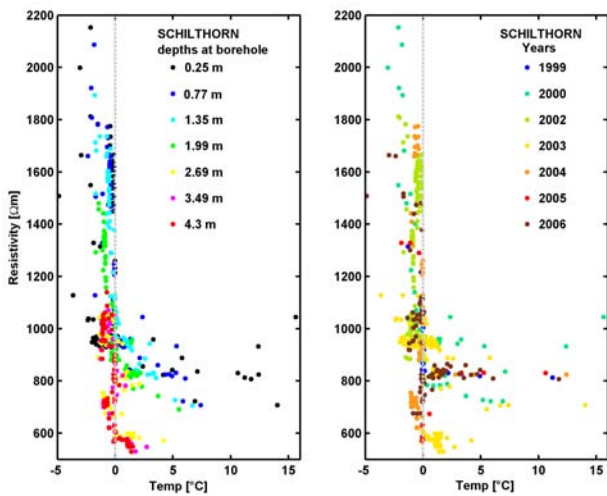


Figure 7: Resistivity at borehole location against subsurface temperatures for the 8-year *Schilthorn* dataset. Colors highlight depths (left panel) and years (right panel). Note that temporal resolution and number of measurements per year are not regular.

At subzero temperatures the reverse effect is visible at all sites: starting at temperatures slightly below the freezing point resistivities increase exponentially while temperature decrease is almost negligible. Comparing the ρ - T relationship for different depths it is apparent that although the shape of the curves is similar the resistivities are decreasing with depth, indicating higher amounts of unfrozen water at greater depths of the active layer (according to Archie’s Law). During freezing unfrozen water contents remain higher in the deeper parts represented by the still lower resistivities (Hauck 2002).

Analyzing the same data set with respect to different years, the exceptional low resistivity values of 2003 and the following years become evident as being completely below the main part of the ρ - T curve, again confirming the hypothesis of substantial ground ice degradation at *Schilthorn* in the summer of 2003.

Figure 8 shows the data from all monitoring sites. The amplitude of the resistivity increase for subzero temperatures differs significantly between the sites. While values approximately duplicate at *Schilthorn* from ca. 800 m in unfrozen state to 1600 – 2000 m in frozen state, they rise over more than an order of magnitude from < 100 k Ω m to > 2 M Ω m at *Murtèl*. Unfrozen values at *Lapires* and *Stockhorn* are similar to *Murtèl*, reflecting the blocky active layers, but frozen values are significantly lower due to the lower ice contents. Unfrozen resistivity values of *Stockhorn* cover a wide range due to high variations between dry and wet surface conditions.

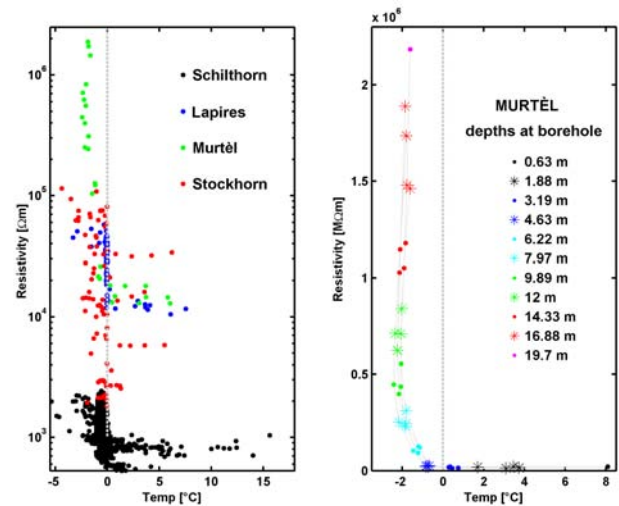


Figure 8: Left panel: comparison of amplitudes of resistivity-temperature relationships for all sites. Right panel: ρ - T relation for 4 different measurement dates at *Murtèl* with colors highlighting different depths. Note that temporal resolution and number of measurements per year are not regular.

The right panel in Figure 8 shows the ρ - T relationships for different measurement dates (lines) and depths (colors) at *Murtèl*. In contrast to *Schilthorn*, values are constant over time, showing almost the same relationship at all temporal reference points. This high degree of repeatability highlights the thermally inert role of the rockglacier and further confirms the reliability of the ERT monitoring approach, even on blocky and highly resistive terrain. A striking feature is the clear dependence of the ρ - T relation on depth. At *Murtèl* (and also at *Stockhorn* and *Lapires*, not shown here) the reverse pattern of *Schilthorn* is visible: Values increase with increasing depths. In contrast to *Schilthorn* (Fig. 7) values in Figure 8 mainly represent conditions below the permafrost table and are therefore interpreted as being due to decreasing unfrozen water contents with depth. However, also decreasing intensity of weathering, higher density and less pore space with depth may be contributing parameters.

Conclusion

Results from an ERT monitoring network at four sites in the Swiss Alps are presented and analyzed in combination with borehole temperature data. Key results from the landform-specific approach can be summarized as follows:

- Both total resistivity ranges and amplitudes of temporal resistivity changes differ markedly for the observed landforms. This is due to site-specific differences of material properties (lithology, pore volume, contents of air, ice and unfrozen water within the pore space, etc.), seasonal dynamics, temperature ranges and the hierarchy of dominating factors.
- Three-dimensional topographic effects influence radiation and turbulent heat transfer to the ground in ridge situations and complicate the pattern of resistivity distribution and seasonal changes, as shown by the example of the rock plateau *Stockhorn*.
- Small seasonal changes are recorded at the *Murtèl* site due to thermally inert characteristics of rockglaciers as opposed to high seasonal dynamics at the other sites as a consequence of internal ventilation (*Lapires* talus slope), high unfrozen water and low ice contents (*Schilthorn*) and 3D effects (*Stockhorn*).
- From the ρ -T relationships a significant dependence on depth becomes evident, with opposite behavior observed in the active layer (at *Schilthorn*) and below the permafrost table (*Stockhorn*, *Lapires*, *Murtèl*) due to differences in unfrozen water content.

A long-term continuation of the ERT monitoring in the scope of PERMOS is intended and aims at a site-specific assessment of climate related ground ice degradation.

Acknowledgments

We thank Schilthornbahn AG, Zermatt Bergbahnen AG and Corvatsch AG for logistical, and the PERMOS network (BAFU, Switzerland) for financial support, and all students that helped in the field.

References

- Beniston, M., Diaz, H.F. & Bradley, R.S. 1997: Climatic change at high elevation sites: An overview. *Climatic Change* 36(2): 233-251.
- Bundesamt für Umwelt BAFU 2006. Hinweiskarte Permafrost Schweiz. <http://www.bafu.admin.ch>.
- Claerbout, J.F. & Muir, F. 1973. Robust modeling with erratic data. *Geophysics* 38: 826-844.
- Delaloye, R. & Lambiel, C. 2005. Evidences of winter ascending air circulation throughout talus slopes and rock glaciers situated in the lower belt of alpine discontinuous permafrost (Swiss Alps). *Norwegian Journal of Geography* 59(2): 194-203.
- Fortier, R., Allard, M. & Seguin, M.K. 1994. Effect of physical properties of frozen ground on electrical resistivity logging. *Cold Regions Science and Technology* 22: 361-384.
- Frauenfeld, O.W., Zhang, T. & Barry, R.G. 2004. Interdecadal changes in seasonal freeze and thaw depths in Russia. *Journal of Geophysical research* 109: 1-12.
- Gruber, S., Hoelzle, M. & Haeberli, W. 2004. Permafrost thaw and destabilization of Alpine rock walls in the hot summer of 2003. *Geophysical Research Letters* 31: 1-4.
- Harris, C. 2001. Permafrost and Climate in Europe (PACE), *Permafrost and Periglacial Processes*, 12 (1): 156.
- Hauck, C. 2002. Frozen ground monitoring using DC resistivity tomography. *Geophysical Research Letters* 29(21): 2016.
- Hauck, C. & Kneisel C. 2008a. *Applied geophysics in periglacial environments*. Cambridge: Cambridge University Press, in press.
- Hilbich, C., Hauck, C., Hoelzle, M., Scherler, M., Schudel, L., Völksch, I., Vonder Mühl, D. & Mäusbacher, R. 2008. Monitoring of mountain permafrost evolution using electrical resistivity tomography: A seven-year study of seasonal, annual and long-term variations at Schilthorn, Swiss Alps. *Journal of Geophysical Research*, 113, F01S90.
- Hoelzle, M., Mittaz, C., Etzelmüller, B. & Haeberli, W. 2001. Surface energy fluxes and distribution of permafrost in European mountain areas: an overview of current developments. *Permafrost and Periglacial Processes* 12: 53-68.
- Intergovernmental Panel on Climate Change (IPCC) 2007. Climate change 2007: The physical science basis. Summary for policy makers. <http://www.ipcc.ch/>
- Loke, M.H. & Barker, R.D. 1995. Least-squares deconvolution of apparent resistivity. *Geophysics* 60: 1682-1690.
- Marescot, L., Loke, M.H., Chapellier, D., Delaloye, R., Lambiel, C. & Reynard, E. 2003. Assessing reliability of 2D resistivity imaging in mountain permafrost studies using the depth of investigation index method. *Near Surface Geophysics* 1.2: 57-67.
- Nelson, F.E., Anisimov, O.A. & Shiklomanov, N.I. 2001. Subsidence risk from permafrost thaw. *Nature* 410: 889-890.
- Noetzli, J., Hilbich, C., Hauck, C., Hoelzle, M. & Gruber, S. 2008. Comparison of Transient 2D Temperature Fields with Time-Lapse Electrical Resistivity Data at the Schilthorn Crest, Switzerland. *This proceedings*.
- Osterkamp, T.E. 1983. Response of Alaskan permafrost to climate. 4th International Conference on Permafrost, Fairbanks, Alaska, USA: 145-152.
- Telford, W.M., Geldart, L.P. & Sheriff, R.E. 1990. *Applied geophysics*. 2nd edition, Cambridge: Cambridge University Press, 770 pp.
- Vonder Mühl, D., Noetzli, J., Makowski, K. & Delaloye, R. (eds.) 2004. *Permafrost in Switzerland 2000/2001 and 2001/2002*. Glaciological Report (Permafrost) of the Glaciological Commission of the Swiss Academy of Sciences 2, 3.

6 Applicability of electrical resistivity tomography monitoring to coarse blocky and ice-rich permafrost landforms

Citation

Hilbich, C., Marescot, L., Hauck, C., Loke, M.H. & Mäusbacher, R. (in press). Applicability of ERT monitoring to coarse blocky and ice-rich permafrost landforms. *Permafrost and Periglacial Processes*.

This paper analyses the reliability of the inverted resistivities and their temporal changes on coarse blocky and ice-rich permafrost sites, where the most challenging conditions for conducting ERTM on alpine terrain can be found. Three different appraisal techniques are presented and applied to data sets from the Murtèl rockglacier and the Lapires talus slope². The combination of different techniques led to the identification of unreliable model regions and a refinement of the information content of the ERT images, consequently allowing a thorough evaluation of the quality of information provided by time-lapse inversion.

Main findings

- ▷ The application of forward-inverse-cycles using synthetic models representing the general characteristics of a specific study site should be conducted prior to a monitoring installation to analyse the potential of ERTM to resolve anticipated spatio-temporal resistivity changes under certain site-specific conditions.
- ▷ The depth of investigation index (DOI) not only determines the maximum investigation depth of an ERT survey, but is also useful to estimate the reliability of ERT images in transition zones with gradational resistivity changes, which are usually important features in ERTM studies on permafrost.
- ▷ The resolution matrix approach generally gives similar results as the DOI method, and places low confidence in model regions dominated by very high resistivities.

² The originally submitted version of this manuscript contained two case studies. Due to the restrictions of the page limit in the journal *Permafrost and Periglacial Processes*, the editor and one reviewer suggested to restrict the manuscript to one case study (Murtèl rockglacier). Accordingly, the Lapires case study was removed in the revised manuscript. As this decision was only due to the page limit, the results of the appraisal analysis for the Lapires talus slope are added as an appendix to *publication #3* in this thesis.

- ▷ For ice-rich permafrost landforms (such as Murtèl rockglacier), the inverted resistivities in zones of massive ground ice and in model regions with strong resistivity contrasts (e.g. between active layer and massive ground ice) are severely influenced by the inversion process and therefore of very critical reliability. Such inversion artefacts may superimpose e.g. on the general relationship between resistivity and subsurface temperatures, or between the resistivity of different ice types. Consequently, temporal resistivity variations in zones with massive ice can very likely be caused solely by the inversion process and do not necessarily indicate true variations in the permafrost regime.
- ▷ Conversely, degradation phenomena close to the surface and in the uppermost part of the ice core can successfully be identified by ERTM. At Murtèl rockglacier, a significant resistivity decrease at the top of the ice core (indicative for increasing unfrozen water contents under still negative temperatures) and a small zone with pronounced active layer deepening was observed as a consequence of the warm winter 2006/2007. As the borehole is located in a part with only minor resistivity changes, these observations again demonstrate the striking potential of ERTM for the detection of climate related changes in the permafrost regime.
- ▷ In comparison with the Lapires talus slope it could be shown, that both resolution capacity and investigation depth increase substantially for landforms with comparatively lower (i.e. not supersaturated) ice content, such that even complex spatio-temporal resistivity changes can be reliably resolved by ERTM. The monitoring data from the Lapires site indicate that ERTM is in principle capable of detecting zones with preferential air flow (ventilation funnels) within ventilated talus slopes and may thus contribute to an increased process understanding.

Applicability of Electrical Resistivity Tomography Monitoring to Coarse Blocky and Ice-rich Permafrost Landforms

C. Hilbich¹, L. Marescot², C. Hauck³, M.H. Loke⁴ and R. Mäusbacher¹

¹ Geographical Institute, University of Jena, Germany

² Institute of Geophysics, ETH, Zurich, Switzerland

³ Department of Geosciences, University of Fribourg, Switzerland

⁴ Geotomo Software, Malaysia

ABSTRACT

The inversion and interpretation of electrical resistivity tomography (ERT) data from coarse blocky and ice-rich permafrost sites is challenging due to strong resistivity contrasts and high contact resistances. To assess temporal changes during ERT monitoring (ERTM), corresponding inversion artefacts have to be separated from true subsurface changes. Appraisal techniques serve to analyse an ERTM data set from a rockglacier, including synthetic modelling, the depth of investigation index technique, and the so-called resolution matrix approach. The application of these methods led step by step to the identification of unreliable model regions and thus to the improvement of the interpretation of temporal resistivity changes. An important result is that resistivity values of model regions with strong resistivity contrasts and highly resistive features are generally of critical reliability, and resistivity changes within or below the ice core of a rockglacier should therefore not be interpreted as a permafrost signal. Conversely, long-term degradation phenomena in terms of warming of massive ground ice at the permafrost table are detectable by ERTM.

KEY WORDS: Electrical Resistivity Tomography (ERT); Murtèl rockglacier; depth of investigation (DOI) index; resolution matrix; forward-inverse-modelling

INTRODUCTION

The application of geophysical techniques and in particular of electrical resistivity tomography (ERT) to permafrost related problems has become a standard approach in recent years and is commonly used for the detection, mapping and characterisation of mountain permafrost (for a review see Kneisel & Hauck, 2008). However, within the context of global warming not only the assessment of its present state but also the temporal evolution of permafrost is of particular interest. In addition to 1-dimensional (1D) thermal monitoring techniques (e.g. in boreholes), 2D ERT monitoring (ERTM) is a promising geophysical method for the observation of possible permafrost degradation. Since the measured resistivity is largely controlled by the electrolytic conduction of unfrozen water that is distributed across grain boundaries or contained in pores, fractures and faults (e.g. Schön, 2004), ERTM is mainly sensitive to changes in the amount of unfrozen water in the subsurface material. ERTM can therefore provide information on relative changes in ice and water content with time.

Hauck (2002) and Hilbich *et al.* (2008) have proven that ERTM can successfully be applied in permafrost conditions with fine grained material providing good electrode coupling and relatively low resistivities. Based on the results from the Schilthorn monitoring site (Bernese Alps, Switzerland) presented in these studies, ERTM was recently included in the monitoring approach of a number of different permafrost landforms within the Swiss permafrost monitoring network PERMOS (Vonder Mühll *et al.*, 2007). This network involves coarse blocky permafrost sites such as rockglaciers or talus slopes, that usually constitute a challenging terrain for ERT surveys. Whereas several ERT surveys on permafrost sites with coarse blocky surface characteristics showed good results regarding a qualitative analysis of the permafrost conditions (e.g. Marescot *et al.*, 2003, Ikeda & Matsuoka, 2006, Kneisel & Käab, 2007, Maurer & Hauck, 2007, Hauck & Kneisel, 2008), their potential for quantitative ERTM purposes is still unclear.

Common problems of ERT surveying on coarse blocky material comprise the weak (and seasonally variable) electrode coupling to the ground (i.e. the blocks) and the bad electrical contact between the individual blocks within the uppermost layer of a rockglacier or talus slope. Dahlin & Loke (1998) have noted, that high electrode contact resistances often lead to higher measurement uncertainties. Another problem is the often ice-rich permafrost conditions that cause extremely high resistivities and strong resistivity contrasts between frozen and unfrozen material. In this context, Marescot *et al.* (2003) have emphasised the high probability of the occurrence of artefacts within the inverted tomograms (provoking misinterpretations) and thus the need for a methodology to evaluate the reliability of inversion results. They have shown that, while the existence and lateral extent of the ice body can be delineated, the resistivity of massive ice can not be determined accurately. In an attempt to analyse the application of ERT on talus slopes and rockglaciers, they have also indicated that the reliability of information on bedrock underneath massive ice is very limited.

The described uncertainties demonstrate that electrical resistivity measurements in such extreme environments are close to the limit of reliable data acquisition and inversion. In view of these limitations and the anticipated small temporal resistivity changes on annual time scales, ERT monitoring results in coarse blocky permafrost terrain have to be carefully analysed in terms of reliability and possible resolution of the inverted image. In order to extend the usually qualitative application of ERT to quantitative analyses of the resistivity signal, appraisal analysis is an important next step after the inversion to evaluate what features in image are influenced by artefacts due to the inversion and what regions are constrained by the data. Appraisal methods aim at evaluating (a) the confidence we can have in the existence of features observed in the inverted image, (b) the level of detail that can be obtained and (c) the resolution capability at depth (Oldenburg & Li, 1999). Different appraisal methods were presented and discussed by Oldenburg & Li (1999), Alumbaugh & Newman (2000), Friedel (2003), Stummer *et al.* (2004), and Routh & Miller (2006).

In this paper we aim to evaluate whether information provided by time-lapse ERT measurements in coarse blocky terrain is reliable enough to assess long-term permafrost degradation. We use different appraisal approaches: the calculation of the depth of investigation (DOI) index (introduced by Oldenburg & Li, 1999), and the analysis of the resolution matrix in terms of the formal model resolutions (e.g. Menke, 1984), and will extend their application to repeated ERT surveys with the aim of analysing the possibility of differentiating between the signal (i.e. the temporal resistivity change) and the uncertainties induced by data acquisition (noise), inversion (artefacts), and interpretation. In addition, we apply synthetic modelling to

demonstrate the usefulness of the DOI and resolution matrix techniques for the analysis of ERTM data, and to evaluate the internal structure of Murtèl rockglacier (Swiss Alps), that provides coarse blocky surface conditions and massive ice underneath.

We will show that the applied appraisal methods help to identify unreliable model regions, which considerably improves the interpretation of time-lapse data sets, and that ERTM is basically capable of detecting ground ice degradation under coarse blocky surface conditions.

APPRAISAL TECHNIQUES FOR ERTM

FORWARD AND INVERSE MODELLING OF SYNTHETIC RESISTIVITY MODELS

The *inverse problem* in geophysics represents the link of measured data by a mathematical relationship with the specific properties of the earth. In practical ERT applications all inverse problems are underdetermined, which is due to limited data coverage (finite number of electrodes), the resulting limited measurement precision, and inevitable noise. This leads to a non-uniqueness of the solution, meaning that an infinite number of solutions exist that fit the data equally well (Scales & Snieder, 2000, Friedel, 2003). The *forward problem* represents the prediction of a set of geophysical data based on a specific subsurface model and a set of specific model parameters. In ERT surveys this corresponds to a data set of expected measured apparent resistivities that can be calculated (predicted) from a model of synthetic (i.e. known) specific resistivities.

The inversion of the resistivity data can e.g. be carried out using the 2D inversion program RES2DINV (Loke & Barker, 1996; Loke & Dahlin, 2002) that uses a Gauss-Newton algorithm to determine the change in the model parameters:

$$\left(\mathbf{J}_k^T \mathbf{J}_k + \lambda_k \mathbf{F}\right) \Delta \mathbf{m}_k = \mathbf{J}_k^T \mathbf{d}_k - \lambda_k \mathbf{F}(\mathbf{m}_{k-1} - \mathbf{m}_0) \quad (1)$$

$$\text{with } \mathbf{F} = \alpha_s \mathbf{W}_s + \alpha_x \mathbf{C}_x^T \mathbf{W}_x \mathbf{C}_x + \alpha_z \mathbf{C}_z^T \mathbf{W}_z \mathbf{C}_z \quad (2)$$

$\Delta \mathbf{m}_k$ is the change in the model parameters for the iteration k , \mathbf{m}_{k-1} is the model parameter vector (the logarithms of the model resistivity values) at the iteration $k-1$, \mathbf{m}_0 is a homogeneous half space reference model, \mathbf{d}_k is the discrepancy vector, the difference between the logarithms of measured and calculated apparent resistivity values. \mathbf{W}_x , \mathbf{W}_z , and \mathbf{W}_s and \mathbf{C}_x and \mathbf{C}_z are weighting and smoothing matrices, respectively, and the damping factor λ_k determines the relative importance given to minimising the model roughness. α_x and α_z are the relative weights (which are both normally set to 1.0) for the roughness filters in horizontal and vertical direction. α_s is the relative weight (usually set to a smaller value such as 0.01 to 0.05) for the damping factor that minimises the deviation of the model resistivity from a reference model (see Loke & Dahlin, 2002, Oldenburg & Li, 1999). \mathbf{J}_k is the Jacobian matrix of partial derivatives (sensitivity), which is entirely recalculated after each iteration. For ERTM data sets, a joint inversion technique can be carried out in RES2DINV, which is based on cross-model constraints that uses the model obtained from the so-called time-lapse inversion of an initial data set as a reference model to constrain the inversion of the later time-lapse data sets (Loke 1999).

In contrast to the inverse problem, the solution of the forward problem is unique. Forward modelling of a synthetic resistivity model thus allows us to investigate the response of the in-

version process to a given subsurface structure to evaluate the possible resolution of features of interest, the depth of investigation, or the occurrence of inversion artefacts. As ERT data with high resistivities and/or high resistivity contrasts are known to favour the development of inversion artefacts (e.g. Rings *et al.*, 2008), forward/inverse modelling is particularly important for ERT surveys on permafrost. For ERTM purposes it is further useful to investigate the response of the inverted model to the expected time-dependent variations of specific resistivities and its resolution potential. By this, interpretation methods can be tested under controlled circumstances to overcome the problem of only limited in situ control (e.g. only by 1D boreholes) of the subsurface structures in a natural environment (Dahlin & Loke, 1998, Olayinka & Yaramanci, 2000, Hauck & Vonder Mühll, 2003, Fortier *et al.*, 2008).

Fig. 6.1 illustrates the concept of forward/inverse modelling for an example from Murtèl rockglacier (which will be introduced in the following section). Based on the results of a real ERT data set obtained in August 2006 at Murtèl rockglacier (Fig. 6.1a and Fig. 6.1b) and the information from a borehole we generated a synthetic model (Fig. 6.1c) consisting of (1) an unfrozen coarse blocky active layer (20 k Ω m), (2) an unfrozen fine-grained rockglacier front (10 k Ω m), (3) a highly resistive ice core (2000 k Ω m) segmented by (4) a less resistive anomaly (200 k Ω m), (5) an underlying layer of unfrozen blocks and debris (20 k Ω m) possibly including a talik (according to Vonder Mühll & Holub, 1992), and (6) frozen coarse blocks or bedrock (200 k Ω m). The simulated data set of expected apparent resistivities was calculated for the same electrode configuration as applied for collecting the real data (Wenner array, 48 electrodes, 5 m spacing), using the software RES2DMOD (Loke, 2002). To approximate field conditions, Gaussian random noise (Press *et al.*, 1992) of 5% was added to the simulated data, which were then inverted with the robust inversion scheme of the software RES2DINV (Loke *et al.*, 2003). The iterative inversion procedure was stopped as soon as the absolute data misfit value fell below the noise level. The inverted synthetic model (Fig. 6.1d) is compared to the inversion of the real data (Fig. 6.1b), and, if necessary, the synthetic model is adapted and the forward-inverse-cycle repeated until both synthetic and real data inversion produce similar results. According to this back-and-forth procedure (described by Fortier *et al.*, 2008) we developed the synthetic model shown in Fig. 6.1c and Fig. 6.1d, that can be regarded as a possible representation of the subsurface of Murtèl rockglacier.

THE DEPTH OF INVESTIGATION INDEX (DOI)

The Depth Of Investigation (DOI) index technique was introduced by Oldenburg & Li (1999) and first used by Marescot *et al.* (2003) for permafrost studies. In this appraisal technique, two inversions of the same data sets are carried out using equation (1), but with two different reference models with homogeneous resistivity values \mathbf{m}_{01} and \mathbf{m}_{02} . In practice, the DOI index is normalised using the DOI value at the bottom of the model $\mathbf{DOI}_{\text{bottom}}$, and is defined by:

$$\mathbf{DOI}(\mathbf{x}, \mathbf{z}) = \frac{\mathbf{m}_1(\mathbf{x}, \mathbf{z}) - \mathbf{m}_2(\mathbf{x}, \mathbf{z})}{\mathbf{DOI}_{\text{bottom}}(\mathbf{m}_{01} - \mathbf{m}_{02})} \quad (3)$$

where \mathbf{m}_1 and \mathbf{m}_2 are the resistivity values of the same particular cell for the two inversion results. The DOI value will be close to 0 in regions of the models well constrained by the data since the two inversions produce the same results. Conversely, the DOI will approach unity in regions of the model, where the inversion result is only controlled by the reference models and the data have negligible influence.

In this paper, the two reference models used are 0.1 and 10 times the average of the observed apparent resistivity of the data sets. The depth range of the models was extended to 5 times the median depth of investigation of the largest array spacing used (Edwards, 1977), so that the resistivity of the deepest model cells in the inversion model will be close to the reference model used. Moreover, a high damping factor of $\alpha_s = 0.05$ (Equation 2) was used, thus giving a large impact to the reference model used.

The technique is illustrated for Murtèl rockglacier (Fig. 6.2). The average observed apparent resistivities (\mathbf{m}_0) of the exemplary data set is 86.7 k Ω m, the two inversions of the synthetic data set were thus carried out using two reference models with resistivities of $\mathbf{m}_1 = 8.67$ k Ω m and $\mathbf{m}_2 = 867$ k Ω m (Fig. 6.2a and Fig. 6.2b). The DOI index is then calculated using Equation (3) (Fig. 6.2c). The two inversions produce similar models close to the surface (DOI close to 0), where the data have a superior influence, but only reflect the reference model at depth (DOI ~ 1). When a cut-off value of the DOI index (e.g. > 0.2 , as suggested by Oldenburg & Li, 1999) is used to disregard unreliable model regions, the two inversion results depict very similar images (Fig. 6.2d and Fig. 6.2e). Using the DOI index technique, unreliable resistivity zones, which are not constrained by the data, can be identified and the misinterpretation of inversion artefacts can be avoided. The resulting resistivity image is very similar to the synthetic model presented in Fig. 6.1 in the zones where the DOI index is lower than 0.2.

Fig. 6.3 shows the vertical resistivity distribution for the two inversions along the black lines at horizontal distances of 90 and 140 m drawn in Fig. 6.2a and Fig. 6.2b. Close to the surface at depths less than 5 m, both inversions produce similar results, confirming that the active layer is reasonably well resolved. In this region, the DOI index is close to 0. In the middle of the resistive body (between 20-30 m in depth), the two inversions produce still similar results at 90 m, but very different results at 140 m, thus showing that no reliable information can be obtained for electrical properties of the highly resistive ice body, whereas in a zone with lower resistivities (at 90 m) the reliability is much higher. Below, the resistivities approach the values of the reference models used, and thus will cross at a certain point, resulting in a DOI index of 0, although this does not mean that that part of the model is reliable. This clearly shows that DOI patterns should not be interpreted as such, but have to be used as a guideline to highlight regions of the model that are not very well constrained by the data. We therefore avoid the choice of an arbitrary cut-off value and will use the DOI index to scale the intensity of the colours of the inversion results in this study.

THE MODEL RESOLUTION MATRIX

As a further appraisal technique, the resolution matrix technique identifies model regions, where the model parameters (e.g. the specific resistivities) can be independently resolved. Following Menke (1984), the model resolution can be expressed as:

$$\mathbf{m}^{\text{est}} = \mathbf{R} \mathbf{m}^{\text{true}} \quad (4)$$

where \mathbf{R} is the model resolution matrix. If \mathbf{R} equals the identity matrix \mathbf{I} ($\mathbf{m}^{\text{est}} = \mathbf{m}^{\text{true}}$), each model parameter is uniquely determined and its resolution equals 1. Conversely, when \mathbf{R} is not an identity matrix, the estimates of the model parameters are then weighted averages of the true model parameters and their resolution is < 1 . The resolution matrix for iteration k is computed using Equation (1), but with no reference model included:

$$\mathbf{R}_k = (\mathbf{J}_k^T \mathbf{J}_k + \lambda_k \mathbf{F})^{-1} \mathbf{J}_k^T \mathbf{J}_k \quad (5)$$

This relation is strictly valid only for linear problems. As electrical inversion is non-linear, the resolution matrix in this case is only an approximation. Fig. 6.2f shows an example of a resolution matrix used for the Murtèl synthetic example. We can observe a high resolution in the active layer and low resolution in the ice core at larger depths.

The information we get from \mathbf{R} and \mathbf{DOI} is slightly different and thus a complementary use of both techniques is used to assess the reliability of inversion images in this study.

FIELD SITE

Murtèl rockglacier is located near Piz Corvatsch on the northern slope of the Upper Engadine valley (eastern Swiss Alps). It is one of the most intensely investigated rockglaciers worldwide. Borehole temperatures, recorded since 1987 (Haeberli *et al.*, 1998, Hoelzle *et al.*, 2002, Vonder Mùhll *et al.*, 2007), provide the longest temperature record in Alpine permafrost. Apart from borehole observations (Vonder Mùhll & Holub, 1992, Arenson *et al.*, 2002), no direct information exist of the interior of the rockglacier. Indirect information could be inferred from geophysical surveys (Vonder Mùhll & Klingelé, 1994, Vonder Mùhll *et al.*, 2000, Hauck & Vonder Mùhll, 2003, Maurer & Hauck, 2007).

The stratigraphy revealed by drilling (Haeberli *et al.*, 1988, Vonder Mùhll & Holub, 1992) comprises (1) a ca. 3 m thick active layer (consisting of large blocks and debris), (2) a zone with massive ice between 3 and 15 m depth (ice content ca. 80-90%; Arenson & Springman, 2005), and (3) a layer with ice and frozen sand between 15 and 30 m depth (ice content 30-35%). (4) A layer with boulders (low ice content) underneath is followed by (5) probable bedrock at about 52 m in depth. The geophysical surveys on the rockglacier revealed that this vertical structure is basically homogeneously distributed in lateral direction (Hauck *et al.*, 2003, Maurer & Hauck, 2007).

Creep rates derived from photogrammetry are relatively slow with surface velocities between 5 and 15 cm per year (Kääb *et al.*, 1998). As many rockglaciers in the Alps experienced a pronounced acceleration in recent years (Roer *et al.*, 2005, Kääb *et al.*, 2007, Delaloye *et al.*, 2008), also Murtèl shows a small increase in horizontal velocity, although the rates range between a few cm to dm per year and are much lower than for most other accelerating rockglaciers (pers. comm. I. Roer, 2008).

Due to its inert role the expected response of the rockglacier to climate change seems to be rather small, and no distinct degradation phenomena were observed so far. However, the ERTM results presented in this study hint at a more heterogeneous internal structure and temporal changes than previously assumed.

DATA ACQUISITION

A 235 m long fixed electrode array (48 electrodes, 5 m spacing) was installed in longitudinal direction across the lower part and the front of the rockglacier in summer 2005 (Fig. 6.1a). The array was installed in the vicinity of a 145 m long ERT survey (dashed line in Fig. 6.1a) conducted in July 1998 (Hauck *et al.*, 2003). Electrode coupling was extremely difficult in the blocky surface layer and considerable efforts were undertaken to fix the electrodes as deep and as firm as possible in blocky ground. In critical cases significant improvement was achieved by

parallel coupling of two electrodes (partly screwed into the blocks), which finally revealed sufficient electric contact to the ground in summer (when it is not too dry). We used a Syscal system (Iris Instruments) with high internal impedance to collect the data. Experiences on different rockglaciers showed, that contact resistances can sometimes be as high as 500 k Ω and more, only allowing input currents of predominantly < 2 mA, often even as low as 0.03 mA, but still yielding good results. As one aim of the study is to evaluate the feasibility of ERTM for automated data acquisition in the near future, we avoid the supply of water to the electrodes in this case, although contact resistances can be reduced by its usage.

For all presented data sets the Wenner array was used for the ERT measurements. Using stacking operations on the measured V/I ratio to evaluate measurement standard deviation, data with a standard deviation larger than 10% were discarded. Under less demanding permafrost conditions (i.e. fine-grained material and good electrode coupling) the variations usually remain around zero and exceed 5% only in a few cases. On coarse blocky landforms similar values are achieved under favourable conditions, but with a higher amount of outliers that must be deleted. In general, a full measurement data set is considered successful, when less than 10% of the data have to be deleted. From the ERTM data obtained at Murtèl rockglacier, three data sets are of high quality, where only 2 to 7% of the data had to be deleted: August 17, 2006, August 30, 2007, and September 09, 2008. Another data set from July 09, 2007, which is of lower quality, is presented here (15% deleted). Although the original intention was a long-term comparison with the ERT survey from July 1998 (Hauck *et al.*, 2003), this profile has even worse overall data quality (23% deleted) and was therefore not included in this analysis.

In wintertime, when the active layer is frozen, the electric contact becomes extremely weak and contact resistances rise to > 2000 k Ω , resulting in input currents < 0.02 mA. Data quality decreases substantially with many outliers with a standard deviation $> 10\%$. As no satisfying measurements could be obtained during the winters so far, only ERTM results from July to September are presented here.

RESULTS

FORWARD-INVERSE MODELLING

Prior to the analysis of field data, a synthetic rockglacier model was used to evaluate the resolution potential of ERTM regarding different scenarios and the accuracy of time-dependent resistivity changes in different model regions. The synthetic model in Fig. 6.1c was simplified (Fig. 6.4a, upper panel) and is referred to as the initial model (IM) in the following. It was then altered within the uppermost 10 m to resemble idealised freezing and thawing scenarios in the active layer and at the top of the ice core (Fig. 6.4a).

Analysis of individual inversion results

The first three scenarios in Fig. 6.4a illustrate resistivity changes within the active layer: (1) frozen (50 k Ω m), and (2) unfrozen moist conditions (2 k Ω m), and (3) a scenario identical to the IM (20 k Ω m), but with an extremely low resistive (saturated) layer (0.2 k Ω m) at the bottom of the active layer. Scenario (3) represents an idealised case of fast water infiltration through the active layer but delayed runoff on the impermeable ice core during the snow melt season. In scenario (4) the resistivities are identical to the IM, but the thickness of the active

layer is increased by 1 m at the expense of the uppermost part of the ice core. In scenarios (5) and (6) the IM was locally modified to illustrate potential causes for local anomalies in the inversion result (motivated by observed low resistive anomalies at Murtèl rockglacier, that will be discussed later): (5) a situation similar to scenario (3), but with a locally confined low resistive layer (2 k Ω m), and (6) a restricted version of scenario (4) with only local active layer thickening on the expense of the ice core.

Fig. 6.4b shows the inversion results of the different scenarios. In general, the inverted resistivities of the active layer largely satisfy the preset values, while larger deviations from the preset values are found at the right boundary of the model (corresponding to the rockglacier front), and at greater depth (comprising both ice core and bedrock). Note, that the synthetic resistivities of the ice core and bedrock remained unchanged in all scenarios, such as all deviations in the inverted resistivities of the frontal part, the ice core, and the bedrock layer from the IM are a consequence of resistivity changes within the active layer.

The inversion results of scenarios (2) and (3), characterised by low active layer resistivities, constitute major exceptions from the general model responses. Even though the inverted resistivities of the ice core are largely underestimated in *all* inverted models, inversion responses of scenarios (2) and (3) rather deny the presence of the ice core. In case (2) the resistivity of the active layer is so low that almost no current flows through deeper model regions. The saturated layer in case (3) is extremely narrow (ca. 1 m), obviously causing the emergence of an inversion artefact (ca. 25 m thick low resistive layer). According to Dahlin & Loke (1998), calculation errors usually increase with both resistivity contrast and decreasing thickness of the low resistive layer, what may explain the extreme response of the inversion. The inverted resistivities at greater depth in both models do not represent the data but are largely influenced by the resistivity of the starting models (by default the average apparent resistivity in RES2DINV), which are much lower than for the other scenarios (Table 1).

A clear detection of the lower boundary of the ice core is not evident in the different synthetic models. The limited ability to resolve stratigraphic information below the transition zone to the ice core is due to the very limited resolution capacity of the Wenner configuration at depth (e.g. Stummer *et al.*, 2004) and also to the concentration of the current flow within the least resistive upper layer. This is supported by the more detailed synthetic model of Murtèl rockglacier shown in Fig. 6.1c, where a vertical intersection of the ice core was introduced to account for the higher complexity in the interior of the rockglacier (Fig. 6.1b). The continuous vertical zone of significantly lower resistivities (200 k Ω m) enabled current flow around the right part of the ice core, and realistically reproduced the resistivity pattern of the observed ERT data (cf. Fig. 6.1c and Fig. 6.1d). Conversely, the results from a synthetic model without this vertical layer (not shown) were less consistent with the observed data. As a consequence of this “channelled” current flow, the lower boundary of the ice-rich layer can only be identified in the right part of Murtèl rockglacier (Fig. 6.1d). The capacity of ERT to delineate the thickness of such ice-rich layers can further be increased by extending the survey line into unfrozen regions at both ends of a rockglacier to enable current flow below the highly resistive core (see also results by Hauck *et al.* (2003) for an ice-cored moraine).

A vertical cut through the synthetic and inverted synthetic models at 90 m horizontal distance is shown in Fig. 6.5. The difference between the sharp resistivity contrasts of the synthetic models and the smooth contrasts of the inversion models, caused by the least-squares approach of the algorithm, is clearly seen. Apart from that, the inverted resistivities of scenarios (1), (4), and (6) largely correspond to their synthetic models in the upper part of the profile. In

all scenarios the thickness of the active layer, defined as the depth where resistivity sharply increases, is relatively well resolved, despite the large electrode spacing, but the resistivity of the ice core is underestimated (cf. Fig. 6.5). In contrast, the resistivity of the very low resistive layers in scenarios (3) and (5) is overestimated and they completely fail to resolve the thickness of the low resistive layer. Sharp boundaries between stratigraphic interfaces of the synthetic models generally appear gradational, which is a consequence of the imposed damping and smoothness constraints and hence a common characteristic of tomographic inversion results (Stummer *et al.*, 2004).

However, Fig. 6.5 also indicates that, within moderate bounds, relative differences between the synthetic models are properly resolved by the inversion, as is the case for scenarios (1), (4), and (6), which are characterised by the lowest model misfits in Table 1. Temporal resistivity changes due to freezing/thawing of the active layer or melting of the top of the ice core should therefore be detectable by ERTM. Further synthetic modelling tests (not shown here) revealed that thawing of the ice core from below would not be detectable under the given circumstances.

Another important result of the synthetic modelling is that the large differences in the inverted models are a consequence of the different starting models and the limited resolution at depth. Absolute resistivity values of the ice core are very likely a function of the resistivity of the active layer, and hence the resistivity contrast. In ERT applications that aim at relating absolute resistivity values of highly resistive ice bodies to, e.g. possible origins of the ice in rockglaciers (e.g. Haeberli & Vonder Mühll, 1996, Ishikawa *et al.*, 2001), to the ice content, or to subsurface temperature data, this problem related to strong resistivity contrasts has to be taken into account. Concerning ERTM, resistivity changes in the ice core are therefore not reliably interpretable if temporal resistivity changes within the active layer are present.

Analysis of time-lapse inversion results

Time-lapse inversion was performed for all scenarios (with the inversion result of the IM used as reference model) to analyse the accuracy of modelled resistivity changes relative to the IM (Fig. 6.4c). Since the reliability of the results for scenarios (2) and (3) is low (see above), we will only address resistivity changes from the IM to scenarios (1), (4), (5), and (6).

Freezing of the active layer causes a significant resistivity increase of more than 100% in the upper part of the time-lapse tomogram in scenario (1) (Fig. 6.4c: IM to (1)). But also at greater depths pronounced resistivity increases of up to 50%, and even 100% close to the transition to the front, are visible. As the reduction of the resistivity contrast (by the frozen active layer) improves the resolution of the true resistivity of the ice core (cf. Fig. 6.5), the observed temporal resistivity increase reflects only the different resolution capacities of both scenarios, and not a change in true resistivity. This is also supported by the lowest data misfit value of all time-lapse inversions revealed for the frozen active layer scenario.

Scenario (4) (Fig. 6.4c: IM to (4)) strikingly illustrates the capability of ERTM to detect a melting of massive ground ice from above, while the resistivity in the active layer remains unchanged. However, the reduction in ice core thickness is largely overestimated (5-10 m instead of 1 m)! This is partly due to a decrease in the resolution of the electrical method with depth, but a major factor is the limited vertical resolution (5 m electrode spacing), resulting in an increased thickness of the zone with changed resistivity in the time-lapse tomogram. As a consequence of the principle of equivalence, the overall resistivity decrease obtained (about 60-

70%) is lower than in the synthetic model (99%). Similar to scenario (1), the resistivity decrease below the melted ice core is very likely to be associated with the different resolution capacities of both models at depth.

Time-lapse responses of scenarios (5) and (6) (Fig. 6.4c: IM to (5) and IM to (6)) are similar, though their causes differ significantly. Although the introduced anomaly in scenario (5) is smaller in size than in scenario (6), its response in the time-lapse inversion is larger. As discussed earlier, the presence of a low resistive layer at the transition to a highly resistive layer (5) causes an inversion artefact, suggesting a “block” with decreased resistivity *within* rather than a thin low resistive layer *on* the ice core. Interestingly, the locally restricted scenario of ice core melting (6) provides a more realistic estimate of its depth extent than scenario (4), though still overestimated by a factor of 6 to 7.

Even though the overall trends are well reproduced in all cases, it can be stated that the interpretation of time-lapse tomograms of rockglaciers is generally difficult due to the high probability of contamination with inversion artefacts. Moreover, one should be aware of the sometimes misleading resistivity changes as a consequence of limited resolution power. Nevertheless, the analysis showed that freezing or thawing of the active layer, as well as a degradation (shrinking) of the ice core are well detectable by ERTM, whereas the accuracy in the estimation of both spatial dimension and quantity may be limited in some cases.

ERTM RESULTS

After the analysis of the general applicability of ERTM to the observation of permafrost evolution, ERTM data from Murtèl rockglacier from August 2006, July 2007, August 2007, and September 2008 will be studied in the following. The synthetic modelling tests indicate a rather low reliability of the resistivity values below the active layer as a consequence of the extremely resistive ice core. The DOI index technique and the resolution matrix approach will now be applied to further appraise the reliability of the spatial resistivity distribution and temporal changes.

Analysis of the DOI index

Fig. 6.6a and Fig. 6.6b show the calculated DOI index and the inversion results from the four measurement dates with the intensity of the colours scaled by DOI values > 0.2 (pale colours are associated with a high DOI index and thus denote unreliable inversion results). At first glance the tomograms do not differ much. Striking features are the comparably low resistive active layer (ca. 20 k Ω m), the highly resistive ice core (> 1000 k Ω m), and a zone in the central part of the ice core with lower resistivities (ca. 300-500 k Ω m). On closer inspection, the resistivity of the ice core (especially the left part) changes considerably between the subsequent measurement dates (by up to 500 k Ω m). Also the thickness of the active layer exhibits a pronounced variability in the central part (especially in August 2007). Note, that the bedrock underneath the rockglacier (expected at about 50 m depth) is not resolved in all tomograms. Small data misfit values (referred to as absolute errors in the figures) in all cases confirm the good principal quality of these inversion results.

The calculated DOI indices (Fig. 6.6a) vary slightly between the measurement dates, but a common pattern can be identified in all tomograms: DOI values remain very low (< 0.2) in the active layer, show several intermediate zones (0.2 – 0.4) in the region of the ice core and

the front of the rockglacier and increase rapidly at a depth of about 50 m, indicated by the complete fade out of the colours in Fig. 6.6b.

Notwithstanding the original sense of the DOI concept to define the depth region where the image is no longer constrained by the data, the method is also sensitive to zones with distinct resistivity gradients, as the strength of the resistivity gradient will significantly depend on the reference model used. This is the case for the transition between active layer and ice core, between ice core and the rockglacier front, and within the vertical anomaly (between 80 and 120 m horizontal distance) in the neighbourhood of the most resistive zone of the profile. Especially around these transition zones the DOI index can be a valuable measure of how well gradational transitions reflect the subsurface conditions.

Apart from the transition zones, the DOI index clearly indicates low sensitivity within the ice core, especially in the left part, which corresponds to the above mentioned zone with strong (but unexpected) resistivity changes between subsequent measurements. The DOI values in the upper 10-20 m of the ice core are below 0.2, suggesting that this is the part of the ice core best constrained by the data. Interestingly, the vertical zone intersecting the ice core is attributed with low reliability in all data sets. However, the forward modelling tests revealed that a vertical anomaly with comparatively low resistivity is a necessary condition to reproduce the measured data (see also Fig. 6.1c and Fig. 6.1d), and that the resistivity of this zone was over-estimated by a factor of > 2 in most inversion results. As discussed earlier, current flow is basically restricted to the active layer and the front of the rockglacier, and, by the presence of this vertical anomaly, around the frontal part of the ice core. The different reference models used for the calculation of the DOI significantly influence the resistivity of this zone, causing high DOI values. Consequently, the presence of a less resistive zone within the ice core is very likely but the reliability of the resistivity values is, however, rather low.

In addition to the individual tomograms, a time-lapse inversion was carried out for the data set (with the inversion result from August 17, 2006 used as reference model for the later ERTM data). Resistivity changes were calculated for subsequent time steps and for the full two-year period (August 2006 - September 2008) and are plotted in Fig. 6.6c. Blue and red colours stand for a resistivity increase and decrease, respectively. For the time-lapse studies, separate DOI distributions were calculated for each tomogram. From these we chose the maximum DOI distribution for each pair of tomograms as an upper bound for the reliability of the calculated resistivity changes (referred to as DOI_{max} in Fig. 6.6c).

The time-lapse results show (a) horizontally irregular changes within the active layer attributed to differences in water saturation, (b) a zone of more homogeneous changes at the transition to or within the uppermost part of the ice core, with a decrease of up to 75% between summers 2006 and 2007, and (c) zones with large positive and negative changes (up to 40%) in deeper parts of the profile and close to the rockglacier front. However, high DOI values in the zone of massive ice point to an increased risk of inversion artefacts or limited accuracy in the resistivity values. Borehole temperatures, that do not indicate large temperature variations in deeper parts of the rockglacier, support the assumption that resistivity changes in this zone are of low reliability.

According to relatively low DOI values in the upper parts of the time-lapse tomograms, calculated resistivity changes in this zone are reliable results, and can be interpreted as true freeze/thaw processes (in agreement with the synthetic modelling results).

Analysis of the formal model resolution

The formal model resolution for the Murtèl data set (Fig. 6.6d) is largest in the active layer and the frontal part, and diminishes rapidly at the transition to the highly resistive ice core in all tomograms. Stummer *et al.* (2004) showed that electrical current concentration (resulting in larger formal model resolutions) occurs above and below resistive blocks or layers and give a threshold of about 0.05, below which model resolutions are considered to indicate only poorly resolved model regions. This value roughly corresponds to the red colour in Fig. 6.6d, i.e. yellow and white colours stand for an unsatisfactory resolution. The conclusions for the Murtèl site are straightforward and confirm the findings of the synthetic modelling and DOI analyses: for rockglaciers with a highly resistive core of massive ice and the corresponding strong resistivity contrast between active layer and ice core the resolution capacity of ERT data is very limited and can be described roughly as a function of conductivity. Consequently, the resolution increases in the zones with locally increased active layer depth and lower resistivities at the surface of the ice core, as observed in both data sets from 2007 compared to 2006 and 2008 (Fig. 6.6b). Also the less resistive vertical zone within the ice core is accentuated by slightly higher, but still poor, resolution. This implies that long-term permafrost degradation (associated with a resistivity decrease) would increase the resolution in the respective model region, and should therefore be detectable by ERTM.

DISCUSSION OF TIME-LAPSE ERTM RESULTS

Using the above results, we are now able to restrict the interpretation of the time-lapse inversion results between summer 2006 and 2008 to reliable model regions, i.e. to the active layer and the top of the ice core. Apart from seasonal variations in the active layer, reflecting moister or drier conditions, a significant decrease in resistivities can be observed along the whole survey line at the transition between active layer and ice core in 2007, which is still present in September 2008 (Fig. 6.6c, zone A). Hoelzle & Gruber (2008) report that air temperatures in winter 2006/2007 at nearby meteorological stations were the warmest ever recorded. Although snow cover thickness was the lowest since 1972, this prevented an effective cooling and caused significantly higher temperatures in the uppermost 15 m of the rockglacier in summer 2007 compared to 2006. The observed resistivity changes near the borehole position (indicated in Fig. 6.6c) correspond well to the borehole temperatures that indicate for August 2006 and 2007 a temperature difference of 0.2 - 0.8 K between 3.8 and 15 m depth (frozen), and even more in the uppermost 3 m (unfrozen). Note, that the borehole is located in a zone with only minor resistivity changes, and that the more pronounced variations between 0 and 50 m, and 80 and 120 m horizontal distance can not be verified by temperature data. We suggest that the exceptionally warm winter 2006/2007 led to a sustained warming at the top of the ice core (zone A), with different magnitudes along the survey line and persisting for at least 2 years (summers 2007 and 2008). The negligible difference between August 2007 and September 2008 confirms that the impact from winter 2007 was not yet compensated in 2008.

As the active layer thickness can not grow over massive ice due to the absent supply of rock material from the ice itself (Haeberli & Vonder Mühll, 1996), a detection of permafrost degradation by ERTM would, strictly spoken, only be possible in terms of a resistivity decrease due to a warming (not melting) of the permafrost. This is what we observe in zone A, where resistivity values of $> 200 \text{ k}\Omega\text{m}$ still indicate frozen conditions. Conversely, a resistivity decrease to less than $30 \text{ k}\Omega\text{m}$, as observed in zone B in August 2007, points to unfrozen conditions. This in turn reflects a locally increased active layer depth and indicates that the ice content must

have been significantly lower in this part of the rockglacier (see above: otherwise thaw subsidence should have occurred rather than a thickening of the active layer). The anomalous zone B amounts to 3-4 m thickness in the ERTM data, but, as discussed above, its true vertical extent is unknown. This local active layer thickening is remarkable, since maximum active layer depths (obtained from borehole temperatures) only varied by a few centimetres in the last 20 years (Vonder Mühll *et al.*, 2007, Bauder *et al.*, 2008), and by only 1 cm between 2006 and 2007 (note, that almost no resistivity change is visible at the borehole position). According to the synthetic modelling (Fig. 6.4, scenario (6)) we interpret the observed local active layer thickening in summer 2007 to be a real feature, whereas the resolution capacity of its vertical extent is critical due to the large electrode spacing. In contrast to scenario (6), an interpretation according to scenario (5) is less probable as a decreasing resistivity of the active layer due to a local formation of a moist layer would be expected (cf. Fig. 6.4), which was not observed.

We conclude from the time-lapse analysis that ERTM revealed a spatially heterogeneous impact of the warm winter 2006/2007 on the permafrost regime of Murtèl rockglacier that is in general more severe than observed at the borehole position: The top of the ice layer shows a significant resistivity decrease, and locally (in a zone where less ice content is assumed) even a melting of the ice (i.e. a thickening of the active layer) is indicated. In contrast to the overall resistivity decrease at the top of the ice core (zone A), the local active layer thickening (zone B) did not persist until summer 2008. ERTM will be continued in the following years to evaluate whether the observed resistivity changes indicate long-term permafrost degradation.

CONCLUSIONS

Strong resistivity contrasts and high contact resistances make the acquisition, inversion and interpretation of ERT data from coarse blocky and ice-rich permafrost sites difficult. To assess changes during ERT monitoring (ERTM) it is essential to separate changes due to corresponding inversion artefacts from true temporal subsurface changes. Three appraisal methods were used to analyse an ERTM data set from Murtèl rockglacier. The application of these methods led step by step to the identification of unreliable model regions.

The strengths of the applied methods are:

- Forward-inverse-cycles using synthetic models served to analyse structural information and potential temporal resistivity changes inferred from inversion results before the interpretation of time-lapse data. Valuable insights into the potential to detect anticipated spatio-temporal resistivity changes are possible with this method.
- The DOI method provides information which model regions are well constrained by the data and which regions are mainly influenced by the resistivity of the applied reference model. Not only the maximum investigation depth can be estimated, but also the reliability of the image in transition zones with gradational resistivity changes.
- The formal model resolution is roughly a function of electrical conductivity, and generally places low confidence to the inverted resistivities of highly resistive model regions.

From the analysis of the applied appraisal techniques it turned out that the information content of ERTM results could be refined by the combination of these methods, allowing a responsible evaluation of the information provided by time-lapse inversion. The general implications for the applicability of ERTM to coarse blocky and ice-rich permafrost sites are:

- Without additional constraints in the inversion algorithm, temporal resistivity variations in zones with massive ice are most likely a function of a change in resistivity contrast, and therefore caused by the inversion process. Such features do not necessarily indicate true variations in the permafrost conditions!
- Temporal degradation phenomena in terms of long-term changes in active layer thickness or rather a melting of the ground ice at the permafrost table are suggested to be detectable by ERTM. The accuracy in determining the vertical extent of such features is, however, a function of the electrode spacing and depth of investigation.
- Absolute resistivity values in zones of massive ground ice and in model regions with strong resistivity contrasts (e.g. between active layer and massive ground ice) are strongly influenced by the inversion process and thus of very critical reliability. This has to be taken into account for ERT applications that relate absolute resistivity values to subsurface temperatures or the ice-origin of rockglaciers, for example.
- As the inversion process is sensitive to strong resistivity contrasts, this problem can be minimised by conducting ERTM measurements (also) during winter, when the active layer is frozen (if electrode coupling is sufficient). It is also recommended to extend survey lines into unfrozen surroundings at both ends of rockglaciers or other ice-rich landforms, to increase the resolution near the lower boundary of the ice core.
- For Murtèl rockglacier all the above limitations prohibit a detailed detection of processes within or below the ice core, but degradation phenomena from above, such as the observed local active layer thickening and the pronounced resistivity decrease at the top of the ice core in 2007, can be identified.

Apart from the limiting factors mentioned above, ERTM has a large potential regarding the identification of the spatio-temporal heterogeneity of the anticipated climate-induced degradation of mountain permafrost and the relative quantification of ground ice degradation.

Acknowledgements

We like to thank all students that helped with the data acquisition, especially Martin Baum and Sebastian Klein. Many thanks also to Martin Hoelzle for making us available the borehole data of Murtèl and for fruitful discussions of the ERTM results, and to the two reviewers for their constructive comments. The study was funded by the PERMOS network (BAFU, Switzerland) and by the DFG (MA1308_22-1).

REFERENCES

- Alumbaugh DL, Newman GA. 2000. Image appraisal for 2-D and 3-D electromagnetic inversion. *Geophysics* **65**(5): 1455-1467. DOI:10.1190/1.1444834
- Arenson L, Hoelzle M, Springman S. 2002. Borehole deformation measurements and internal structure of some rock glaciers in Switzerland. *Permafrost and Periglacial Processes* **13**(2): 117-135. DOI: 10.1002/ppp.414

- Arenson L, Springman S. 2005. Triaxial constant stress and constant strain rate tests on ice-rich permafrost samples. *Canadian Geotechnical Journal* **42**(2): 412-430. DOI: 10.1139/t04-111
- Bauder A, Marty C, Noetzi J. 2008: Schnee, Gletscher und Permafrost 2005/06 und 2006/07. *Die Alpen* **9**: 47-56.
- Dahlin T, Loke MH. 1998. Resolution of 2D Wenner resistivity imaging as assessed by numerical modelling. *Journal of Applied Geophysics* **38**(4): 237-249. DOI: 10.1016/S0926-9851(97)00030-X
- Delaloye R, Perruchoud E, Avian M, Kaufmann V, Bodin X, Hausmann H, Ikeda A, Käab A, Kellerer-Pirklbauer A, Krainer K, Lambiel C, Mihajlovic D, Staub B, Roer I, Thibert E. 2008. Recent Interannual Variations of Rock Glacier Creep in the European Alps. *Proceedings of the Ninth International Conference on Permafrost*, Fairbanks, Alaska, Volume I: 343-348.
- Edwards LS. 1977. Modified Pseudo-Section for Resistivity and IP. *Geophysics* **42**(5): 1020-1036. DOI: 10.1190/1.1440762
- Fortier R, LeBlanc AM, Allard M, Buteau S, Calmels F. 2008. Internal structure and conditions of permafrost mounds at Umiujaq in Nunavik, Canada, inferred from field investigation and electrical resistivity tomography. *Canadian Journal of Earth Sciences* **45**(3): 367-387. DOI: 10.1139/E08-004
- Friedel S. 2003. Resolution, stability and efficiency of resistivity tomography estimated from a generalized inverse approach. *Geophysical Journal International* **153**(2): 305-316. DOI: 10.1046/j.1365-246X.2003.01890.x
- Haerberli W, Huder J, Keusen HR, Pika J, Röthlisberger H. 1988. Core drilling through rock glacier-permafrost. *Proceedings of the 5th International Conference on Permafrost*, Trondheim, Norway, Volume 2: 937-942.
- Haerberli W Vonder Mühl D. 1996. On the characteristics and possible origins of ice in rock glacier permafrost. *Zeitschrift für Geomorphologie*, N.F. Suppl. **1004**: 43-57.
- Haerberli W, Hoelzle M, Käab A, Keller F, Vonder Mühl D, Wagner S. 1998. Ten years after drilling through the permafrost of the active rock glacier Murtèl, eastern Swiss Alps: answered questions and new perspectives. *Proceedings of the 7th International Conference on Permafrost*, Yellowknife, Canada: 403-410
- Hauck C. 2002. Frozen ground monitoring using DC resistivity tomography. *Geophysical Research Letters* **29**(21): 2016. DOI: 10.1029/2002GL014995
- Hauck C, Vonder Mühl D, Maurer H. 2003. Using DC resistivity tomography to detect and characterize mountain permafrost. *Geophysical Prospecting* **51**(4): 273-284. DOI: 10.1046/j.1365-2478.2003.00375.x
- Hauck C, Vonder Mühl D. 2003. Inversion and interpretation of two-dimensional geoelectrical measurements for detecting permafrost in mountainous regions. *Permafrost and Periglacial Processes* **14**(4): 305-318. DOI: 10.1002/ppp.462
- Hauck C, Kneisel C. 2008: *Applied geophysics in periglacial environments*. Cambridge University Press: Cambridge, 240 pp.
- Hilbich C, Hauck C, Hoelzle M, Scherler M, Schudel L, Völksch I, Vonder Mühl D, Mäusbacher R. 2008. Monitoring mountain permafrost evolution using electrical resistivity tomo-

- graphy: A 7-year study of seasonal, annual, and long-term variations at Schilthorn, Swiss Alps. *Journal of Geophysical Research* **113**: F01S90. DOI: 10.1029/2007JF000799
- Hoelzle M, Vonder Mühll D, Haeberli W. 2002. Thirty years of permafrost research in the Corvatsch-Furtschellas area, Eastern Swiss Alps: a review. *Norwegian Journal of Geography* **56**: 137-145. DOI: 10.1080/002919502760056468
- Hoelzle M, Gruber S. 2008. Borehole and Ground Surface Temperatures and Their Relationship to Meteorological Conditions in the Swiss Alps. *Proceedings of the Ninth International Conference on Permafrost*, Fairbanks, Alaska, Volume I: 723-728.
- Ikeda A, Matsuoka N. 2006. Pebbly versus bouldery rock glaciers: Morphology, structure and processes. *Geomorphology* **73**(3-4): 279–296. DOI: 10.1016/j.geomorph.2005.07.015
- Ishikawa M, Watanabe T, Nakamura N. 2001. Genetic differences of rock glaciers and the discontinuous mountain permafrost zone in Kanchanjunga Himal, Eastern Nepal. *Permafrost and Periglacial Processes* **12**(2): 243-253. DOI: 10.1002/ppp.394
- Kääb A, Gudmundsson GH, Hoelzle M. 1998. Surface deformation of creeping mountain permafrost. Photogrammetric investigations on rock glacier Murtél, Swiss Alps. *Proceedings of the 7th International Conference on Permafrost*, Yellowknife, Canada: 531-537.
- Kääb A, Frauenfelder R, Roer I. 2007. On the response of rockglacier creep to surface temperature increase. *Global and Planetary Change* **56**(1-2): 172-187. DOI: 10.1016/j.gloplacha.2006.07.005
- Kneisel C, Kääb A. 2007. Mountain permafrost dynamics within a recently exposed glacier forefield inferred by a combined geomorphological, geophysical and photogrammetrical approach. *Earth Surface Processes and Landforms* **32**(12): 1797-1810. DOI: 10.1002/esp.1488
- Kneisel C, Hauck C. 2008. Electrical Methods. In *Applied geophysics in periglacial environments*, Hauck C, Kneisel C (eds.). Cambridge University Press: Cambridge: 3-27.
- Kneisel C, Hauck C, Fortier R, Moorman B. 2008. Advances in geophysical methods for permafrost investigations. *Permafrost and Periglacial Processes* **19**(2): 157-178. DOI: 10.1002/ppp.616
- Loke MH, Barker, RD. 1996. Rapid least-squares inversion of apparent resistivity pseudosections by a quasi-Newton method. *Geophysical Prospecting* **44**(1): 131-152. DOI: 10.1111/j.1365-2478.1996.tb00142.x
- Loke MH. 1999. Time lapse resistivity imaging inversion. *Proceedings of the 5th Meeting of the EEGS European Section*, Em1.
- Loke MH, Dahlin T. 2002. A comparison of Gauss-Newton and quasi-Newton methods in resistivity imaging inversion. *Journal of Applied Geophysics* **49**: 149-162. DOI: 10.1016/S0926-9851(01)00106-9
- Loke MH. 2002. RES2DMOD ver. 3.01: Rapid 2D resistivity forward modelling using the finite-difference and finite-element methods.
- Loke MH, Acworth I, Dahlin T. 2003. A comparison of smooth and blocky inversion methods in 2D electrical imaging surveys. *Exploration Geophysics* **34**(3): 182-187. DOI: 10.1071/EG03182

- Marescot L, Loke MH, Chapellier D, Delaloye R, Lambiel C, Reynard E. 2003. Assessing reliability of 2D resistivity imaging in mountain permafrost studies using the depth of investigation index method. *Near Surface Geophysics* **1**(2): 57-67.
- Maurer H, Hauck C. 2007. Geophysical imaging of alpine rock glaciers. *Journal of Glaciology* **53**(180): 110-120. DOI: 10.3189/172756507781833893
- Menke W. 1984. *Geophysical data analysis: Discrete inverse theory*. Academic Press, Inc.: Orlando, 260 pp.
- Olayinka AI, Yaramanci U. 2000. Assessment of the reliability of 2D inversion of apparent resistivity data. *Geophysical Prospecting* **48**(2): 293-316.
- Oldenburg DW, Li YG. 1999. Estimating depth of investigation in dc resistivity and IP surveys. *Geophysics* **64**(2): 403-416. DOI: 10.1190/1.1444545
- Press WH, Teukolsky SA, Vetterling WT, Flannery BP. 1992. Numerical recipes in C. Cambridge University Press: Cambridge, 994 pp.
- Rings J, Scheuermann A, Preko K, Hauck C. 2008: Soil water content monitoring on a dike model using electrical resistivity tomography. *Near Surface Geophysics* **6**: 123-132.
- Roer I, Käab A, Dikau R. 2005. Rockglacier acceleration in the Turtmann valley (Swiss Alps): Probable controls. *Norwegian Journal of Geography* **59**: 157-163. DOI: 10.1080/00291950510020655
- Routh PS, Miller CR. 2006. Image interpretation using appraisal analysis. *SAGEEP Proceedings*, 1812–1820.
- Scales J.A, Snieder R. 2000. The anatomy of inverse problems. *Geophysics* **65**(6): 1708-1710.
- Schön JH. 2004. *Physical properties of rocks: Fundamentals and principles of petrophysics*. Elsevier: Amsterdam, 600 pp.
- Stummer P, Maurer H, Green AG. 2004. Experimental design: Electrical resistivity data sets that provide optimum subsurface information. *Geophysics* **69**(1): 120-139. DOI: 10.1190/1.1649381
- Vonder Mühl D, Holub P. 1992. Borehole logging in Alpine permafrost, Upper Engadine, Swiss Alps. *Permafrost and Periglacial Processes* **3**(2): 125-132. DOI: 10.1002/ppp.3430030209
- Vonder Mühl DS, Klingele EE. 1994. Gravimetric Investigation of Ice-Rich Permafrost within the Rock Glacier Murtèl-Corvatsch (Upper Engadin, Swiss Alps). *Permafrost and Periglacial Processes* **5**(1): 13-24. DOI: 10.1002/ppp.3430050103
- Vonder Mühl DS, Hauck C, Lehmann F. 2000. Verification of geophysical models in Alpine permafrost using borehole information. *Annals of Glaciology* **31**: 300-306. DOI: 10.3189/172756400781820057
- Vonder Mühl D, Noetzi J, Roer I, Makowski K, Delaloye R. 2007. Permafrost in Switzerland 2002/2003 and 2003/2004. Glaciological Report (Permafrost) No. 4/5 of the Cryospheric Commission (CC) of the Swiss Academy of Sciences (SCNAT) and the Department of Geography, University of Zurich, 107 pp.

TABLE:

Tab. 6.1: Absolute model misfits ($1/N \sum k (|m_{k+1} - m_k| / |m_k|)$) (according to Equation 2) within the upper 40 m, and average apparent resistivities of the initial rockglacier model and the different freezing and thawing scenarios.

		(1)	(2)	(3)	(4)	(5)	(6)
Model	initial	frozen active layer	moist active layer	saturated layer	thawed ice core	saturated layer (local)	thawed ice core (local)
absolute model misfit	0.25%	0.24%	0.29%	1.46%	0.23%	0.29%	0.25%
average ρ_a (starting model)	100 k Ω m	205 k Ω m	11 k Ω m	7 k Ω m	78 k Ω m	69 k Ω m	76 k Ω m

FIGURE CAPTIONS:

Fig. 6.1: a) Photo of Murtèl rockglacier with the position of the borehole (dot), the ERTM line (bold) and the ERT line of 1998 (dashed), b) inverted image of an ERT measurement in August 2006, and a possible representation of the real data set in terms of c) a synthetic model and d) the corresponding inversion result. Numbers in c) indicate the various elements of the model and are described in the text. The location of the site within Switzerland is indicated in the inset.

Fig. 6.2: Illustration of the two inversion results of the synthetic Murtèl rockglacier model based on the different reference models with factors 0.1 (a) and 10 (b) of the average apparent resistivity, and c) the calculated DOI index. The inverted resistivity models a) and b) were cut according to a DOI index > 0.2 in d) and e). The formal model resolution of the synthetic rockglacier model is shown in f).

Fig. 6.3: A vertical cut through DOI models a) and b) in Figure 6.2 at 90 and 140 m horizontal distance.

Fig. 6.4: The initial rockglacier model (upper panel) and different freezing and thawing scenarios: a) synthetic resistivity models, b) inverted synthetic resistivity models, and c) percentage change in resistivities relative to the initial model revealed by time-lapse inversion.

Fig. 6.5: Resistivity-depth plots representing a cut through a) the synthetic and b) the inverted synthetic rockglacier models in Figure 6.4a and 6.4b at 90 m horizontal distance.

Fig. 6.6: a) Calculated DOI index, b) inverted models with the intensity of the colours scaled by the DOI index (for better visibility scaled by DOI index > 0.2), c) time-lapse tomograms scaled by DOI_{max} > 0.2 , and d) formal model resolution for the Murtèl data set. Pale colours in b) and c) are associated with unreliable inversion results. Highlighted zones A and B are described in the text.

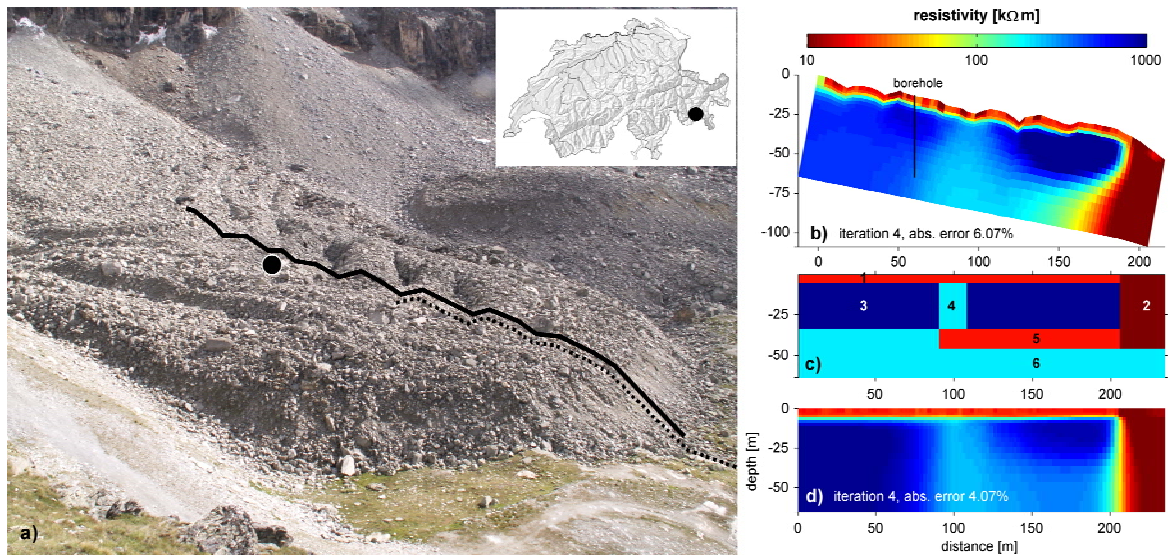


Fig. 6.1: a) Photo of Murtèl rockglacier with the position of the borehole (dot), the ERTM line (bold) and the ERT line of 1998 (dashed), b) inverted image of an ERT measurement in August 2006, and a possible representation of the real data set in terms of c) a synthetic model and d) the corresponding inversion result. Numbers in c) indicate the various elements of the model and are described in the text. The location of the site within Switzerland is indicated in the inset.

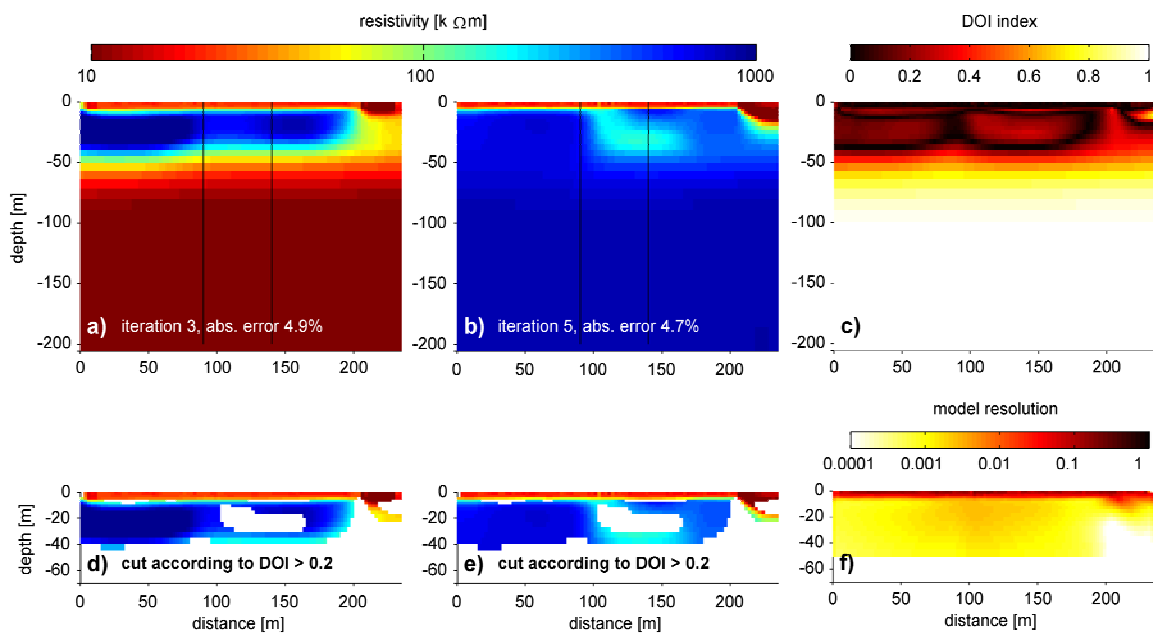


Fig. 6.2: Illustration of the two inversion results of the synthetic Murtèl rockglacier model based on the different reference models with factors 0.1 (a) and 10 (b) of the average apparent resistivity, and c) the calculated DOI index. The inverted resistivity models a) and b) were cut according to a DOI index > 0.2 in d) and e). The formal model resolution of the synthetic rockglacier model is shown in f).

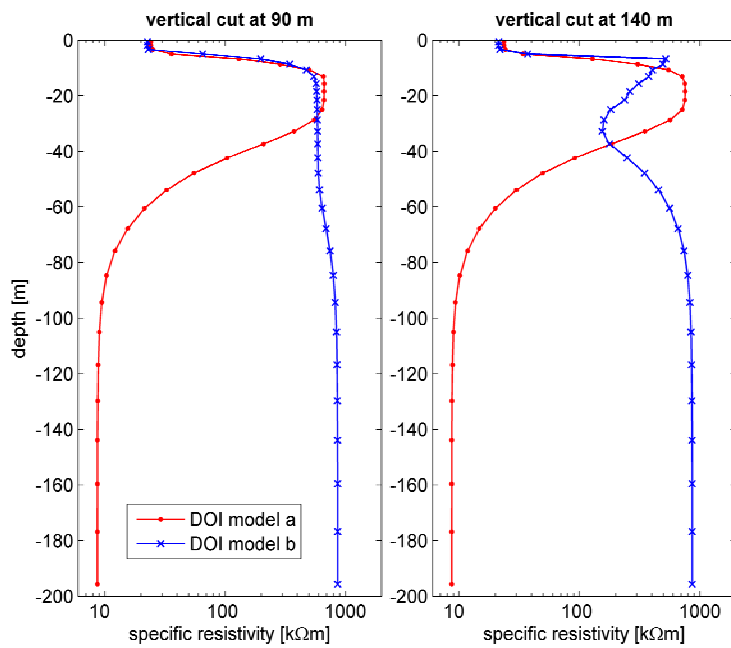


Fig. 6.3: A vertical cut through DOI models a) and b) in Figure 6.2 at 90 and 140 m horizontal distance.

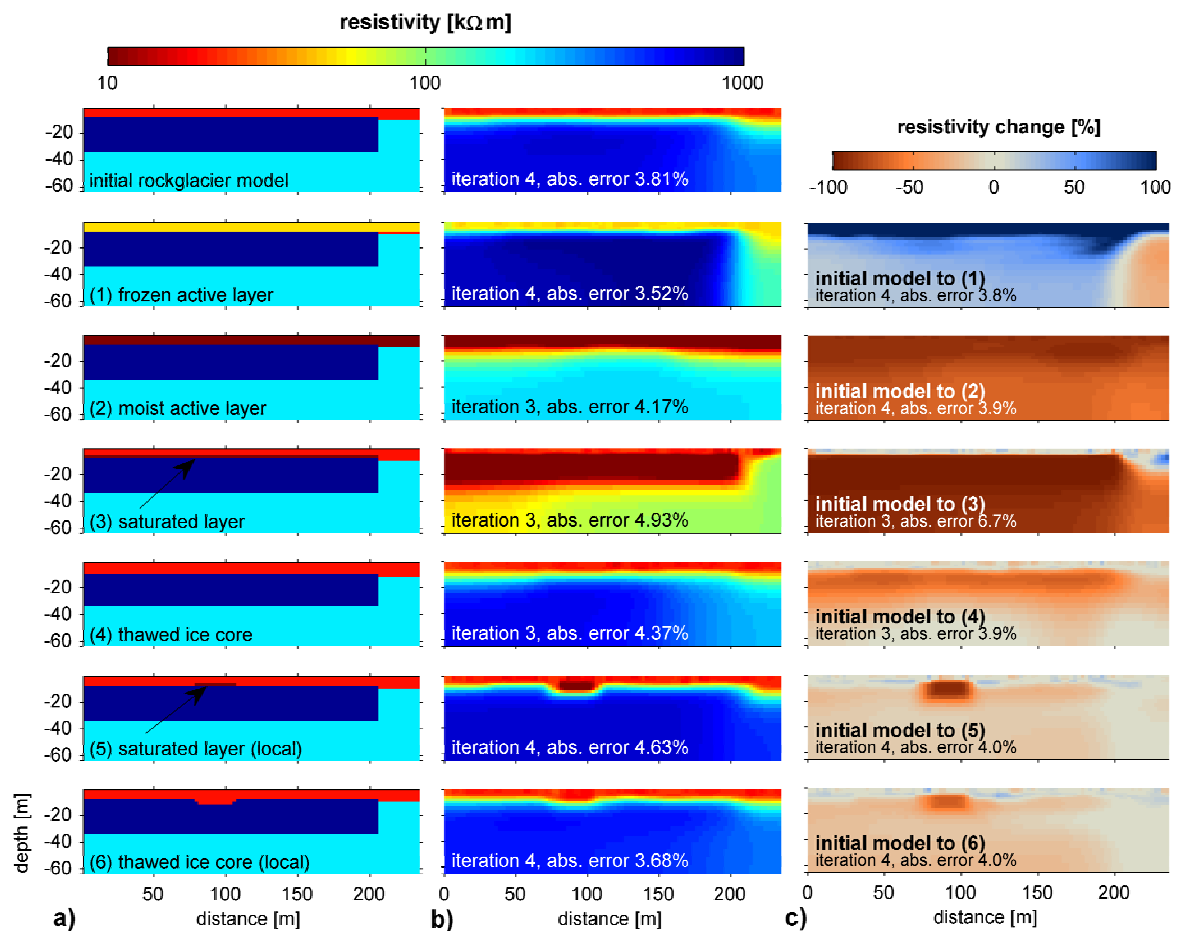


Fig. 6.4: The initial rockglacier model (upper panel) and different freezing and thawing scenarios: a) synthetic resistivity models, b) inverted synthetic resistivity models, and c) percentage change in resistivities relative to the initial model revealed by time-lapse inversion.

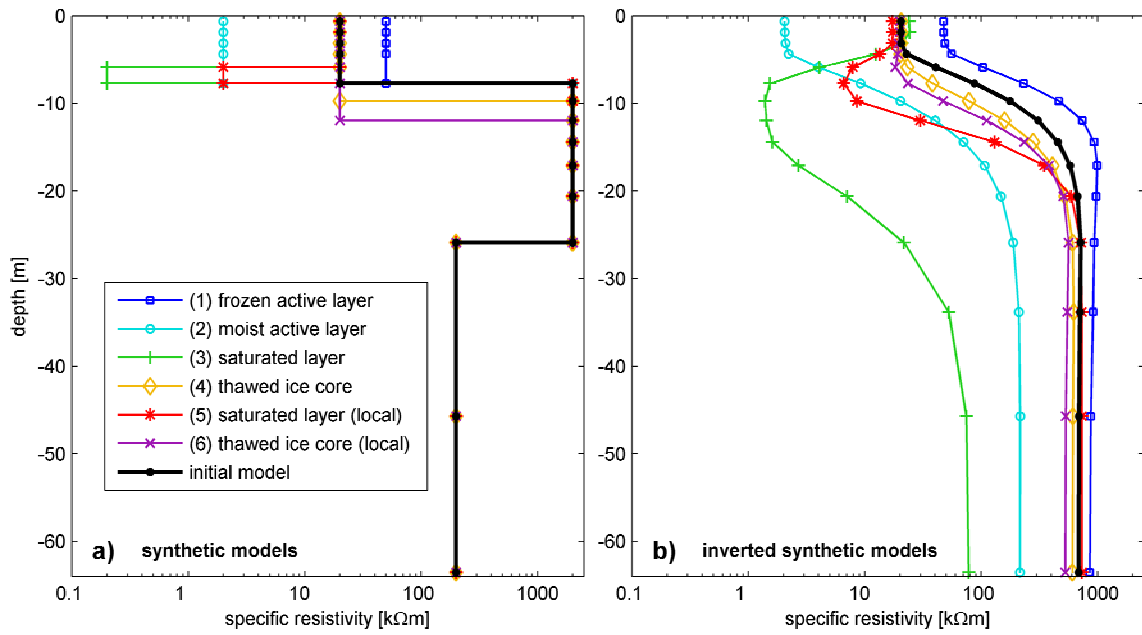


Fig. 6.5: Resistivity-depth plots representing a cut through a) the synthetic and b) the inverted synthetic rockglacier models in Figure 6.4a and 6.4b at 90 m horizontal distance.

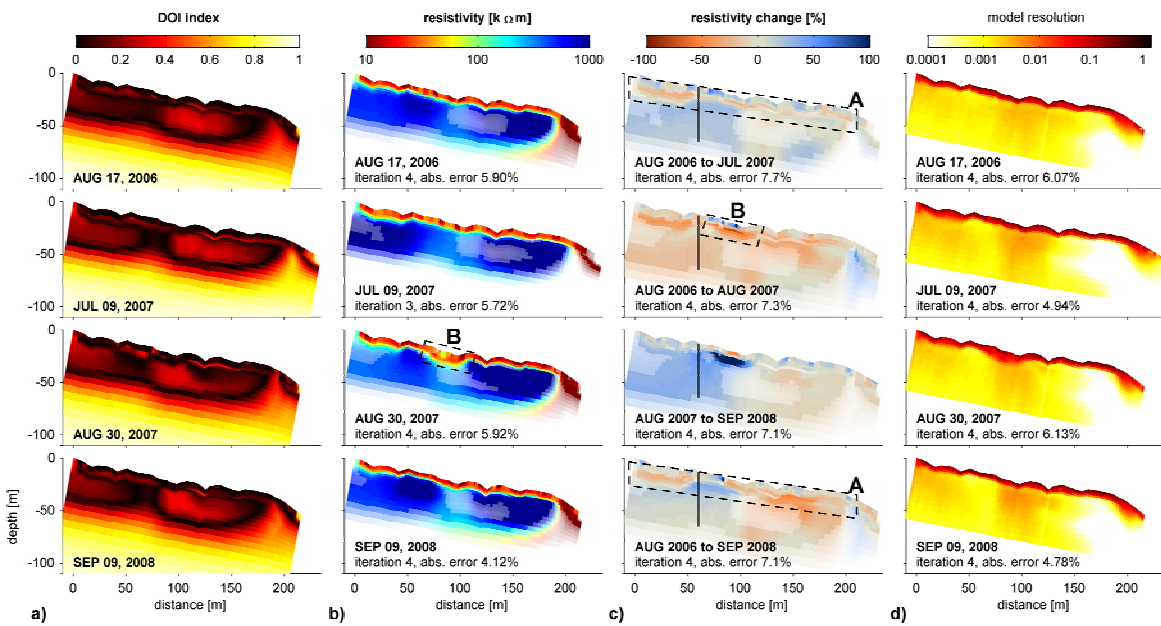


Fig. 6.6: a) Calculated DOI index, b) inverted models with the intensity of the colours scaled by the DOI index (for better visibility scaled by $DOI_{max} > 0.2$), c) time-lapse tomograms scaled by $DOI_{max} > 0.2$, and d) formal model resolution for the Murtèl data set. Pale colours in b) and c) are associated with unreliable inversion results. Highlighted zones A and B are described in the text.

APPENDIX TO PUBLICATION #3

In addition to the Murtèl rockglacier, the appraisal analyses were also carried out for a data set from the Lapires talus slope. Similar to Murtèl rockglacier, this site also provides coarse blocky surface conditions, but constitutes different subsurface conditions (not supersaturated with ice) and permafrost dynamics, resulting in different challenges for conducting ERTM. According to the structure of *publication #3*, the Lapires field site is introduced in the next section followed by the presentation and discussion of the results from the appraisal analysis of an exemplary data set.

THE VENTILATED LAPIRES TALUS SLOPE

The Lapires talus slope is located in NE orientation at the foot of the Pointe des Lapires summit in the Valais (Swiss Alps) extending over more than 500 m width between 2350 and 2700 m altitude (Fig. 3.6). In 1998 considerable amounts of ground ice were found at Lapires during the construction of two cable car pylons within the talus slope (Delaloye et al. 2001). Comprehensive investigations followed in order to map the permafrost distribution and to understand its controlling factors, including the measurement of ground temperatures in a borehole (20 m, drilled in 1999) and the foundation of one of the pylons (down to 6 m), BTS (bottom temperature of winter snow cover) measurements, vertical electrical soundings, and ERT surveys along several transects (Delaloye et al. 2001; Marescot et al. 2003; Delaloye 2004). In addition, new drillings were conducted in autumn 2008, with the deepest borehole located about 10 m left of the pylon, where no bedrock was encountered down to a depth of 40 m (pers. comm. R. Delaloye and C. Scapozza, 2008).

Internal air circulation has been evidenced as one of the key factors controlling the permafrost distribution, and contributes (at least partly) to the cooling of the Lapires talus slope (Delaloye 2004; Delaloye & Lambiel 2005). The ventilation acts through the porous coarse blocky surface material depending on the contrast in temperature between the interior of the scree and the outside. The ascent of relatively warm air towards the top of the scree in wintertime facilitates the aspiration of cold air deep inside the talus slope. A gravity discharge of cold air may then occur during summer. The ventilation process of talus slopes is described in more detail e.g. by Sawada et al. (2003), Delaloye & Lambiel (2005), and Zacharda et al. (2007).

ERTM on talus slopes may contribute to the investigation of the spatio-temporal permafrost dynamics controlled by the internal air circulation. Besides the electrode coupling, the challenges of conducting an ERTM at this site are related to the seasonal temperature changes inside the talus slope, causing a complex response in the resistivity pattern. Image appraisal methods shall therefore help to evaluate the reliability and resolution capacity concerning pronounced resistivity contrasts in spatial and temporal dimension. The pylon P10 in the immediate vicinity of the ERTM profile (indicated in Fig. 3.6 and Fig. 6.7) may complicate the inversion of the data. Special attention will therefore be paid to the possible influence of the low resistive anomaly caused by the foundation of the pylon to judge the significance of resistivity changes as indication for changes in material properties.

DATA ACQUISITION

A fixed electrode array with a total length of 168 m (43 electrodes, 4 m spacing) was installed in horizontal orientation at the talus slope in summer 2006 (see Fig. 3.6). Compared to Murtèl, electrode coupling was slightly less challenging here and provided maximum contact resistances of about 300 to 400 k Ω . In parts of the profile line, where large blocks dominated the surface, electrode coupling could be improved considerably by adding fine-grained material from a nearby debris flow deposit to the electrodes. Filtering of the data was the same as described for Murtèl. In contrast to the rockglacier site, high data quality is obtained at Lapires in all seasons (only 0 - 4.5% of the raw data were deleted). Up to now the Lapires ERTM data set comprises more than 19 measurements between August 2006 and April 2009 from all seasons at irregular time instances of roughly 1 to 3 months.

RESULTS

ERTM RESULTS

The analysis of the complete data set of up to now 19 measurements (not shown here) revealed two distinct patterns of resistivity distribution corresponding to a summer and a winter state. The shift from one state to the other occurs between October and December, and between April and June. Fig. 6.7 representatively illustrates both states by inversion results from January 29, 2008 and August 19, 2008. Common features of both images are (1) a resistive anomaly (ca. 50 - 100 k Ω m) of about 20 m vertical and 70 m horizontal extent in the central part of the tomogram (indicating the occurrence of ground ice, supported by ground truth observations during the construction of the cable car pylon (Delaloye et al. 2001)), (2) a small and very low resistive anomaly (0.5 - 3 k Ω m) at the surface at 85 m horizontal distance (caused by the foundation of the cable car pylon), and (3) the host material consisting of loose debris in the left part of the profile and underneath the resistive anomaly with resistivities of ca. 1.5 - 6 k Ω m. In winter, the resistivities of the uppermost few meters are much higher than in summer, corresponding to the frozen and unfrozen states of the active layer. Another pronounced change is visible in the zone underneath the low resistive pylon with maximum resistivities of > 100 k Ω m in summer and a resistivity minimum within the permafrost body during winter.

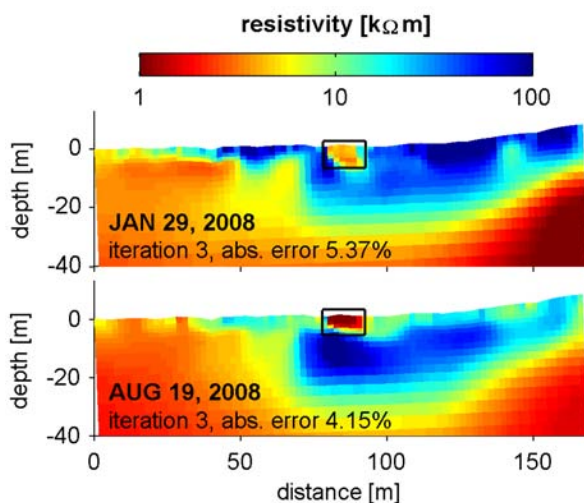


Fig. 6.7: Inverted resistivity data for representative data sets from the Lapires talus slope (January 29, 2008, and August 19, 2008). The rectangles mark the position of the pylon foundation.

FORWARD-INVERSE MODELLING

Unlike Murtèl rockglacier the interior of the Lapires talus slope is characterised by a much more heterogeneous pattern. The derivation of appropriate synthetic models approximating the subsurface structure and the seasonal dynamics related to internal air circulation is a very complex process. A comprehensive discussion of the forward-inverse-cycles is therefore beyond the scope of this paper, and in the following the most important results from this synthetic modelling are briefly summarised:

- Due to the strong resistivity contrasts the low resistive foundation of the cable car pylon very likely influences the resistivity values of the permafrost body underneath (see rectangle in Fig. 6.7). Absolute resistivity changes around the pylon may consequently be of limited reliability. However, the presence of a resistivity maximum below the pylon was a necessary condition to reproduce the observed pattern, which is supported by observations from Delaloye et al. (2001) that revealed higher seasonal dynamics in the vicinity of the pylon compared to the borehole position.
- Seasonal resistivity changes in the interior (beyond the influence of the pylon) are not only caused by active layer dynamics and a delayed response at greater depth. An inverse behaviour of resistivity changes between the active layer and the interior (uppermost 15-20 m) is observed that is very likely a reliable feature, and not an inversion artefact caused by resistivity contrasts due to active layer dynamics. This feature will further be discussed in the next section.

ANALYSIS OF THE DOI INDEX

Calculated DOI indices for the two representative data sets from Lapires and the superposition of the DOI index on the respective resistivity tomograms are illustrated in Fig. 6.8a and Fig. 6.8b.

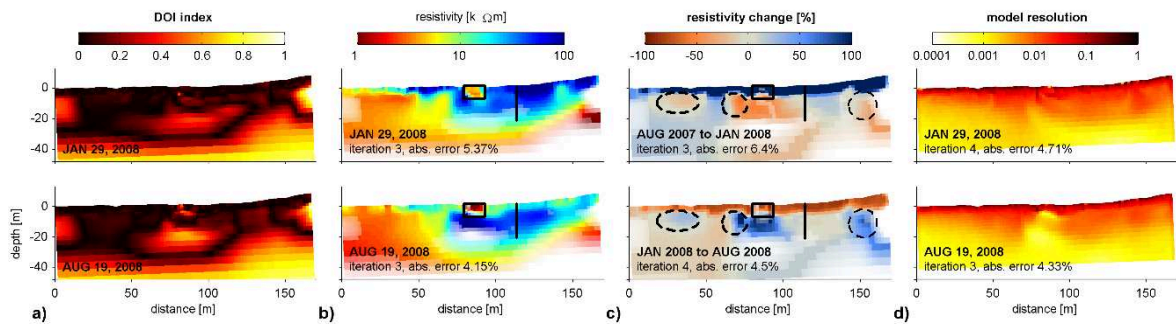


Fig. 6.8: a) Calculated DOI index, b) inverted models scaled by $DOI > 0.2$, c) time-lapse tomograms scaled by $DOI_{max} > 0.2$ (circles mark features described in the text), and d) formal model resolution for representative data sets from winter and summer.

In large parts of the profile DOI values are generally lower than for the Murtèl data set. Particularly the left part of the profile is characterised by low DOI values indicating high confidence down to 30 m depth. This difference in DOI values between the rather low resistivities (unfrozen) in the left and high values (frozen) in the central and right part of the tomogram strikingly illustrates the inherent limitations in resolution capacity concerning ERT surveys in ice-rich permafrost environments. The distribution of DOI values does not change significantly between winter and summer, pointing to a comparable quality of the inversion results.

Except for marginal and deep zones of the tomogram, where reliability is low due to limited data coverage, maximum DOI values occur in the central resistive anomaly. The values are highest for the summer state, where the resistivity contrast between the pylon and the permafrost body is largest. This implies that the resistivity increase of the permafrost body may at least partly be caused by the decreased resistivity of the foundation of the pylon (due to warmer and/or moister conditions) and therefore by the inversion process rather than by true variations in material properties. Apart from the critical zone around the pylon, the generally low DOI values within the uppermost 15-20 m of the profile suggest that the resistivity values are well constrained by the data and exhibit high reliability.

Assuming that the resistivities of the host material represent scree rather than firm bedrock (that would have higher resistivities than the observed 3 k Ω m), the base of the talus slope is expected at a depth > 30 m in the left part of the profile. In the right part of the tomogram, the base of the talus slope cannot be resolved, even if it is located at shallower depth, because the high DOI values in that part point to a high influence of the reference model and hence to a low confidence below the resistive permafrost body. First data from a new drilling site 10 m left of the pylon confirm that no bedrock was encountered down to a depth of 40 m (pers. comm. R. Delaloye and C. Scapozza, 2008).

Fig. 6.8c shows the results from time-lapse inversion of three data sets for subsequent time steps, again with the colours scaled by DOI_{max} values > 0.2. The active layer is clearly visible in terms of significant resistivity changes between summer and winter. Compared to the processes close to the surface, zones with an *inverse response of resistivities* are detected in the interior of the talus slope: while the active layer freezes during winter, several zones underneath indicate resistivity decrease. The same zones exhibit increasing resistivities as opposed to decreasing values related to thawing of the active layer in summer. DOI values are generally very low and do not indicate inversion artefacts in these zones.

ANALYSIS OF THE FORMAL MODEL RESOLUTION

Model resolution of the winter and summer state (Fig. 6.8d) are in large parts of the tomograms significantly better than for Murtèl. Zones with adequate resolution capacity (≥ 0.05) extend to a depth of ca. 10 m. The part of the permafrost body underneath the pylon exhibits low resolution in summer, whereas in winter its resolution equals the values of the entire permafrost body. This is due to the reduced resistivity contrast and/or the reduced resistivity below the pylon in winter. For the winter season the overall resolution of the permafrost body is relatively high, with a higher reliability in the frozen region compared to Murtèl rockglacier.

DISCUSSION OF TIME-LAPSE ERTM RESULTS

Having analysed the Lapires data set by appraisal methods we can now omit zones of critical reliability from the interpretation of the time-lapse inversion results (Fig. 6.8c). Apart from marginal and deep zones these include the resistive zone beneath the foundation of the pylon P10, and the entire region below the resistive permafrost body in the right part of the image.

As described above, an inverse relationship between a superficial resistivity increase in the active layer (freezing) and a resistivity decrease in small zones underneath is observed between August 2007 and January 2008, and similarly, decreasing resistivities in the active layer (thawing) are accompanied by increasing values between January and August 2008 (dashed circles in Fig. 6.8c). The inverse character of these resistivity changes appears to be, in contrast to a

delayed advance of the summer warming front at greater depth in winter, in accordance with observed inverse temperature effects inside and outside the talus slope (reported by Delaloye, 2004). These observations were made at different locations on the talus slope, and especially in the central part of the ERTM profile (around the pylon P10). However, because temperature records at this pylon cover only the uppermost 6 m of the talus slope, where the ERT data are disturbed by the foundation of the pylon, the observed inverse resistivity effects in deeper parts cannot be verified by in situ temperature measurements. Based on the findings of Delaloye (2004) and our data, we note that there is a probability that these effects are indeed related to the internal air circulation. Some indications of this are given by the fact that the borehole, where no inverse temperature effects are observed, is located in a zone without significant resistivity changes below the active layer (indicated in Fig. 6.8b and Fig. 6.8c). We therefore assume that zones with preferential air flow (ventilation funnels) may be in principle delineated and visualised by time-lapse inversion of ERTM data.

It is important to note, that apart from the differences between August and January presented here, resistivity changes can differ remarkably in terms of position and magnitude depending on the observed time span. The selected data sets only served to analyse the general applicability of ERTM to visualise the internal air circulation and do not provide sufficient insights into the spatio-temporal dynamics of the process. This will be subject to further studies.

CONCLUSIONS

In addition to the conclusions in *publication #3*, the appraisal of the ERTM data set from the Lapires talus slope revealed that ERT resolution capacity and investigation depth increase substantially for landforms with comparatively lower (i.e. not supersaturated) ice content characterised by lower resistivity values (one order of magnitude compared to Murtèl). Such conditions allow even complex spatio-temporal resistivity changes to be reliably resolved by ERTM. In comparison with subsurface temperature data the observed seasonal resistivity changes within the talus slope point to a relation to the ventilation process described by Delaloye & Lambiel (2005). The significance of these resistivity changes will be analysed in more detail in future studies.

7 On the potential of time-lapse refraction seismic for the detection of changes in ground ice content

7.1 Motivation

The ERTM approach to assess percentage changes in electrical resistivity is only one possible method to monitor mountain permafrost evolution. In principle, also other geophysical methods are suitable for monitoring purposes. The requirements for an adequate method to observe changes in ground ice content comprise a) a pronounced contrast of the measured signal between ground ice, frozen material containing no (or only little) ice, and unfrozen material, and b) the reproducibility of measurement conditions. The latter can best be achieved by permanently installed survey lines, but also fixed positions of transmitters and receivers are possible.

From the range of geophysical methods tested for their applicability concerning detection, mapping and characterisation of mountain or discontinuous polar permafrost (Hauck 2001; Ingeman-Nielsen et al. 2005; Yoshikawa et al. 2006), the best potential was attributed to ERT (due to the large resistivity contrast between ice and unfrozen material and the reasonable horizontal and vertical resolution). Due to its complementary nature, seismic refraction is often considered to be a valuable additional method to verify subsurface structures identified by ERT (e.g. Hauck 2001; Kneisel et al. 2008). As shown in chapter 2, seismic refraction is generally capable of discriminating unfrozen and frozen sediments or massive ice, and is thus a common method to determine active layer thickness. However, the largely overlapping ranges of P-wave velocities for ice and bedrock (both frozen and unfrozen) make a differentiation of stratigraphic details in bedrock and/or below the permafrost table often difficult. Together with the comparatively high measurement and processing efforts, this may be a reason why refraction seismic surveys are less popular in permafrost research than e.g. ERT or GPR measurements. Nevertheless, numerous studies successfully applied refraction seismic surveys in permafrost terrain (e.g. Vonder Mühl 1993; Musil et al. 2002; Hauck et al. 2004; Ikeda & Matsuoka 2006; Hausmann et al. 2007; Maurer & Hauck 2007), and main advantages of the method, compared to ERT surveys, are e.g. the less challenging coupling of the sensors in blocky terrain, or the applicability in terrain with conductive infrastructure contaminating the resistivity signal.

From a monitoring point of view, time-lapse refraction seismic theoretically has a considerable potential. Main advantages comprise the ground contact of the sensors (that can be permanently fixed), the complementary nature of the method compared to ERT, and the strong sensitivity of the seismic P-wave velocity to variations in ice content of a given medium (see chapter 2). With regard to time-lapse data sets the latter allows, despite the limitations concerning qualitative stratigraphic interpretation, even comparatively small temporal changes in

P-wave velocities to be attributed to zones with significant changes in subsurface conditions (e.g. seasonally or long-term varying ground ice content).

As outlined in chapter 2, apart from a vast research related to *reflection* seismic monitoring of deep reservoirs in exploration geophysics, similar efforts to investigate the potential of a *refraction* seismic monitoring approach for the observation of shallow targets have not been undertaken so far. According to the theoretical suitability of a RSTM approach to permafrost related research, in the following, the potential of an independent (complementary) monitoring method to determine relative ice (and water) content changes in the subsurface will be evaluated based on the analysis of repeated refraction seismic measurements at two different test sites.

The approach (presented in chapter 2) comprises a qualitative and quantitative analysis and comparison of a) time-lapse seismograms, b) time-lapse travel time curves and corresponding velocities, and c) the inverted tomograms.

7.2 Time-lapse refraction seismic data sets

To evaluate the RSTM approach repeated refraction seismic measurements were carried out at two different test sites for intervals of roughly 1.5 months, respectively, in the summer season. The test sites comprise the ventilated Lapires talus slope (2500 m altitude), and the north oriented slope of the Schilthorn summit (2970 m) (see chapter 3 for detailed description of both sites). The measurements were conducted in July and August 2008, respectively, with the first measurement date roughly representing the end of the snowmelt season, where the active layer starts thawing. The respective active layer depths in the nearby boreholes at the date of the first measurement were 2.5 m (3.5 at pylon) for Lapires, and 2 m and 0.5 m (B14 and B100) for Schilthorn (see Fig. 3.2 and Fig. 3.6 for position of the boreholes). After 40 and 47 days the active layer depth increased by 1.5 m (B20 and pylon) at Lapires, and by 3 m (B14 and B100) at Schilthorn. Tab. 7.1 summarises the details of data acquisition for both test sites. The positions of the RST profiles equal the positions of the ERTM profiles, which are discussed in detail in *publication #1* (chapter 4) for Schilthorn and in the appendix of *publication #3* (chapter 6) for Lapires.

Tab. 7.1: Measurement details for the seismic monitoring test sites.

	number of geophones	geophone spacing	profile length	number of shot points	off-end shots (distance from first/last geophone)
Lapires	23	8 m	176 m	24	4/4 m
Schilthorn	24	2 m	46 m	24	-/1 m

7.3 Analysis of time-lapse refraction seismic data sets

In the following, the two data sets acquired during a time span of 40 days in summer 2008 at the Lapires talus slope will be analysed first regarding different parameters, followed by comparison with the data set measured in parallel to this survey at Schilthorn.

7.3.1 Analysis of seismograms

Lapieres

Fig. 7.1 exemplarily illustrates a detailed view of an unfiltered part of a selected seismogram with the traces for two measurement dates: July 10 (grey) and August 18, 2008 (red). Striking features of this seismogram are a) the very similar waveforms of corresponding traces from both dates pointing to a high reproducibility of the seismic signal for subsequent measurements, and b) the generally earlier arrival times of the waves in July compared to those from August with a time shift of about 1-3 ms between the two dates (highlighted in Fig. 7.1). Geophones closest to the shot point are often disturbed by inevitable noise caused by the person hitting the hammer, making the identification of the first break sometimes difficult (see traces at 1144 and 1152 m horizontal distance in Fig. 7.1).

Schilthorn

A detailed view of an unfiltered part of a selected time-lapse seismogram from Schilthorn is shown in Fig. 7.2 with the traces for the dates: July 11 (grey) and August 26, 2008 (red). Compared to Fig. 7.1 the time shift of first arrivals between July and August is with about 3-8 ms considerably more pronounced. The waveforms of coincident traces from both dates show less correspondence, which may be caused by considerably longer travel paths of the waves due to a lowered refractor depth in August and a correspondingly altered seismic signal.

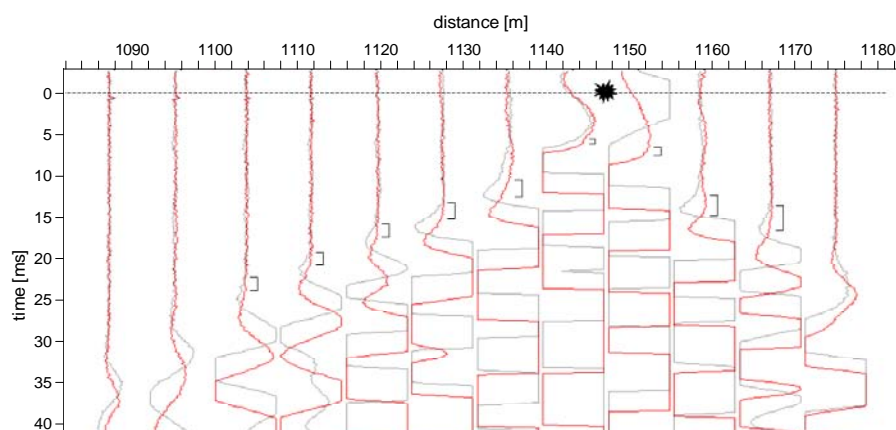


Fig. 7.1: Detailed view of a time-lapse seismogram from Lapieres for the shot position at 1148 m with traces from July 10 (grey) and August 18, 2008 (red). Time shifts of the first arrivals are highlighted.

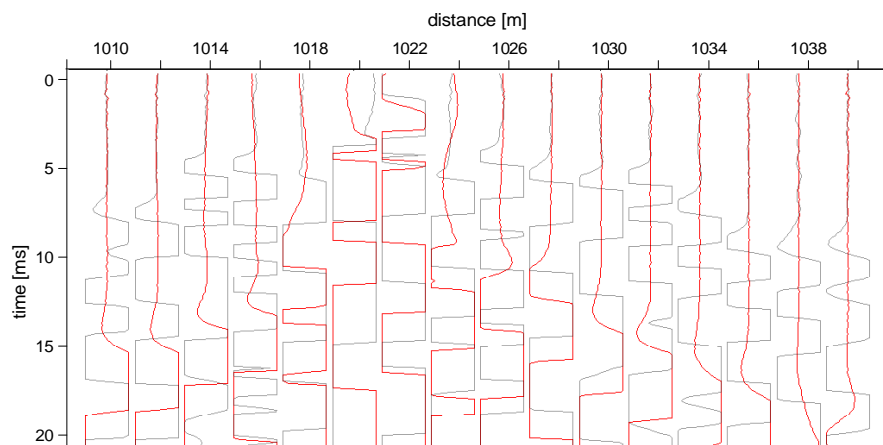


Fig. 7.2: Detailed view of a time-lapse seismogram from Schilthorn at the shot position at 1021 m with traces from July 11 (grey) and August 26, 2008 (red).

7.3.2 Analysis of travel time curves

Lapires

First arrivals were picked manually for all 24 seismograms corresponding to 24 shot points. For data sets from coarse blocky sites with considerable surface roughness the identification of the first arrivals is sometimes complicated by their irregular distribution. In this context the high reproducibility of the signal was therefore utilised to increase the confidence in the identification of the first arrivals by jointly analysing both data sets for first arrival picking (as illustrated in Fig. 7.1). Especially at far distances from the shot points, where the signal-to-noise ratio usually decreases, this “constrained picking” considerably improved the accuracy in identifying the first breaks.

In Fig. 7.3 all picked first arrivals are displayed as combined travel time curves for both dates. Significant temporal differences can be observed by visual inspection and comparison of both plots. They provide information on a) changes in seismic velocities (the slope of the travel time curve) indicating altered ice and water contents of certain layers, and/or b) time shifts in travel times indicating a shift in the depth of a refractor (i.e. the seasonally varying interface between frozen and unfrozen conditions).

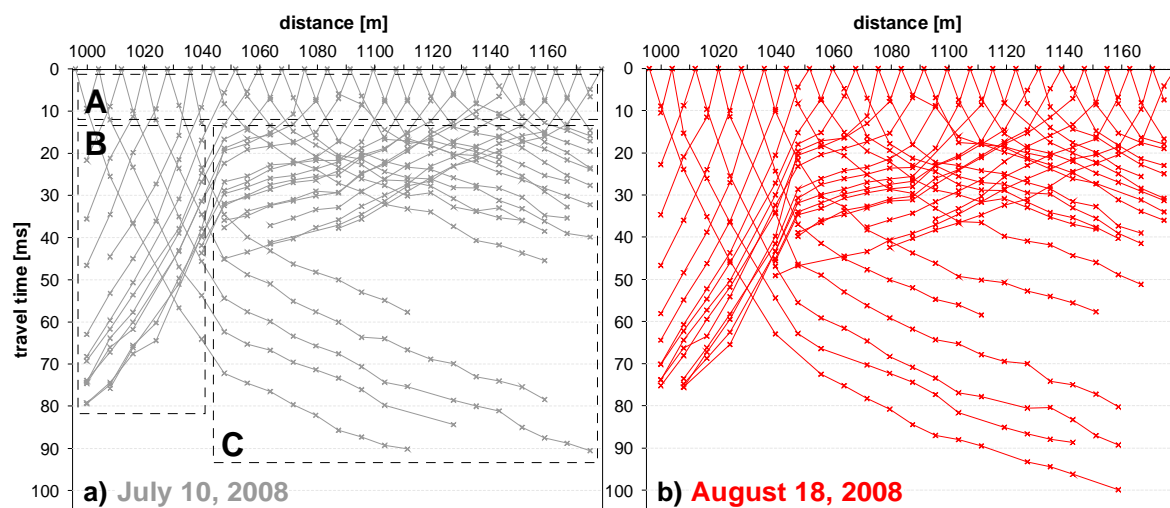


Fig. 7.3: Combined travel time curves for the measurement from a) July 10, 2008 (grey) and b) August 18, 2008 (red).

Comparing Fig. 7.3a and Fig. 7.3b confirms the general reproducibility of the overall pattern of first arrivals. Note, that several picks (crosses) are missing due to occasional low signal-to-noise ratios making the identification of some first breaks uncertain or even impossible. The differences in total travel times for corresponding forward and reverse traverses are mainly due to the missing picks for far geophones from the far reverse shots.

General features of the travel time curves can be described as follows (indicated in Fig. 7.3a):

- **Zone A** represents homogeneously low velocities of 400-700 m/s in the uppermost layer of the whole profile.
- **Zone B** exhibits no clear refractor and velocities do not exceed 800-1000 m/s also for later arrivals from far shots.
- **Zone C** is characterised by a sharp velocity increase and thus by a clear refractor with mean velocities of about 3000 to 4500 m/s. In the absence of a strong superficial relief a

considerable subsurface topography of this refractor is indicated by significant velocity differences between forward (about 5000-6500 m/s) and reverse (about 2600-4000 m/s) shots between ca. 1050 and 1090 m horizontal distance.

The differences between the two dates are highlighted in Fig. 7.4 by the superposition of corresponding pairs of travel time curves (distributed into three different plots for better visibility). Apart from a few exceptions (e.g. for the shot at 996 m horizontal distance) the first arrivals for the data set from July are generally slightly earlier than for the second measurement in August. The following features can be recognised from visual inspection of the time-lapse travel time plot:

- In zones A and B the travel time differences are small or even absent.
- Within zone C the difference between July and August is not equal for all travel times. For some shots (e.g. at 1044, 1124, 1172, and 1180 m horizontal distance) the difference is significantly larger than the mean displacement. According to Reynolds (1997) the form of the travel time curves may indicate a change in the form of the refractor, that is the differences in displacement may indicate locally pronounced changes in the refractor depth.
- The differences between both dates are generally characterised by time shifts of the travel time curves rather than by clear changes in the velocities of certain layers. A slight velocity decrease from July to August may be identified at the transition between zone A and the strong refractor of zone C), but, regarding the absence of additional geophones supporting this assumption, this feature more likely points to a lowering of the refractor depth.

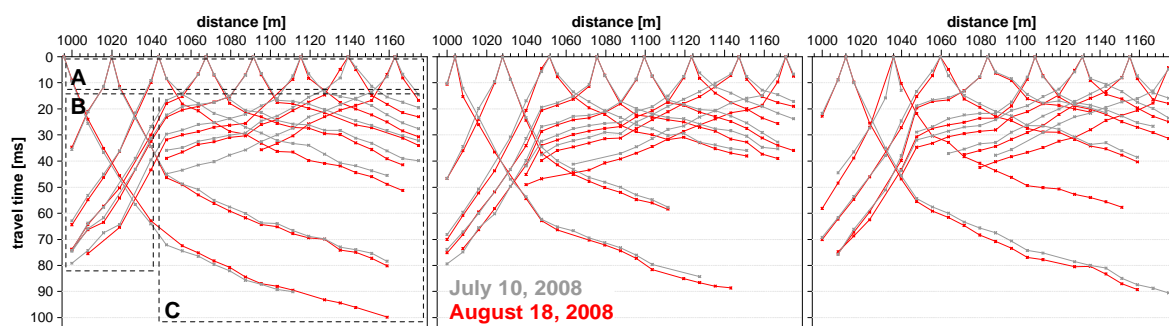


Fig. 7.4: Comparison of travel times from July 10 (grey) and August 18, 2008 (red), distributed into three separated plots for clarity. Note, that in some cases the absence of single picks may change the form of the travel time curve.

Plotting the travel times against the absolute offset between source and receiver (after Hausmann et al. 2007) reveals a clustering according to the dominant layers of the subsurface that allows a rough estimation of the mean velocities of the respective materials (indicated in Fig. 7.5a). As the Lapires site exhibits pronounced lateral differences (referred to as zone B and C in Fig. 7.3a) the common offset plot shows two separate branches. The lowermost branch is a result of the low velocity in zone B, causing a delayed arrival (longer travel time) of waves from far shots, while the velocities are equal for all waves travelling through zone C.

The mean velocity close to the surface is with ca. 650 m/s quite low and corresponds to the unconsolidated coarse blocky layer of the talus slope. Almost no increase in velocity is observed within zone B (mean velocity about 780 m/s), indicating that no clear refractor is detectable within the investigation depth of the survey geometry, thus strongly restricting the information on the left side of the profile. The mean velocity of the only significant refractor observed amounts to 3500 m/s and is indicative for ground ice (Röthlisberger 1972).

The travel time differences between July and August (Fig. 7.4 and Fig. 7.5a) were plotted against the absolute source-receiver offset (Fig. 7.5b) and against the shot position (Fig. 7.5c). The majority of travel time differences between August and July are positive indicating an increase in travel time. The dependence of the travel time differences from the shot location is small for all offsets greater 20 m (Fig. 7.5b), meaning that the travel time shifts are caused close to the surface and only minor velocity changes (corresponding to ice content changes) are expected at greater depth. Sorting the calculated travel time differences according to shot position proves the existence of lateral differences in the observed changes along the profile line. According to Fig. 7.5c a laterally heterogeneous pattern can be observed for travel times corresponding to shot positions within zone C, with the largest positive changes at the right edge of the profile and the left bound of zone C, and the smallest variations around 1080-1090 m horizontal distance (coinciding with the position of the cable car pylon).

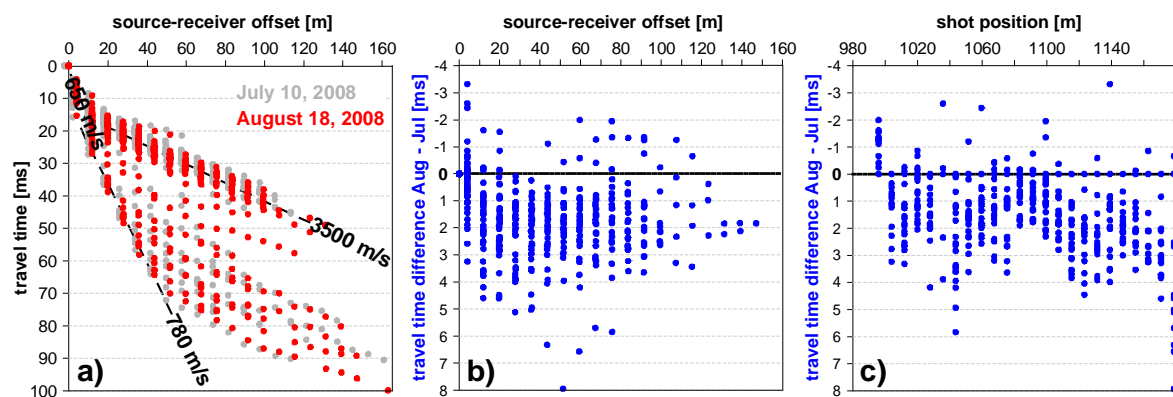


Fig. 7.5: a) Travel times for July 10, 2008 (grey) and August 18, 2008 (red) (as in Fig. 7.3), but sorted by the absolute offset between geophone and shot point (for better visibility of both data sets the x axis was slightly shifted to the right for July 10, 2008). b) Calculated travel time differences between August and July, sorted by source-receiver offset, and c) by shot position along the profile.

Schilthorn

The corresponding travel time curves for the Schilthorn data set are shown in Fig. 7.6. Comparing the travel time curves for both dates emphasises the pronounced difference between July and August observed in the seismogram of Fig. 7.2. The low velocity surface layer has considerably increased in August making a direct comparison of corresponding travel time curves for subsequent measurements difficult (or not useful). However, a close inspection of the travel times reveals some common characteristics (highlighted in Fig. 7.6a and Fig. 7.6b):

- **Zone A** basically exhibits a constant velocity of about 300-600 m/s for both dates.
- **Zone B** intersects the low velocity surface layer by increased velocities.
- The pattern of the travel times in **zone C** points to a irregular topography of the refractor.

The following information can already be derived from a qualitative analysis of both data sets:

- Although the velocities seem to slightly decrease from July to August they remain significantly higher in **zone B** than in the neighbouring zones.
- Similarly, in small regions (**zones D**) previously part of **zone C** the velocities decrease in August, but remain higher than the velocity of **zone A**

- **Zone E** showed a distinct travel time pattern for all waves traversing this zone in July, but exhibits a more regular pattern in August.

A rough interpretation of the observed features includes a significant deepening of the low velocity surface layer, i.e. a lowering of the refractor, as well as the development of zones with intermediate velocities in August that have been part of refractor C in July. Conversely, other zones (E and partly B) showed a specific travel time behaviour in July but seemed to smooth out until August.

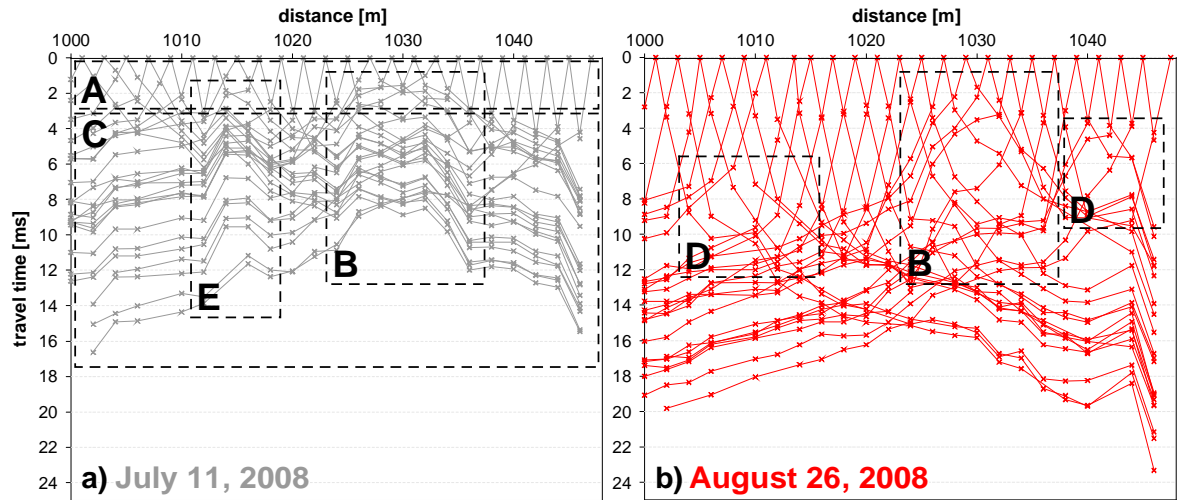


Fig. 7.6: Combined travel time curves for the measurement at Schilthorn from a) July 11, 2008 (grey) and b) August 26, 2008 (red).

The common offset plot of the travel times in Fig. 7.7 shows basically two layers with average velocities of about 590 m/s for the surface layer and 3500 m/s at greater depth. The intermediate velocity of zones B and D (cf. Fig. 7.6) cannot be determined from Fig. 7.7. The travel time pattern appears very similar for both dates, but the values from August exhibit higher variations, especially at far distances. A slight tendency of higher velocities may be indicated at far distances, but cannot be determined with certainty.

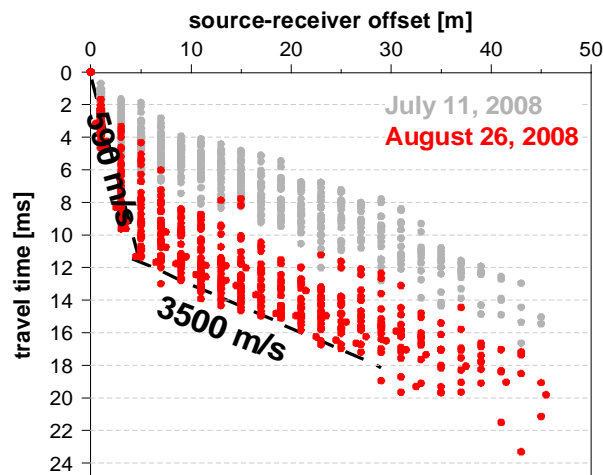


Fig. 7.7: Common offset plot of the travel times at Schilthorn for July 11, 2008 and August 26, 2008.

As the travel time differences are much higher than for Lapires, a systematic analysis of the travel times is only of limited use and the analysis will focus on the inverted tomograms.

7.3.3 Analysis of refraction seismic tomograms and quantification of velocity changes

Lapires

The results of the tomographic inversion of both data sets are shown in Fig. 7.8a (upper panels). To evaluate the RSTM approach in relation to the ERTM approach, the corresponding ERT data sets, that were acquired in parallel on the same survey line, are shown in the lower panels (a combined interpretation follows in section 7.4). The black line delineates the surface, deep red colours above this line are due to the fact that topographic relief is modelled by setting the velocities of cells above the irregular surface to that of air and fixing them during the inversion. As the investigation depth of a refraction seismic survey depends not only on the survey geometry (source-receiver locations) but also on the characteristics of the subsurface layers, at ice-rich permafrost sites the investigation depth is often limited by the presence of a sharp refractor caused by the transition from the unfrozen active layer to the permafrost table. The amount of energy reflected/refracted to the surface is a function of the velocity contrast at an interface, with high velocity contrasts causing greater fractions of energy to be reflected or refracted to the surface (Burger et al. 2006). By this, the potential to resolve additional refractors at greater depth (e.g. the bedrock interface) decreases substantially. The refraction seismic tomograms in Fig. 7.8a illustrate this problem: the investigation depth is relatively shallow and does not exceed 15 m on average. Note, that the inversion scheme extrapolates calculated velocities, which are not covered by rays, from the given velocities of neighbouring cells into deeper areas (Sandmeier 2008), as can be recognised by the diagonal structures at greater depth (the maximum depth of penetration is marked by a dashed line).

The two tomograms from July and August are largely comparable concerning the overall structure, but exhibit different investigation depths and a clear shift in the transition between the low velocity overburden (red colours) and the material indicated by blue colours, corresponding to zone C in Fig. 7.3c, that is interpreted as the zone containing ground ice.

To quantitatively analyse the change in P-wave velocities from July to August, the velocity difference is displayed in terms of absolute velocities (m/s) and percentage change in Fig. 7.8b (upper panels). Additionally, the percentage resistivity change is plotted for comparison (lower panel). For the interpretation of velocity changes it is important to restrict the comparison of refraction seismic tomograms to those parts that are resolved by both data sets (here the penetration depth achieved in the earlier measurement in July 2008, indicated in Fig. 7.8b).

The velocity changes derived from independent tomographic inversion of both data sets largely correspond to the observations made from the analysis of travel time differences. As mentioned earlier, a velocity change may, strictly speaking, be solely a consequence of altered material characteristics, independently from a change in the depth of a refractor. Conversely, a shift in refractor depth (here due to the advance of the thawing front to greater depth) does not necessarily change the mean velocity of the respective layers, but the zone affected by this phase change obviously exhibits a velocity decrease (red colours) by the transition from one state (frozen) to the other (unfrozen), or vice versa (blue colours). Consequently, a thorough interpretation of the velocity change (altered conditions within a layer, or change of refractor depth) is only possible with respect to absolute velocities in the RST tomograms.

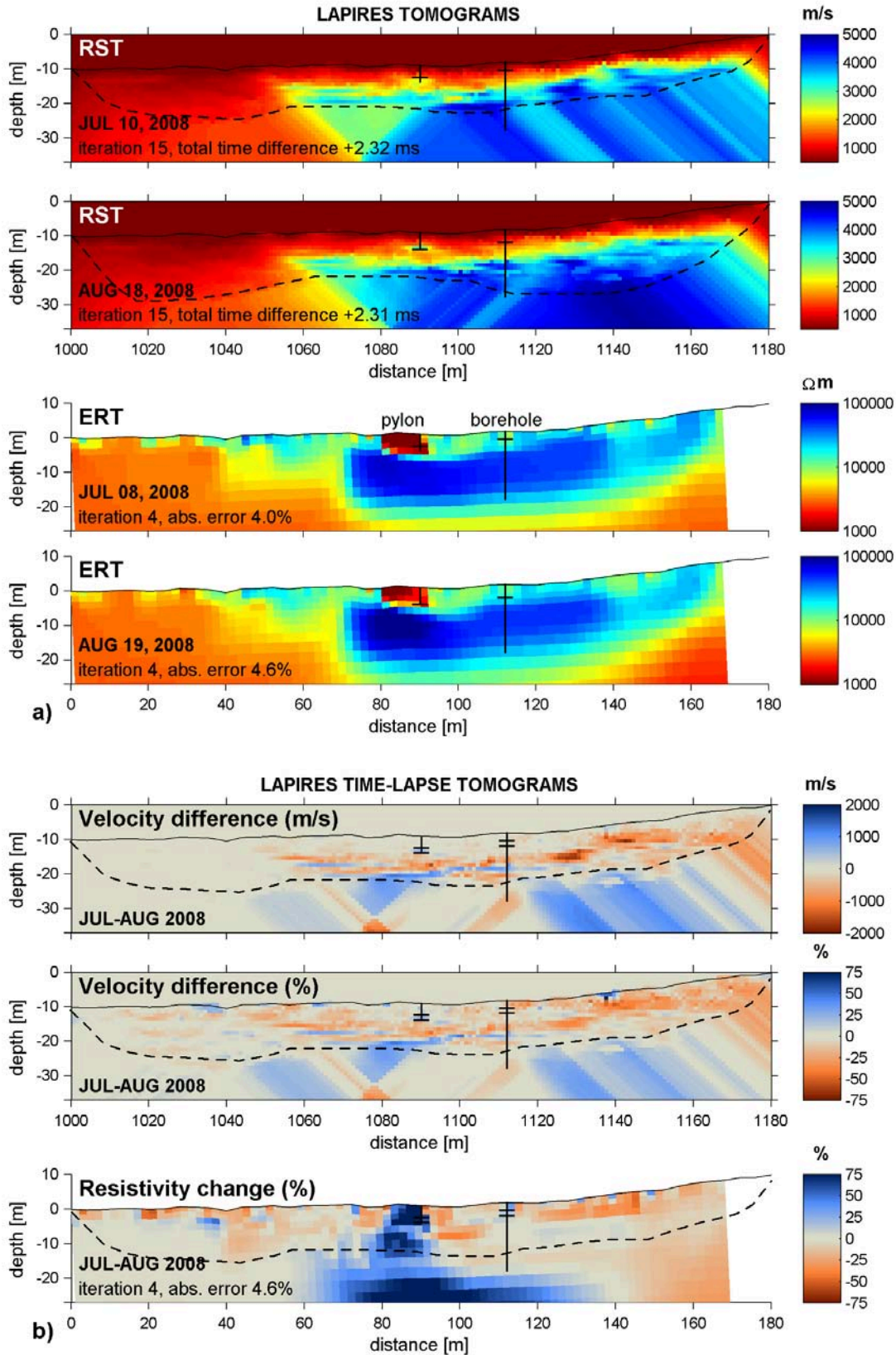


Fig. 7.8: a) Comparison of RST tomograms from July 10 and August 19, 2008 at Lapires with ERT tomograms from comparable dates. b) Comparison of temporal change in seismic velocities with resistivity changes. The resolved investigation depth is marked by a dashed line. Locations of the pylon and the borehole are indicated, as well as the respective active layer depths at both positions (a), and for both dates in (b).

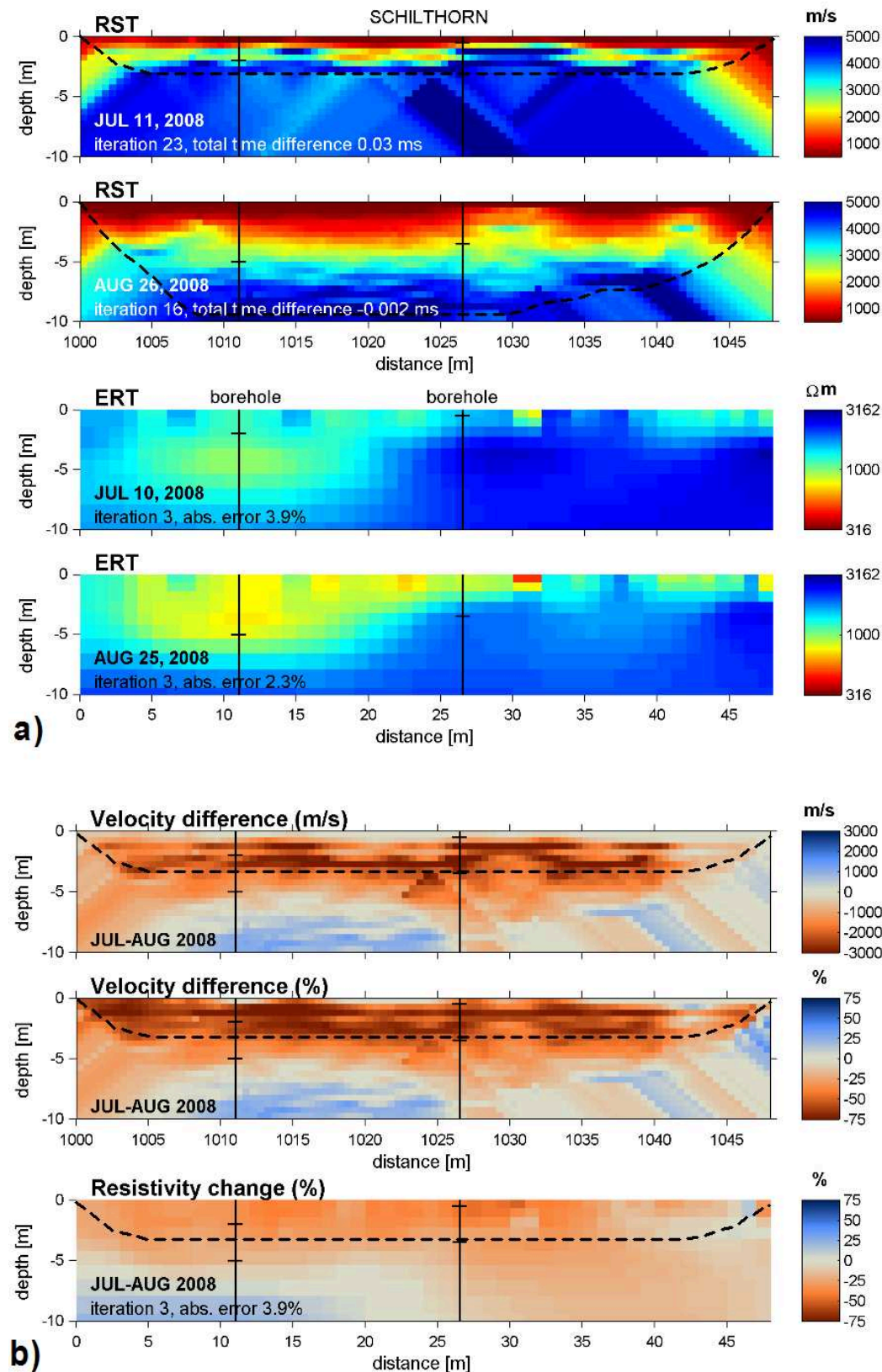


Fig. 7.9: a) Comparison of RST and ERT tomograms for comparable dates in July and August at Schilthorn. b) Comparison of temporal change in seismic velocities with changes in electric resistivities. The resolved investigation depth is marked with dashed lines in (a). The smaller investigation depth from July is the lower boundary for direct comparisons and therefore marked in all tomograms in (b). Vertical lines denote the position of the boreholes with the actual active layer depths highlighted in (a) and the differences in active layer depths highlighted in (b).

The average negative velocity changes calculated from the tomograms are on the order of 20% to >50%, showing that the relatively small increase in travel times from July to August (on average by 2-15% with a maximum around 5%) represents a substantial change in subsurface characteristics.

Schilthorn

The results of tomographic inversion of the Schilthorn data sets are shown in Fig. 7.9a (upper panels) together with the corresponding ERT tomograms from the same date (lower panels). Similar to the Lapires site the investigation depth is small for the measurement in July and significantly larger in August (dashed lines in Fig. 7.9a). A direct comparison is therefore only possible for the depth resolved in both tomograms. A quantification of the velocity differences in terms of absolute and percentage changes is illustrated in Fig. 7.9b, where the dashed line marks the common investigation depth of both dates (upper panels), and can again be compared to the contemporaneous resistivity changes (lower panel).

As discussed earlier, the comparability of both data sets is limited due to the pronounced changes that occurred between the 47 days of the two measurements. However, there are some common features of both tomograms. The tomogram from July shows a shallow refractor ($v_p = 4000\text{-}5000$ m/s) at about 2 m depth but with distinct undulations: high velocity zones are found at shallower depths around 1015 m, between 1025 and 1035 m, and around 1040 m horizontal distance. Accordingly, the tomogram from August, which exhibits generally lower velocities, shows small anomalies with higher velocities (ca. 3500 m/s) than the surroundings around 1030 m and around 1040 m horizontal distance that are slightly deeper. Conversely, no comparable feature is visible around 1015 m.

7.3.4 Evaluation of the time-lapse refraction seismic approach

The reliability of the seismic tomograms can be judged qualitatively on the basis of the ray distributions, where synthetic ray paths are reconstructed by forward modelling based on the final model of the tomographic inversion. The results from network ray tracing for the data sets from both test sites are shown in Fig. 7.10 (Lapires) and Fig. 7.11 (Schilthorn). Note, that for better visibility of the velocity distribution only 25% of the calculated ray paths are plotted. In general, large numbers of crossing rays indicate that velocities are well constrained by the travel time data. Ray coverage, and therefore confidence in the velocity estimates, is generally high, but is reduced below ca. 20 m depth at Lapires and below 2.5 m depth in July and below 9 m in August at Schilthorn. Velocities determined at the base of the lowermost ray paths likely represent average values for the deep regions traversed (Musil et al. 2002), meaning that the confidence of these velocities is limited.

The *total absolute time difference* between observed and calculated travel times (see chapter 2) amounts to 2.64 and 2.71 ms for July and August respectively at Lapires, and to 0.46 and 0.71 ms at Schilthorn. The generally higher values at Lapires are a function of the greater investigation depth and the resulting longer travel times. Whereas this value is well below the observed temporal shift in travel times between July and August at Schilthorn, demonstrating that the observed changes are significantly higher than the uncertainty of the inversion, the overall uncertainty of adaptation is in the same order of magnitude as the observed temporal shift in travel times in Lapires.

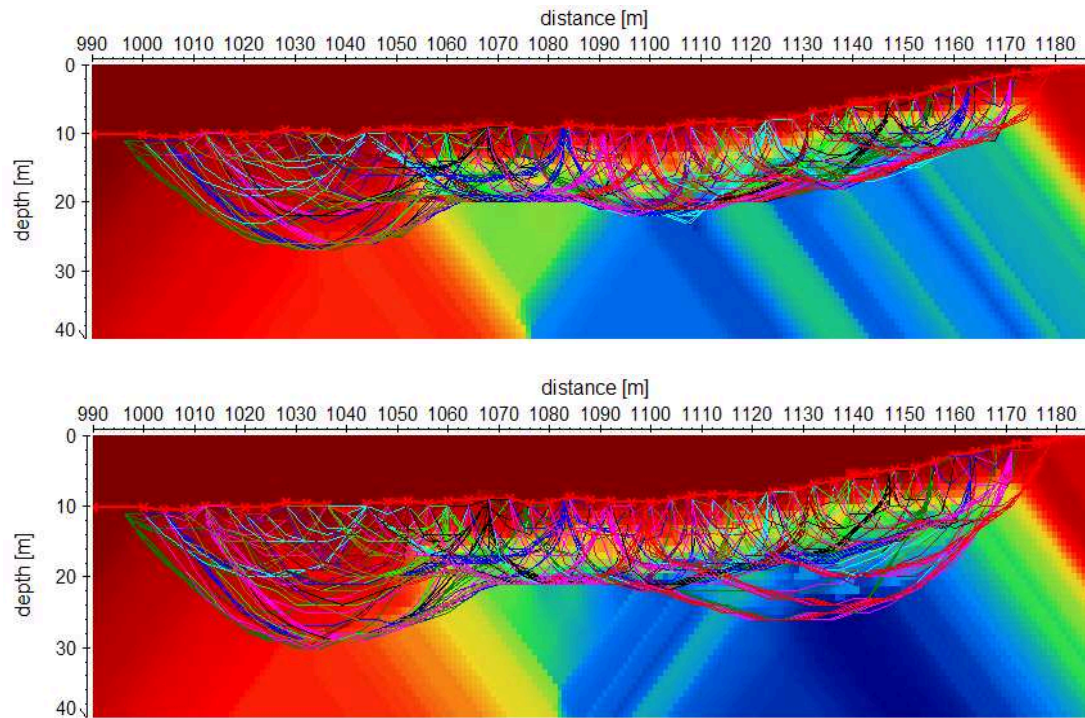


Fig. 7.10: Calculated ray paths for the tomograms from Lapires: July 10, 2008 (top), and August 18, 2008 (bottom).

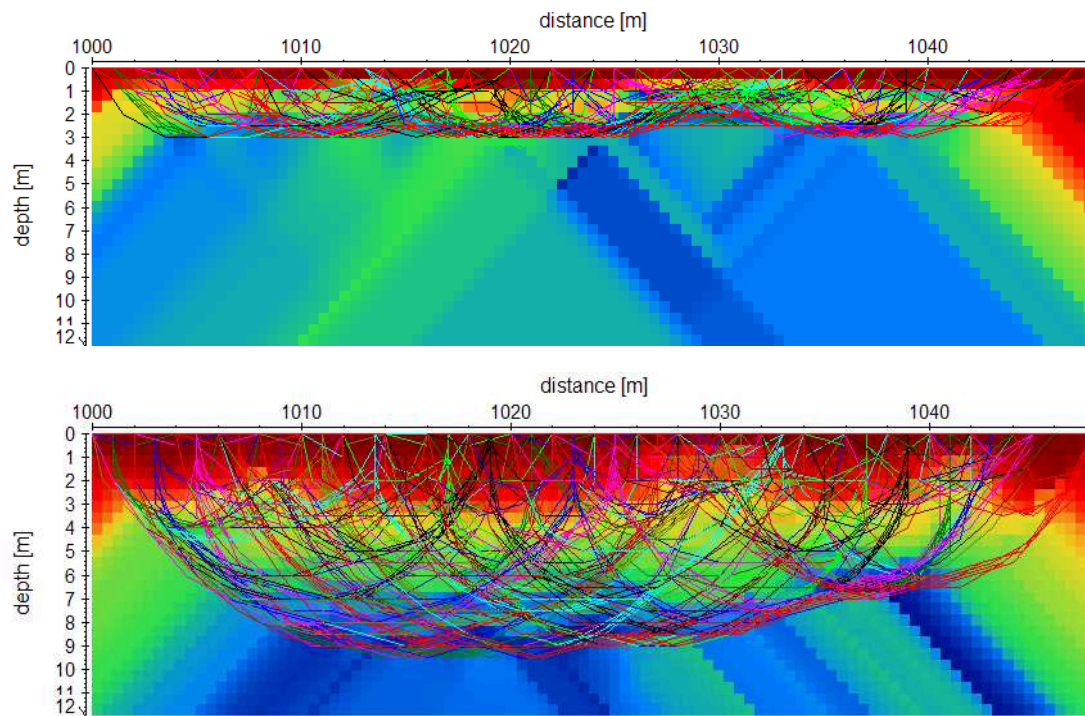


Fig. 7.11: Calculated ray paths for the tomograms from Schilthorn: July 11, 2008 (top), and August 26, 2008 (bottom). Note that the depth scale is smaller than in Fig. 7.10.

The *total time difference* between observed and calculated travel times (see chapter 2) amounts to 2.32 and 2.31 ms at Lapires, and to 0.03 and -0.002 ms at Schilthorn for the July and August tomograms, respectively, meaning that the modelled data slightly tend to underestimate the depth of the real structure in Lapires (i.e. observed – calculated travel times = positive values).

At Schilthorn the very low values prove a high confidence in the depth of the modelled structures. As these values for the July and August measurements are very similar at both sites, respectively, the quality of adaptation can be considered equally well.

To further analyse the reliability of the observed velocity changes at Lapires, the qualitative and quantitative differences between the travel times calculated by forward modelling from the tomographic inversion models of both measurement dates are plotted in Fig. 7.12 (equivalent to Fig. 7.5). Similar to the observed travel times, the calculated travel times show a temporal shift in measured travel times from July to August on the order of 1-4 ms (cf. Fig. 7.5b and 5c). This indicates that the overall misfit between model and data (total absolute time difference) of 2.64 and 2.71 ms does not seriously affect the accuracy of the detection of changes in travel times. Rather do calculated and observed data correspond surprisingly well and demonstrate that the results from the travel time analysis are in good accordance with the results from the tomographic inversion.

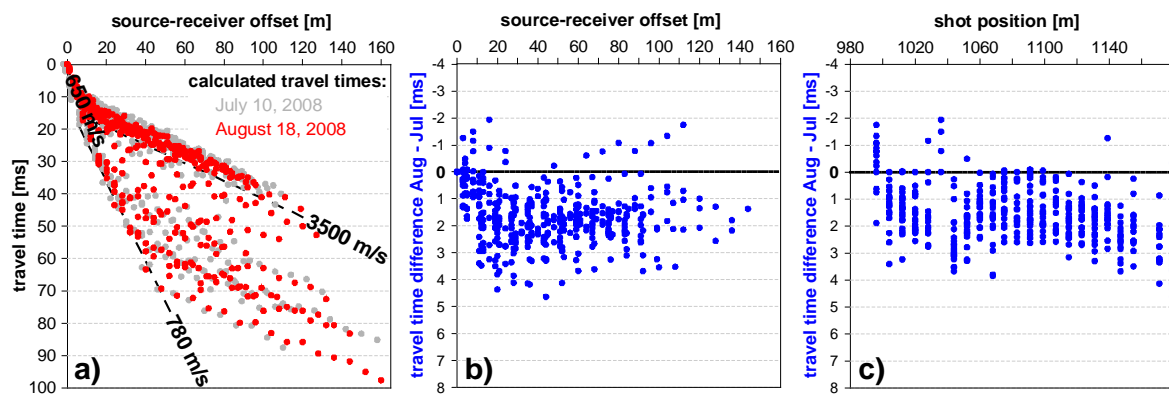


Fig. 7.12: As in Fig. 7.5, but now for a) calculated travel times based on the tomographic inversion models displayed in Fig. 7.8a against source-receiver offset, b) differences in calculated traveltimes against offset, and c) against shot position.

7.4 Interpretation of the results

As both the qualitative and quantitative analysis of the travel times and tomograms revealed a good reliability of the data sets, the tomograms and velocity changes are now interpreted together with the ERT data for both sites.

Lapires

Comparing the seismic data with the ERT tomograms in Fig. 7.8a the results show good agreement and the subsurface structure derived from both methods can be summarised as follows:

- The active layer is characterised by low seismic velocities (due to high amounts of air in the voids between the unconsolidated blocks and fines) and intermediate resistivities (also caused by high amounts of air within the otherwise relatively conductive overburden).
- A small high velocity anomaly is detected that coincides with the very low resistive anomaly in the ERT data due to the conductive (reinforced concrete) foundation of the cable car pylon (at 80-90 m horizontal distance). In contrast to the conductive metal, the seismic

waves are rather sensitive to the dense concrete material of the foundation accelerating the wave speeds in this zone.

- The left side of the profile represents the host material of the talus slope (unconsolidated blocks and fines) by both low seismic velocities and comparatively low electrical resistivities. The investigation depth of both methods is insufficient to detect the depth of the underlying bedrock ($> 40\text{m}$).
- The high velocity and high resistivity anomaly within the central and right part of the tomograms delineate the presence of ice-rich permafrost. The observed average velocity of 3500 m/s could also indicate bedrock, but ground truth observations from an excavation (Delaloye et al. 2001), borehole data and ERT data (Delaloye 2004; see *publication #3*, chapter 6), all indicate the presence of ground ice. Furthermore, during a new borehole drilling close to the pylon (see **Fig. 3.6**) in 2008 no bedrock was encountered down to a depth of 40 m (pers. comm. Reynald Delaloye & Cristian Scapozza 2008), which clearly supports the ground ice hypothesis. As high resistivities would also be caused by large amounts of air within the voids between the blocks, this possibility can now be excluded by the absence of a low velocity layer in this zone, and the seismic data therefore provide valuable complementary information to confirm the identification of ground ice.
- The zone with intermediate velocities between 1060 and 1080 m horizontal distance, corresponding to the zone with intermediate resistivities between 50 and 70 m , may be interpreted in terms of coarser material compared to the very left part of the profile but containing more fines and being more compacted than the blocks at the surface. Due to the generally lower velocities and resistivities this part may contain no or at least less ice than the zone to the right.

According to Lanz et al. (1998) the depth resolution of refraction seismics is much higher than that provided by other geophysical methods, which is clearly seen from comparison with ERT data in Fig. 7.8. However, regarding the geophone spacing of 8 m compared to 4 m electrode spacing, it is remarkable that the RST data sets still provides better resolution, which strikingly demonstrates the high potential of the RST method to resolve small-scale changes.

Regarding the *time-lapse tomograms* in Fig. 7.8b, as expected, the overall trend in velocity shift is negative, i.e. velocities generally decreased from July to August. However, large parts of the tomogram (at the surface and in the left (non-permafrost) part of the profile) exhibit only very small or even no changes in P-wave velocity. According to the above stated hypothesis, no considerable change in the content of frozen or liquid water has occurred in these zones and the general conditions did not change during the 40 days between the two measurements. Realising that the surface was already widely free of snow and unfrozen at the time of the first measurement in July, it is not surprising that changes in the uppermost part of the active layer are small. Also, the absence of pronounced changes in the unfrozen left part of the profile corresponds to the assumption that (from a geophysical point of view) seasonal changes at depth are much smaller in unfrozen regions than under permafrost conditions, as no phase changes between frozen and unfrozen conditions occur.

The red zones in Fig. 7.8b vividly illustrate the advance of the thawing front within the active layer during summer and indicate a reduction in P-wave velocity due to the melting of (seasonal) ground ice and. Note, that this zone is thicker in the right part of the profile, which corresponds to the observed larger travel time differences in Fig. 7.5c. The respective thaw depths (indicated in Fig. 7.8) are in good accordance with the resistivity changes (lower panel

in Fig. 7.8b), and are generally above the zone of main observed velocity changes (upper panels). This suggests that the seismic signal is more sensitive to changes occurring below 0°C, where the amount of unfrozen water already considerably increases with rising temperatures (cf. chapter 2).

The only zone with a significant velocity *increase* (blue colours in Fig. 7.8b) is observed in the central part of the tomogram, beneath the foundation of the cable car pylon. A temporally increased velocity can be attributed to either a reduced water content compared to formerly saturated conditions within unconsolidated sediments (Burger et al. 2006), or to the formation of ice (cf. chapter 2). The high electric resistivities contradict the presence of large amounts of unfrozen water and make the first option unlikely. The latter was already proposed from the analysis of ERT monitoring data (see appendix of *publication #3*), but the interpretation was rendered more difficult due to the conductive anomaly caused by the foundation of the pylon, strongly influencing the inversion result. As seismic monitoring yields comparable results (Fig. 7.8b) this previous interpretation of ERTM results is now strikingly supported.

Schilthorn

Comparing the RST and ERT tomograms from the Schilthorn site (Fig. 7.9a), the velocity and resistivity distributions exhibit clear differences (due to their complementary sensitivity to the physical properties of the subsurface). Regarding the overall temporal change visible in the time-lapse tomograms in Fig. 7.9b, velocity changes correspond remarkably well to resistivity changes.

The combined interpretation of RST and ERT results from Schilthorn (cf. Fig. 7.9a) is summarised as follows:

- In July small parts of the RST and ERT profile were still covered by snow and the surface was very wet as a consequence of snow melt water that could not infiltrate into the still widely frozen ground. Active layer thickness was ca. 2 m at B14 and ca. 0.5 m at B100 (Fig. 7.9). The shallow low velocity layer is interpreted as the active layer, which shows spatially heterogeneous vertical extents around a mean depth, that is in agreement with the borehole data. The velocity of the refractor of 4000-5000 m/s may indicate both frozen conditions as well as bedrock. Due to the strong refractor and its relatively high velocities the investigation depth is limited, and no stratigraphic details can be resolved below ca. 2.5 m.
- At the end of August the snow has disappeared completely and surface conditions were relatively dry. The active layer thickness has increased by 3 m at both boreholes (Fig. 7.9) within 47 days, which is clearly visible by the increased thickness of the red coloured zone indicating the active layer. The investigation depth increased to about 10 m with velocities of about 5000 m/s at the bottom. Velocities of 3000-4500 m/s in the lower part of the profile (between the permafrost table at about 5 m and the bottom) correspond to the frozen conditions recorded in the boreholes. The more heterogeneous velocity distribution in this layer may be attributed to a heterogeneous distribution of debris (lower velocities) and frozen bedrock (higher velocities). As velocities further increase to about 5000 m/s at greater depth it is assumed that the seismic velocity also represents transitions between weathered and firm bedrock.
- The increase in penetration depth is larger at the left side of the profile, which is in accordance to the ERT data that generally exhibit lower resistivities in this part, indicating the

presence of debris compared to prevailing bedrock in the right part (see interpretation of the ERT profile in *publication #1*, chapter 4).

In the *time-lapse tomograms* in Fig. 7.9b an overall velocity decrease is observed throughout the profile (note, that only velocity changes above the dashed line should be interpreted). A very shallow zone at the surface (ca. 0.5 m) shows no change or partly a slight velocity increase, which can be explained by the initially unfrozen conditions with different degrees of saturation that may change depending on weather conditions or water supply from above. Below this superficial layer the P-wave velocity decreased *by more than 3000 m/s*, which is over 75% of the absolute velocity. As major changes in the lithology and porosity can be excluded, this value cannot (only) be explained by seasonal variations in the air and/or water content but clearly indicates that the change in subsurface composition must have involved a significant amount of (seasonal) ground ice in the active layer (cf. Fig. 2.4), i.e. a change from primarily solid matrix conditions (rock-ice matrix) to a solid-liquid or a solid-liquid-gaseous matrix. A comparable order of magnitude could only be achieved by significant changes in the pore volume with time and thus by variations in the air content (which is very unlikely within the observed time span). The hypothesis of melting of ground ice is strongly supported by the borehole temperatures, that change from frozen to unfrozen conditions in the depth range of maximum velocity change (see thaw depths indicated at the boreholes in Fig. 7.9).

Whereas the absolute change in velocity is nearly uniformly distributed along the profile, the relative change is slightly increased in the left part of the profile (around 1005 m and 1015 m horizontal distance), indicating that the pore space and/or the ice content is higher than in the right part. This is in accordance with the findings by Hauck (2001) (based on a RST profile with larger penetration depth) as well as the interpretation of the ERT data (see *publication #1*, chapter 4) that are considered to represent a several meters thick debris cover in the left part and bedrock with lower porosity in the right part. The resistivity changes observed by ERTM agree well with the seismic data set. The relative resistivity changes are even smaller than changes in seismic velocities, which is interpreted to be a consequence of the generally, compared to other permafrost sites, very low resistivities observed at Schilthorn (due to very low ice contents lithology). Both methods reveal the lowest changes at the right end of the profile where bedrock outcrops indicate the occurrence of the bedrock layer close to the surface.

7.5 Conclusions

The novel RSTM application of the presented study is based on the assumption that P-wave velocities within the subsurface are affected by seasonal or inter-annual freezing or thawing processes, and that repeated refraction seismic measurements under constant measurement conditions allow the assessment of such temporal changes. The evaluation strategy of this approach comprised a) the analysis of reproducibility of the seismic signal, b) the analysis of time-lapse travel time curves with respect to resolving possible shifts in travel times, and c) the comparison of inverted tomograms including the quantification of spatio-temporal velocity changes.

Time-lapse data sets from the Lapires talus slope and the Schilthorn rock slope served to evaluate the performance of the RSTM approach. Both sites are characterised by pronounced differences in the seasonal changes during the same period.

Important results from this study are summarised in the following:

- Analysis of the unfiltered *seismograms* revealed a generally good reproducibility of the waveforms and signal strength for subsequent measurements with moderate changes in active layer depth (as observed at Lapires).
- The confidence in the identification of first breaks could be substantially improved by jointly analysing the two data sets and thus enabling a “*constrained picking*”, which was especially helpful for large offsets with reduced signal-to-noise ratios.
- The comparison of *time-lapse travel time curves* showed systematic temporal changes in the seismic response from the subsurface, and the quantification of travel time differences revealed lateral and vertical variations of these subsurface changes.
- *Tomographic inversion results* are largely comparable concerning the overall structure, but exhibit different investigation depths and a clear shift in the transition between the low velocity overburden and the refractor underneath.
- The temporal shift is well reconstructed in the *calculated* travel times from the inverted models (by forward modelling) indicating that the overall misfit between model and observed data does not seriously affect the accuracy of the detection of travel time changes.
- Interpretation of velocity changes from *time-lapse tomograms* corresponds to results from ERT monitoring, and to the thawing front progression. No changes were observed in initially already unfrozen parts of the active layer.
- Refraction seismic tomograms also yield *complementary information* that strongly support the interpretation of ERTM data in ambiguous cases. By this, a critical zone in the ERT images from the Lapires site that was difficult to interpret due to the high probability of an inversion artefact (cf. *publication #3*, chapter 6), could be verified by RSTM. This confirms that resistivity and velocity increases can be observed in summer within ventilated talus slopes. RSTM may therefore contribute to an increased understanding of the ventilation process.
- An important result is, that the observed *velocity change of $\sim 3000\text{m/s}$* at the Schilthorn site *unambiguously* proved the initial presence of significant amounts of ground ice in the active layer that disappeared until the later measurement. Compared to ERTM, this is a great advantage of the RSTM approach. For sites with generally low resistivities of the permafrost material (such as Schilthorn), with corresponding difficulties in the interpretation regarding the existence of ground ice, RST monitoring therefore provides a huge potential to avoid ambiguities.
- Another advantage of the RSTM approach is the generally *higher vertical resolution* than that revealed by Wenner ERT surveys, even for a geophone spacing larger than the corresponding electrode spacing. Together with the high reproducibility of the seismic signal in case of relatively small changes this points to a remarkable potential to resolve anticipated smaller-scale changes in ground ice content for inter-annual comparisons.
- A serious limitations of the approach is the *often small penetration depth* due to strong velocity contrasts between active layer and permafrost table.
- As the acquisition of high-resolution data sets cannot easily be automated and data processing is based on manual picking of first arrivals, the overall efforts of RSTM are much higher than for ERTM. However, for a long-term analysis of climate related ground ice

degradation one data set per site and per year (for comparable dates) should be sufficient, which requires not too much effort.

The time-lapse seismic refraction approach provides a valuable potential in terms of an independent and complementary monitoring approach for the detection of altered subsurface conditions caused by freezing and thawing processes. The approach was tested on a seasonal time scale, but as the expected annual changes in response to global warming are believed to be on a similar order of magnitude as seasonal changes, RSTM will work equally well on longer time scales and will be applied to those within the next years.

Finally, the long-term potential of the refraction seismic monitoring approach comprises the coupled use of time-lapse ERT and RST data sets in a time-lapse application of the 4-phase model for the assessment of changes in volumetric ice and water contents and thus climate related ground ice degradation. This will be a subject of the following chapter.

PART III - SYNTHESIS

Chapter 8

General Discussion

Chapter 9

Conclusions and Outlook

8 General discussion

This chapter provides a synthesis of the results from the previous chapters with the aim to comprehensively discuss the main findings and to evaluate the geoelectric and seismic monitoring approaches in terms of their potentials and limitations. A special focus will lie on the potential of a combined application of geoelectric and seismic monitoring to quantify temporal changes in ground ice content.

Based on the results from a preliminary study on the feasibility of permafrost monitoring by repeated ERT measurements over one year at Schilthorn (Hauck 2002) prior to this study, a systematic evaluation of this ERTM approach was carried out in the framework of this thesis. In addition, a complementary RSTM approach was tested for the first time in periglacial environments. The establishment of a unique geophysical monitoring network allowing repeated ERT and RST measurements at four different permafrost landforms in the Swiss Alps forms the basis of the evaluation of both monitoring approaches. The acquired data sets were analysed for their potential to indicate changes in ground ice content to evaluate the general capability of geophysical monitoring to the estimation of anticipated climate related ground ice degradation. As the monitoring network is still very young with only two to three years of observation (except for the Schilthorn site with 9 years), the evaluation strategy was mainly based on the analysis of seasonal and inter-annual changes. As independent ERT and RST measurements form the input for the time-lapse analysis, in the following, first the *reliability of the inverted tomograms* will be discussed, followed by the evaluation of the significance of the observed *temporal changes*.

8.1 Reliability of inverted ERT and RST tomograms

ERT

In principle, the electrical resistivity of the ground is strongly related to temperature, in particular for temperatures below the freezing point, as the pore water is conductive for positive temperatures, but successively transforms to insulating ice with temperatures decreasing to several degrees below zero. Consequently, the observed resistivity distribution of a subsurface section yields information on the ground ice and water content (and indirectly on the temperature) of a permafrost site. However, several uncertainties are involved, which have to be considered when interpreting resistivity values in terms of a permafrost signal:

The most obvious problem is that resistivities of different materials vary over a wide range depending on a variety of parameters, but primarily on the porosity and the amount of water contained in the pore space of a substrate or rock. The wide and largely overlapping resistivity ranges superimpose on the temperature signal, which makes, in the absence of additional data, a meaningful interpretation of certain resistivity values in terms of temperature or ice content extremely difficult. Exceptions comprise e.g. permafrost landforms consisting of massive ice (supersaturated) that can easily be identified with ERT due to their extremely high resistivities on the order of several M Ω m.

It is important to emphasise that, even if the identification of discontinuous permafrost occurrences by ERT may be straightforward in cases with significant ice contents, the absolute resistivity values are often strongly perturbed by superimposed effects from the inversion process. Consequently, a relation of ice content to resistivity may be very critical in cases of high ice contents and high resistivity contrasts (cf. *publication #3*, chapter 6). Similarly, although differences in specific resistivities in rockglaciers of up to one order of magnitude may principally be indicative for different ice types, a relation of inverted resistivity values to the ice origin of rockglaciers (as suggested by Haeberli & Vonder Mühll 1996) must be treated with great care for the same reasons.

For low to moderate ice contents and resistivity contrasts (as e.g. for Schilthorn) absolute resistivity values are much more reliable, but a differentiation between air, ice and rock is still difficult.

Apart from these uncertainties in the accuracy of absolute values, it could be shown in *publication #2* (chapter 5) that the observed vertical resistivity distribution is encouragingly consistent with overall vertical temperature trends in the subsurface (even for rockglaciers), strongly confirming the general applicability of the concept of relating ERT data to permafrost conditions.

RST

Observed P-wave velocities in refraction seismic surveying are in general well correlated with temperature and hence the ice content of the subsurface. As a fundamental difference to ERT, where electrolytic conduction takes place in the unfrozen portion of the pore water (even for extremely low pore water contents), *seismic waves* are transmitted primarily through the solid matrix (which is significantly influenced by the amount of ice contained in the pore volume), and seismic velocity thus increases as a consequence of *solidification* during the freezing process (Kneisel et al. 2008). The relation between temperature and velocity is more pronounced for saturated substrates compared to unsaturated or even dry conditions. This differentiated temperature relation can cause velocity differences of far more than 1000 m/s for different porosities and/or saturations at equal subzero temperatures. The interpretation of the subsurface stratigraphy in permafrost environments from absolute P-wave velocities alone may therefore be restricted to only a very rough discrimination. Moreover, similar to resistivity, also P-wave velocities exhibit wide and overlapping ranges for different rock types depending mainly on variations in porosity, weathering and fracturing.

The reliability of velocity values is basically a function of the resolution (i.e. the spacing of sources and receivers) and the quality of the data set (signal-to-noise ratio), which can thus largely be controlled by the user. The tomographic inversion is less influenced by artefacts as for ERT, and with some experience, the confidence of the inversion result can more easily be judged (qualitatively) by the user than for ERT. However, it is very important to note, that if the necessary condition of increasing density of the subsurface material with depth is not met, refraction seismic results are by definition unreliable (though basically not easily recognisable). In such cases (in permafrost environments this can e.g. occur in early winter when the active layer already started freezing from above but is still unfrozen in deeper parts, or for taliks), the data may indicate a good signal-to-noise ratio and the data misfit may indicate a high quality of the inversion result, whereas the reliability is rather low. Reducing the risk of so-called blind or hidden layers (Burger et al. 2006) is one of the most important tasks in assuring good reliabil-

ity of (time-lapse) refraction seismic tomograms. Similarly, RST is of very limited use, when no or only weak density contrasts occur in the depth range resolved by the survey geometry.

In contrast to ERT, RST works best for pronounced stratigraphic contrasts and is thus well suited as a complementary method to ERT. Where ERT often suffers from inversion artefacts due to too strong resistivity contrasts (e.g. at the interface between active layer and massive ice), RST provides the potential to considerably improve the reliability of the interpretation.

8.2 Reliability of relative resistivity and velocity changes

The approach of this thesis was to overcome the above listed uncertainties associated with individual geophysical surveys by repeated measurements and the consideration of relative changes instead of absolute values. In all three publications on ERTM and the chapter on RSTM it could be proven that the temporal changes in the observed specific resistivities and P-wave velocities are basically driven by changes in the subsurface temperature regime and are thus clearly related to permafrost dynamics. The reliability of the observed relative changes will now be summarised for both methods.

ERTM

Generally, as could be shown in *publication #1* (chapter 4), the reliability of inverted resistivity changes can be quite high when the overall variation in resistivities, either spatial or temporal, is rather low (i.e. less than one order of magnitude), independent of the time scale.

On the other hand, as for absolute resistivity values, the reliability of resistivity changes derived from rockglaciers and other landforms with coarse blocky surface characteristics and high ice contents can be seriously limited as a consequence of the very high resistivities of the ground ice and the large resistivity contrasts between active layer and permafrost (cf. *publication #3*, chapter 6). This was shown by a systematic appraisal analysis from the application of forward modelling, the depth of investigation index, or the resolution matrix approach, which allowed to identify unreliable model regions and significantly improved the interpretation of resistivity changes. As a general result, zones with strong resistivity gradients are often perturbed by inversion artefacts and should be excluded from the interpretation of resistivity changes. An encouraging result of the appraisal analysis with regard to anticipated changes in the permafrost regime is, that the reliability of temporally decreasing resistivities (as expected for long-term observations in the context of global warming) is higher compared to temporally increasing resistivities.

A satisfying spatial resolution of permafrost related processes is often restricted to the active layer and the uppermost permafrost layers (e.g. the progression of the thawing/freezing front, changes in moisture content within the active layer, or warming of massive ground ice). As the reliability of ERT data considerably decreases with depth, a detection of permafrost degradation at greater depth would consequently hardly be possible. This is strongly supported by the results from appraisal analysis carried out in *publication #3*, chapter 6.

A major uncertainty involved in the concept of relating resistivity changes to ice content changes is that, theoretically, for permafrost conditions only partly saturated with ice, an increase in water content without a considerable reduction in ice content may occur on short time scales during the season of snow-melt and active layer thawing. The corresponding reduction in observed resistivities may in such special cases wrongly lead to an interpretation of

ground ice loss. Similarly, a melting of significant amounts of ground ice may be followed by draining of the unfrozen water, causing the free pore space to be occupied by air, that is equally (or even more) resistive as ice. As before, these events occur on short time scales and are rather difficult to detect correctly by ERTM. Such cases have to be kept in mind when interpreting resistivity changes over long time scales. A third example may be significant for long-term ERTM on rockglaciers: As the active layer thickness cannot grow over massive ice due to the absent supply of rock material from the ice itself, a detection of permafrost degradation in terms of thinning of the ice core may be very difficult by ERTM (cf. *publication #3*, chapter 6). The corresponding ambiguities of these examples can be reduced by an adequate choice of the time for long-term comparisons (e.g. end of summer) and by a number of repeated measurements with high temporal resolution around the time of interest to evaluate the current subsurface dynamics.

RSTM

In RSTM applications the most serious limitation is due to considerable differences in penetration depths depending on the respective subsurface conditions. Although this does not directly affect the reliability of temporal velocity changes, it clearly refers to zones that are subject to considerable change and thus to zones of increased interest. As reliable velocity changes can only be calculated for model regions that are resolved by both involved data sets, changing penetration depths constitute a major restriction of the RSTM approach. However, in practise this might rather be a problem for seasonal than for inter-annual investigations.

An ambiguity that has to be kept in mind, is that temporal velocity changes may be due to either a shift in the refractor depth (without significant changes in the composition of the respective layers), or to changes in the composition of certain layers (without considerable changes of the geometry of the interfaces), or a combination of both. Calculated velocity changes must therefore always be interpreted with respect to absolute velocities in the RST tomograms, as a reliable interpretation of observed changes would otherwise be difficult.

The analysis of the data misfits (i.e. the difference between observed and calculated travel times during tomographic inversion) as well as the reconstruction of ray paths revealed a high reliability of all presented data sets (cf. chapter 7). As no time-lapse RST inversion technique was available for this study, the time-lapse RSTM approach introduced in this thesis is based on velocity differences calculated from independently inverted tomograms. Consequently, the reliability of the calculated changes can be regarded equally high as for absolute velocities.

A major advantage of RSTM compared to ERTM is the capability to unambiguously identify significant changes in ice content under certain conditions. As high *resistivity* values can equally be due to ice or air, large resistivity changes may consequently be caused by several processes involving not only freezing/thawing but also evaporation, infiltration/draining of water, etc. In contrast, a decrease in *seismic velocity* of more than 3000 m/s (as observed at Schilthorn, cf. chapter 7), clearly indicates that (for temporally constant porosity) the change in subsurface composition must have involved a significant amount of ice (cf. Fig. 2.4). Theoretically, a comparable order of magnitude could also be achieved by variations in the air content, but this requires a significant change in pore space with time, which is assumed to be very unlikely within the observed time span.

Similar to ERT, RST data suffer from decreasing resolution with depth, restricting reliable observations to shallow depths. In addition, the methodological condition of increasing ve-

localities with depth makes RSTM generally not applicable to analyse the lower boundary of permafrost or the evolution of taliks.

8.3 Evaluation of the applicability of ERTM and RSTM within an operational geophysical monitoring network

As discussed above, the quality of the acquired data sets may strongly depend on the characteristics of the field sites. Experiences from field work and data processing are therefore summarised in the following to evaluate the applicability of geophysical monitoring of permafrost within operational monitoring networks (such as PERMOS) concerning the strengths and weaknesses of both approaches.

8.3.1 Surface characteristics

The surface characteristics of a field site basically influence the coupling of the sensors (electrodes and geophones) to the ground. In any case, both types of sensors must be connected as firm as possible to achieve good results.

Electrode coupling is most difficult under coarse blocky surface conditions or even on rock faces, as contact resistances are quite high due to both high resistivity of rocks and only punctual coupling. From a monitoring point of view (in particular in view of the envisaged automation of the data acquisition), the often favoured supply of water is not always feasible. Instead, a significant reduction of the contact resistance could be achieved by a) parallel coupling of two or more electrodes, b) using screws (on large fixed blocks, or in rock faces) instead of steel stakes, or c) adding fine-grained material and/or moss to the electrodes.

On fine-grained surfaces, some electrodes were occasionally pushed towards the surface and loosened by frost heave during winter. Some improvement may be achieved by using longer stakes and/or by putting heavy blocks on top of the electrodes.

In contrast to electrodes, the *coupling of geophones* is facilitated by the presence of large blocks (with good ground contact) or rock faces, provided that the geophones can be fixed via screws. However, also under fine-grained or debris covered conditions, fixing of the geophones via spikes is generally relatively easy. If snow was present in the vicinity of the survey line, covering of the geophones with snow showed good improvement of the signal-to-noise ratio.

8.3.2 Seasonal differences of data quality and applicability

As measurements with both methods have been carried out during different seasons, some experiences were made in terms of seasonal differences in applicability and data quality.

Resistivity contrasts between active layer and permafrost table are highest in summer and minimal during winter, when the occurrence of inversion artefacts should theoretically be minimal. Together with the thermal damping effect of the snow cover (acting as a low-pass filter for atmospheric influences) this advantage would call for conducting the long-term ERTM measurements of permafrost evolution in winter. On the other hand, electrode coupling is generally worse in winter often prohibiting reliable data sets to be acquired. Exceptions comprise the Schilthorn and the Lapires sites, where contact resistances are higher in winter as well, but still allow high quality data sets to be measured in winter.

Seasonal aspects for *RST measurements* mainly focus on the accessibility of the ground surface as a) the energy has to be transmitted into the ground (coupling of the source), and b) the geophone array is currently not permanently fixed. In addition, the above mentioned problem of limited penetration depth in case of a widely frozen active layer indicates that RSTM measurements should, whenever possible, be conducted in late summer at the time of maximum active layer depth and before the evolution of a frozen surface.

8.3.3 Spatial resolution vs. penetration depth

Important insights of this thesis are concerned with the compromise between the desired spatial resolution and penetration depth of monitoring profiles. Initially, considerations on the length and investigation depth of the ERTM profiles were governed by the intention to achieve investigation depths that sufficiently cover the expected vertical extent of the considered landforms (in the cases of the Lapires talus slope and Murtèl rockglacier), and to cover a representative length and depth section of the rock slopes observed at Schilthorn and Stockhorn. Electrode spacing and thus spatial resolution was thereby adapted according to the maximum number of available electrodes (depending on the applied resistivity meter, a SYSCAL instrument with 48 electrodes).

However, a major result of the appraisal analysis conducted in *publication #3* (chapter 6) is, that a high spatial resolution is of superior importance. The reliability of resistivity values (and changes) generally decreases considerably with depth, and interpretations at greater depth always remain speculative. For ERTM therefore the smallest possible electrode spacing should be favoured, in particular at challenging sites such as rockglaciers or talus slopes. A small electrode spacing can essentially increase the resolution and reliability within the zone of expected changes (for rockglaciers e.g. in the active layer and the uppermost part of the ice core). As a compromise, singular surveys with larger spacing and corresponding deeper penetration may be carried out prior to the installation of a fixed electrode array, to obtain information on the depth to bedrock or other characteristics of interest, while ERTM should be focused on the uppermost parts of rockglaciers or similar landforms.

For a combined application of ERTM and RSTM similar considerations should be made for the priorities of refraction seismic surveys.

8.3.4 Temporal resolution

Finally, the optimum date for long-term comparisons and the generally desired temporal resolution of ERTM and RSTM shall briefly be discussed.

In principle, annual measurements at comparable dates may be sufficient for the observation of long-term permafrost degradation. In practice the evaluation of long-term changes is facilitated by conducting a number of subsequent measurements throughout the year, and ideally also around the date of “maximum” interest (i.e. the time for year-to-year comparisons).

For manual measurements, regular data acquisition is logistically difficult, and comparable dates for inter-annual comparisons are difficult to determine in advance, as the term ‘comparable’ may include meteorological conditions. As rule of thumb, at least one measurement between the end of August and beginning of September should be realised. This time roughly coincides with the time of maximum active layer depth at most permafrost sites (Vonder Mühl et al. 2007), and generally guarantees snow-free conditions. Ideally, at least a second measurement should be conducted around end of September or beginning of October, to

obtain a data set from the end of summer with the cumulative impact of the whole summer season. As the time of first snow strongly varies between the years and may have occurred before the date of this later measurement, this second late-summer measurement may be inappropriate for long-term comparisons, but nevertheless gives a good approximation of inter-annual differences. For the envisaged automated ERTM acquisition in the near future, a much higher temporal resolution is possible, such that the date used for long-term comparisons may be chosen from a comprehensive data set of e.g. weekly measurements (and additional information from meteorological and borehole temperature data may be used for the selection).

As the efforts for RST surveys are much higher (for both data acquisition and processing) than for ERTM, one measurement per year (ideally contemporaneously with ERTM) should be sufficient.

8.4 Quantification of ground ice degradation using a combined application of ERTM and RSTM data

So far, the considered relative changes in electrical resistivities and seismic velocities provided rough approximations on different amounts of spatio-temporal changes in the subsurface. Compared to temperature monitoring in 1D boreholes, ERTM and RSTM provide additional information on the distribution of higher and lower ice contents within 2D subsurface sections and on spatial differences in temporal changes. However, as straightforward relations between observed resistivity or velocity and ice content do not exist, from the consideration of relative resistivity or velocity changes alone an absolute quantification of long-term ground ice degradation is still not possible.

A novel approach to estimate total volumetric fractions of ice, water, and air within the (prescribed) pore volume of a rock matrix jointly using complementary data sets from non-intrusive geophysical surveys was introduced by Hauck et al. (2008, see chapter 2). The so-called four-phase model (4PM) uses coincident ERT and RST data sets to relate the physical properties of the subsurface to the measured electrical resistivities and seismic velocities. In its current state the 4PM still has a number of shortcomings and provides only rough estimations of the quantities of the solid (ice), liquid (water), and gaseous (air) constituents of the available pore volume (see section 8.4.2). But independently of its problems the combined analysis of ERT and RST data sets in the 4PM already allows for a clearly improved differentiation of the respective fractions.

A step towards reducing the uncertainties and to gain higher confidence in the calculated values may be a time-lapse application of the 4PM. Assuming that the porosity of a subsurface section will not change over the observation period, the calculation of *changes* in ice, water and air contents over time may give a more reliable indication on the subsurface characteristics than the estimation of *total* fractions. Based on these considerations, in the following, a comprehensive outlook on the *extension of the application of the 4PM to monitoring data sets* will be given by an exemplary demonstration for the time-lapse data sets from the Schilthorn site that were shown and discussed in chapter 7. This new approach is only possible by the unique data sets of coinciding ERTM and RSTM data acquired in the geophysical monitoring network. It comprises the estimation of *volumetric ground ice contents* (relative to porosity) for subsequent data sets compared to the estimation of *temporal changes in volumetric ice content* for a prescribed porosity model (assuming that the porosity remains constant over time).

8.4.1 Exemplary data set

The data set was already introduced in chapter 7 and comprises respective pairs of contemporaneous ERTM and RSTM data from July and August 2008 at Schilthorn (illustrated in Fig. 8.1). The ERT profile is 10 m longer than the RST profile and is thus only shown for the section covered by the RST profile (0-48 m length). The RST tomogram from July 2008 was cut for depths larger than 3.8 m to disable calculations for unrealistic velocity values below the overall investigation depth (cf. chapter 7). Moreover, the marginal zones of both data sets should be excluded (due to edge effects) from the interpretation of total amounts or changes in ice, water, and air contents.

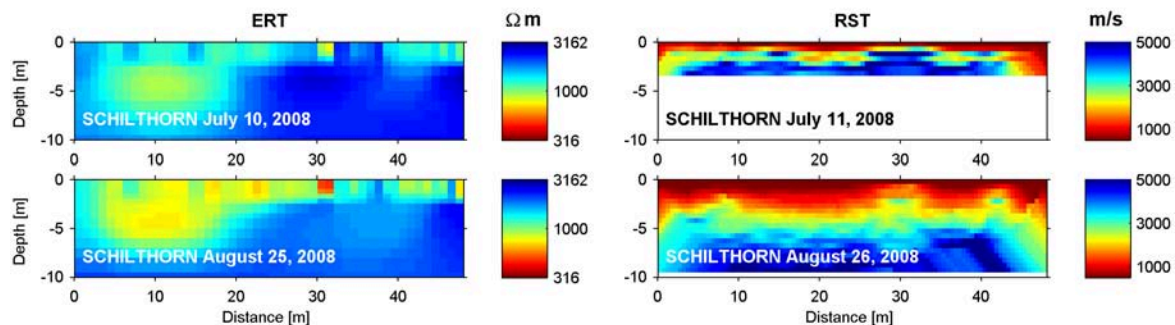


Fig. 8.1: Time-lapse ERT and RST data sets from Schilthorn used for the time-lapse 4PM approach.

8.4.2 Deficiencies of the 4-Phase Model (4PM)

Before the application of the 4PM, its current deficiencies are first briefly discussed. According to Hauck et al. (2008), a major limitation is that the calculated absolute fractions are significantly controlled by the prescribed porosity model. Other prescribed model parameters that influence the quantities of the calculated fractions are the resistivity of the pore water (controlling the amount of water present in a model cell) and, to a lesser extent, also the empirical parameters in Archie's law (m , n) and the seismic velocity of the bedrock material (v_r). Whereas v_r and the Archie parameters have to be assumed from literature (v_r can also be estimated from RST tomograms or from laboratory measurements), the pore water resistivity can be approximated by field measurements. A value of 83 Ωm was measured in August 2008 for water running out of a rock outcrop close to the ERT profile. Compared to a resistivity of 476 Ωm obtained from snow melt water the value of 83 Ωm clearly indicates an increased ionic load of the pore water at this site. Krainer & Mostler (2002) and L. Schrott (pers. communication) report comparable values in the order of 50-150 Ωm measured at springs of rockglaciers that similarly increased to values $> 400 \Omega\text{m}$ during snow melt, confirming that decreased values after the snow melt season rather represent the pore water conditions.

The most serious limitation of the 4PM is that a physical solution of the system of equations is only possible for limited ranges of seismic velocities and electrical resistivities. For example, if the seismic velocity of a certain cell is high (e.g. 4000 m/s) the calculated fraction for air may become negative for low resistivities. Similarly, very low seismic velocities may cause negative (and thus "non-physical") ice contents in case of low resistivity values. This relationship is exemplarily illustrated in Fig. 8.2a, where the resistivity-velocity space for physically correct solutions ($0 \leq \text{ice/water/air} \leq 100\%$) of the 4PM is plotted for a certain parameter configuration. Colours indicate the volumetric fraction, while blank regions indicate resistivity-velocity pairs with non-physical solutions of the 4PM. Note, that the form and size of this resistivity-velocity space depends on the selected prescribed parameters m , n , v_r , ρ_w , and Φ .

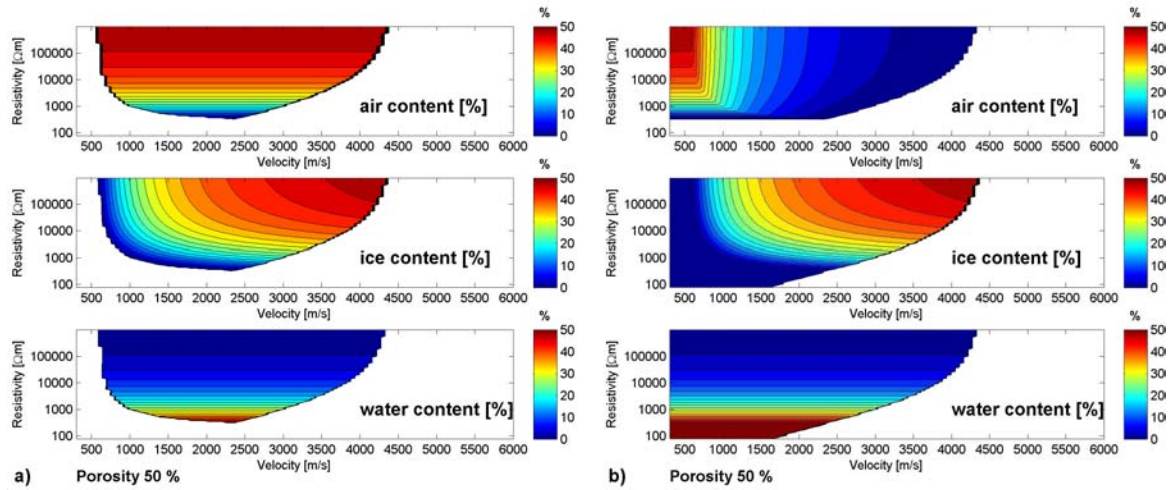


Fig. 8.2: a) Illustration of the resistivity-velocity space for physically correct solutions of the 4PM for a constant porosity of 50%. b) Extension of this space for the assumption that for low seismic velocities the ice content can be set to zero.

Recalling Equation (13) in chapter 2, it is seen that the amount of water content is only controlled by the electrical resistivity (due to the strong sensitivity to unfrozen water defined in Archie's law), which is visible in Fig. 8.2a. Conversely, the ice content is largely controlled by the seismic velocity (Equation 11), and is only restricted by the water content determined from the ERT data. Although ice largely influences the measured resistivities (cf. chapter 2) it is not considered in Archie's Law (originally designed for unfrozen conditions) demonstrating one of the major shortcomings in the current formulation of the 4PM.

To increase the amount of possible solutions to the 4PM, additional assumptions may be included. An admissible assumption may be that for very low seismic velocities the ice content will be close to zero. Including the condition, that negative values for the ice content (that occur for very low seismic velocities) are set to zero, the air content is then a function of the porosity and the water content ($f_a = 1 - \Phi - f_w$) and thus no longer dependent on seismic velocities. Fig. 8.2b illustrates the corresponding resistivity-velocity space for the altered formulation. Similar assumptions for high seismic velocities are more critical as the resistivity-controlled water content would simulate considerably high total water contents for seismic velocities that represent firm bedrock.

In the following, the resulting fractions of ice, water, and air will only be plotted for the adapted resistivity-velocity space of the respective combination of model parameters (similar to Fig. 8.2b but altered for a decreasing porosity model with depth, with lower porosities extending the space to higher seismic velocities).

8.4.3 Calculation of total ice, water and air contents by the 4PM

As a first step, a porosity model has to be prescribed (cf. chapter 2). As the boreholes at Schilthorn were drilled by a destructive technique, no direct information exists for the porosity of the subsurface material at Schilthorn. An approximation of the porosity of the overburden debris cover is given by Scherler (2006), who calculated mean values for the pore volume from grain size analyses of different samples within the upper 50 cm of the subsurface. The calculated values varied around 50% and decreased with depth. For the 4PM a porosity model with a maximum porosity of 50% at the surface was chosen that linearly decreased to 12.5% at 10

m depth. An overview of all selected model parameters (including Φ , Q_w , v_r , v_i , v_w , v_a , m , and n) is given in Tab. 8.1.

Fig. 8.3 illustrates the prescribed porosity model and the calculated volumetric fractions of ice, water, and air for both data sets from July and August 2008. Due to the small penetration depth of the seismic signal in July 2008 (discussed in chapter 7), the results are restricted to the uppermost 3.8 m (cf. Fig. 8.1). In addition, the relationship illustrated in Fig. 8.2b further limits the model results (blank zones).

A qualitative comparison of the 4PM results for July and August reveals largely plausible results: In July the *ice content* is negligible only in the uppermost 0.5-1 m and an extension of this zone to about 3-4 m is observed in August. Below this ice-free layer the calculated ice contents vary between 10 - 25% to a depth of at least 6 m (in August) with higher values in July. Generally, the right part of the profile exhibits higher ice contents (only visible for August).

The calculated *water content* shows a more homogeneous distribution with values of 25-30% in July and up to 40% in August. In contrast to the ice content, maximum values are found around 10 m horizontal distance and in the superficial (ice-free) layer. Significant amounts of *air* (up to 25%) are only found within the uppermost few meters, again with increased values at depth for the later measurement in August.

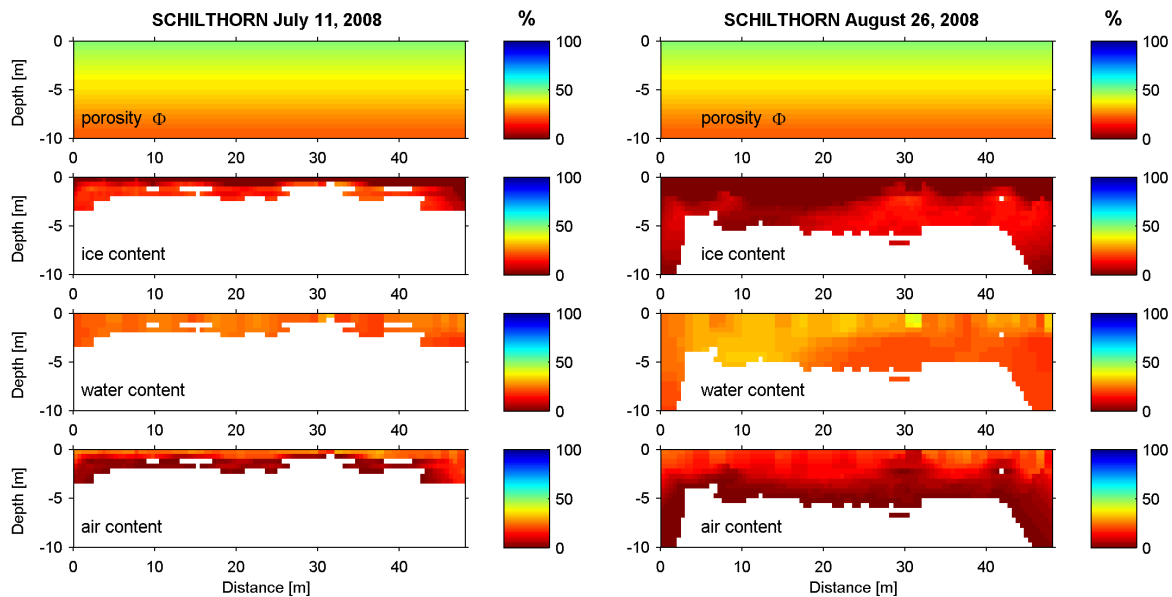


Fig. 8.3: Volumetric fractions of ice, water and air for a resistivity of the pore water of $80 \Omega\text{m}$ and a prescribed porosity model with decreasing porosity with depth.

According to the above mentioned dependence of the calculated fractions on the estimated porosity model, Hauck et al. (2008) emphasise that the consideration of fractions *relative to porosity* may be more appropriate. In Fig. 8.4 the respective fractions of the calculated ice, water, and air contents are shown relative to the porosity for both measurement dates, such that a value of 50% would mean that half of the available pore space is filled with the respective fraction.

Regarding these results relative to the available pore space, both spatial differences within a profile and temporal differences between the two measurement dates become more pronounced. Most striking is the difference between the almost equally distributed fractions of

water and ice (40-60% respectively) in the right part of the profile and the clearly increased water content (up to 80%) compared to much lower ice contents in the left part (around 10 m horizontal distance). The temporal evolution of the respective fractions confirm the interpretations from the resistivity and velocity changes in the ERT and RST data sets: In July the ice content is relatively high (40-60% of the pore space) in the uppermost few meters, and in August the ice has disappeared completely within the uppermost 3 m and decreased significantly at greater depth. Accordingly, the water and air contents increased significantly with the uppermost 5 m from July to August.

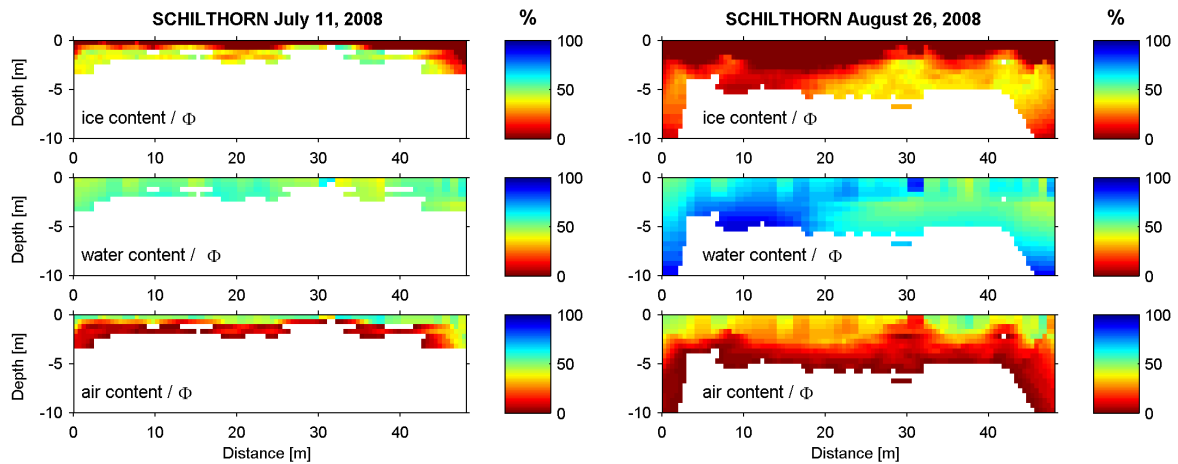


Fig. 8.4: Volumetric fractions of ice, water and air relative to the pore volume for both dates.

The *influence of the porosity model* on the calculated fractions is illustrated in Fig. 8.5 for a slightly altered porosity model of initially 40% porosity at the surface decreasing to 11% at 10 m depth. Compared to Fig. 8.4, the calculated contents of ice, water and air are clearly affected by this small alteration of the porosity model.

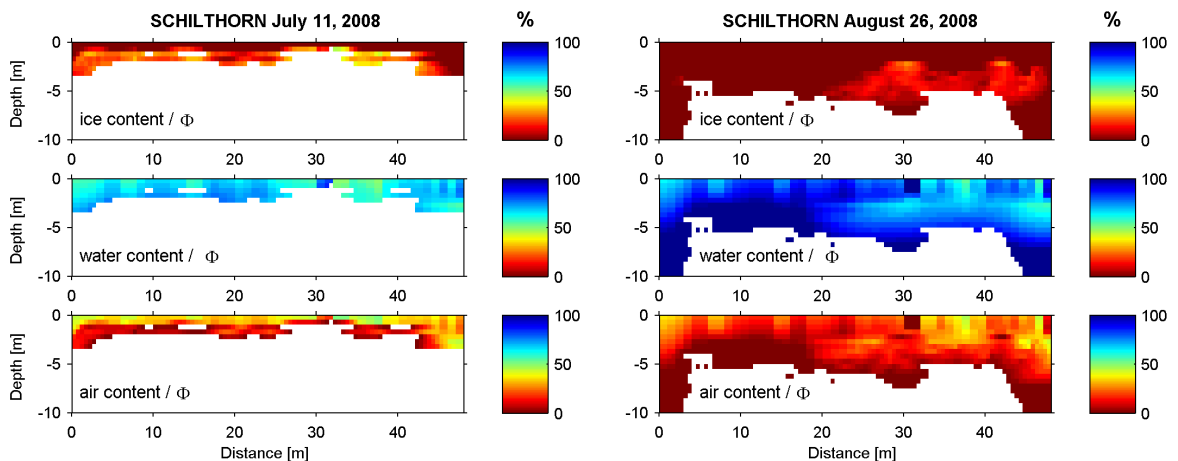


Fig. 8.5: As Fig. 8.4 but calculated for a different porosity model (40% at the surface and linearly decreasing to 11% at 10 m depth).

However, from a monitoring point of view, this uncertainty in the determination of an adequate porosity model is less critical when the *temporal change* in the fractions of ice, water and air are considered *relative to porosity*. Theoretically, the temporal change in the respective fractions should be unaffected from differences due to variations in the model parameters, as they

are equally applied to the data sets of both time instances. In the next section, therefore the calculated temporal changes between July and August 2008 in the respective fractions per porosity are illustrated, and the sensitivity of these changes to variations in model parameters is analysed compared to the sensitivity of the total fractions.

8.4.4 Changes in ice, water and air content determined from a time-lapse application of the 4PM

Fig. 8.6 illustrates the difference in the three calculated percentage fractions relative to porosity between July and August 2008. In this figure, a value of -30% for the change in ice content means a reduction of the ice filled pore space by 30%. Again, due to the limited penetration depth of the seismic survey in July 2008, in this example the change can only be calculated for the uppermost few meters. Apart from the uppermost 0.5-1 m, which were already unfrozen in July, a loss in ice content of up to 50% of the available pore space occurred between July and August. The resulting free pore space was replaced by air (30-50%) rather than water (0-20%). Conversely, within the uppermost 0.5-1 m the water content increased on the expense of air filled pore space.

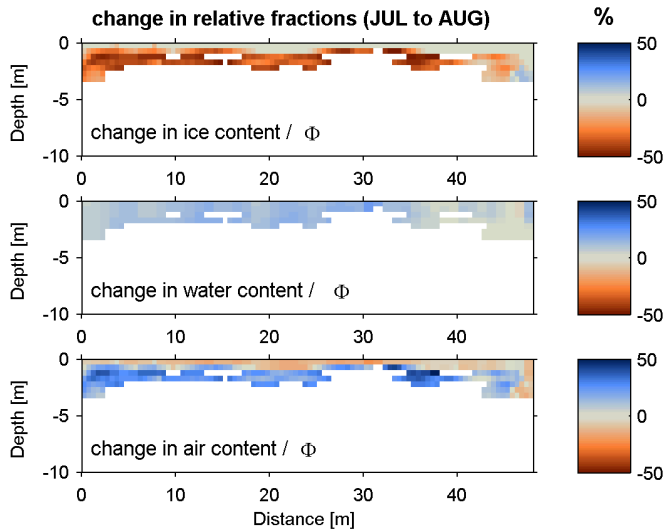


Fig. 8.6: Percentage changes in the ice, water and air content relative to porosity.

A decrease of the ice filled pore space by 30-50% would be, independent of the absolute pore volume, a strong indication for an initially significant ice content, which is in accordance with the qualitative analysis of the RSTM data set from Schilthorn in chapter 7. To evaluate the accuracy of the determined changes, in the following the sensitivity of the calculated relative fractions to the most important prescribed parameters in the 4PM will exemplarily be discussed for the ice content. These parameters include the mean seismic velocity for the rock matrix v_r (v_a , v_i , v_w can be regarded as constants, see Tab. 8.1), the porosity Φ , the resistivity of the pore water ρ_w , and the empirical parameters in Archie's law (m , n).

Fig. 8.7 shows the results for the application of the 4PM for different parameter combinations (within the range specified in Tab. 8.1) along a 1D vertical section at 38 m horizontal distance of the profile. The left panels illustrate the results for calculated total ice contents (according to Fig. 8.3) for July (continuous lines) and August 2008 (dashed lines) to the respective model depths, showing the smallest dependence on the value for the seismic velocity of bedrock, and the largest deviations for different porosity models.

Tab. 8.1: Model parameters used for the calculation of the fractions in the previous figures, and range of values used for the sensitivity analysis of the model results.

parameter	values used for 4PM calculations	range used for sensitivity analysis
v_r	6000 m/s	5000 – 8000 m/s
v_a	300 m/s	-
v_i	3500 m/s	-
v_w	1500 m/s	-
Φ	50 – 12.5% (decreasing with depth)	max. value (at the surface): 40-50% min. value (at 10 m depth): 11-20%
ρ_w	80 Ωm	60 – 120 Ωm
m	2	1.8 – 2.2
n	2	1.6 – 2.2

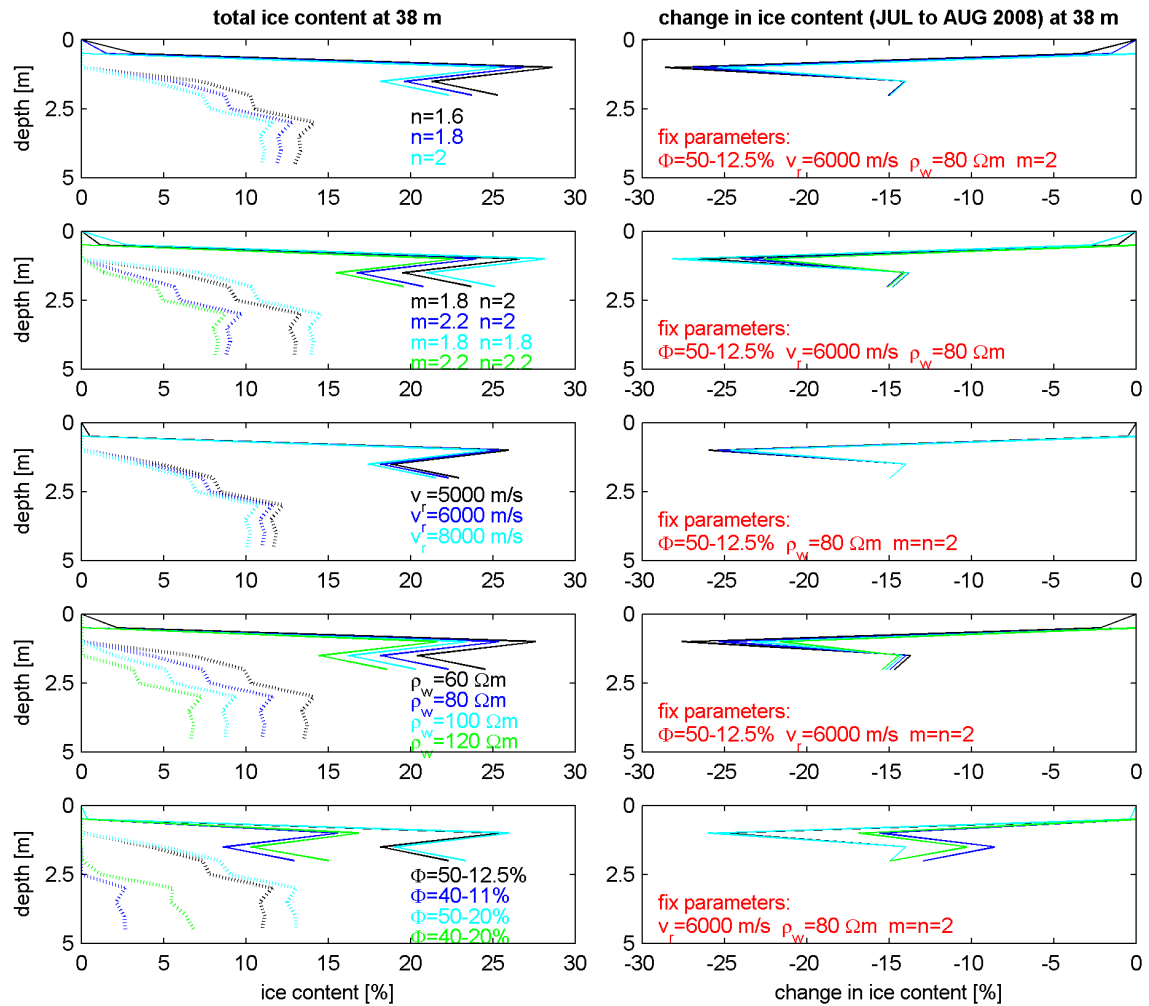


Fig. 8.7: Vertical cut through the tomogram at 38 m horizontal distance for the total ice content (left panels) and the change in ice contents (right panels) for calculated fractions based on different parameter combinations for m , n , v_r , ρ_w , and Φ . Solid and dashed lines correspond to the results from July and August, respectively.

It is seen that for the temporal change in total ice contents (July to August), the effects of different porosity models result in similarly large differences but the effect is much smaller for all other parameter combinations (right panel). As described above, in theory the temporal changes should be unaffected by variations of the model parameters (provided that the model parameters are equal for both time steps). However, an exception occurs at the boundaries of the resistivity-velocity space illustrated in Fig. 8.2b: for cases where slightly altered model parameters decide whether a model cell lies within the physically defined resistivity-velocity space or not (i.e. whether the ice content is very low or is set to zero due to too small seismic velocities), the change in ice content is no longer a continuous function of the resistivity-velocity relation. As the porosity model has the strongest influence on the extent of the valid resistivity-velocity space, different porosity models can lead to significantly altered ice contents. The sensitivity of the observed changes is therefore largest for the prescribed porosity.

For the presented data set from Schilthorn the selection of an appropriate porosity model is therefore still crucial, but for the analysed porosity differences a maximum difference in the change of ice content of 10% was observed. As a rough approximation, the estimated change in ice content at Schilthorn may have an accuracy of $\pm 5\text{-}10\%$, meaning that the observed changes of 30-50% are still significant.

8.4.5 Discussion and implications for future applications of the 4PM

The presented time-lapse approach of the 4PM allows for a partial compensation of current deficiencies of the 4PM, as inaccuracies in the prescribed model parameters will not affect the relative temporal change of the ice, water, and air content within the available pore space (provided that the porosity remains constant over time, and that model parameters are equally applied to both time instances).

However, not all deficiencies of the current formulation of the 4PM are reduced by the time-lapse approach. The limited resistivity-velocity space for correct solutions of the system of equations, that was artificially extended for low-velocity conditions (assuming that they point to zero ice contents), seriously affects also the calculated changes of the respective fractions. In this context, the presented data set from Schilthorn suffers from anomalously low resistivity values (due to the strongly weathered and rather low resistive limestone schists forming the host material of the permafrost), causing a large number of model cells to lie outside the resistivity-velocity space. Together with the limited investigation depth of the first RST data set in July, restricting the calculation of temporal changes to only a limited number of model cells, the example from Schilthorn is only of limited use for a thorough analysis of the advantages of a time-lapse 4PM approach. More appropriate data sets are necessary to exploit the potential of this approach. However, up to now, coincident and contemporaneous ERTM and RSTM data sets are only available on a seasonal scale, which leads to similar limitations described above. The acquisition of contemporaneous ERTM and RSTM data sets will be continued on an annual scale including at least one measurement in late summer (for maximum active layer depth), and more appropriate data sets for inter-annual comparisons will be available soon.

As the 4PM jointly uses the information of ERT and RST data, it does not provide new information that is not available from a separate analysis of both data sets, but it is rather a visualisation tool to aid interpretation. Compared to only ERTM or only RSTM data sets a temporal change in the geophysical signals can be interpreted more precisely, i.e. a decrease in the electrical resistivity may be due to a reduction in ice content but may also be caused by the

replacement of air by water with the ice content remaining unaffected. Similarly, a decrease of seismic velocity from 5000 to 3000 m/s may be interpreted as a decrease in ice content, but it is not clear whether the pore space is now filled with water or air. This qualitative interpretation is highly improved by the time-lapse application of the 4PM, giving clear indications on the spatial distribution of ice, water and air, and their temporal change.

The current limitations of the 4PM mainly affect the accuracy of the estimated quantities rather than the detection of the relative distribution of the respective fractions. The model is still under development, and an improved formulation of the 4PM should aim for a more advanced electrical mixing rule taking into account the different electrical characteristics of the three non-conducting phases air, ice and rock, or include additional geophysical data sets. A successful future improvement of the 4PM will provide a large potential to “translate” geophysical signals and their temporal changes into a vivid image of the subsurface composition in permafrost environments.

9 Conclusions and outlook

9.1 Main findings of the thesis

As a first step to improve the knowledge of processes and physical parameters in the frozen subsurface (as emphasised in the recent review paper of Harris et al. (2009)), it could be shown in this thesis that geophysical monitoring approaches are applicable to the determination of changes in ice and unfrozen water contents at different landforms and on different time scales in mountain permafrost terrain.

Evaluation of the ERT monitoring approach

The results of all three publications that are part of this thesis strongly emphasised that temporal changes in the observed electrical resistivities in periglacial environments are directly associated with changes in the content of ground ice and unfrozen water. The ERTM approach tested at four different landforms in mountain permafrost allows a relative quantification of these changes on different time scales.

The unique ERTM data set from the Schilthorn site comprising more than 9 years of observations revealed evidence for sustained ground ice degradation related to the heat wave that occurred in summer 2003. The severity of this impact, that is a persisting ice loss for several years, was not detected by borehole temperatures but only by geoelectric monitoring.

The observed discrepancy between temperature and resistivity evolution at Schilthorn, i.e. the delayed redeveloping of ground ice despite favourable temperature conditions, is interpreted to be indicative of a limited availability of unfrozen water (prohibiting refreezing to the previous amount of ice in the following winter) or by changes in materials characteristics, e.g. pore volume change by subsidence.

The need for detailed information on the varying response of heterogeneous landforms in mountain permafrost was emphasised by e.g. Harris et al. (2001b), Luetschg & Haeberli (2005), and Haeberli et al. (2006). To account for this heterogeneity, an ERTM network was established on four different landforms. The resistivity-temperature relations analysed for all sites showed a pronounced site-specific behaviour, confirming the dependence of resistivity on site characteristics, such as e.g. lithology, porosity, or ice content. At the same time it emphasises that, without additional knowledge, resistivities are not generally applicable as a proxy for subsurface temperatures in the absence of borehole data.

To address the problems related to the possible occurrence of inversion artefacts, identified by Marescot et al. (2003), a combination of different appraisal techniques (forward modelling, the depth of investigation index, and the resolution matrix approach) was applied that allowed the identification of unreliable model regions and thus a responsible interpretation of calculated resistivity changes. It could be demonstrated that even under the challenging conditions of coarse blocky terrain, such as rockglaciers or talus slopes, the ERTM approach is successfully applicable, provided that the reliability of the inverted tomograms is carefully analysed.

For ice-rich permafrost sites (such as Murtèl rockglacier) the inverted resistivities in zones of massive ground ice and in model regions with strong resistivity contrasts (e.g. between active layer and the ice body) are severely influenced by the inversion process and therefore of very critical reliability. Such inversion artefacts may superimpose on the general relationship between resistivity and subsurface temperatures, or between resistivity and different ice types. Consequently, temporal resistivity variations in zones with massive ice can very likely be caused solely by the inversion process and do not necessarily indicate true variations in the permafrost regime.

Conversely, degradation phenomena close to the surface and in the uppermost part of the ice core can successfully be identified by ERTM. At Murtèl rockglacier a small zone with pronounced active layer thickening was identified in summer 2007. In addition, at the top of the ice core a significant decrease in resistivities (indicative for warming permafrost with increasing unfrozen water contents within the still frozen ice core) was observed as a consequence of the warm winter 2006/2007. As rather stable borehole temperatures were recorded in a part with only minor resistivity changes, these observations are consistent with the borehole record, but again demonstrate the striking advantages of 2-dimensional ERTM for the detection of climate related changes in the permafrost regime.

In comparison with the Lapires talus slope it could be shown, that both resolution capacity and investigation depth increase substantially for landforms with comparatively lower (i.e. not supersaturated) ice content, such that even complex spatio-temporal resistivity changes can be reliably resolved by ERTM. The monitoring data from the Lapires site indicate that ERTM is in principle capable of detecting zones with preferential air flow (ventilation funnels) within ventilated talus slopes and may thus contribute to an increased understanding of this process.

As a conclusion, the ERTM approach proved to be a suitable approach to assess long-term ground ice degradation even on very blocky and therefore challenging surface conditions and contributes valuable additional information to traditional thermal monitoring records.

Potential of a complementary RST monitoring approach

The need for complementary methods to reduce the ambiguities inherently involved in geophysical methods is often emphasised (e.g. Hauck & Vonder Mühl 2003; Kneisel et al. 2008). The concept of time-lapse measurements instead of singular surveys, which is more and more used in ERT applications (e.g. Loke 1999), was therefore transferred to repeated refraction seismic measurements. It was demonstrated that refraction seismic monitoring is generally capable of detecting altered subsurface conditions caused by freezing and thawing processes. The results from this novel RSTM application confirmed its general applicability to permafrost sites making it a valuable complementary monitoring approach to support the interpretation of ERTM results.

Although the effort in data acquisition and processing is much higher than for ERTM, a combined application of ERTM and RSTM can strongly improve the interpretation in ambiguous cases. Besides the high spatial resolution, a particular strength of the RSTM approach is its good performance for subsurface conditions with pronounced interfaces, providing valuable complementary information in zones where the resolution of ERTM is strongly limited due to the occurrence of large resistivity gradients. In addition, RSTM may successfully be applied at

sites where ERT data are perturbed e.g. due to contamination by electrically conductive infrastructure.

Under certain conditions, the identification of ice content changes by RSTM can even be completely unambiguous, as a velocity decrease around 3000 m/s can only be a result of severe ice content losses in the subsurface. This could be observed at Schilthorn, where a seasonal velocity decrease by more than 3000 m/s clearly proved the initial presence of significant amounts of ground ice in the active layer that disappeared in the following month.

In the same period, the subsurface changes at the Lapires site were considerably smaller. The analysis of the time-lapse data set showed a striking reproducibility of the waveforms and signal strength, which points to a considerable potential to resolve even small-scale inter-annual changes in ground ice content.

Quantification of ground ice degradation

The role of ice within fine and coarse debris and in bedrock, and the significance of percolating water for the mass and heat transfer in permafrost are often regarded as key parameters concerning a more sophisticated permafrost modelling (Riseborough et al. 2008; Harris et al. 2009). To achieve improvements in subsurface models (Noetzli et al. 2008) and their coupling to Regional Climate Models (Salzmann et al. 2007b), approaches are required to estimate spatially distributed volumetric ice contents and their temporal changes. A coincident and contemporaneous application of ERTM and RSTM over several years is an important prerequisite to determine not only relative resistivity or velocity changes, but to estimate changes in volumetric ice and water contents from the coupled analysis of both methods. A further improvement of the formulation of the so-called four-phase model (4PM), that relates the measured geophysical variables to quantities of the subsurface constituents, will allow for a better estimation of the amount of climate related ground ice degradation. The potential of this quantification approach was demonstrated for a seasonal example from Schilthorn.

9.2 Outlook and implications for future research

The work has focused on the assessment of the general applicability of geophysical techniques to monitor permafrost evolution. A further continuation of the monitoring in the following years to decades is intended by the PERMOS network, and the assessment of permafrost evolution under current warming trends will then be possible for different sites and landforms. In addition, the monitoring network will be extended to further sites in the Swiss Alps within the scope of PERMOS. Experiences made during the pilot phase of the geophysical monitoring network in the framework of this PhD project inspired new ideas on the improvement of data acquisition, data quality, and data processing and analysis.

An important task is to improve the coupling of the permanently installed electrodes to enable high-quality measurements during the winter season. First tests with screws fixed to large blocks were promising, but still do not reliably provide sufficient contact under frozen surface conditions. As the contact resistance decreases as a function of the “common surface” between an electrode and e.g. a rock, using longer screws and always three (or more) electrodes/screws in parallel instead of only one may already lead to considerable improvements. The performance of contact enhancing means (e.g. pole grease) should be tested for long-term application in cold environments. Finally, an innovative technique to prevent fixed electrodes

(and also permanent cables) from loosening or damage on creeping rockglaciers (that are usually moving faster than Murtèl) has to be found.

In the beginning of the project for practical reasons the Wenner configuration was chosen for the geoelectrical measurements. Improvements in data acquisition now allow the acquisition of a variety of different electrode configurations, and the corresponding joint inversion of the combined data set will significantly improve the spatial resolution achieved by the ERT data sets, as proposed by Stummer et al. (2004). First tests with data sets based on Wenner, Wenner-Schlumberger, and Dipole-Dipole configurations yielded very promising results at all sites (provided that electrode coupling is sufficient to allow a large dipole spacing). The increased resolution will also contribute to an improved accuracy and reliability of volumetric quantities of ice as calculated by the 4PM.

The development of an automated ERTM system is already in progress and a first prototype will soon be installed at Schilthorn, and successively at the other monitoring sites. The main advantage of automated data acquisition lies of course in an immense reduction in logistical efforts for data acquisition. Moreover, a huge potential also lies in the collection of data sets with a daily or weekly resolution, as such comprehensive data sets will not only allow for a thorough investigation of short-term events (e.g. thawing of the active layer in summer or refreezing in autumn), but also provide a valuable data base for inter-annual comparisons. The analysis of the long-term evolution of permafrost will no longer depend on a few arbitrarily chosen measurement dates, but the selection of data sets for inter-annual comparisons can then be based on meteorological data and statistical parameters. Also, a combined analysis of geophysical, thermal and meteorological monitoring data will be possible by ERTM data sets with high temporal resolution.

Finally, for future improvements the application of joint inversion techniques of ERT and RST would be desirable. Some theoretical concepts and first algorithms are existent (e.g. Gallardo & Meju 2004), but have not yet been applied to mountain permafrost. Resulting tomograms with increased accuracy will not only facilitate the interpretation, but they can also contribute to a better performance of the 4PM and thus to the reliability of estimated total fractions of ice and water in the subsurface.

References

- Aaltonen, J. 2001. Ground monitoring using resistivity measurements in glaciated terrains. Ph.D. thesis, *Department of Civil and Environmental Engineering, Royal Institute of Technology, Stockholm*: 61 pp.
- Aaltonen, J. & Olofsson, B. 2002. Direct current (DC) resistivity measurements in long-term groundwater monitoring programmes. *Environmental Geology* **41**(6): 662-671.
- Archie, G.E. 1942. The electrical resistivity log as an aid in determining some reservoir characteristics. *Trans. AIME, Metallurgy and Petroleum Engineers* **146**: 54-62.
- Arenson, L., Hoelzle, M. & Springman, S. 2002. Borehole deformation measurements and internal structure of some rock glaciers in Switzerland. *Permafrost and Periglacial Processes* **13**(2): 117-135.
- Arenson, L. & Springman, S. 2005. Triaxial constant stress and constant strain rate tests on ice-rich permafrost samples. *Canadian Geotechnical Journal* **42**(2): 412-430.
- Arenson, L.U., Almasi, N. & Springman, S.M. 2003. Shearing response of ice-rich rock glacier material. *Proceedings of the 8th International Conference on Permafrost, Zürich*: 39-44.
- Barsch, D. 1973. Refraktionsseismische Bestimmung der Obergrenze des gefrorenen Schuttkörpers in verschiedenen Blockgletschern Graubündens, Schweizer Alpen. *Zeitschrift für Gletscherkunde und Glazialgeologie* **9**(1-2): 143-167.
- Baum, M. 2008. Potential und Grenzen eines geoelektrischen Monitorings zur Untersuchung der active layer Dynamik und möglicher Permafrostdegradation am Stockhorn (Wallis, Schweizer Alpen). Diploma thesis, *Institut für Geographie, Jena, University of Jena*: 68 pp.
- Beniston, M. 2006. Mountain weather and climate: A general overview and a focus on climatic change in the Alps. *Hydrobiologia* **562**: 3-16.
- Berthling, I., Etzelmüller, B., Wåle, M. & Sollid, J.L. 2003. Use of Ground Penetrating Radar (GPR) soundings for investigating internal structures in rock glaciers. Examples from Prins Karls Forland, Svalbard. *Zeitschrift für Geomorphologie, N.F. Suppl.* **132**: 103-121.
- Brown, J. & Romanovsky, V.E. 2008. Report from the International Permafrost Association: State of permafrost in the first decade of the 21st century. *Permafrost and Periglacial Processes, Special Issue: Recent advance in permafrost and periglacial research* **19**(2): 255-260.
- Bucki, A.K., Echelmeyer, K.A. & MacInnes, S. 2004. The thickness and internal structure of Fireweed rock glacier, Alaska, USA, as determined by geophysical methods. *Journal of Glaciology* **50**(168): 67-75.
- Burger, H.R., Sheehan, A.F. & Jones, C.H. 2006. *Introduction to applied geophysics - Exploring the shallow subsurface*. W.W. Norton & Company, Inc., London, 554 pp.
- Daily, W., Ramirez, A. & Binley, A. 2004a. Remote monitoring of leaks in storage tanks using electrical resistance tomography: Application at the Hanford site. *Journal of Environmental and Engineering Geophysics* **9**(1): 11-24.
- Daily, W., Ramirez, A., Binley, A. & D., L. 2004b. Electrical resistance tomography. *The Leading Edge* **23**(5): 438-442.

- Daniels, J.J., Keller, G.V. & Jacobson, J.J. 1976. Computer-Assisted Interpretation of Electromagnetic Soundings over a Permafrost Section. *Geophysics* **41**(4): 752-765.
- Davies, M.C.R., Hamza, O. & Harris, C. 2001. The effect of rise in mean annual temperature on the stability of rock slopes containing ice-filled discontinuities. *Permafrost and Periglacial Processes* **12**(1): 137-144.
- Delaloye, R. 2004. Contribution à l'étude du pergélisol de montagne en zone marginale. PhD thesis, *Département de Géosciences - Géographie*. Fribourg, University of Fribourg: 242 pp.
- Delaloye, R. & Lambiel, C. 2005. Evidences of winter ascending air circulation throughout talus slopes and rock glaciers situated in the lower belt of alpine discontinuous permafrost (Swiss Alps). *Norwegian Journal of Geography* **59**(2): 194-203.
- Delaloye, R., Perruchoud, E., Avian, M., Kaufmann, V., Bodin, X., Hausmann, H., Ikeda, A., Käab, A., Kellerer-Pirklbauer, A., Krainer, K., Lambiel, C., Mihajlovic, D., Staub, B., Roer, I. & Thibert, E. 2008. Recent interannual variations of rock glacier creep in the European Alps. *Proceedings of the 9th International Conference on Permafrost*, Fairbanks, Alaska **1**: 343-348.
- Delaloye, R., Reynard, E. & Lambiel, C. 2001. Pergélisol et construction de remontées mécaniques: l'exemple des Lapires (Mont-Gelé, Valais). *Le gel en géotechnique, Publications de la Société Suisse de Mécanique des Sols et des Roches*. **141**: 103-113.
- Delaney, A., Sellmann, P. & Arcone, S. 1988. Seasonal variations in resistivity and temperature in discontinuous permafrost. *Proceedings of the 5th International Conference on Permafrost*, Trondheim, Norway: 927-932.
- Fisch, W., Fisch, W. & Haeberli, W. 1977. Electrical DC resistivity soundings with long profiles on rock glaciers and moraines in the Alps of Switzerland. *Zeitschrift für Gletscherkunde und Glazialgeologie* **13**(1-2): 239-260.
- Fischer, L., Käab, A., Huggel, C. & Noetzi, J. 2006. Geology, glacier retreat and permafrost degradation as controlling factors of slope instabilities in a high-mountain rock wall: the Monte Rosa east face. *Natural Hazards and Earth System Sciences* **6**(5): 761-772.
- Fortier, R., Allard, M. & Seguin, M.K. 1994. Effect of Physical-Properties of Frozen Ground on Electrical-Resistivity Logging. *Cold Regions Science and Technology* **22**(4): 361-384.
- French, H.K., Hardbattle, C., Binley, A., Winship, P. & Jakobsen, L. 2002. Monitoring snow-melt induced unsaturated flow and transport using electrical resistivity tomography. *Journal of Hydrology* **267**(3-4): 273-284.
- Gallardo, L.A. & Meju, M.A. 2004. Joint two-dimensional DC resistivity and seismic travel time inversion with cross-gradients constraints. *Journal of Geophysical Research* **109**: B03311.
- Gruber, S. & Haeberli, W. 2007. Permafrost in steep bedrock slopes and its temperature-related destabilization following climate change. *Journal of Geophysical Research-Earth Surface* **112**: F02S18.
- Gruber, S., Hoelzle, M. & Haeberli, W. 2004a. Permafrost thaw and destabilization of Alpine rock walls in the hot summer 2003. *Geophysical Research Letters* **31**: L13504.
- Gruber, S., King, L., Kohl, T., Herz, T., Haeberli, W. & Hoelzle, M. 2004b. Interpretation of geothermal profiles perturbed by topography: the Alpine permafrost boreholes at Stockhorn Plateau, Switzerland. *Permafrost and Periglacial Processes* **15**(4): 349-357.
- Gude, M. & Barsch, D. 2005. Assessment of geomorphic hazards in connection with permafrost occurrence in the Zugspitze area (Bavarian Alps, Germany). *Geomorphology* **66**(1-4): 85-93.

- Günzel, F. 2008. Shear strength of ice-filled rock joints. *Proceedings of the 9th International Conference on Permafrost*, Fairbanks, Alaska **1**: 581-586.
- Haerberli, W. 1973. Die Basis-Temperatur der winterlichen Schneedecke als möglicher Indikator für die Verbreitung von Permafrost in den Alpen. *Zeitschrift für Gletscherkunde und Glazialgeologie* **9**(1-2): 221-227.
- Haerberli, W. 1978. Special aspects of high mountain permafrost methodology and zonation in the Alps. *Proceedings of the 3rd International Conference on Permafrost*, Edmonton, Canada: 379-384.
- Haerberli, W. 1990. Glacier and permafrost signals of the 20th-century warming. *Annals of Glaciology* **14**: 99-101.
- Haerberli, W. & Gruber, S. 2008. Research challenges for permafrost in steep and cold terrain: an alpine perspective. *Proceedings of the 9th International Conference on Permafrost*, Fairbanks, Alaska **1**: 597-605.
- Haerberli, W., Hallet, B., Arenson, L., Elconin, L., Humlum, O., Kääb, A., Kaufmann, V., Ladanyi, B., Matsuoka, N., Springman, S. & Vonder Mühll, D. 2006. Permafrost creep and rock glacier dynamics. *Permafrost and Periglacial Processes* **17**: 189-214.
- Haerberli, W., Hoelzle, M., Kääb, A., Keller, F., Vonder Mühll, D. & Wagner, S. 1998. Ten years after drilling through the permafrost of the active rock glacier Murtèl, eastern Swiss Alps: answered questions and new perspectives. *Proceedings of the 7th International Conference on Permafrost*, Yellowknife, Canada: 403-410.
- Haerberli, W., Huggel, C., Kääb, A., Zraggen-Oswald, S., Polkvoj, A., Galushkin, I., Zotikov, I. & Osokin, N. 2004. The Kolka-Karmadon rock/ice slide of 20 September 2002: an extraordinary event of historical dimensions in North Ossetia, Russian Caucasus. *Journal of Glaciology* **50**(171): 533-546.
- Haerberli, W., Kääb, A., Mühll, D.V. & Teyssie, P. 2001. Prevention of outburst floods from periglacial lakes at Grubengletscher, Valais, Swiss Alps. *Journal of Glaciology* **47**(156): 111-122.
- Haerberli, W. & Vonder Mühll, D. 1996. On the characteristics and possible origins of ice in rock glacier permafrost. *Zeitschrift Für Geomorphologie, N.F. Suppl.* **1004**: 43-57.
- Harris, C., Arenson, L.U., Christiansen, H.H., Etzelmüller, B., Frauenfelder, R., Gruber, S., Haerberli, W., Hauck, C., Hoelzle, M., Humlum, O., Isaksen, K., Kääb, A., Kern-Lütsch, M.A., Lehning, M., Matsuoka, N., Murton, J.B., Noetzli, J., Phillips, M., Ross, N., Seppälä, M., Springman, S. & Vonder Mühll, D. 2009. Permafrost and climate in Europe: Monitoring and modelling thermal, geomorphological and geotechnical responses. *Earth Science Reviews* **92**: 117-171.
- Harris, C., Davies, M.C.R. & Etzelmüller, B. 2001a. The assessment of potential geotechnical hazards associated with mountain permafrost in a warming global climate. *Permafrost and Periglacial Processes* **12**: 145-156.
- Harris, C., Haerberli, W., Vonder Mühll, D. & King, L. 2001b. Permafrost monitoring in the high mountains of Europe: the PACE project in its global context. *Permafrost and Periglacial Processes* **12**(1): 3-11.
- Harris, C., Vonder Mühll, D., Isaksen, K., Haerberli, W., Sollid, J.L., King, L., Holmlund, P., Dramis, F., Guglielmin, M. & Palacios, D. 2003. Warming permafrost in European mountains. *Global and Planetary Change* **39**(3-4): 215-225.

- Hauck, C. 2001. Geophysical methods for detecting permafrost in high mountains. PhD thesis, *Mitteilungen der Versuchsanstalt für Wasserbau, Hydrologie und Glaziologie der Eidgenössischen Technischen Hochschule Zürich*, Nr. 171, ETH Zürich: 204 pp.
- Hauck, C. 2002. Frozen ground monitoring using DC resistivity tomography. *Geophysical Research Letters* **29**(21): 2016.
- Hauck, C., Bach, M. & Hilbich, C. 2008. A 4-phase model to quantify subsurface ice and water content in permafrost regions based on geophysical data sets. *Proceedings of the 9th International Conference on Permafrost*, Fairbanks, Alaska **1**: 675-680.
- Hauck, C., Guglielmin, M., Isaksen, K. & Vonder Mühll, D. 2001. Applicability of frequency-domain and time-domain electromagnetic methods for mountain permafrost studies. *Permafrost and Periglacial Processes* **12**(1): 39-52.
- Hauck, C., Isaksen, K., Mühll, D.V. & Sollid, J.L. 2004. Geophysical surveys designed to delineate the altitudinal limit of mountain permafrost: An example from Jotunheimen, Norway. *Permafrost and Periglacial Processes* **15**(3): 191-205.
- Hauck, C. & Kneisel, C. (Eds.) 2008. *Applied geophysics in periglacial environments*. Cambridge, Cambridge University Press, 240 pp.
- Hauck, C. & Vonder Mühll, D. 2003. Evaluation of geophysical techniques for application in mountain permafrost studies. *Zeitschrift für Geomorphologie, N.F., Suppl.* **132**: 159-188.
- Hauck, C., Vonder Mühll, D. & Maurer, H. 2003. Using DC resistivity tomography to detect and characterize mountain permafrost. *Geophysical Prospecting* **51**(4): 273-284.
- Hauck, C. & Wagner, U. 2003. Combining and interpreting geoelectric and seismic surveys in permafrost studies using fuzzy logic. *Geophysical Research Abstracts* **5**: 00807.
- Hausmann, H., Krainer, K., Brückl, E. & Mostler, W. 2007. Internal structure and ice content of Reichenkar rock glacier (Stubai Alps, Austria) assessed by geophysical investigations. *Permafrost and Periglacial Processes* **18**(4): 351-367.
- Hilbich, C., Hauck, C., Delaloye, R. & Hoelzle, M. 2008a. A geoelectric monitoring network and resistivity-temperature relationships of different mountain permafrost sites in the Swiss Alps. *Proceedings of the 9th International Conference on Permafrost*, Fairbanks, Alaska **1**: 699-704.
- Hilbich, C., Hauck, C., Hoelzle, M., Scherler, M., Schudel, L., Völksch, I., Vonder Mühll, D. & Mäusbacher, R. 2008b. Monitoring mountain permafrost evolution using electrical resistivity tomography: A 7-year study of seasonal, annual, and long-term variations at Schilthorn, Swiss Alps. *Journal of Geophysical Research* **113**: F01S90.
- Hilbich, C., Marescot, L., Hauck, C., Loke, M.H. & Mäusbacher, R. in press. Applicability of electrical resistivity tomography monitoring to coarse blocky and ice-rich permafrost landforms. *Permafrost and Periglacial Processes*.
- Hoekstra, P. & McNeill, D. 1973. Electromagnetic probing of permafrost. *Proceedings of the 2nd International Conference on Permafrost*, Yakutsk, Russia: 517-526.
- Hoelzle, M. & Gruber, S. 2008. Borehole and ground surface temperatures and their relationship to meteorological conditions in the Swiss Alps. *Proceedings of the 9th International Conference on Permafrost*, Fairbanks, Alaska **1**: 723-728.
- Hoelzle, M., Mittaz, C., Etzelmüller, B. & Haeberli, W. 2001. Surface energy fluxes and distribution models of permafrost in European mountain areas: an overview of current developments. *Permafrost and Periglacial Processes* **12**(1): 53-68.

- Hoelzle, M., Vonder Mühll, D. & Haerberli, W. 2002. Thirty years of permafrost research in the Corvatsch-Furtschellas area, Eastern Swiss Alps: a review. *Norsk Geografisk Tidsskrift* **56**: 137-145.
- Huggel, C., Caplan-Auerbach, J. & Wessels, R. 2008. Recent extreme avalanches: Triggered by climate change? *EOS. Transactions. American Geophysical Union* **89**(47): 469-484.
- IEEE (Ed.) 1983. *IEEE Guide for Measuring Earth Resistivity, Ground Impedance, and Earth Surface Potentials of a Ground System*. New York, USA, 49 pp.
- Ikeda, A. 2006. Combination of conventional geophysical methods for sounding the composition of rock glaciers in the Swiss Alps. *Permafrost and Periglacial Processes* **17**(1): 35-48.
- Ikeda, A. & Matsuoka, N. 2002. Degradation of talus-derived rock glaciers in the Upper Engadin, Swiss Alps. *Permafrost and Periglacial Processes* **13**(2): 145-161.
- Ikeda, A. & Matsuoka, N. 2006. Pebbly versus bouldery rock glaciers: Morphology, structure and processes. *Geomorphology* **73**(3-4): 279-296.
- Imhof, M., Pierrehumbert, G., Haerberli, W. & Kienholz, H. 2000. Permafrost investigation in the Schilthorn massif, Bernese Alps, Switzerland. *Permafrost and Periglacial Processes* **11**: 189-206.
- Ingeman-Nielsen, T., Villumsen, A. & Baumgartner, F. 2005. Geophysical techniques applied to permafrost investigations in Greenland. PhD thesis, *Technical University of Denmark*: 177 pp.
- IPCC 2007. Climate change 2007: The physical science basis. Summary for policy makers: 1-21.
- Kääb, A., Frauenfelder, R. & Roer, I. 2007. On the response of rockglacier creep to surface temperature increase. *Global and Planetary Change* **56**(1-2): 172-187.
- Kääb, A., Gudmundsson, G.H. & Hoelzle, M. 1998. Surface deformation of creeping mountain permafrost. Photogrammetric investigations on rock glacier Murtél, Swiss Alps. *Proceedings of the 7th International Conference on Permafrost*, Yellowknife, Canada: 531-537.
- Keller, G.V. & Frischknecht, F.C. 1966. *Electrical methods in geophysical prospecting*. Pergamon Press, Oxford, 523 pp.
- Kemna, A., Vanderborght, J., Kulesa, B. & Vereecken, H. 2002. Imaging and characterisation of subsurface solute transport using electrical resistivity tomography (ERT) and equivalent transport models. *Journal of Hydrology* **267**: 125-146.
- King, M.S. 2005. Rock-physics developments in seismic exploration: A personal 50-year perspective. *Geophysics* **70**(6): 3-8.
- King, M.S., Zimmerman, R.W. & Corwin, R.F. 1988. Seismic and Electrical-Properties of Unconsolidated Permafrost. *Geophysical Prospecting* **36**(4): 349-364.
- Klein, S. 2008. Untersuchung des Potenzials und der Grenzen eines refraktionsseismischen Monitorings im Hinblick auf die Beobachtung der active layer Dynamik und möglicher Permafrostdegradation am Stockhorn (Wallis, Schweizer Alpen). Diploma thesis, University of Jena: 59 pp.
- Kneisel, C. 2004. New insights into mountain permafrost occurrence and characteristics in glacier forefields at high altitude through the application of 2D resistivity imaging. *Permafrost and Periglacial Processes* **15**(3): 221-227.
- Kneisel, C. 2006. Assessment of subsurface lithology in mountain environments using 2D resistivity imaging. *Geomorphology* **80**(1-2): 32-44.

- Kneisel, C. & Hauck, C. 2003. Multi-method geophysical investigation of a sporadic permafrost occurrence. *Zeitschrift für Geomorphologie, N.F. Suppl.* **132**: 145-159.
- Kneisel, C., Hauck, C., Fortier, R. & Moorman, B. 2008. Advances in geophysical methods for permafrost investigations. *Permafrost and Periglacial Processes* **19**(2): 157-178.
- Krainer, K. & Mostler, W. 2002. Hydrology of active rock glaciers: Examples from the Austrian Alps. *Arctic, Antarctic, and Alpine Research* **34**(2): 142-149.
- Krauer, M. 2008. Versuch einer 3-dimensionalen Erfassung des Permafrostes in der Gipfelregion des Schilthorns mittels Geoelektrik. MSc thesis, University of Zurich: 112 pp.
- Krautblatter, M. & Hauck, C. 2007. Electrical resistivity tomography monitoring of permafrost in solid rock walls. *Journal of Geophysical Research-Earth Surface* **112**(F2).
- LaBrecque, D.J., Sharpe, R., Wood, T. & Heath, G. 2004. Small-scale electrical resistivity tomography of wet fractured rocks. *Ground Water* **42**(1): 111-118.
- Lambiel, C. 1999. Inventaire des glaciers rocheux entre la Val de Bages et le Val d'Hérémence (Valais). PhD thesis, University of Lausanne: 167 pp.
- Landrø, M., Nguyen, A.K. & Mehdizadeh, H. 2004. Time lapse refraction seismic – a tool for monitoring carbonate fields? *SEG International Exposition and 74th Annual Meeting, 10-15 October 2004*, Denver, Colorado: 1-4.
- Lanz, E., Maurer, H. & Green, A.G. 1998. Refraction tomography over a buried waste disposal site. *Geophysics* **63**(4): 1414-1433.
- Lehmann, F. & Green, A.G. 2000. Topographic migration of georadar data: Implications for acquisition and processing. *Geophysics* **65**(3): 836-848.
- Loke, M.H. 1999. Time lapse resistivity imaging inversion. *Proceedings of the 5th Meeting of the EEGS European Section Em1*: 2.
- Loke, M.H. 2003. Tutorial: 2-D and 3-D electrical imaging surveys: 1-127.
- Loke, M.H., Acworth, I. & Dahlin, T. 2003. A comparison of smooth and blocky inversion methods in 2D electrical imaging surveys. *Exploration Geophysics* **34**: 182-187.
- Loke, M.H. & Barker, R.D. 1995. Least-squares deconvolution of apparent resistivity. *Geophysics* **60**: 1682-1690.
- Loke, M.H. & Barker, R.D. 1996. Rapid least-squares inversion of apparent resistivity pseudosections by a quasi-Newton method. *Geophysical Prospecting* **44**(1): 131-152.
- Luetschg, M. & Haeberli, W. 2005. Permafrost evolution in the Swiss Alps in a changing climate and the role of the snow cover. *Norwegian Journal of Geography* **59**: 78-83.
- Luetschg, M., Lehning, M. & Haeberli, W. 2008. A sensitivity study of factors influencing warm/thin permafrost in the Swiss Alps. *Journal of Glaciology* **54**(187): 696-704.
- Lugon, R., Gardaz, J.M. & Vonder Mühl, D. 2000. The partial collapse of Dolent glacier moraine (Mont Blanc Range, Swiss Alps). *Zeitschrift für Geomorphologie, N.F. Suppl.* **122**: 191-208.
- Marescot, L., Loke, M.H., Chapellier, D., Delaloye, R., Lambiel, C. & Reynard, E. 2003. Assessing reliability of 2D resistivity imaging in mountain permafrost studies using the depth of investigation index method. *Near Surface Geophysics* **1**(2): 57-67.
- Matsuoka, N. & Humlum, O. 2003. Monitoring periglacial processes: New methodology and technology. *Permafrost and Periglacial Processes* **14**: 299-303.
- Maurer, H. & Hauck, C. 2007. Geophysical imaging of alpine rock glaciers. *Journal of Glaciology* **53**(180): 110-120.

- Maurer, H.R., Springman, S.M., Arenson, L.U., Musil, M. & Vonder Mühll, D. 2003. Characterisation of potentially unstable mountain permafrost - a multidisciplinary approach. *Proceedings of the 8th International Conference on Permafrost*, Zurich, Switzerland: 741-746.
- McGinnis, L.D., Nakao, K. & Clark, C.C. 1973. Geophysical identification of frozen and unfrozen ground, Antarctica. *Proceedings of the 2nd International Conference on Permafrost*, Yakutsk, Russia: 136-146.
- Menke, W. 1984. *Geophysical data analysis: Discrete inverse theory*. Academic Press, Orlando, 260 pp.
- MeteoSchweiz 2006. Witterungsbericht Jahr 2006. Zürich, MeteoSchweiz.
- MeteoSchweiz 2007. Witterungsbericht Jahr 2007. Zürich, MeteoSchweiz.
- Mittaz, C., Hoelzle, M. & Haeberli, W. 2000. First results and interpretation of energy-flux measurements over Alpine permafrost) *Annals of Glaciology, Vol 31, 2000*. **31**: 275-280.
- Musil, M., Maurer, H., Green, A.G., Horstmeyer, H., Nitsche, F.O., Vonder Mühll, D. & Springman, S. 2002. Shallow seismic surveying of an Alpine rock glacier. *Geophysics* **67**(6): 1701-1710.
- Noetzli, J. 2008. Modeling transient three-dimensional temperature fields in mountain permafrost. PhD thesis, *Glaciology, Geomorphodynamics and Geochronology*. Zurich, University of Zurich: 150 pp.
- Noetzli, J., Hilbich, C., Hauck, C., Hoelzle, M. & Gruber, S. 2008. Comparison of simulated 2D temperature profiles with time-lapse electrical resistivity data at the Schilthorn crest, Switzerland. *Proceedings of the 9th International Conference on Permafrost*, Fairbanks, Alaska **2**: 1293-1298.
- Noetzli, J., Hoelzle, M. & Haeberli, W. 2003. Mountain permafrost and recent Alpine rock-fall events: a GIS-based approach to determine critical factors. *Proceedings of the 8th International Conference on Permafrost*, Zürich, Switzerland: 827-832.
- Olhoef, G.R. 1978. Electrical properties of permafrost. *Proceedings of the 3rd International Conference on Permafrost*, Edmonton, Canada: 127-131.
- Osterkamp, T.E. 1983. Response of Alaskan permafrost to climate. *Proceedings of the 4th International Conference on Permafrost*, Fairbanks, Alaska, USA: 145-152.
- Otto, J.C. & Sass, O. 2006. Comparing geophysical methods for talus slope investigations in the Turtmann valley (Swiss Alps). *Geomorphology* **76**(3-4): 257-272.
- Pandit, B.I. & King, M.S. 1979. Study of the Effects of Pore-Water Salinity on Some Physical-Properties of Sedimentary-Rocks at Permafrost Temperatures. *Canadian Journal of Earth Sciences* **16**(8): 1566-1580.
- PERMOS 2009. *Permafrost in Switzerland 2004/2005 and 2005/2006*. Noetzli, J., Naegeli, B. & Vonder Mühll, D. (Eds.). Glaciological Report (Permafrost) No. 6/7 of the Cryospheric Commission (CC) of the Swiss Academy of Sciences (SCNAT) and the Department of Geography, University of Zurich, 61 pp.
- Reynolds, J.M. 1997. *An introduction to applied and environmental geophysics*. Wiley, Chichester, 796 pp.
- Riseborough, D., Shiklomanov, N., Etzelmüller, B., Gruber, S. & Marchenko, S. 2008. Recent advance in permafrost modelling. *Permafrost and Periglacial Processes* **19**(2): 137-156.
- Roer, I., Haeberli, W., Avian, M., Kaufmann, V., Delaloye, R., Lambiel, C. & Kääh, A. 2008. Observations And Considerations On Destabilizing Active Rockglaciers In The Euro-

- pean Alps. *Proceedings of the 9th International Conference on Permafrost*, Fairbanks, Alaska **2**: 1505-1510.
- Roer, I., Kääb, A. & Dikau, R. 2005. Rockglacier acceleration in the Turtmann valley (Swiss Alps): Probable controls. *Norwegian Journal of Geography* **59**: 157-163.
- Romanovsky, V.E., Kholodov, A.L., Marchenko, S.S., Oberman, N.G., Drozdov, D.S., Malkova, G.V., Moskalenko, N.G., Vasiliev, A.A., Sergeev, D.O. & Zheleznyak, M.N. 2008. Thermal state of permafrost in Russia: First results of IPY. *Proceedings of the 9th International Conference on Permafrost*, Fairbanks, Alaska **2**: 1511-1518.
- Röthlisberger, H. 1972. *Seismic exploration in cold regions*. Cold Regions Research and Engineering Laboratory, Hanover, 139 pp.
- Routh, P.S. & Miller, C.R. 2006. Image interpretation using appraisal analysis. *SAGEEP Proceedings*: 1812-1820.
- Rubin, Y. & Hubbard, S.S. (Eds.) 2005. *Hydrogeophysics*. Water science and technology library. Dordrecht, Springer, 523 pp.
- Salzmann, N., Frei, C., Vidale, P.L. & Hoelzle, M. 2007a. The application of Regional Climate Model output for the simulation of high-mountain permafrost scenarios. *Global and Planetary Change* **56**(1-2): 188-202.
- Salzmann, N., Noetzli, J., Hauck, C., Gruber, S., Hoelzle, M. & Haeberli, W. 2007b. Ground surface temperature scenarios in complex high-mountain topography based on regional climate model results. *Journal of Geophysical Research-Earth Surface* **112**: F02S12.
- Sandmeier, K.J. 2008. REFLEXW - Windows™ 9x/NT/2000/XP-program for the processing of seismic, acoustic or electromagnetic reflection, refraction and transmission data.
- Sawada, Y., Ishikawa, M. & Ono, Y. 2003. Thermal regime of sporadic permafrost in a block slope on Mt. Nishi-Nupukaushinupuri, Hokkaido Island, Northern Japan. *Geomorphology* **52**(1-2): 121-130.
- Scales, J.A. & Snieder, R. 2000. The anatomy of inverse problems. *Geophysics* **65**(6): 1708-1710.
- Schär, C., Vidale, P.L., Lüthi, D., Frei, C., Häberli, C., Liniger, M.A. & Appenzeller, C. 2004. The role of increasing temperature variability in European summer heatwaves. *Nature* **427**(6972): 332-336.
- Scherler, M. 2006. Messung und Modellierung konvektiver Wärmetransportprozesse in der Auftauschicht von Gebirgspermafrost am Beispiel des Schilthorns. unpubl. Diploma thesis, *Geographical Institute*, University of Zurich: 100 pp.
- Schiermeier, Q. 2003. Alpine thaw breaks ice over permafrost's role. *Nature* **424**(6950): 712-712.
- Schön, J.H. 2004. *Physical properties of rocks: fundamentals and principles of petrophysics*. Helbig, K. & Treitel, S. (Eds.) Handbook of geophysical exploration - Seismic exploration. Elsevier, Amsterdam, Boston, Heidelberg, 583 pp.
- Schrott, L. & Hoffmann, T. 2008. Refraction seismics. in: Hauck, C. & Kneisel, C. (Eds.) *Applied geophysics in periglacial environments*. Cambridge, Cambridge University Press: 57-80.
- Schudel, L. 2003. Permafrost Monitoring auf dem Schilthorn mit geophysikalischen Methoden und meteorologischen Daten. unpubl. Diploma thesis, *Geographical Institute*, University of Zurich: 82 pp.
- Scott, W.J., Sellmann, P.V. & Hunter, J.A. 1990. Geophysics in the study of permafrost. in: Ward, S. (Ed.) *Geotechnical and Environmental Geophysics*. Tulsa: 355-384.

- Singha, K. & Gorelick, S.M. 2006. Hydrogeophysical tracking of three-dimensional tracer migration: The concept and application of apparent petrophysical relations. *Water Resources Research* **42**(6).
- Slater, L., Binley, A., Versteeg, R., Cassiani, G., Birken, R. & Sandberg, S. 2002. A 3D ERT study of solute transport in a large experimental tank. *Journal of Applied Geophysics* **49**(4): 211-229.
- Smith, S.L. & Burgess, M.M. 1998. Mapping the response of permafrost in Canada to climate warming, Geological Survey of Canada, Current Research 1998-E: 163-171.
- Smith, S.L., Burgess, M.M., Riseborough, D. & Nixon, F.M. 2005. Recent trends from Canadian permafrost thermal monitoring network sites. *Permafrost and Periglacial Processes* **16**: 19-30.
- Sondergeld, C.H. & Rai, C.S. 2007. Velocity and resistivity changes during freeze-thaw cycles in Berea sandstone. *Geophysics* **72**(2): E99-E105.
- Stummer, P., Maurer, H. & Green, A.G. 2004. Experimental design: Electrical resistivity data sets that provide optimum subsurface information. *Geophysics* **69**(1): 120-139.
- Timur, A. 1968. Velocity of compressional waves in porous media at permafrost temperatures. *Geophysics* **33**(4): 584-595.
- Vesnaver, A.L., Accainoz, F., Bohmz, G., Madrussaniz, G., Pajchel, J., Rossiz, G. & Dal Moro, G. 2003. Time-lapse tomography. *Geophysics* **68**(3): 815-823.
- Völksch, I. 2004. Untersuchung und Modellierung kleinräumiger Unterschiede im Verhalten von Gebirgspermafrost. unpubl. Diploma Thesis, *Geographical Institute*, University of Zurich pp.
- Vonder Mühl, D., Hauck, C. & Gubler, H. 2002. Mapping of mountain permafrost using geophysical methods. *Progress in Physical Geography* **26**(4): 643-660.
- Vonder Mühl, D., Noetzli, J., Roer, I., Makowski, K. & Delaloye, R. 2007. Permafrost in Switzerland 2002/2003 and 2003/2004, Glaciological Report (Permafrost) No. 4/5 of the Cryospheric Commission (CC) of the Swiss Academy of Sciences (SCNAT) and the Department of Geography, University of Zurich: 106.
- Vonder Mühl, D.S. 1993. Geophysikalische Untersuchungen im Permafrost des Oberengadins. PhD thesis, *ETH Zürich, Diss. ETH Nr. 10107*: 222 pp.
- Vonder Mühl, D.S., Noetzli, J. & Roer, I. 2008. PERMOS - A comprehensive monitoring network of mountain permafrost in the Swiss Alps. *Proceedings of the 9th International Conference on Permafrost*, Fairbanks, Alaska **2**: 1869-1874.
- Wyllie, M.R.J., Gregory, A.R. & Gardner, L.W. 1956. Elastic wave velocities in heterogeneous and porous media. *Geophysics* **XXI**(1): 41-70.
- Yoshikawa, K., Leuschen, C., Ikeda, A., Harada, K., Gogineni, P., Hoekstra, P., Hinzman, L., Sawada, Y. & Matsuoka, N. 2006. Comparison of geophysical investigations for detection of massive ground ice (pingo ice). *Journal of Geophysical Research-Planets* **111**(E6): E06S19.
- Zacharda, M., Gude, M. & Ruzicka, V. 2007. Thermal regime of three low elevation scree slopes in central Europe. *Permafrost and Periglacial Processes* **18**(3): 301-308.
- Zimmerman, R.W. & King, M.S. 1986. The Effect of the Extent of Freezing on Seismic Velocities in Unconsolidated Permafrost. *Geophysics* **51**(6): 1285-1290.

Appendix

A Selected plots from publication #1 actualised for 1999-2008

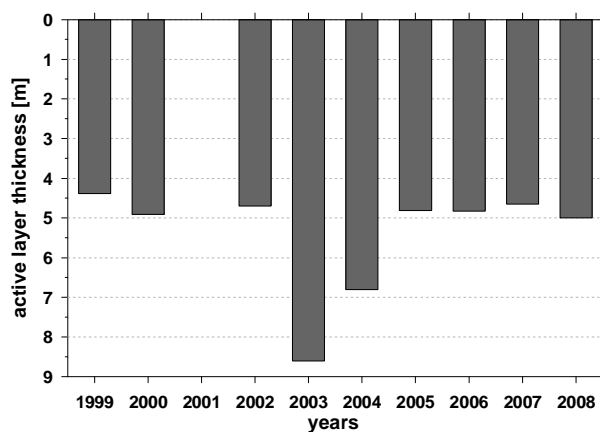


Fig. A-1: Maximum active layer thickness at Schilthorn in the observation period between 1999-2008.

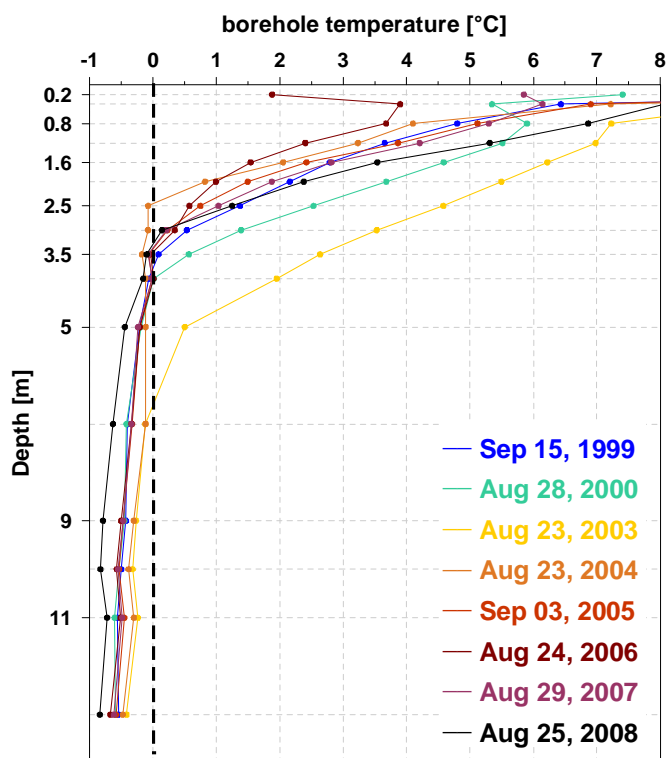


Fig. A-2: Temperature-depth plots for the borehole (B14) at Schilthorn from the ERT measurement dates between 1999-2008 (similar to Fig. 6b in publication #1). For clarity, temperatures above 8°C are not shown.

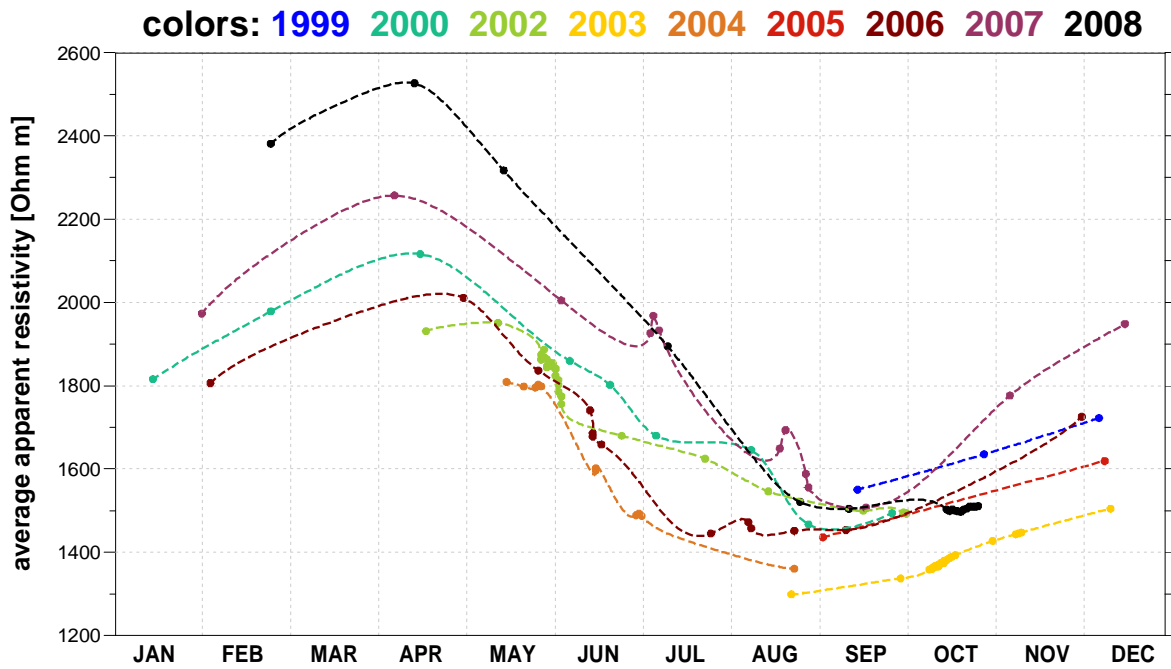


Fig. A-3: The bulk apparent resistivity (average value for the full profile) displayed as annual cycle for the observation period 1999-2008 at Schilthorn (similar to Fig. 7d in publication#1).

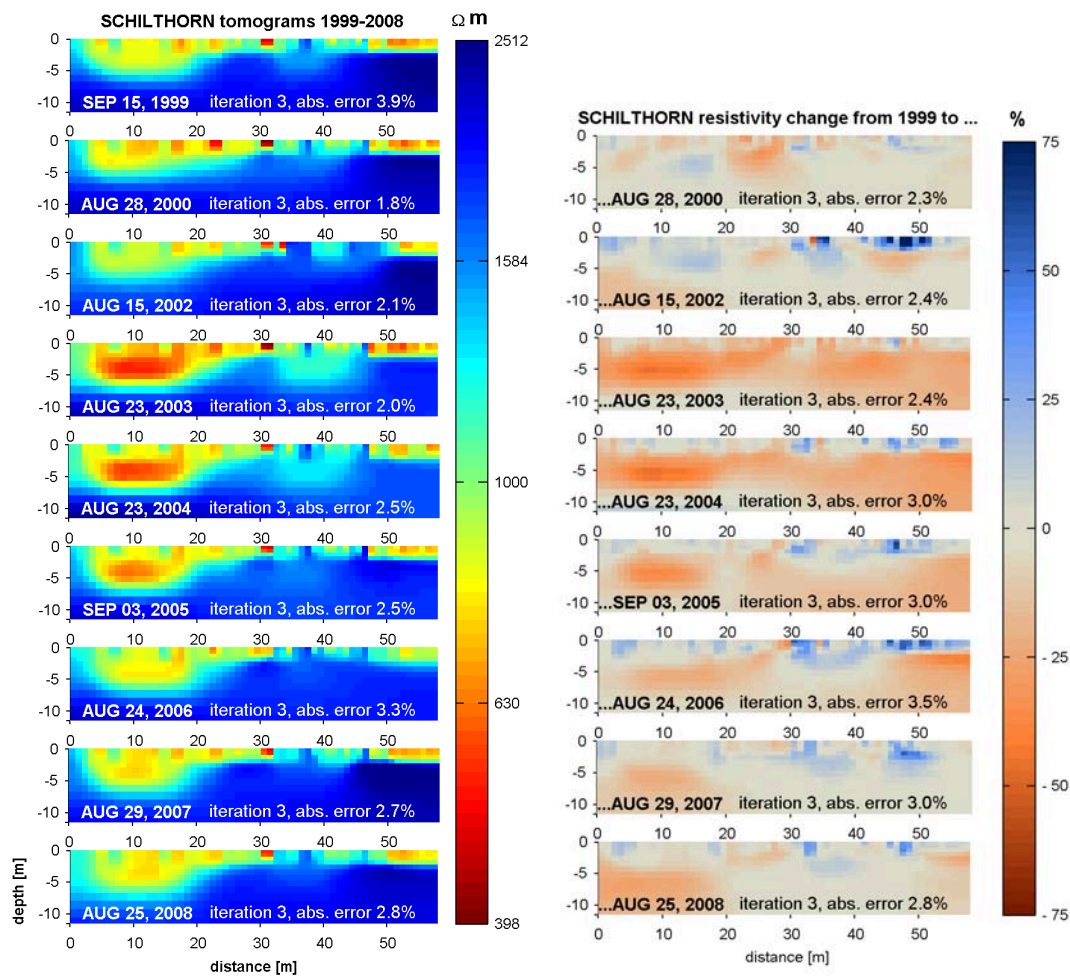


Fig. A-4: Tomograms (left) and time-lapse tomograms of the percentage resistivity change (right) at Schilthorn for the observation period 1999-2008 (similar to Fig. 10 in publication #1).

B Additional publication

The following publication is included as supplementary material to this thesis:

Noetzi, J., Hilbich, C., Hauck, C., Hoelzle, M. & Gruber, S. 2008. Comparison of simulated 2D temperature profiles with time-lapse electrical resistivity data at the Schilthorn crest, Switzerland. *Proceedings of the 9th International Conference on Permafrost*, Fairbanks, Alaska **2**: 1293-1298.

Comparison of Simulated 2D Temperature Profiles with Time-Lapse Electrical Resistivity Data at the Schilthorn Crest, Switzerland

JEANNETTE NOETZLI

Glaciology, Geomorphodynamics, Geochronology, Geography Department, University of Zurich, Switzerland

CHRISTIN HILBICH

Department of Geography, University of Jena, Germany

CHRISTIAN HAUCK

Institute for Meteorology and Climate Research, University of Karlsruhe/Forschungszentrum, Karlsruhe, Germany

MARTIN HOELZLE

Glaciology, Geomorphodynamics, Geochronology, Geography Department, University of Zurich, Switzerland

STEPHAN GRUBER

Glaciology, Geomorphodynamics, Geochronology, Geography Department, University of Zurich, Switzerland

Abstract

THE SCHILTHORN CREST IN THE BERNESE ALPS IS AN IMPORTANT PERMAFROST RESEARCH SITE. TOPOGRAPHIC AND ASPECT EFFECTS INFLUENCE THE TEMPERATURE FIELD BELOW THE EAST-WEST ORIENTED CREST. MEASURED TEMPERATURE PROFILES, HOWEVER, DO NOT PROVIDE SUFFICIENT INFORMATION FOR A COMPREHENSIVE DESCRIPTION OF THE SUBSURFACE PERMAFROST DISTRIBUTION. WE COMBINE GROUND TEMPERATURE MEASUREMENTS, ELECTRICAL RESISTIVITY TOMOGRAPHY (ERT) MONITORING AND NUMERICAL MODELING TO INVESTIGATE THE 3-DIMENSIONAL THERMAL REGIME BELOW THE CREST. THE MODELED SOUTH-NORTH ORIENTED CROSS SECTION AGREES WELL WITH ERT RESULTS ALONG THE SAME PROFILE. THE SUBSURFACE PERMAFROST BELOW THE SCHILTHORN IS CHARACTERIZED BY GENERALLY WARM PERMAFROST, WITH THE COLDEST ZONE BEING LOCATED ON THE NORTH-FACING SLOPE. THE COMBINATION OF MEASUREMENTS AND GEOPHYSICAL MONITORING BEARS POTENTIAL TO IMPROVE SIMULATION AND VALIDATION OF PERMAFROST MODELS.

Keywords: ALPINE PERMAFROST DISTRIBUTION; THERMAL MODELING; ELECTRICAL RESISTIVITY TOMOGRAPHY; PERMAFROST MONITORING AND TOPOGRAPHICAL TEMPERATURE EFFECTS

Introduction

PERMAFROST WAS FIRST FOUND ON SCHILTHORN SUMMIT IN SWITZERLAND, WHEN THE FACILITIES FOR THE CABLE CAR WERE BUILT BETWEEN 1965 AND 1967. DURING THE CONSTRUCTION OF THE BUILDINGS SEVERAL ICE LENSES WITH A THICKNESS OF UP TO 1 M WERE ENCOUNTERED. SINCE THEN, EXTENSIVE RESEARCH HAS TAKEN PLACE ON SCHILTHORN (E.G., IMHOF 2000, VONDER MUEHLL ET AL. 2000, HAUCK 2001, MITTAZ ET AL. 2002, HILBICH ET AL. 2008). IT IS ONE OF THE MOST INTENSIVELY INVESTIGATED PERMAFROST SITES IN THE EUROPEAN ALPS. THREE BOREHOLES IN PERENNIALY FROZEN GROUND WERE DRILLED WITHIN THE PACE-PROJECT BETWEEN 1998 AND 2001 (HARRIS 2001). THESE BOREHOLES PROVIDE THE BASIS FOR MONITORING AND QUANTIFICATION OF PERMAFROST IN THE PERMAFROST THERMAL REGIME.

IN MOUNTAIN AREAS THE INTERPRETATION OF MEASURED TEMPERATURE PROFILES IN BOREHOLES WITH RESPECT TO CLIMATE SIGNALS IS COMPLICATED BY TOPOGRAPHIC EFFECTS (GRUBER ET AL. 2001). THE SCHILTHORN REPRESENTS AN EAST-WEST ORIENTED MOUNTAIN WITH A WARM SOUTH FACING AND A COLDER NORTH FACING SLOPE. THOUGH MEASURED TEMPERATURE PROFILES IN BOREHOLES PROVIDE AN INITIAL ASSESSMENT OF TOPOGRAPHY RELATED PERMAFROST EFFECTS, THEY ARE ONLY REPRESENTATIVE OF ISOLATED POINTS. A COMPREHENSIVE ANALYSIS OF PERMAFROST DISTRIBUTION AND EVOLUTION BELOW THE CREST CAN ONLY BE ACHIEVED BY INTEGRATING ADDITIONAL SUBSURFACE DATA.

IN THIS PAPER, WE COMBINE MEASUREMENTS OF SUBSURFACE TEMPERATURES, ELECTRICAL RESISTIVITY TOMOGRAPHY (ERT), AND NUMERICAL MODELING OF A SUBSURFACE TEMPERATURE FIELD FOR A 2-DIMENSIONAL INVESTIGATION OF PERMAFROST DISTRIBUTION BELOW THE SCHILTHORN CREST. A 2D HEAT TRANSFER MODEL WAS FORCED BY MEASURED NEAR-SURFACE TEMPERATURES AT THE BOUNDARY TO SIMULATE THE THERMAL FIELD OF A NORTH-SOUTH ORIENTED CROSS SECTION OF THE RIDGE. AN ERT MONITORING SYSTEM WAS INSTALLED ACROSS THE SAME PROFILE, WHICH PROVIDES ADDITIONAL INFORMATION ON SUBSURFACE CONDITIONS, AND ENABLES COMPARISON OF MODELING RESULTS FOR A QUALITATIVE VALIDATION.

The Field Site

THE SCHILTHORN (2970 M ASL., 46.56° N/7.83° E, FIGS. 1 AND 2) IS LOCATED IN THE BERNESE OBERLAND IN THE NORTHERN PART OF THE ALPS. THE THREE BOREHOLES ARE LOCATED ON A SMALL PLATEAU ON THE NORTH-FACING SLOPE APPROXIMATELY 60 M BELOW THE CREST.



FIGURE 1. VIEW OF THE SCHILTHORN CREST IN THE BERNESE ALPS FROM THE EASTWARD. THE ERT-PROFILE STARTS JUST BELOW THE METEO STATION ON THE NORTHERN SLOPE AND REACHES ACROSS THE CREST APPROXIMATELY 60 M BELOW THE SOUTHERN BORDER OF THE PHOTO.

SUMMIT. AIR TEMPERATURES RECORDED AT THE METEOROLOGICAL STATION CLOSE TO THE BOREHOLES INDICATE AN ANNUAL MEAN FOR THE YEARS 1999–2007. THE ANNUAL PRECIPITATION ESTIMATED TO 2700 MM AND ABOUT 90% OF IT FALLS AS SNOW (IMHOF 2000). AS THE PRECIPITATION MAXIMUM OCCURS DURING WINTER AND DUE TO ADDITIONAL SNOW INPUT THROUGH WIND TRANSPORT, THE SNOW COVER ON THE NORTHERN SLOPE OF THE SCHILTHORN PERSISTS FROM OCTOBER UNTIL JUNE OR EVEN JULY (HAUCK 2009). THE AVERAGE SNOW DEPTH SINCE THE BEGINNING OF THE PERMAFROST MEASUREMENTS AT THE METEOROLOGICAL STATION IN 1999 IS AROUND 10 CM. THE SCHILTHORN CONSISTS OF DARK MICACEOUS SHALES. UNDER WINTER WEATHER TO FORM A FINE-GRAINED DEBRIS LAYER OF UP TO 10 METERS IN THICKNESS COVERING THE ENTIRE SUMMIT. THE ICE CONTENT OF THE SUBSURFACE MATERIAL IS ASSUMED TO BE GENERALLY LOW (AROUND 5-10% IN THE UPPER METERS, AS DEDUCED FROM DIRECT OBSERVATIONS, IMHOF ET AL. 2000, MÜHLL ET AL. 2000).

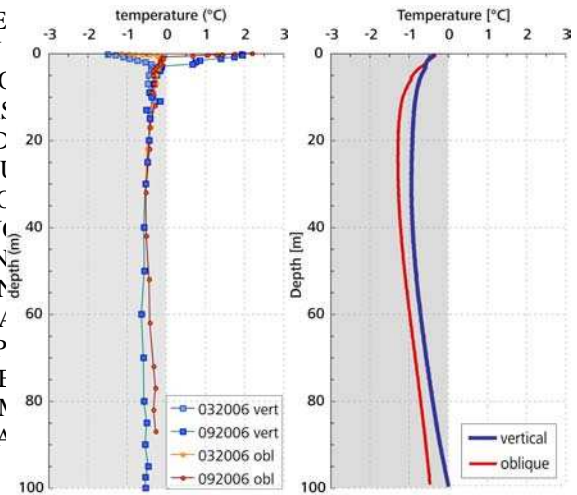


FIGURE 3. T(Z)-PROFILES FOR THE 101 M VERTICAL (VERT, BLACK) AND OBLIQUE (OBL, GRAY) BOREHOLES ON THE SCHILTHORN FOR SPRING AND AUTUMN 2006 (LEFT). MODELED T(Z)-PROFILES EXTRACTED FROM THE TEMPERATURE FIELD IN FIG. 4 AT THE LOCATIONS OF THE TWO BOREHOLES (RIGHT).

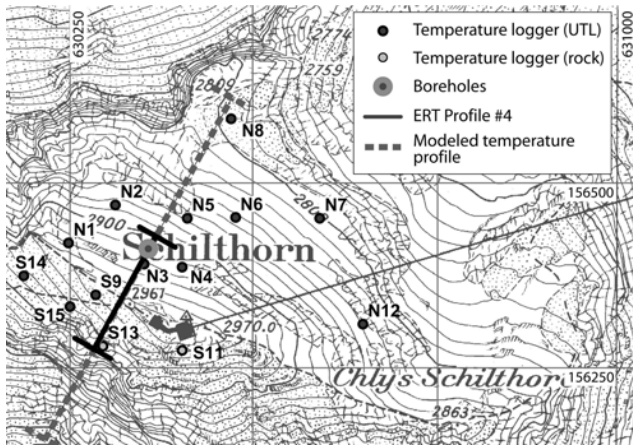


FIGURE 2. OVERVIEW OF THE FIELD SITE SCHILTHORN CREST SHOWING THE LOCATIONS OF THE NEAR-SURFACE TEMPERATURE LOGGERS, THE BOREHOLES, THE MEASURED ERT PROFILE, AND THE MODELED NORTH-SOUTH CROSS SECTION. MAP: SWISSTOPO.

Ground surface temperatures

IN ADDITION TO THE BOREHOLE MEASUREMENTS, 14 TEMPERATURE LOGGERS WERE DISTRIBUTED ON BOTH SIDES OF THE CREST IN 2005 AND 2006 TO MEASURE NEAR SURFACE-TEMPERATURES (SEE FIG. 2). THE LOGGERS WERE INSTALLED AT A DEPTH OF 5 CM (UTL MINI LOGGERS) AND 10 CM (ROCK TEMPERATURE LOGGERS) RESPECTIVELY, AND TEMPERATURES ARE RECORDED EVERY 15 MINUTES. THE ACCURACY OF THE TEMPERATURE LOGGERS IS GIVEN AS ± 0.1 °C AND ± 0.1 °C, RESPECTIVELY. AS THE LOWER PARTS OF THE SOUTHERN SLOPE ARE DIFFICULT TO ACCESS, LOGGERS WERE ONLY PLACED IN THE UPPER PART OF THE SLOPE. THESE NEAR-SURFACE TEMPERATURE MEASUREMENTS PROVIDE THE UPPER BOUNDARY CONDITION FOR THE NUMERICAL HEAT TRANSFER MODEL PRESENTED IN THE FOLLOWING SECTION. IN ADDITION, THEY CAN BE USED TO CHECK THE INTERPRETATION OF THE GEOPHYSICAL RESULTS CONCERNING THE SUBSURFACE THERMAL REGIME.

Temperature Measurements

Boreholes

IN THE SCOPE OF THE PACE PROJECT, A 14 M BOREHOLE WAS DRILLED IN 1998 AND COMPLEMENTED BY TWO 101 M BOREHOLES IN 2000. TODAY, THESE BOREHOLES ARE PART OF THE PERMAFROST MONITORING SWITZERLAND (PERMOS). THE DEEPER BOREHOLES WERE DRILLED VERTICAL AND WITH AN ANGLE OF 60° TO THE VERTICAL IN ORDER TO ACCOUNT FOR TOPOGRAPHY RELATED EFFECTS. TEMPERATURES MEASURED IN THESE BOREHOLES POINT TO WARMER PERMAFROST CONDITIONS WITH TEMPERATURE VALUES BETWEEN -1.5°C AND -2.5°C BELOW DEPTH OF THE ZERO ANNUAL AMPLITUDE (ZAA) AT APPROXIMATELY 20 M, AND TO A VERY SMALL TEMPERATURE GRADIENT WITH DEPTH (FIG. 3, LEFT). THE TEMPERATURE GRADIENT IN THE OBLIQUE BOREHOLE IS SLIGHTLY GREATER THAN IN THE VERTICAL BOREHOLE. GROUND TEMPERATURES ARE CONSIDERABLY WARMER COMPARED TO OTHER SITES AT SIMILAR ALTITUDE AND EXPOSITION, WHICH IS PROBABLY DUE TO THE LOW BEDROCK ALBEDO, LOW SNOW COVER, AND LOW ICE CONTENT AT THE SITE (HAUCK 2009).

Numerical Modeling of Subsurface Temperatures

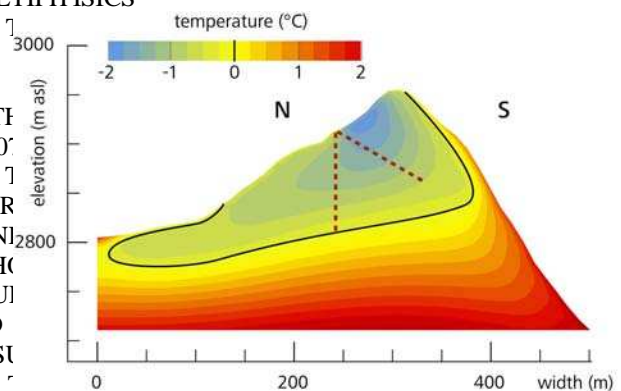
WE CONSIDERED A PURELY CONDUCTIVE TRANSIENT THERMAL PROBLEM IN AN ISOTROPIC AND HOMOGENEOUS MEDIUM ACCORDING TO CARSLAW AND JAEGER (1959). IN ORDER TO ACCOUNT FOR TOPOGRAPHY RELATED EFFECTS, WE USED A 3D HEAT TRANSFER MODEL. TEMPERATURES ARE CALCULATED FOR A PERMAFROST THERMAL YEAR 2006/2007 (I.E., 1 OCT TO 30 SEP). THE MODEL IS BASED ON MEAN ANNUAL CONDITIONS AT THE SURFACE. SEASONAL VARIATIONS AT THE SURFACE ARE NOT INCLUDED IN THE MODEL. TEMPERATURE VARIATIONS ABOVE THE ZAA ARE NOT SIMULATED IN THE MODEL. DURING WARMING BY THE UPTAKE OF LATENT HEAT DURING WARMING. THIS IS ADDRESSED IN OUR FINITE-ELEMENT TRANSPORT MODEL BY APPARENT HEAT CAPACITY, WHICH IS A FUNCTION OF THE VOLUMETRIC HEAT CAPACITY IN THE HEAT TRANSFER

AND INCLUDES ENERGY CONSUMED DURING PHASE CHANGE AND ESTIMATIONS FROM GEOPHYSICAL MEASUREMENTS. WE USED THE APPROACH DESCRIBED BY MOTTAGHY & RATH (2008) FOR THE UPPER LAYERS, A UNIFORM IC

THE RESULTING TEMPERATURE PATTERN IS EXPECTED TO BE SIMILAR FOR THE ENTIRE PROFILE WAS ASSUMED IN THE SIMULATIONS. THE UNFROZEN WATER CONTENT IS DESCRIBED BY THE BENTONITE INDEX FUNCTION AND THE STEEPNESS FACTOR WAS ASSUMED AS 0.01 (KFASSOMPAUNDY & RATH 2006).

OF SYMMETRY IN EAST-WEST DIRECTION IS SUPPORTED BY FIRST ORDER RESULTS OF A QUASI-3D GEOELECTRICAL INVESTIGATION IN THE LASTING

FOUR PARALLEL AND TWO ORTHOGONAL ERT-PROFILES THROUGH THE SCHILTHORN SUMMIT AREA (KRAUER, IN PREP.). THE SELECTED PROFILE IS SHOWN IN FIGURE 4. MAXIMUM PERMAFROST THICKNESS WAS EXTRACTED FROM A DIGITAL ELEVATION MODEL (DEM) WITH 10 M HORIZONTAL RESOLUTION (DATA SOURCE: SWISS PHOTOGRAMMETRY CENTER). ISOTHERMS ARE STEEPLY INCLINED IN THE NORTHERN ELEMENT (FE) MESH WAS GENERATED FOR THIS PART OF THE MODEL. LATERAL HEAT FLOW EXISTS FROM THE WARMER SLOPE WITH CORRESPONDING 10 M RESOLUTION AT THE SURFACE TO THE COLDER NORTH FACE. SIMULATED PERMAFROST TEMPERATURE FIELD WITH RESOLUTION AT GREATER DEPTH. THE MESH CONSISTS OF 1,000,000 ELEMENTS. THE SOFTWARE PACKAGE COMSOL MULTIPHYSICS WAS USED FOR FORWARD MODELING OF SUBSURFACE



Boundary conditions

FOR ALL NEAR-SURFACE TEMPERATURE LOGGERS THE MEASURED TEMPERATURE FOR THE HYDROLOGICAL YEAR 2006/2007 WAS USED AND SET AS UPPER BOUNDARY CONDITION AT THE SURFACE. A TYPICAL THERMAL OFFSET BETWEEN THE GROUND AND AIR TEMPERATURE AT THE SURFACE IS SMALL AT SCHILTHORN (ABOUT 0.3 °C; C.F. HUBER & GRUBER 2008) AND IS, HENCE, NEGLECTED IN THE SIMULATION.

THE YEARS 2006 AND 2007 WERE VERY WARM AND ABOVE THE LONG TERM AVERAGE. THEREFORE, MEASUREMENTS OF SURFACE TEMPERATURES ARE NOT REPRESENTATIVE FOR CURRENT CONDITIONS AT THE SURFACE DURING THE PAST DECADES. TRANSIENT EFFECTS ARE LIKELY TO OCCUR AND, THEREFORE, A FULLY TRANSIENT HEAT CONDUCTION MODEL IS REQUIRED IN ORDER TO PERFORM A REALISTIC SIMULATION OF THE CURRENT SUBSURFACE TEMPERATURE FIELD. BASED ON THE ASSUMPTION THAT SURFACE TEMPERATURE FLUCTUATIONS MAINLY FOLLOW AIR TEMPERATURES, WE USED MEAN ANNUAL AIR TEMPERATURES (MAAT) FROM THE METEOSTATION AT JUNGFAUJOCH (3576 M ASL, DATA SOURCE: METEOSWISS) SOME 10 KM EAST OF SCHILTHORN TO DESCRIBE THE EVOLUTION OF SURFACE TEMPERATURES. FOR JUNGFAUJOCH, AIR TEMPERATURE DATA IS AVAILABLE BACK TO 1933. THE TOTAL DIFFERENCE BETWEEN 2006 AND THE MEAN OF THE PERIOD 1933-1950 IS +1.52 °C. WE ADDITIONALLY ASSUMED A DIFFERENCE IN AIR TEMPERATURE OF +0.5 °C BETWEEN THE START OF THE DATA RECORDINGS AND THE LITTLE ICE AGE (CA. 1850). THE MODEL INITIALIZATION WAS STARTED IN 1850, AND DAILY TIME STEPS WERE TAKEN. A UNIFORM LOWER BOUNDARY HEAT FLUX OF 0.05 W M⁻² WAS ASSUMED AT SEA LEVEL, AND THERMAL INSULATION WAS ASSUMED FOR THE LATERAL BOUNDARIES OF THE GEOMETRY.

Subsurface properties

SUBSURFACE MATERIAL PROPERTIES WERE ASSIGNED TO THE HOMOGENEOUS AND DIFFUSIVE AND TRANSIENT SIMULATIONS. THERMAL CONDUCTIVITY, VOLUMETRIC HEAT CAPACITY, AND THE ICE WATER CONTENT ARE THE PETROPHYSICAL PARAMETERS OF IMPORTANCE. HOWEVER, ONLY LITTLE IS KNOWN ON THE SUBSURFACE CHARACTERISTICS BELOW STEEP TOPOGRAPHY AND THE PARAMETERS WERE SET BASED ON PUBLISHED VALUES: THERMAL CONDUCTIVITY WAS ASSUMED AS 2.5 W M⁻¹, AND HEAT CAPACITY TO 210 X 10⁶ J M⁻³ K⁻¹ FOR THE BULK MATERIAL (CERMAK & RYBACH 1982). THE COLDTEST TEMPERATURES EXIST BELOW THE NORTHERN SLOPE. THE REASON IS THAT COLDER TEMPERATURES ARE FOUND IN THE STEEP PART OF THE NORTHERN SLOPE (MAINLY DUE TO REDUCED SOLAR RADIATION AND LONG COVER DURATION), AND THAT SURFACE TEMPERATURES ARE MAINLY POSITIVE IN THE SMALL PLATEAU WHERE THE BOREHOLES ARE LOCATED. ON THE SOUTHERN SIDE, THE SOUTHERN SLOPE IS MAINLY FROST-FREE AT THE SURFACE. HOWEVER, DUE TO THE COLDER TEMPERATURES BELOW THE SURFACE, PERMAFROST CAN BE FOUND BELOW THE SURFACE. ADDITIONALLY, THIS IS CAUSED BY THE CENTURY-WIDE WARMING HAS NOT YET PENETRATED TO GREATER DEPTH IN THE MOUNTAIN. ADDITIONALLY, LATERAL HEAT FLOW LOWERS THE TEMPERATURES A FEW TENS OF DEGREES BELOW THE SURFACE COMPARED TO PRESENT-DAY STEADY STATE CONDITIONS. SIMILARLY, PERMAFROST REMAINS BELOW THE SURFACE AT THE FOOT OF THE NORTHERN SLOPE. THESE RESULTS POINT TO THE IMPORTANCE OF TRANSIENT 2D/3D MODELING, AS SUCH TRENDS AND TOPOGRAPHY RELATED EFFECTS COULD NOT BE DETECTED BY 1D MODELS. IN COMPARISON TO ERT PROFILES (C.F., NEXT SECTION), VERIFICATION OF THE MODEL MADE IN FIGURE 4 IS POSSIBLE. A QUALITATIVE VALIDATION OF THE GENERAL CHARACTER OF TEMPERATURE DISTRIBUTION, COMPARISON WITH EXTRACTION OF TEMPERATURE PROFILES AT THE LOCATIONS OF THE BOREHOLES SHOWS THAT THE MODELED TEMPERATURE VALUES (FIG. 3). IN GENERAL, THE MODELED PROFILES CORRESPOND TO THE MEASURED DATA.

3 AS TEMPERATURES ARE BELOW -1.5 °C FOR THE ENTIRE PROFILE, YIELD INFORMATION ON THE CHANGES AND TEMPERATURE GRADIENTS WITH DEPTH ARE SMALL. THE OBLIQUE BOREHOLE SHOWS TIME (FORTIER ET AL. 1994). A SLIGHTLY MORE CURVED PROFILE. HOWEVER, TEMPERATURE MONITORING DATA OF THE CROSS-CREST PROFILE (FIG. 1) THE MODELED PROFILE AVERAGE ABOUT 0.2 °C COLDER THAN THE MEASURED VALUES, BUT RANGE UP TO 1 °C IN THE UPPER PART OF THE PROFILE. FURTHER, IN THE LOWER PARTS THE OBLIQUE PROFILE IS WARMER THAN THE VERTICAL PROFILE, WHICH COULD BE DUE TO THE HIGHER RESISTIVITY CHANGES BETWEEN 2005 AND 2006. WHEREAS THE ANNUAL RESOLUTION PRODUCED IN THE SIMULATION. THE RESULTS ARE ENCOURAGING THAT THE MODEL ERROR SOURCES, WHICH INCLUDE: (1) SUBSURFACE PROPERTIES (I.E., ICE CONTENT, THERMAL CONDUCTIVITY) AS HOMOGENOUS FOR THE ENTIRE PROFILE AND ARE NOT KNOWN AT DEPTH. (2) THE TEMPERATURE EVOLUTION AT THIS SITE MAY BE INFLUENCED BY EFFECTS OF SOLAR RADIATION COVER AND DO NOT EXACTLY FOLLOW AIR TEMPERATURE. (3) SMALL SCALE VARIABILITY AT THE SITE THAT MY CAUSE ERRORS IN LOGGER MEASUREMENTS, AND (4) PROCESSED HEAT TRANSPORT BY CONVECTION ARE NOT TAKEN INTO ACCOUNT COMPARED TO OTHER PERMAFROST SITES AND EXCEED 4000 ΩM. THIS IS MAINLY DUE TO THE THICK FINE GRAINED DEBRIS LAYER COVERING THE SUMMIT REGION. (5) OF THE UNDERLYING BEDROCK ALSO INDICATE STRONGLY CONDITIONS OF THE MICACEOUS SHALES WITH CREVICES WATER CAN PERCOLATE. IN ADDITION TO THE COMPARABLE HOST MATERIAL, THE LOW ICE CONTENT IS IN ACCORDANCE WITH THE RESISTIVITY VALUES.

Geophysical Measurements

Electrical Resistivity Tomography (ERT)

IN 1999 A SEMI-AUTOMATIC ERT MONITORING SYSTEM WAS INSTALLED ON A 60 M LINE CLOSE TO THE THREE BORINGS IN THE NORTH FACING SLOPE TO OBSERVE SUBSURFACE RESISTIVITY CHANGES WITH RESPECT TO GROUND ICE AND WATER CONTENT (HILBICH ET AL. 2008). IN SUMMER 2005, A SECOND ERT MONITORING LINE (188 M) WAS INSTALLED ACROSS THE CREST MENTED BY A QUASI-3D ERT SURVEY ALONG FOUR TRANSECTS ACROSS THE CREST TO ANALYZE THE 3D PERMAFROST DISTRIBUTION.

THE MEASURED SIGNAL IS SENSITIVE TO TEMPORAL VARIATIONS IN PROPERTIES SUCH AS TEMPERATURE, VIA THE UNFROZEN WATER, AND

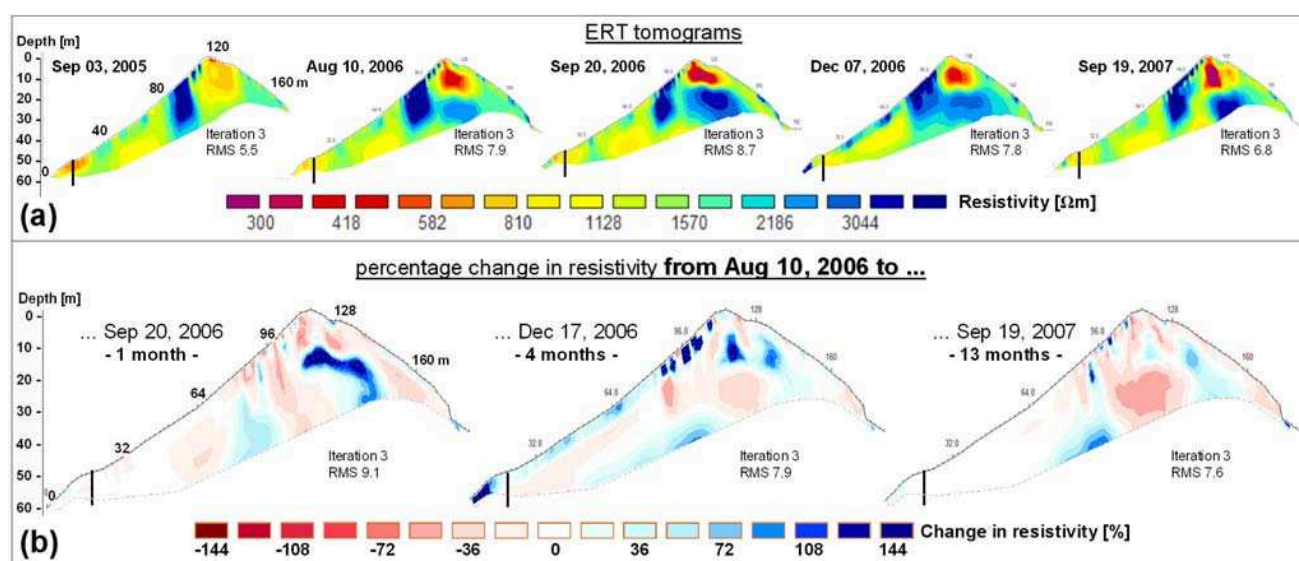


FIGURE 5. ERT MONITORING DATA ILLUSTRATED AS INDIVIDUAL RESISTIVITY TOMOGRAMS FOR SUBSEQUENT MEASUREMENTS IN SLOPE (A) AND PERCENTAGE CHANGE IN RESISTIVITY BASED ON THE REFERENCE PROFILE FROM AUGUST 10, 2006 OVER ONE, FOUR AND 13 MONTHS (B).

BOTH POSSIBILITIES WOULD RESULT IN INCREASED RESISTIVITY VALUES. ALSO THE RESULTS FROM ERT COMPARED TO REGIONS WITH LOWER ICE CONTENTS FROM MORE WETTEST HIGH AMOUNTS OF UNFROZEN WATER HERED BEDROCK OCCURRENCES, RESPECTIVELY. THE LOW RESISTIVITY ANOMALY (HAUCK ET AL. 2008). ANOMALY AT THE CREST (D) IS DIFFICULT TO INTERPRET. IN THE UPPER PART OF THE NORTHERN SLOPE A ZONE OF HOMOGENEOUS PERMAFROST WITH LOW ICE-CONTENT EXISTS. THE CORRESPONDING ZONE OF HIGH RESISTIVITY ASSOCIATED WITH VERY HIGH AMOUNTS OF UNFROZEN WATER IN THE ERT PROFILE IS, HENCE, PROBABLY CAUSED BY CONDUCTIVE MAN MADE STRUCTURES (E.G., CABLES). THE PRESENCE OF PERMAFROST RATHER THAN BY GEOLOGICAL CHARACTERISTICS SUCH A LARGE AMOUNT OF WATER IS VERY UNLIKELY SINCE THE CREST IS COVERED BY THE LARGER SEASONAL RESISTIVITY ANOMALY. THE CREST CONSISTS OF FIRM BEDROCK WITHOUT A SUPERFICIAL PERMAFROST COVER. HIGHER CONTENTS OF ICE AND UNFROZEN WATER IN THE LOWER PART OF THE NORTHERN SLOPE. WHEREAS METALLIC REMNANTS FROM THE CONSTRUCTION OF THE CREST ARE FOUND ALL OVER THE CREST PERMAFROST BOUNDARY ON THE SOUTHERN SLOPE. A MAN-MADE LOW RESISTIVE ANOMALY CAN THEREFORE NOT BE EXTENDED ONLY LITTLE BELOW THE SURFACE, AN EFFECT WHICH IS BELIEVED TO BE AN INVERSION ARTIFACT, WHICH IS NOT YET AFFECTED GREATER DEPTHS. SEASONALLY CHANGING PROPERTIES. FROM THIS, ZONE (A) ON THE NORTHERN SLOPE CAN BE SEEN AS A REGION WITH LITTLE PERMAFROST BUT WITH PRONOUNCED RESISTIVITY CHANGES NEAR THE SURFACE. THIS CLEARLY INDICATES THE PRESENCE OF PERMAFROST WITH ACTIVE LAYER FREEZING IN WINTER. ZONE (B) IN THE LOWER PARTS TEND TO EXHIBIT SLIGHTLY LOWER RESISTIVITIES IN WINTER WHICH WE INTERPRET AS DELAYED ADVANCE OF THE PERMAFROST ZONE IN THE LOWER NORTHERN SLOPE WITH A HIGH ICE-CONTENT. ZONE (C) IN THE SOUTHERN SLOPE IS CHARACTERIZED BY A HOMOGENEOUS RESISTIVITY AND DECREASES DURING SUMMER, BUT SHOWS ALMOST NO CHANGES BETWEEN AUGUST AND DECEMBER, I.E., NO ACTIVE LAYER FREEZING CAN BE REACHED BY GEOPHYSICAL MEASUREMENTS OR DIRECTLY OBSERVED. IN CONTRAST TO THE VERY SIMILAR ABSOLUTE RESISTIVITIES IN BOREHOLES. ADDITIONALLY, THE NUMERICAL MODEL IS USED TO CALCULATE SCENARIOS OF THE EVOLUTION OF THE SURFACE TEMPERATURES AND OF FUTURE PERMAFROST (ICE) CONTENT. BELOW THE SCHILTHORN CREST BY PRESCRIBING THE EVOLUTION OF THE UPPER BOUNDARY CONDITION OR BY COUPLING THE MODEL TO A SURFACE ENERGY BALANCE MODEL AND/OR USING REGIONAL CLIMATE MODEL OUTPUT (CF., NOETZLI ET AL. 2007).

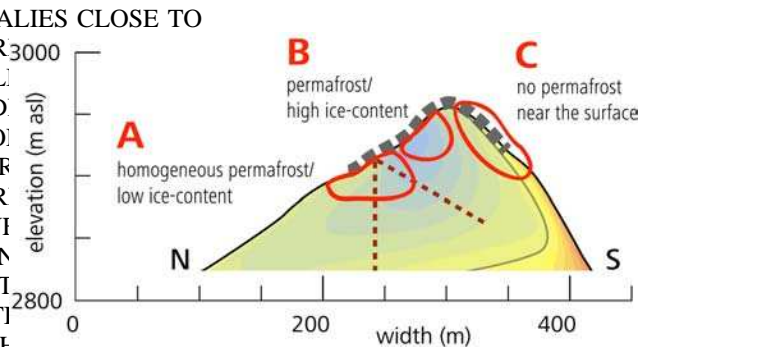


FIGURE 6. THREE FEATURES THAT ARE ADDRESSED IN THE DISCUSSION ARE HIGHLIGHTED BY BLACK CIRCLES: (A) A HOMOGENEOUS PERMAFROST ZONE IN THE LOWER NORTHERN SLOPE WITH A HIGH ICE-CONTENT, (B) PERMAFROST WITH ACTIVE LAYER FREEZING IN WINTER, AND (C) NO PERMAFROST NEAR THE SURFACE ON THE SOUTHERN SLOPE. ADDITIONALLY, GREY DASHED LINES INDICATE THE EXTENT OF THE BOREHOLES.

APART FROM THE HIGH AND LOW RESISTIVE ANOMALIES CLOSE TO THE CREST, THE CHARACTERISTICS OF THE NORTHERN (B) SLOPE SEEM TO BE SIMILAR. FROM THE QUALITATIVE ANALYSIS OF THE INDIVIDUAL TOMOGRAMS NO CLEAR INFERENCES IN PERMAFROST OCCURRENCE AND ICE CONTENT BETWEEN THE TWO SLOPES IS APPARENT. CALCULATING THE PERCENTAGE OF RESISTIVITIES BETWEEN SUBSEQUENT MEASUREMENTS OF THE TOMOGRAMS CAN BE TRANSFERRED INTO INVERSELY SEASONALLY CHANGING PROPERTIES. FROM THIS, ZONE (A) ON THE NORTHERN SLOPE CAN BE SEEN AS A REGION WITH LITTLE PERMAFROST BUT WITH PRONOUNCED RESISTIVITY CHANGES NEAR THE SURFACE. THIS CLEARLY INDICATES THE PRESENCE OF PERMAFROST WITH ACTIVE LAYER FREEZING IN WINTER. ZONE (B) IN THE LOWER PARTS TEND TO EXHIBIT SLIGHTLY LOWER RESISTIVITIES IN WINTER WHICH WE INTERPRET AS DELAYED ADVANCE OF THE PERMAFROST ZONE IN THE LOWER NORTHERN SLOPE WITH A HIGH ICE-CONTENT. ZONE (C) IN THE SOUTHERN SLOPE IS CHARACTERIZED BY A HOMOGENEOUS RESISTIVITY AND DECREASES DURING SUMMER, BUT SHOWS ALMOST NO CHANGES BETWEEN AUGUST AND DECEMBER, I.E., NO ACTIVE LAYER FREEZING CAN BE REACHED BY GEOPHYSICAL MEASUREMENTS OR DIRECTLY OBSERVED. IN CONTRAST TO THE VERY SIMILAR ABSOLUTE RESISTIVITIES IN BOREHOLES. ADDITIONALLY, THE NUMERICAL MODEL IS USED TO CALCULATE SCENARIOS OF THE EVOLUTION OF THE SURFACE TEMPERATURES AND OF FUTURE PERMAFROST (ICE) CONTENT. BELOW THE SCHILTHORN CREST BY PRESCRIBING THE EVOLUTION OF THE UPPER BOUNDARY CONDITION OR BY COUPLING THE MODEL TO A SURFACE ENERGY BALANCE MODEL AND/OR USING REGIONAL CLIMATE MODEL OUTPUT (CF., NOETZLI ET AL. 2007).

Discussion

IN BOTH THE MODELED TEMPERATURE FIELDS AND THE ERT PROFILES, THREE ZONES IN THE INVESTIGATED CROSS SECTION OF THE SCHILTHORN CREST CAN BE DISTINGUISHED THAT ARE PARTICULARLY INTERESTING (FIG. 6). CROSS VALIDATION OF THE RESULTS OF THE TWO COMPLEMENTARY APPROACHES ENABLES AN INTERPRETATION AS FOLLOWS.

(A) IN THE LOWER PART OF THE NORTHERN SLOPE A HOMOGENEOUS PERMAFROST WITH LOW ICE-CONTENT EXISTS. THE CORRESPONDING ZONE OF HIGH RESISTIVITY ASSOCIATED WITH VERY HIGH AMOUNTS OF UNFROZEN WATER IN THE ERT PROFILE IS, HENCE, PROBABLY CAUSED BY CONDUCTIVE MAN MADE STRUCTURES (E.G., CABLES). THE PRESENCE OF PERMAFROST RATHER THAN BY GEOLOGICAL CHARACTERISTICS SUCH A LARGE AMOUNT OF WATER IS VERY UNLIKELY SINCE THE CREST IS COVERED BY THE LARGER SEASONAL RESISTIVITY ANOMALY. THE CREST CONSISTS OF FIRM BEDROCK WITHOUT A SUPERFICIAL PERMAFROST COVER. HIGHER CONTENTS OF ICE AND UNFROZEN WATER IN THE LOWER PART OF THE NORTHERN SLOPE. WHEREAS METALLIC REMNANTS FROM THE CONSTRUCTION OF THE CREST ARE FOUND ALL OVER THE CREST PERMAFROST BOUNDARY ON THE SOUTHERN SLOPE. A MAN-MADE LOW RESISTIVE ANOMALY CAN THEREFORE NOT BE EXTENDED ONLY LITTLE BELOW THE SURFACE, AN EFFECT WHICH IS BELIEVED TO BE AN INVERSION ARTIFACT, WHICH IS NOT YET AFFECTED GREATER DEPTHS. SEASONALLY CHANGING PROPERTIES. FROM THIS, ZONE (A) ON THE NORTHERN SLOPE CAN BE SEEN AS A REGION WITH LITTLE PERMAFROST BUT WITH PRONOUNCED RESISTIVITY CHANGES NEAR THE SURFACE. THIS CLEARLY INDICATES THE PRESENCE OF PERMAFROST WITH ACTIVE LAYER FREEZING IN WINTER. ZONE (B) IN THE LOWER PARTS TEND TO EXHIBIT SLIGHTLY LOWER RESISTIVITIES IN WINTER WHICH WE INTERPRET AS DELAYED ADVANCE OF THE PERMAFROST ZONE IN THE LOWER NORTHERN SLOPE WITH A HIGH ICE-CONTENT. ZONE (C) IN THE SOUTHERN SLOPE IS CHARACTERIZED BY A HOMOGENEOUS RESISTIVITY AND DECREASES DURING SUMMER, BUT SHOWS ALMOST NO CHANGES BETWEEN AUGUST AND DECEMBER, I.E., NO ACTIVE LAYER FREEZING CAN BE REACHED BY GEOPHYSICAL MEASUREMENTS OR DIRECTLY OBSERVED. IN CONTRAST TO THE VERY SIMILAR ABSOLUTE RESISTIVITIES IN BOREHOLES. ADDITIONALLY, THE NUMERICAL MODEL IS USED TO CALCULATE SCENARIOS OF THE EVOLUTION OF THE SURFACE TEMPERATURES AND OF FUTURE PERMAFROST (ICE) CONTENT. BELOW THE SCHILTHORN CREST BY PRESCRIBING THE EVOLUTION OF THE UPPER BOUNDARY CONDITION OR BY COUPLING THE MODEL TO A SURFACE ENERGY BALANCE MODEL AND/OR USING REGIONAL CLIMATE MODEL OUTPUT (CF., NOETZLI ET AL. 2007).

THE RESULTS OF THIS QUALITATIVE VALIDATION CORROBORATE THE ASSUMPTION THAT THE GENERAL PATTERN OF THE SUBSURFACE TEMPERATURE FIELDS CAN BE MODELED USING DIFFUSIVE AND TRANSPORT EQUATIONS. USING SUCH AN APPROACH ENABLING THE CALCULATION OF TEMPERATURE FIELDS AT GREATER DEPTHS CAN BE REACHED BY GEOPHYSICAL MEASUREMENTS OR DIRECTLY OBSERVED. IN CONTRAST TO THE VERY SIMILAR ABSOLUTE RESISTIVITIES IN BOREHOLES. ADDITIONALLY, THE NUMERICAL MODEL IS USED TO CALCULATE SCENARIOS OF THE EVOLUTION OF THE SURFACE TEMPERATURES AND OF FUTURE PERMAFROST (ICE) CONTENT. BELOW THE SCHILTHORN CREST BY PRESCRIBING THE EVOLUTION OF THE UPPER BOUNDARY CONDITION OR BY COUPLING THE MODEL TO A SURFACE ENERGY BALANCE MODEL AND/OR USING REGIONAL CLIMATE MODEL OUTPUT (CF., NOETZLI ET AL. 2007).

Conclusions and Perspectives

THE SURFACE THERMAL FIELD OF A 2-D SECTION ACROSS THE SCHILTHORN WAS MODELED ASSUMING A PURELY CONDUCTIVE UNDERGROUND IN A FIRST APPROACH. COMPARISON WITH MEASURED GROUND TEMPERATURES AND ERT PROFILES YIELDS THE FOLLOWING CONCLUSIONS: THE SURFACE THERMAL REGIME OF THE SCHILTHORN IS MAINLY INFLUENCED BY BOTH TOPOGRAPHY AND CLIMATE.

Acknowledgements

Establishing and managing a monitoring network means a lot of field work at different places and learning to know and working with many different people. I am very grateful to a large number of colleagues, field helpers, advisors and friends who accompanied me through the last three years, for their support and encouragement in various fields. My sincerest thanks go to:

- my doctor father Roland Mäusbacher (University of Jena), who encouraged me to start a doctoral thesis and who gave me the rare opportunity to freely choose an exciting research field. He always showed a great portion of trust in my skills and supported me not only during the proposal of the PhD project but also with good advice and constructive criticism whenever needed.
- Christian Hauck (University of Fribourg) for offering me this really exciting topic and for his infectious enthusiasm about science as a whole and geophysics in particular. He not only laid the future of ‘his’ first monitoring site at Schilthorn into my hands but also entrusted me with the configuration of the whole network and actively supported me during field work and with many, many fruitful discussions.
- Daniel Vonder Mühl, who had the confidence to entrust me with the responsible task to establish a geophysical monitoring network within the PERMOS network, although I was a completely unknown quantity to him in the beginning.
- all assistants who helped me in the field, which was quite a hard job especially for those who had to carry all the heavy equipment to remote places, and those who had to swing the sledge hammer several hundred times for the refraction seismic measurements. I really appreciate the invaluable support from: Damien Abbet, Vanessa Baptista, Martin Baum, Jonathan Dorthe, Stephan Gruber, Andi Hasler, Christian Hauck, Marian Hertrich, Ulrich Hilbich, Tobias Hördt, Sebastian Klein, Michael Krauer, Ina Leiterer, Sebastien Morard, Isabelle Roer, Tommy Sickel, Andrea Stocker, Jan Walbrecker. Special thanks to Reynald Delaloye and colleagues for logistics and broad personal support at the Lapires site.
- PERMOS as a whole, and Reynald Delaloye (University of Fribourg), Martin Hoelzle (University of Fribourg) and Jeannette Noetzli (University of Zurich) in particular, who kindly provided me with the borehole data from all monitoring sites.
- Laurent Marescot (Department of Geophysics, ETH Zurich) for pushing me to an advanced application of the RES2DINV software and for guiding me through the inverse problems in geophysics.
- Karl-Josef Sandmeier (Sandmeier Software, Karlsruhe) for his straightforward help concerning the REFLEX software.
- Meng Heng Loke (Geotomo Software, Malaysia) for providing me with the Beta version of RES2DINV that allowed me to conduct the DOI and resolution matrix calculations for the appraisal analysis.
- Christian Hauck for encouraging me to learning to speak MATLAB, which I can’t imagine to do without any more, and also to Laurent Marescot for supporting me with his scripts.

- a whole bunch of people responsible for the mostly excellent logistics of the geophysical monitoring network. Starting with the equipment I want to thank Ralf Wagner and Hubert Müller (Institute of Materials Science and Technology, University of Jena) for constructing the contact boxes and geophone fixations for the geoelectric and seismic monitoring. As I carried out the geoelectric monitoring while being at an Institute without an own resistivity instrument, I sincerely want to thank all the persons and institutions who let me use their equipment during the last three years: Thomas Jahr and Corinna Kroner (Department of Applied Geophysics, University of Jena), Werner Scherer and Thomas Forbriger (Geophysical Institute, University of Karlsruhe), Reynald Delaloye (University of Fribourg), and Martin Hoelzle (University of Zurich). Special thanks also to Martin Gude (University of Jena), who always had a complete and well sorted tool kit and a simple solution to any technical problem.
- the cable car companies at Schilthorn, Stockhorn and Murtèl/Corvatsch and their helpful personnel, because all the equipment would not have been used at the right place without their support. Many thanks to Hedwig Carlen and the Matterhorn Gotthard Bahn, and Silvia Condemì and the Zermatt Bergbahnen AG for organising free transport to and from the Gornergrat, to Hermann Mooser and colleagues from the Stockhorn Bahn for their manifold support and free transport to the Stockhorn plateau, Bruno Paganini and the Corvatsch Bahn for transport to the Murtèl station, and finally Ruedi Lauri and the Schilthornbahn not only for free transport to the Schilthorn, but also for generous logistical support. Also, I am very grateful to Ueli Frei from the Schilthornbahn for always keeping me safe by giving good advice on the avalanche conditions in the Schilthorn slope.
- all, who generously allowed me to spend the nights in the cable car stations and other exciting places with mostly spectacular views, which I enjoyed very much: Rudolph Florian (Restaurant Murtèl Mittelstation), Lorenz King (University of Giessen) for staying in the Rotenboden Hütte at Gornergrat, Hermann Mooser (Stockhornbahn) for staying at the Rote Nase station, Martin Bäni (Birg station), Christine Hari (Schilthorn Restaurant) and especially the Gipfelwärter from Schilthorn (René and Brigitte Abgotschpon, and Res) for their hospitality on Schilthorn and Birg.
- my colleagues, friends and family in Jena and at all the other places and institutions for their advice, motivation, and any kind of individual support during the ups and downs of this dissertation.
- and finally Christian, for his imperturbable optimism and patience, and much more!

The establishment and installation of the geophysical monitoring network was funded by PERMOS (BAFU, Switzerland). The PhD study was part of the DFG Bündelprojekt “Sensitivity of mountain permafrost to climate change (SPCC)” within the sub-project “Geophysical Observation and 4-phase modelling of ice content evolution (GO4ICE)”.

Contribution of Christin Hilbich to the Publications that are part of this Dissertation

Publication #1

Hilbich, C., Hauck, C., Hoelzle, M., Scherler, M., Schudel, L., Völksch, I., Vonder Mühl, D. & Mäusbacher, R. 2008. Monitoring mountain permafrost evolution using electrical resistivity tomography: A 7-year study of seasonal, annual, and long-term variations at Schilthorn, Swiss Alps. *Journal of Geophysical Research* **113**: F01S90. doi: 10.1029/2007JF000799.

- Christin Hilbich is the first author and is responsible for writing this paper. She carried out the collection of the data since 2005 and the analysis and discussion of the complete data set. She is responsible for literature review and publishing the manuscript.

Publication #2

Hilbich, C., Hauck, C., Delaloye, R. & Hoelzle, M. 2008. A geoelectric monitoring network and resistivity-temperature relationships of different mountain permafrost sites in the Swiss Alps. *Proceedings of the 9th International Conference on Permafrost*, Fairbanks, Alaska **1**: 699-704.

- Christin Hilbich is the first author and responsible for writing this paper. She performed the installation of the monitoring profiles at Murtèl rockglacier, Lapires talus slope and Stockhorn rock plateau and collected the data. She is additionally responsible for literature review, the combined analysis and discussion of resistivity and temperature data, and publishing the manuscript.

Publication #3

Hilbich, C., Marescot, L., Hauck, C., Loke, M.H. & Mäusbacher, R. in press. Applicability of ERT monitoring to coarse blocky and ice-rich permafrost landforms. *Permafrost and Periglacial Processes*.

- Christin Hilbich is the first author and is responsible for writing this paper. She collected the presented data set, performed the appraisal analyses, discussed the data, and is responsible for literature review and publishing the manuscript.

PERSONAL BIBLIOGRAPHY

Publications are listed chronologically. The papers that form this thesis are highlighted with an asterisk (*).

PEER-REVIEWED PUBLICATIONS

- * **Hilbich, C.**, Marescot, L., Hauck, C., Loke, M.H. & Mäusbacher, R. in press. Applicability of ERT monitoring to coarse blocky and ice-rich permafrost landforms. *Permafrost and Periglacial Processes*.
- * **Hilbich, C.**, Hauck, C., Delaloye, R. & Hoelzle, M. 2008. A geoelectric monitoring network and resistivity-temperature relationships of different mountain permafrost sites in the Swiss Alps. *Proceedings of the 9th International Conference on Permafrost*, Fairbanks, Alaska **1**: 699-704.
- Noetzli, J., **Hilbich, C.**, Hauck, C., Hoelzle, M. & Gruber, S. 2008. Comparison of simulated 2D temperature profiles with time-lapse electrical resistivity data at the Schilthorn crest, Switzerland. *Proceedings of the 9th International Conference on Permafrost*, Fairbanks, Alaska **2**: 1293-1298.
- Hauck, C., Bach, M. & **Hilbich, C.** 2008. A 4-phase model to quantify subsurface ice and water content in permafrost regions based on geophysical data sets. *Proceedings of the 9th International Conference on Permafrost*, Fairbanks, Alaska **1**: 675-680.
- Frauenfelder, R., Hauck, C., **Hilbich, C.**, Kneisel, C. & Hoelzle, M. 2008. An integrative observation of kinematics and geophysical parameters of Gianda Grischa rockglacier, Upper Engadine, Swiss Alps. *Proceedings of the 9th International Conference on Permafrost*, Fairbanks, Alaska **1**: 463-468.
- * **Hilbich, C.**, Hauck, C., Hoelzle, M., Scherler, M., Schudel, L., Völksch, I., Vonder Mühl, D. & Mäusbacher, R. 2008. Monitoring mountain permafrost evolution using electrical resistivity tomography: A 7-year study of seasonal, annual, and long-term variations at Schilthorn, Swiss Alps. *Journal of Geophysical Research* **113**: F01S90. doi: 10.1029/2007JF000799.
- Hilbich, C.**, Mügler, I., Daut, G., Frenzel, P., van der Borg, K. & Mäusbacher, R. 2008. Reconstruction of the depositional history of the former coastal lagoon of Vilamoura (Algarve, Portugal): A sedimentological, microfaunal and geophysical approach. *Journal of Coastal Research* **24**(2b): 83-91, doi: 10.2112/04-0411.

PUBLICATIONS WITHOUT PEER REVIEW

- Helmschrot, J., **Hilbich, C.**, Mäusbacher, R. & Daut, G. 2007. Geophysikalische und sedimentologische Untersuchungen zur Entstehung und Ausprägung von Feuchtgebieten im semi-ariden Südafrika. *Zentralblatt für Geologie und Paläontologie, Teil I*, 2006, **1-4**: 63-78.
- Hilbich, C.**, Helmschrot, J., Mäusbacher, R. & Daut, G. 2006. A landscape-based model to characterize the evolution and recent dynamics of wetlands in the Umzimvubu headwa-

ters, eastern cape, South Africa. in: Kotowski, W., Maltby, E., Miroslaw–Swiatek, D., Okruszko, T. and Szatyłowicz, J. (eds) *Wetlands: modelling, monitoring, management*, Taylor & Francis The Netherlands/A.A. Balkema Publisher. pp. 61-69 (ISBN: 10-041508202).

Hilbich, C., Mügler, I., Daut, G., Frenzel, P., Teichner, F. & Mäusbacher, R. 2005. Geophysikalische, sedimentologische und mikrofaunistische Methoden zur Rekonstruktion der Paläogeographie einer Römischen Hafensiedlung: Die Landschaftsgenese der Lagune von Vilamoura (Portugal) während der letzten 6000 Jahre. in: Beck, N. (Ed.) *Neue Ergebnisse der Meeres- und Küstenforschung*. 23. Jahrestagung des Arbeitskreises Geographie der Meere und Küsten, Koblenz. Schriften des Arbeitskreises Landes- und Volkskunde 4: 51-71.

Hilbich, C. 2003. *Rekonstruktion der holozänen Paläoumweltbedingungen der ehemaligen Lagune von Vilamoura (Algarve/Portugal) – Sedimentologische und geophysikalische Untersuchungen*. unpubl. Diploma thesis, University of Jena, 113 pp.

Curriculum vitae

Persönliche Daten

Name	Christin Hilbich
Geburtsdatum	20. Februar 1977
Geburtsort	Jena
Familienstand	ledig

Kurzbiographie

09/1983 - 06/1991	Grundschule in Jena
09/1991 - 06/1995	Gymnasium in Jena Allgemeine Hochschulreife (Abitur)
09/1995 - 07/1997	Fachschule für Technik und Gestaltung, Hermsdorf Abschluss als Technische Assistentin für Gestaltung
10/1997 - 04/2004	Studium der Geographie an der Friedrich Schiller Universität Jena Abschluss als Diplom-Geographin (<i>Gesamtnote 1,3</i>)
10/1998 - 07/2003	studentische Hilfskraft an der FSU Jena
seit 05/2004	Wissenschaftliche Mitarbeiterin am Institut für Geographie, Lehrstuhl Physische Geographie, FSU Jena
seit 04/2009	Wissenschaftliche Mitarbeiterin am Institut für Geographie, Abteilung Glaziologie, Geomorphodynamik und Geochronologie, Universität Zürich

Jena, 15.04.2009

Selbständigkeitserklärung

Ich erkläre, dass ich die vorliegende Arbeit selbständig und unter Verwendung der angegebenen Hilfsmittel, persönlicher Mitteilungen und Quellen angefertigt habe.

.....

Ort, Datum

.....

Christin Hilbich

Erratum

The RMS (root mean square) error given for all tomograms in publications #1 and #2 is in fact the absolute data misfit value in percent. The value of the given error is correct.